

DTIC FILE COPY

GL-TR-90-0005

2

**INVESTIGATION OF STRUCTURE AND TRANSPORT PROCESSES
IN THE HIGH LATITUDE IONOSPHERIC PLASMA USING
GROUND BASED AND AIRBORNE DIGISONDES**

Bodo W. Reinisch
Klaus Bibl
Terence W. Bullett
Paul S. Cannon
Geoffrey Crowley
Claude G. Dozois
Robert R. Gamache
David F. Kitrosser
Eric Li
Gary S. Sales
Jane S. Tang

AD-A224 397

DTIC
S **ELECTE** **D**
JUL 30 1990
D **CS**

University of Lowell
Center for Atmospheric Research
450 Aiken Street
Lowell, MA 01854

January 1990

Final Report

August 8, 1986 - December 7, 1989

Approved for public release; distribution unlimited.

GEOPHYSICS LABORATORY
AIR FORCE SYSTEMS COMMAND
UNITED STATES AIR FORCE
HANSCOM AFB, MASSACHUSETTS 01731-5000

90 07 30 109

"This technical report has been reviewed and is approved for publication"



JURGEN BUCHAU
Contract Manager



WILLIAM K. VICKERY
Branch Chief

FOR THE COMMANDER



ROBERT A. SKRIVANEK
Division Director

This report has been reviewed by the ESD Public Affairs Office (PA) and is releasable to the National Technical Information Service (NTIS).

Qualified requestors may obtain additional copies from Defense Technical Information Center. All others should apply to the National Technical Information Service (NTIS).

If your address has changed, or if you wish to be removed from the mailing list, or if the addressee is no longer employed by your organization, please notify GL/IMA, Hanscom AFB, MA 01731. This will assist us in maintaining a current mailing list.

Do not return copies of this report unless contractual obligations or notice on a specific document requires that it be returned.

Unclassified

SECURITY CLASSIFICATION OF THIS PAGE

REPORT DOCUMENTATION PAGE

Form Approved
OMB No. 0704-0188

1a. REPORT SECURITY CLASSIFICATION Unclassified			1b. RESTRICTIVE MARKINGS		
2a. SECURITY CLASSIFICATION AUTHORITY			3. DISTRIBUTION / AVAILABILITY OF REPORT Approved for public release; distribution unlimited.		
2b. DECLASSIFICATION / DOWNGRADING SCHEDULE					
4. PERFORMING ORGANIZATION REPORT NUMBER(S) ULRF-455/CAR			5. MONITORING ORGANIZATION REPORT NUMBER(S) GL-TR-90-0005		
6a. NAME OF PERFORMING ORGANIZATION University of Lowell	6b. OFFICE SYMBOL (If applicable)	7a. NAME OF MONITORING ORGANIZATION Geophysics Laboratory (AFSC)			
6c. ADDRESS (City, State, and ZIP Code) Center for Atmospheric Research 450 Aiken Street Lowell, MA 01854			7b. ADDRESS (City, State, and ZIP Code) Hanscom AFB Massachusetts 01731-5000		
8a. NAME OF FUNDING / SPONSORING ORGANIZATION Geophysics Laboratory	8b. OFFICE SYMBOL (If applicable) LIS	9. PROCUREMENT INSTRUMENT IDENTIFICATION NUMBER F19628-86-K-0036			
8c. ADDRESS (City, State, and ZIP Code) Hanscom AFB Massachusetts 01731-5000		10. SOURCE OF FUNDING NUMBERS			
		PROGRAM ELEMENT NO 62101F	PROJECT NO 4643	TASK NO 08	WORK UNIT ACCESSION NO AJ
11. TITLE (Include Security Classification) INVESTIGATION OF STRUCTURE AND TRANSPORT PROCESSES IN THE HIGH LATITUDE IONOSPHERIC PLASMA USING GROUND BASED AND AIRBORNE DIGISONDES					
12. PERSONAL AUTHOR(S) Bodo W. Reinisch; Klaus Bibl; Terence W. Bullett; Paul S. Cannon; Geoffrey Crowley; Claude G. Dozois; Robert R. Gamache; David F. Kitrosser; Eric Li; Gary S. Sales;					
13a. TYPE OF REPORT Final	13b. TIME COVERED FROM 8/8/86 TO 12/7/89	14. DATE OF REPORT (Year, Month, Day) 1990 January		15. PAGE COUNT 172	
16. SUPPLEMENTARY NOTATION <i>Keywords:</i>					
17. COSATI CODES			18. SUBJECT TERMS (Continue on reverse if necessary and identify by block number)		
FIELD	GROUP	SUB-GROUP	Polar Ionosphere, Drift Measurements, <i>John</i> Ionospheric Convection, Ionospheric Sounding,		
19. ABSTRACT (Continue on reverse if necessary and identify by block number) The Digisonde 256 is an advanced ionospheric sounder developed by the University of Lowell Center for Atmospheric Research (ULCAR). It is a new and exciting tool for obtaining important ionospheric information. Like a conventional ionosonde, the Digisonde yields vertical electron density profiles. However, the antenna arrangement and sophisticated data handling system also permits plasma drift velocities to be derived from the ionospheric reflections. The F-region plasma drifts perpendicular to the magnetic field at the $E \times B$ velocity, and electric fields can therefore be deduced from the Digisonde drift measurements. This final report describes the development of the drift analysis techniques and highlights some of the exciting scientific results obtained by the Air Force Digisonde network, including the Airborne Ionospheric Observatory (AIO) of the Geophysics Laboratory. Digisonde data have been applied to the study of large scale ionospheric features such as high latitude convection, polar cap patches, sun aligned arcs and the midlatitude trough.					
20. DISTRIBUTION / AVAILABILITY OF ABSTRACT <input checked="" type="checkbox"/> UNCLASSIFIED/UNLIMITED <input type="checkbox"/> SAME AS RPT <input type="checkbox"/> DTIC USERS			21. ABSTRACT SECURITY CLASSIFICATION Unclassified		
22a. NAME OF RESPONSIBLE INDIVIDUAL Jurgen Buchau			22b. TELEPHONE (Include Area Code) 617-377-2390	22c. OFFICE SYMBOL GL/LIS	

12. PERSONAL AUTHOR(S)

Jane S. Tang

19. ABSTRACT

A good data base now exists for the further study of these phenomena.

Accession For	
NTIS CRA&I	<input checked="checked" type="checkbox"/>
DTIC TAB	<input type="checkbox"/>
Unannounced	<input type="checkbox"/>
Justification _____	
By _____	
Distribution /	
Availability Codes	
Dist	Avail and/or Special
A-1	



TABLE OF CONTENTS

	Page
1.0 INTRODUCTION	1
2.0 ANALYSIS AND MEASURING TECHNIQUES	6
2.1 Electron Densities	6
2.2 Plasma Drift	6
2.2.1 Automation of Drift Measurements	7
2.2.2 Echo Source Determination	10
2.2.3 The Effects of Refraction	13
2.2.4 Drift Data Processing	19
2.2.5 Special Processing Concerns	25
2.2.6 Validation of New Phase Only Analysis Technique	26
3.0 OBSERVATIONS AND CAMPAIGNS	28
3.1 Drift	28
3.2 Oblique Ionogram Measurements	30
3.2.1 Oblique Sounding Between Goose Bay and Argentina	31
3.2.2 Oblique Sounding Between Argentina and Millstone	31

TABLE OF CONTENTS (Continued)

	Page
3.2.3 Oblique Sounding Between Goose Bay and Millstone	43
3.2.4 Trough Studies	43
3.3 Campaigns	53
4.0 SONDRESTROM DRIFT OBSERVATIONS	62
5.0 SCIENTIFIC RESULTS	69
5.1 Published Papers	69
5.2 Scientific Reports	70
5.3 Conference Presentations	70
6.0 REFERENCES	73
APPENDIX A Inventory of Drift Observations from Argentina, Goose Bay and Qaanaaq	
APPENDIX B Copies of Publications	

LIST OF FIGURES

Figure No.		Page
1	High Latitude Digisonde Network	3
2	Station Locations	4
3	Lines of Equal Doppler Velocity	12
4	Ionospheric Model to Estimate Refraction Effects	14
5	Seven Antenna Receiving Array	21
6	Individual Skymaps Argentina, Newfoundland 20 October 1987 2201 - 2203 UT	23
7	Comparing the FWPD and PO Analysis Techniques	27
8	Reception in Argentina of Oblique Ionograms from Goose Bay	32
9	Variability of the Virtual Transmission Factor (M-Factor) Assuming Linear Gradients in foF2. Argentina - Millstone Day 87293	46
10	Goose Bay to Millstone Oblique Bistatic Ionograms	47
11 a	Trough Signatures for Five Days in 1988	50

LIST OF FIGURES (Continued)

Figure No.		Page
11b	Trough Signatures for Five Days in 1988	51
12	Motion of Trough Over Three Station Chain	52
13	Qaanaaq, Greenland Digital Ionogram 14 August 1987, 1456 UT	55
14	Qaanaaq, Greenland Digital Ionogram 14 August 1987, 1706 UT	56
15	Andoya Ionogram and Electron Density Profiles	59
16	Sondrestrom Drift Data, 89188 to 89192	63
17	Qaanaaq Drift Data, 89188 to 89192	64
18	Drift at Sondrestrom and Qaanaaq	66
19	By Prediction Based on Qaanaaq Drift	68

LIST OF TABLES

Table No.		Page
1 A	Argentina Drift Inventory	29
2 A	Oblique Propagation (from Argentina) Received at Millstone	38
2 B	Oblique Propagation (from Millstone) Received at Argentina	38
3 A	Oblique Propagation (from Argentina) Received at Millstone	39
3 B	Oblique Propagation (from Millstone) Received at Argentina	40
4 A	Oblique Propagation (from Argentina) Received at Millstone	41
4 B	Oblique Propagation (from Argentina) Received at Millstone	42
5 A	Oblique Propagation Received Simultan- eously at Millstone and Argentina	44
5 B	Oblique Propagation Received Simultan- eously at Millstone and Argentina	45
6	Available Ionogram Surveys	49
7	AIO Ionogram Observations Andoya Round Trips 1988	58
8	Digisonde Data in Support of the CEDAR- HLPS (February 1988)	61

1.0 INTRODUCTION

This manuscript represents the final report for Geophysics Laboratory Contract No. F19628-86-K-0036: Investigation of Structure and Transport Processes in the High Latitude Ionosphere Plasma Using Aircraft and Ground Based Digital Ionosondes.

The project addressed three topics identified by a GL Program Research and Development Announcement:

- i) Specification of structure, dynamic behavior and transport of ionization at high latitudes.
- ii) Measurements and long term data base development.
- iii) Analysis and interpretation.

The University of Lowell Center for Atmospheric Research (ULCAR) has designed and built an advanced ionospheric sounder, the Digisonde. Several of these have been purchased and deployed by the Air Weather Service (AWS) for real time ionospheric data acquisition. The Geophysics Laboratory (GL) uses several high latitude systems for scientific studies. ULCAR contracted to use these instruments to address three specific aspects of the above topics:

- i) Determination of ionospheric convection patterns.
- ii) Observations of the E-region trough.
- iii) Definition of the source and structure of polar cap arcs and F-layer patches.

For the purposes of this report, the research has been broken down into three different categories: analysis techniques (Section 2.0); observations and campaigns (Section 3.0); and

interpretation of data (Section 4.0). Section 5.0 lists the publications and presentations that resulted from this research.

The high latitude ionosphere is a complex region because of the two forms of solar energy transfer: electromagnetic radiation and solar wind particles. The coupling of the magnetic fields of the earth and the sun (or the solar wind) leads to magnetospheric electric fields that control the dynamics in the magnetosphere. These electric fields are also mapped along magnetic field lines into the polar cap ionosphere producing an $\mathbf{E} \times \mathbf{B}$ drift that drives the plasma across the polar cap [Dungey, 1961; Cauffman and Gurnett, 1972; Heppner, 1977]. Magnetospheric accelerated particles impacting onto the atmosphere produce the aurora and the auroral oval surrounding the polar cap. The size, or diameter, of the polar cap and the cross polar cap potential are direct measures of the energy transfer from the solar wind into the ionosphere. F region plasma enhancements, or patches, observed to move in the antisunward direction across the polar cap [Buchau et al., 1983; Weber et al., 1984] have been explained as the result of variations in the diameter of the polar cap [Anderson et al., 1988]. When the polar cap convection pattern expands so that sunlit regions at noon magnetic local time (MLT) become part of the pattern, then higher density plasma is carried from the sunlit ionosphere into the dark polar cap, with its lower electron density.

The study of the convection pattern is one of the major tasks of GL's Digisonde network (Figure 1). In Figure 2, the locations of the four high latitude Digisondes are shown in a corrected geomagnetic latitude versus geomagnetic local time (CGLT) system [Hakura, 1965; Whalen, 1970]. The locations of the Millstone Hill and EISCAT incoherent scatter radars are also shown for reference. The initial observations were conducted at Qaanaaq, Greenland (87° CGLAT), Goose Bay, Labrador (65° CGLAT), and Argentia, Newfoundland (57° CGLAT). The station locations are marked by Q,

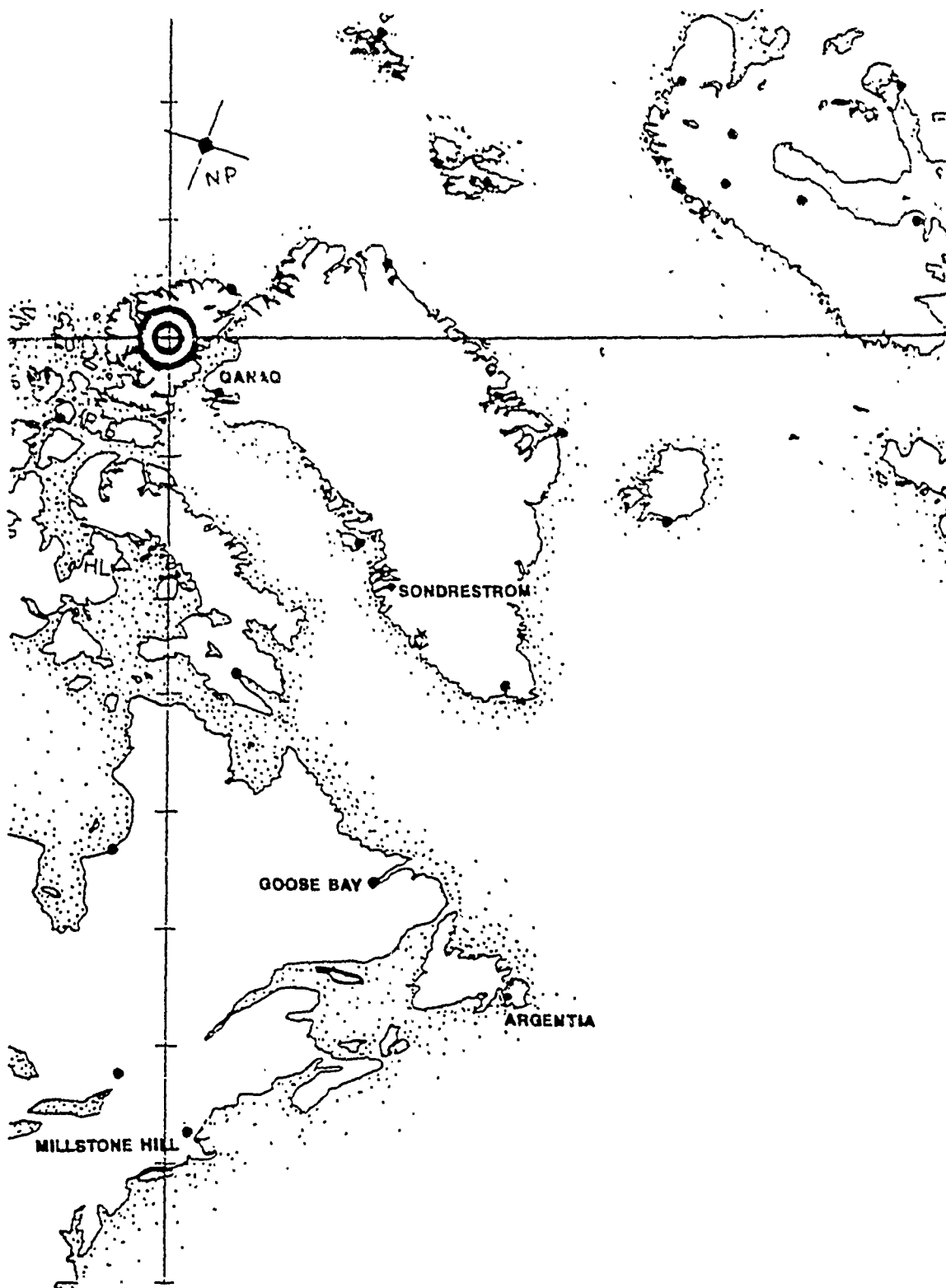


Figure 1. High Latitude Digisonde Network

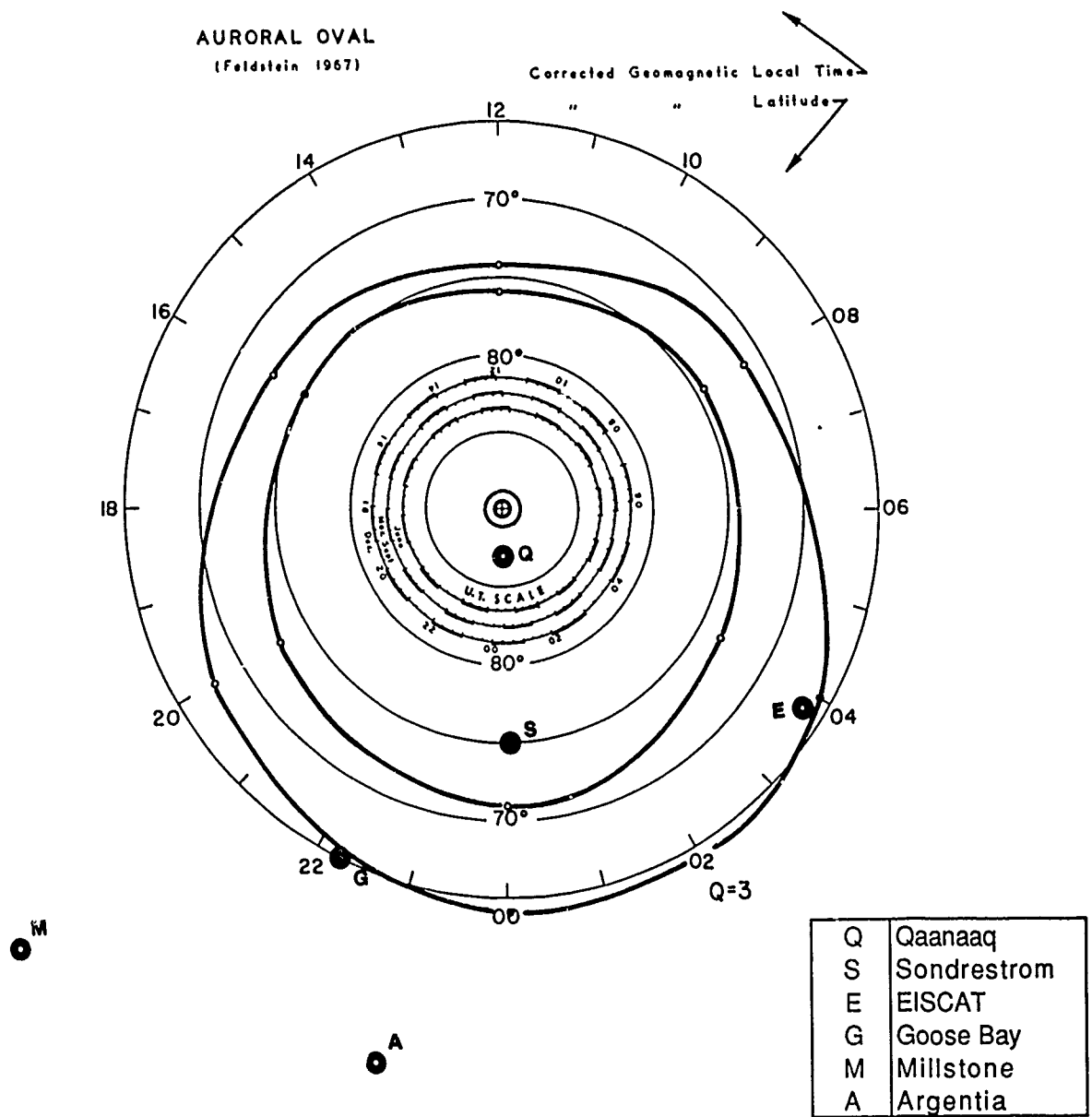


Figure 2. Station Locations

G, and A for 02 universal time (UT), when Qaanaaq is at midnight magnetic local time. The plasma convection pattern is monitored at its center by Qaanaaq, and in the auroral oval and trough regions by the Goose Bay and Argentia stations, respectively. A fourth high latitude Digisonde was installed at Sondre Stromfjord, Greenland (77° CGLAT) in June 1989, and the first observations are discussed in this report. The Sondrestrom Digisonde fills the gap between Qaanaaq and Goose Bay. The Sondrestrom station is important because it monitors the plasma flow in the dayside throat region and enables the development of ionospheric irregularities to be investigated as they cross the polar cap.

For the modeling and forecasting of the high latitude ionosphere the plasma convection is an important driver, and one of the exciting results of the work reported here is the validation of the Digisonde drift measurements as a monitor of the polar cap convection. The characteristic flow patterns as a function of B_y , for B_z negative, had been established by statistical evaluation of satellite plasma flow measurements [Heppner and Maynard, 1987]. Using similar statistical techniques, we have evaluated the Digisonde drift data from the central polar cap station at Qaanaaq, and found excellent agreement with the Heppner-Maynard models.

Understanding of the polar ionization distribution involves the entire polar cap/oval/suboval region, including the formation of the night and daytime F region trough [Whalen, 1989, and references therein]. Whalen concluded from his analysis of ionosonde data that the trough in the daytime F layer is a regular feature, controlled by the magnetospheric-ionospheric convection.

2.0 ANALYSIS AND MEASURING TECHNIQUES

2.1 Electron Densities

The labor intensive ionogram scaling and evaluation required by conventional ionosondes has been replaced by automatic techniques. The Automatic Real Time Ionospheric Scaling Technique (ARTIST) developed by ULCAR is a PC-based system which determines values for the important parameters from an ionogram. The operation and testing of ARTIST has been described by Gamache et al. [1988] associated with this contract, and by Reinisch et al., 1988a.

Inversion of ionograms to yield electron density profiles is also performed automatically by ARTIST. The current software includes two inversion techniques. These are the ULCAR modified Chebyshev polynomial method and the Titheridge POLAN method [Titheridge, 1985]. Both are described in Scientific Report No. 2, and by Reinisch et al. [1988b]. A third representation of the F-region electron density profile in terms of LAY functions has also been investigated [Bossy et al., 1988]. McNamara et al. [1987] compiled statistics on the comparison of hmF2 values derived from the POLAN model with those obtained by the simple methods of Dudeney [1983] and Bilitza et al. [1979].

2.2 Plasma Drift

A very important aspect of the Digisonde is its ability to measure ionospheric plasma drift velocities, from which electric fields may be derived. Until early 1986 drift measurements had been made by manually selecting frequencies and setting sampling gates, thereby requiring continuous manning of the Digisonde during

drift measurements. During the time covered by this contract, the drift measurements have been automated. The drift analysis programs (running on GL's Cyber computer) have also been significantly improved. This work is summarized below.

2.2.1 Automation of Drift Measurements

The automatic drift mode operations of the Digisonde are based on ARTIST trace-identification software. The drift measurements use phase coherent pulse transmission on two HF frequencies which are selected to sample desired heights in the F-region. During normal measurement campaigns, ionograms are taken in 5-minute intervals to monitor the dynamic environment. The time between ionograms is used to collect a series (nominally twelve) of drift measurements (cases) of typically 10-s each.

The commonly used drift mode in the Digisonde 256 multiplexes four sounding frequencies and samples the echoes at one range gate for each of the four frequencies. Automation of the drift operation requires selection of appropriate frequencies F1, F2, F3 and F4, corresponding range gates H1, H2, H3 and H4, and receiver gain settings G1, G2, G3 and G4. The "AUTODRIFT" software residing in the ARTIST PC/AT selects frequencies and range settings from the autoscaled ionograms. To allow for height (or range) changes during the drift observation intervals, a range tracking algorithm is included in AUTODRIFT. The initial settings are $F1 = F2$ and $F3 = F4$; and $H2 = H1 + 10$ km and $H4 = H3 + 10$ km. At the end of each drift case (nominally 10 sec) the amplitudes at HL (larger range) and HS (smaller range), i.e. AL and AS are compared and the range gates are corrected for the next drift case in the following way:

If $AS > AL \rightarrow$ decrease HL by 20 km

If $AS < AL \rightarrow$ increase HS by 20 km.

The two sounding frequencies are selected at the end of the ionogram, as soon as the autoscaling is completed, and then remain constant during the drift interval. The frequency selection criteria are simple: one, find interference-free frequencies, and two, choose frequencies that are reflected at the bottom of the F layer. The reason for the first criterion is clear; good signal-to-noise ratio. The rationale for the second criterion is the Digisonde drift analysis technique [Reinisch et al., 1987] which is summarized in the following paragraphs.

A wide beam transmit antenna, fed by 10 kW of pulsed HF signal, illuminates a large area of the F region above the ionosonde. All areas in the F region where the plasma frequency is equal to the sounding frequency and where the area surface vector is parallel to the incident wave vector generate an echo. The reflection point is called a source [Dozois, 1983]. The Doppler shift of the source signal is determined by the location and the velocity of the source. The Digisonde determines the Doppler shifts by forming the discrete Fourier transforms [Bibl and Reinisch, 1978] of the signals received on four or seven spaced receiving antennas. To find the locations of the sources, two assumptions are made: one, that one source contributes to a given Doppler line, and two, that the incidence angle calculated by using the measured spectral phases at the spaced antennas specifies the source location. This latter assumption is justified when refraction in the ionosphere is small, which is the case for signals reflected at the bottom of the F layer where the vertical plasma density gradient is steep. It is for this reason that AUTODRIFT selects frequencies in the flat part of the F trace in the ionogram. The discussion on refraction effects and on the source/Doppler relation is continued in Section 2.2.2.

The method of selecting the drift sounding frequencies is as follows. The AUTODRIFT algorithm divides the frequency interval $f_oF2 - f_oF1$ (or $f_oF2 - f_oE$, or $f_oF2 - f_{minF}$, depending on ionospheric

conditions), obtained from the last ionogram, into four equal intervals. From the two central intervals, one frequency with the best signal-to-noise ratio (as measured in the ionogram) is determined for each interval. The virtual echo heights for these two frequencies are obtained from the ionogram autoscaling data. The initial receiver gain control is set to -20 dB ($G = 2$). For each of the two frequencies, the gain is adjusted at the end of each drift case until the larger signal amplitude (of the two range gates) is within 6 to 12 dB of the maximum allowable digital signal.

The first automatic drift measurements were made at Argentia, Newfoundland, in October 1986. Since then, several adjustments have been made to the AUTODRIFT program, which is now operating reliably at Argentia, Goose Bay, Sondrestrom, and Qaanaaq.

To measure in the AUTODRIFT mode, Digisonde preface parameter P3 [Bibl et al., 1981] must be ≥ 8 . Different automatic operational modes can be selected by the appropriate setting of the 8, 4, 2 and 1 bits of preface parameter P7:

Bit	On	Off
8	automatic frequency selection from ionogram	manual frequency selection
4	automatic gain control	manual gain control
2	automatic range tracking	manual range setting
1	select sounding frequencies close to foF2 from ionogram	select center frequencies from ionogram

For routine drift observations the 1-bit is off and the two sounding frequencies are selected close to the center of the F2 trace as discussed before. When the 1-bit is on, the sounding frequencies are selected from the interval $0.7 f_oF2 < f < 0.9 f_oF2$.

2.2.2 Echo Source Determination

This section discusses the assumption mentioned in the previous section, that the spectral (Doppler) analysis uniquely identifies the echo sources, i.e. that each Doppler line corresponds to one source. This is, of course, not generally true since even for a horizontal reflection plane that moves with velocity

$$\mathbf{v} = (v_x, v_y, v_z) \quad (1)$$

there exists a line of potential source points that have identical Doppler frequency

$$d = - \frac{\pi}{\lambda r} \mathbf{r} \cdot \mathbf{v} \quad (2)$$

where λ is the wave length and \mathbf{r} the position vector of the source. The loci for which the Doppler frequency or the radical velocity v_r is constant is given by

$$\frac{\mathbf{r}}{r} \cdot \mathbf{v} = v_r = \text{const.} \quad (3)$$

The position vector \mathbf{r} is

$$\mathbf{r} = (x, y, H),$$

where H is the height of the reflecting plane. By appropriate choice of the x , y -directions, equation (1) becomes

$$\mathbf{v} = (v_X, 0, v_Z), \quad (4)$$

and equation (3) can be written as

$$(xv_X + zv_Z)^2 = r^2 v_r^2, \quad (5)$$

or for $v_X \neq 0$:

$$(x + x_0)^2 - Ay^2 = AH^2 \quad (6)$$

where

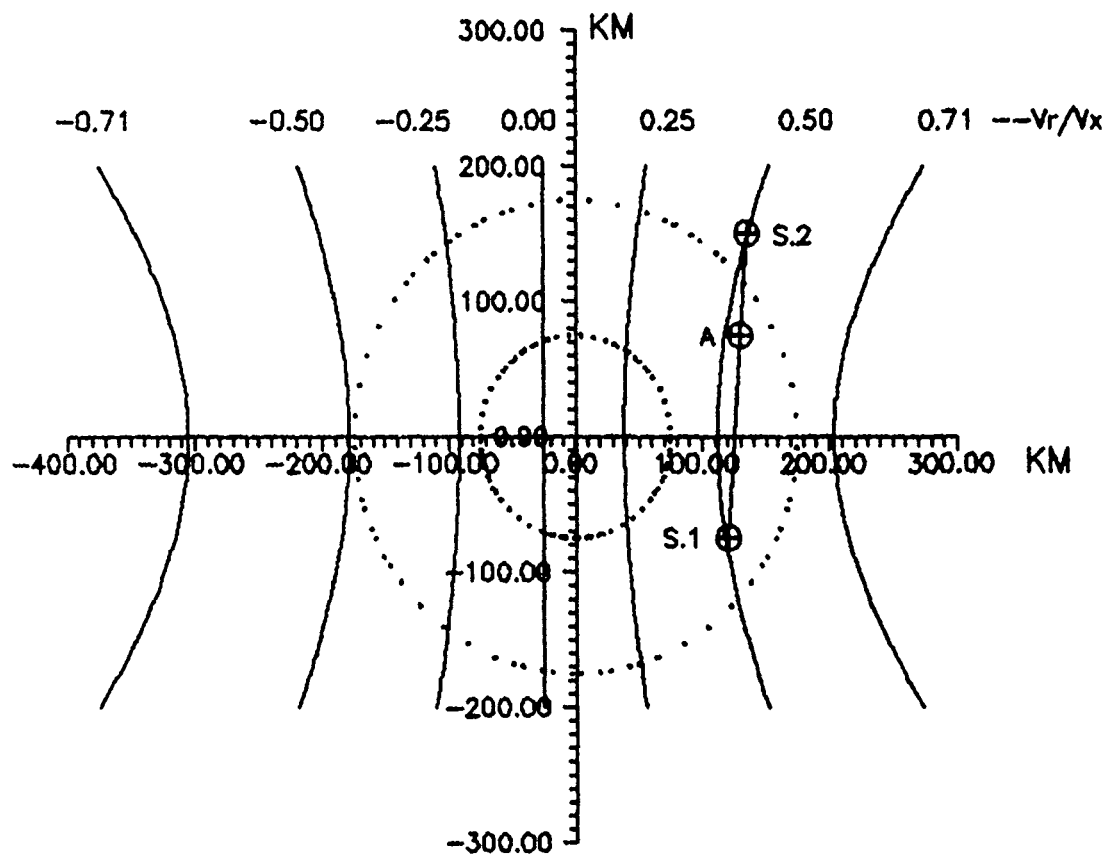
$$A = \frac{(v_r/v_X)^2}{1 - (v_r/v_X)^2}$$

This is a set of hyperbolas shifted along the x -axis by

$$x_0 = -\frac{v_r/v_Z}{1 - (v_r/v_X)^2} H. \quad (7)$$

Figure 3 shows the lines of equal Doppler velocity for different values of v_r/v_X for a reflection height of $H = 250$ km, and a vertical velocity of $v_Z = 0.1 v_X$. The zero Doppler line is the straight line $x = -x_0$. When the vertical velocity v_Z is zero, the zero Doppler line goes through zero (zenith).

The probability that iso-Doppler lines are populated with several sources is small, since the vector normal to the reflecting surface must be parallel to the wave vector of the incident wave. However, when it happens that two sources with the same Doppler exist, like sources $S1$ and $S2$ for $v_r/v_X = 0.5$ in Figure 3, then an error



Lines of equal Doppler velocity. Reflecting plane is at 250 km altitude moving with velocity $V=(V_x, 0, V_z)$. It is assumed that V_z is 10% of V_x .

Figure 3. Lines of Equal Doppler Velocity

in the calculation of the source location may occur. Dozois [1983] has shown, that dependent on the amplitudes and initial phases of the two sources, the apparent Doppler source will be put somewhere between S1 and S2, like point A in Figure 3. Fortunately, the distance of A from its Doppler line is small for most configurations, causing only small errors in the drift velocity calculation.

Only parts of the iso-Doppler lines are within the Digisonde's field of view which is limited by the fact that the ionosphere is illuminated with HF pulses of 66 μ s duration, corresponding to 10 km in range. For a perfect plane at $H = 250$ km this limits the field of view to a circle with 71 km radius, i.e. a zenith angle of 16°. Where the equidensity surfaces are rough with height variations of $\Delta z = 40$ km, the radius becomes 166 km, corresponding to a zenith angle of 34°. The circles with $R = 75$ km and $R = 175$ km in Figure 3 illustrate the fields of view for different ionospheric roughness.

2.2.3 The Effects of Refraction

To estimate the effects of ionospheric refraction on the drift analysis, a simple model calculation was conducted, that neglects the earth's magnetic field and horizontal gradients in ionization. The electron density $N(h)$ in the horizontally stratified ionosphere increases linearly with height

$$\begin{aligned} N(h) &= \alpha (h-h_0) & \text{for } h \geq h_0 \\ &= 0 & \text{for } h < h_0 \end{aligned} \quad (8)$$

Reflections occur at overdense irregularities on a point A on the ray path such that $\mu = 0$ at this point, but $\mu_A \neq 0$ just before (see Figure 4). In our model, the irregularities move together with the

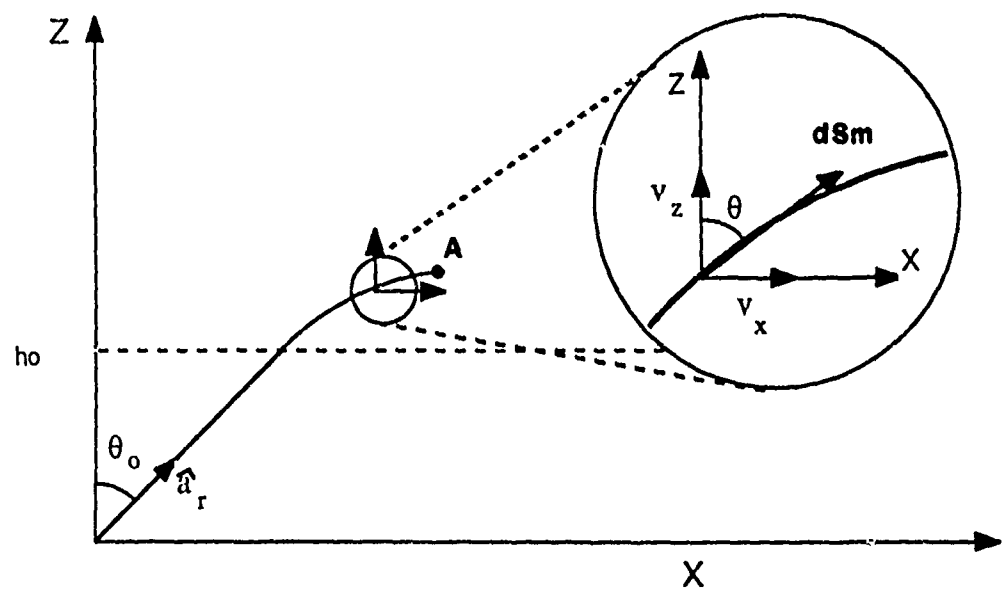


Figure 4. Ionospheric Model to Estimate Refraction Effects

ionosphere with the velocity v . The rate of change of the phase P , i.e. the Doppler velocity v_r is [Kelso, 1964, p. 278]

$$v_r = \frac{dP}{dt} = 2 \left\{ \mu_A m \cdot v + \int_s \frac{\partial}{\partial t} \mu(h,t) dS \right\}$$

m = Unit vector in the ray direction at point v .

v = Velocity at point A .

μ_A = Index of refraction at point A .

P = Phase path.

Integral is over the ray path S .

Vertical and horizontal velocities are considered separately. If we assume the ionized layer is drifting upward at a velocity v_z . Then the following relationships hold:

$$N(h,t) = \alpha(h - h_0 - v_z t) \quad (1)$$

$$\mu^2(h,t) = 1 - \frac{K\alpha}{f^2} (h - h_0 - v_z t) \quad (1)$$

$$\frac{\partial}{\partial t} \mu(h,t) = \begin{cases} \frac{K\alpha}{f^2} \frac{v_z}{2\mu} & \text{for } h > h_0 + v_z t \\ 0 & \text{for } h < h_0 + v_z t \end{cases} \quad (1)$$

$$dS = \frac{\mu dh}{\sqrt{\mu^2 - \sin^2 \theta_0}} \quad (1)$$

ionosphere with the velocity v . The rate of change of the phase path P , i.e. the Doppler velocity v_r is [Kelso, 1964, p. 278]

$$v_r = \frac{dP}{dt} = 2 \left\{ \mu_A \mathbf{m} \cdot \mathbf{v} + \int_s \frac{\partial}{\partial t} \mu(h,t) dS \right\} \quad (9)$$

\mathbf{m} = Unit vector in the ray direction at point v .

\mathbf{v} = Velocity at point A .

μ_A = Index of refraction at point A .

P = Phase path.

Integral is over the ray path S .

Vertical and horizontal velocities are considered separately. First, assume the ionized layer is drifting upward at a velocity v_z . Then the following relationships hold:

$$N(h,t) = \alpha(h - h_0 - v_z t) \quad (10)$$

$$\mu^2(h,t) = 1 - \frac{K\alpha}{f^2} (h - h_0 - v_z t) \quad (11)$$

$$\frac{\partial}{\partial t} \mu(h,t) = \begin{cases} \frac{K\alpha}{f^2} \frac{v_z}{2\mu} & \text{for } h > h_0 + v_z t \\ 0 & \text{for } h < h_0 + v_z t \end{cases} \quad (12)$$

$$dS = \frac{\mu dh}{\sqrt{\mu^2 - \sin^2 \theta_0}} \quad (13)$$

$$dh = \frac{-f^2}{K\alpha} 2\mu d\mu \quad (14)$$

Using (10) - (14) in the integral portion of equation (9):

$$\int_s \frac{\partial}{\partial t} \mu(h,t) dS = \frac{K\alpha}{f^2} \frac{v_z}{2} \int_{Z_0(t)}^{Z_A(t)} \frac{dh}{\sqrt{\mu^2 - \sin^2 \theta_0}} \quad (15)$$

$$= -v_z \int_{\mu=1}^{\mu_A} \frac{\mu d\mu}{\sqrt{\mu^2 - \sin^2 \theta_0}}$$

Let $u^2 = \mu^2 - \sin^2 \theta_0$ and the integral becomes:

$$-v_z \int du = -v_z u = -v_z \left[\sqrt{\mu^2 - \sin^2 \theta_0} \right]_1^{\mu_A} \quad (16)$$

or:

$$\int_s \frac{\partial}{\partial t} \mu(h,t) dS = v_z \left[\sqrt{1 - \sin^2 \theta_0} - \sqrt{\mu_A^2 - \sin^2 \theta_0} \right] \quad (17)$$

Snell's law relates the angle θ_A to the index of refraction μ_A and the zenith angle θ_0 :

$$\mu_A \sin \theta_A = \sin \theta_0 \text{ or } \mu_A = \frac{\sin \theta_0}{\sin \theta_A} \quad (18)$$

So:

So:

$$\int_s \frac{\partial}{\partial t} \mu(h,t) dS = v_z \left[\cos \theta_o - \frac{\cos \theta_A}{\sin \theta_A} \sin \theta_o \right] \quad (19)$$

Add to this the dot product:

$$\mu_A \mathbf{m} \cdot \mathbf{v} = \frac{\sin \theta_o}{\sin \theta_A} v_z \cos \theta_A \quad (20)$$

$$\text{to get a Doppler velocity of: } \frac{dP}{dt} = 2 v_z \cos \theta_o \quad (21)$$

This means that for this case the true velocity is correctly obtained from the measured radial velocity:

$$v = v_z = v_r / 2 \cos \theta_o \quad (22)$$

Assume now that the ionized layer is moving in the +x direction with a velocity v_x . In this case N and μ are no longer functions of time (between the bottom of the layer and the position of the irregularity) so:

$$N(h) = \alpha (h - h_o) \quad (23)$$

$$\mu^2(h) = 1 - \frac{K\alpha}{f^2} (h - h_o) \quad (24)$$

$$\frac{\partial}{\partial t} \mu(h) = 0 \quad (25)$$

$$\int_s \frac{\partial}{\partial t} \mu(h) dS = 0 \quad (26)$$

The irregularity moves with velocity v_x , so:

$$\begin{aligned} \mu_A \mathbf{m} \cdot \mathbf{v} &= \mu_A v_x \cos(90 - \theta_A) = \mu_A v_x \sin \theta_A \\ &= v_x \frac{\sin \theta_o}{\sin \theta_A} \sin \theta_A = v_x \sin \theta_o \end{aligned} \quad (27)$$

By the principle of superposition, if the ionospheric velocity is

$$\mathbf{v} = v_x \hat{\mathbf{a}}_x + v_z \hat{\mathbf{a}}_z \quad (28)$$

the Doppler velocity becomes:

$$\frac{dP}{dt} = 2 (v_z \cos \theta_o + v_x \sin \theta_o) \quad (29)$$

or (see Figure 4)

$$\frac{dP}{dt} = 2 \mathbf{v} \cdot \hat{\mathbf{a}}_r. \quad (30)$$

Bullett [1990] has generalized this result to nonlinear profiles and has shown that the measured rate of change of the phase path is the dot product of the actual velocity and the unit vector $\hat{\mathbf{a}}_r$ in the direction of the ray at the ground. These calculations show that at least to first order there are no refraction effects. Inclusion of the magnetic field will not fundamentally alter these results.

2.2.4 Drift Data Processing

The ability of the Digisonde to make drift measurements automatically is an exciting achievement, which led to a new difficulty: how to handle the vast quantity of data generated by these measurements. A significant amount of effort has been involved in mitigating this problem, leading to the development of more efficient techniques which take advantage of the strengths of the GL Cyber computer on which the processing is currently done.

The plasma drifts were originally computed by the Frequency-Wavenumber Power Density (Scanning) technique described by Dozois [1983]. The FWPD was calculated for a 41×41 pixel area covering the Digisonde viewing area. Only certain spectral lines were used, selected according to their amplitude. The FWPD method used both amplitude and phase measurements to determine source locations. Originally, the FWPD method was thought to be able to separate multiple sources contributing to the same spectral line. However, Dozois [1983] determined that multiple sources could not be reliably separated by this method, which required 10,000 CPU seconds for the processing of one magnetic tape containing one day of drift measurements.

Dozois simulated the multiple sources case and found that two sources can be separately identified when their angular separation is larger than the 6 dB beamwidth of the antenna array, otherwise the FWPD method determines one apparent source located somewhere between the two sources. The exact location depends on the relative amplitudes and phases of the two sources, which are unknown. As discussed in Section 2.2.3, the apparent source location is generally close to its proper iso-Doppler line, so that the effect on the accuracy of the drift vector calculation is small. Nevertheless, being unable to reliably separate multiple sources the computer intensive FWPD method was discarded in favor of a computationally more economic technique that calculates the source location using the

phase only (PO), assuming that there is only one source (for each Doppler).

In the PO method, spectral amplitudes are used as criteria for data selection/rejection, while source locations are computed from phases only. The approach used is as follows. For a given source k with Doppler d_k , the phase ϕ_{ik} measured at antenna i is

$$\phi_{ik} = \mathbf{k} \cdot \mathbf{r}_i + \delta + 2\pi n_i, \quad (31)$$

where

$$k = 2\pi/\lambda$$

$$\lambda = \text{wavelength}$$

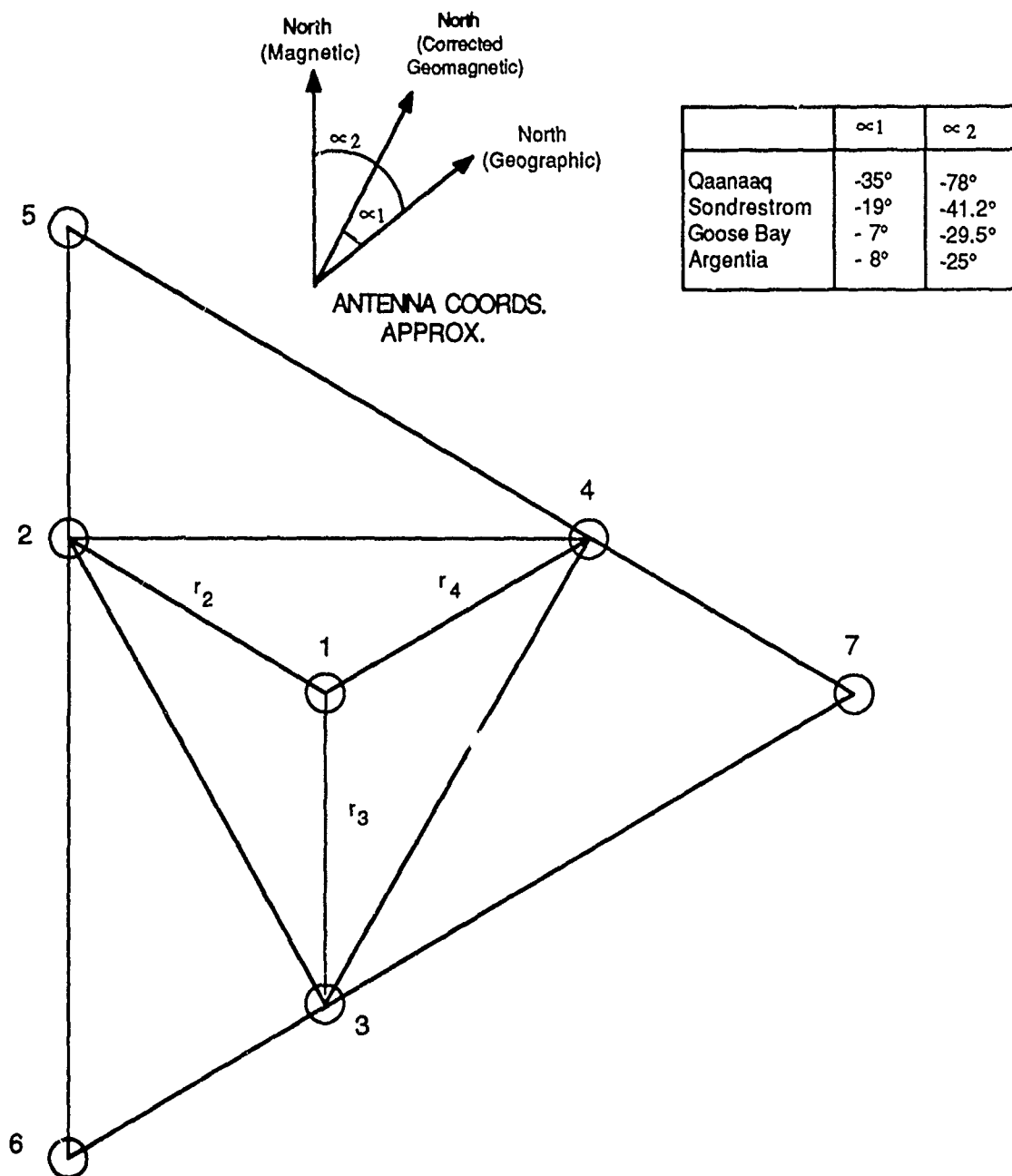
$$\delta = \text{initial phase of the source}$$

$$2\pi n_i = \text{phase ambiguity.}$$

\mathbf{r}_i is the horizontal antenna-position vector pointing from the central antenna 1 to antenna i . The seven antenna array used for these measurements is shown in Figure 5. (Antennas 1, 5, 6 and 7 are used for four-antenna measurements.) Only source locations that produce phase differences of less than π at the spaced antennas are considered here. These sources are located in the primary region for which the zenith angle is smaller than Z_{\max} , where

$$\sin(Z_{\max}) = \frac{\lambda}{a} \quad (32)$$

where a is the antenna separation between antennas 2-3, 3-4 or 2-4. For these sources the integer n_i is 0 or 1: 0 if $\mathbf{k} \cdot \mathbf{r}_i$ is positive; 1 if $\mathbf{k} \cdot \mathbf{r}_i$ is negative, i.e. the (positive) measured phase is greater than $\mathbf{k} \cdot \mathbf{r}_i$ by 2π . Sources outside Z_{\max} are "aliased" into the primary zone, by the sidelobes of the array. The same situation existed for the FWPD calculations.



The relative directions of geographic north, corrected geomagnetic north and compass north (i.e. as measured with a compass) are indicated for key Digisonde locations. Compass north was taken from navigation charts for 1982 in each case except Goose Bay, which was for 1983. The antenna arrays are aligned with compass north (#6 → #5).

Figure 5. Seven Antenna Receiving Array

The symmetry of the four- and seven-antenna arrays used for drift measurements allows us to determine which values need to be decremented to obtain the corrected phase $\mathbf{k} \cdot \mathbf{r}_i + \delta$. A least-squares fit procedure is then used to determine the components of the vector \mathbf{k} . The least-squares error is

$$\epsilon_k^2 = \sum_{i=1}^{N-1} \sum_{j=i+1}^N \left[(\mathbf{k} \cdot \mathbf{r}_i - \mathbf{k} \cdot \mathbf{r}_j) - (\phi'_{ik} - \phi'_{jk}) \right]^2 / [N(N-1)/2] \quad (33)$$

where N is the number of antennas (typically 7 or 4), and ϕ'_{ik} and ϕ'_{jk} are the corrected phases; by working with phase differences, the initial phase δ cancels out. (The denominator in the above equation is the total number of terms in the double sum, normalizing ϵ_k with regard to the number of antennas used.) Taking the derivatives of ϵ_k^2 w.r.t. k_x and k_y and setting them each equal to zero yields the two equations needed for determining the unknowns k_x and k_y . Sources with large r.m.s. errors are deleted from the analysis.

A new skymap printing program MAPTILT was developed that permits different types of skymaps to be displayed. One of the new features is the ability to plot skymaps for each of four frequency-range bins in a case, side by side, to separate the information from different heights, as shown in Figure 6. When these are stacked on a page, the temporal development of the skymaps also becomes apparent. Only sources whose amplitudes are within 10 dB of the maximum amplitude for each subcase are printed, as indicated on the right side of each row. This type of display is useful, for example, in data consistency checks and for ionospheric tilt studies.

The calculation of the three dimensional drift velocity vector from the Doppler sources has remained unchanged. Assuming a uniform velocity field \mathbf{v} , the vector is determined by a least-squares process including all qualified sources $s = 1, 2, \dots, S$. The error to be minimized is:

$$\epsilon^2 = \frac{\sum_s A_s \left[d_s - \frac{1}{\pi} (v_x k_{sx} + v_y k_{sy} + v_z k_{sz}) \right]^2}{\sum_s A_s} \quad (34)$$

where k_{sx} and k_{sy} specify the location for source s with Doppler d_s , and $k_{sz}^2 = (2\pi/\lambda)^2 - k_{sx}^2 - k_{sy}^2$; the weights A_s are (linear) source amplitudes obtained from a combination of the amplitudes measured at each of the four (or seven) antennas.

The PO method gives a higher precision for the source locations. With the FWPD scanning method, the source locations were quantized: in order to avoid a prohibitive number of calculations, the map representing the sky above the Digisonde station was divided into a 41-by-41 set of pixels, and the FWPD was calculated only at these 1681 pixel locations. Sources between these locations ended up at the closest pixel in the map array, and only one source per pixel could be kept in the map array when there were several sources close together. The analytical PO method is not limited to quantized locations. It keeps the same visual map representation of the source locations (coordinates $(X,Y) = 0, \pm 1, \pm 2, \dots, \pm 20$), but for the drift velocity calculations the coordinates are given with one decimal place instead of being integers. The accuracy of our measurements does not justify keeping more than one decimal place.

2.2.5 Special Processing Concerns

The new drift processing software has achieved two objectives: (1) reduction in CPU time, (2) improved data validation. The time required to process one magnetic tape containing the 5 minute data for one day is approximately 500 CPU seconds, a factor of 20 improvement over the FWPD method.

Identification of "good" sources is most important if valid drift velocities are to be derived. The measured drift data consist of four or seven 64-line spectra, one for each receiving antenna. Each spectrum is thresholded by zeroing those spectral lines which have an amplitude below the most-probable-amplitude of the spectrum. Any such "noise" lines are not used for the drift velocity calculation. The remaining spectral lines are considered potential Doppler sources unless a spectral amplitude varies from antenna to antenna by 20 dB or more. The latter case indicates that more than one source exists with the same Doppler shift, and therefore the spectral line is not used.

The phases of the surviving set of S spectral lines are 2π -corrected, and then checked for consistency. Because of the geometry of the antenna array, the corrected phases must fulfill the conditions [Bibl, 1983]:

$$\Delta_i = \phi_{2s} + \phi_{3s} + \phi_{4s} - 3\phi_{1s} = 0 \quad (\text{inner antennas})$$

and

(35)

$$\Delta_0 = \phi_{5s} + \phi_{6s} + \phi_{7s} - 3\phi_{1s} = 0 \quad (\text{outer antennas})$$

These equations are easily verified by inspection of Figure 4:

$$\begin{aligned} (k_s \cdot r_2 + \delta) + (k_s \cdot r_3 + \delta) + (k_s \cdot r_4 + \delta) - 3(k_s \cdot r_1 + \delta) &= k_s \cdot (r_2 + r_3 + r_4) + 3\delta - 3\delta \\ &= 0 \end{aligned} \quad (36)$$

since $r_2 + r_3 + r_4 = 0$

and $r_1 = 0$.

Because of noise and round-out errors, these sums are generally not exactly zero. If a Δ is larger than 80° , the spectral line is not used for skymap and drift calculations. Testing the distribution of Δ 's is a convenient way of checking the proper operation of the receiving array. A defective antenna results in systematically large values for Δ .

2.2.6 Validation of New Phase Only Analysis Technique

To verify that the new analysis program, based on the PO technique is performing correctly, three days of data from Qaanaaq were processed twice using alternately the proven FWPD based program and the new PO based program. Figure 7 shows the results of this test for drift measurements made during the October-November 1986 Viking campaign. The velocities calculated from the FWPD skymaps are joined by a dashed line. It is clear from this comparison that the two methods of calculating the source positions are virtually equivalent.

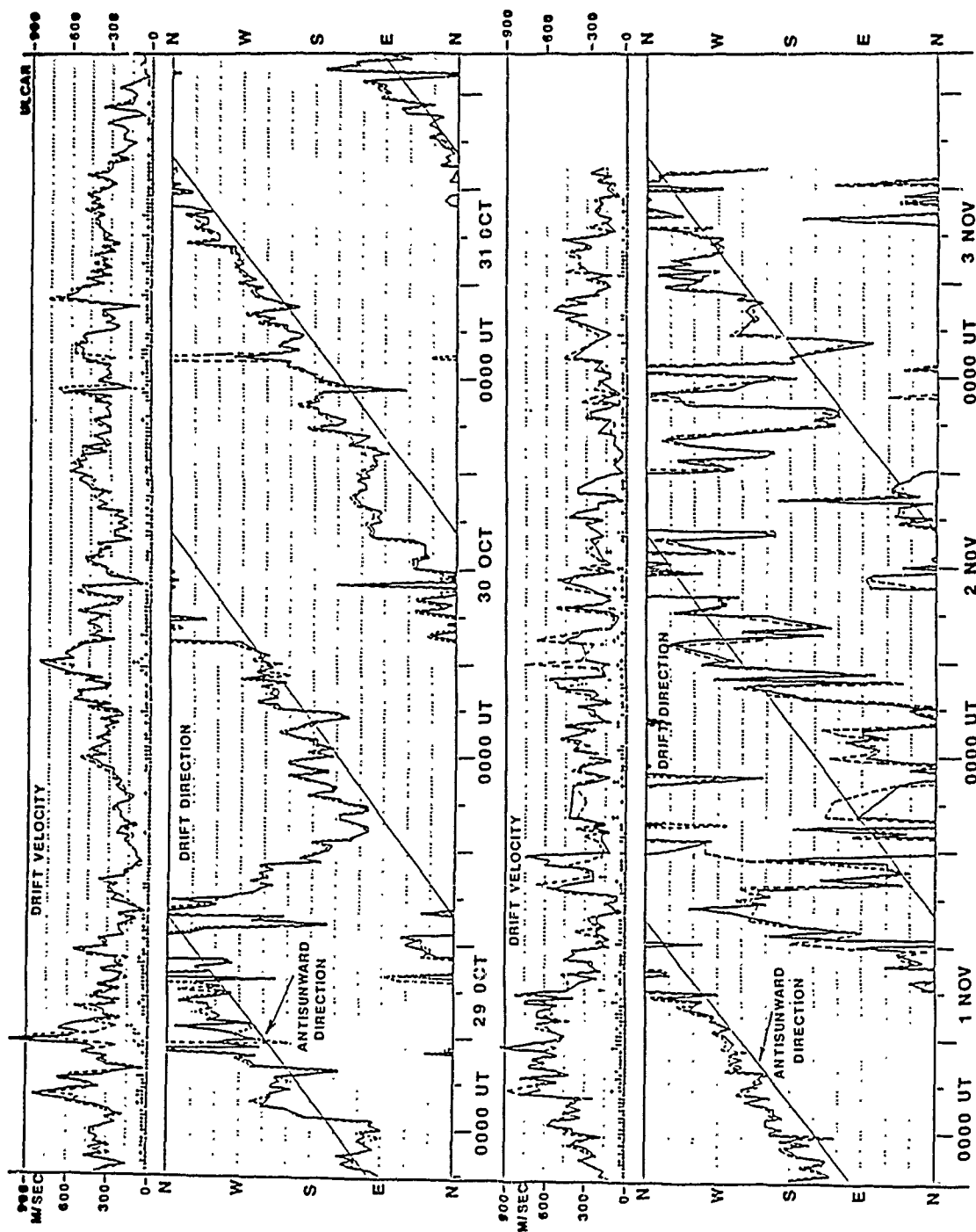


Figure 7. Comparing the FWP and PO Analysis Techniques. The velocities joined by a solid line were calculated from sources which were determined by the scanning method, with the Frequency-Wavenumber Power Density correlation of amplitudes and phases. The velocities joined by a dashed line were calculated from sources which were determined by direct phase comparison. The drift data was measured at Qaanaaq from 28 October to 3 November 1986.

3.0 OBSERVATIONS AND CAMPAIGNS

3.1 Drifts

Development of the instruments at the three Digisonde sites Argentia, Goose Bay, and Qaanaaq has progressed at different rates for a number of reasons including previous history, accessibility, and equipment failure. Consequently, the amount and quality of the data obtained from each site has also varied. Due to the large quantities of data collected by these instruments, and the availability of different modes of operation, a computerized inventory technique was developed.

Tables 1 to 3 in Appendix A depict the drift observing schedules for Argentia (operating autodrift since October 1986), Goose Bay (autodrift since January 1988 when the DGS 256 replaced the DGS 128PS), and Qaanaaq (autodrift since October 1986) for the years 1986, 1987, 1988 and 1989. Table 1A is also shown on the next page. Each line on the table includes a "time line" which is divided into 288 columns (one column for each five minutes of a 24-hour period), preceded by the date and "WD" for the world days. On the time line, the start time of each group of continuous drift measurements (rounded to 5-minute increments) is indicated by a tic mark. To ease reading the inventory over a day, the tic marks are longer on the hour (3 dots instead of 2), with an additional fourth dot every 6 hours. The "p" following some of the time lines indicates the days whose data has been processed into drift velocity graphs. All of the data from all three stations has been processed, except for about 12 months of Argentia. The latter was omitted because of a hardware fault at the station, discovered in August 1989, which had started about one year earlier, and resulted in erroneous values being recorded on the tapes. Note that the ionograms recorded in

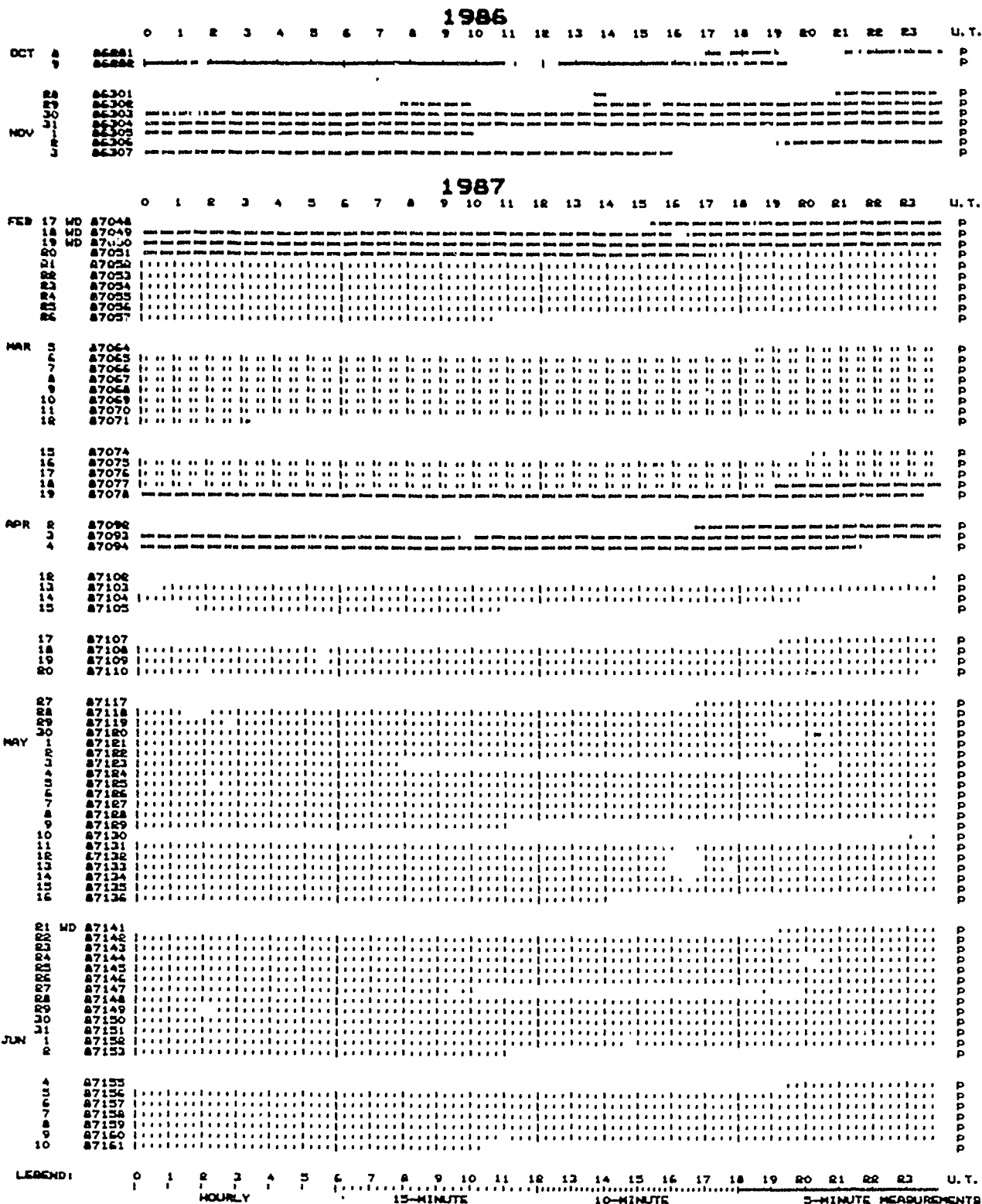


Table 1A. Argentina Drift Survey

this period are correct. The hardware problem could not be fixed until March 1989, when routine processing of the data resumed.

In general, the drift mode operated at each station on the three World Days of every month as specified in the contract. The sounding schedule for the World Days was one ionogram every five minutes, with drifts measured between ionograms. In addition to the contractual requirements, drift data were also taken on a 15 minute schedule on many other days. Thus a substantial data base of drift measurements has been compiled, parts of which have been used in the research leading to the publications listed in Sections 5.0 and Appendix B.

3.2 Oblique Ionogram Measurements

The objective of this part of the project was to develop and use oblique ionospheric sounding between existing Digisonde (DISS) stations in order to increase the effective density of ionospheric sensors. This is clearly necessary to monitor the occurrence, location and extent of the F layer trough. The intent was to use the vertical ionograms from Argentia and Goose Bay together with oblique ionograms between these two stations for the trough monitoring. The Goose Bay Digisonde 256 (DISS) was not installed until 1988, therefore the initial oblique propagation experiments were conducted between Argentia and Millstone Hill. Sample data for the Goose-Argentia link are also now available for limited periods and they show that oblique monitoring is a valuable tool, as discussed below.

3.2.1 Oblique Sounding Between Goose Bay and Argentina

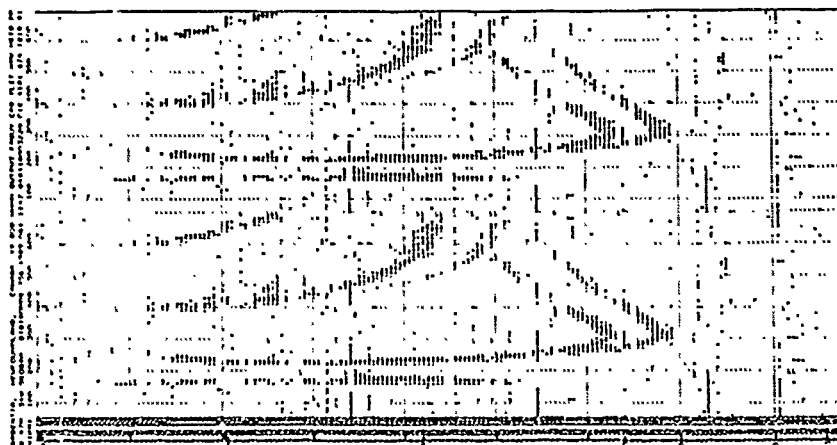
In a feasibility study, good echoes were obtained at Argentina during most of the times of day (see Figures 8a to 8f) in spite of strong interference from Europe at many frequency bands. For most of the recordings, both sounders transmitted and received simultaneously. This was done for testing purposes, but is not generally advisable because of the large difference in signal amplitudes between the vertical and oblique signals. At low frequencies the automatic receiver gain and printer gain squelch the oblique signals because the vertical echoes are so strong. Conversely, the vertical signals near foF2 are gain-reduced, because the oblique signals are strong. However, the variations in the maximum observable frequency (MOF) are clearly identified, and can be used to aid in monitoring the trough region.

3.2.2 Oblique Sounding Between Argentina and Millstone

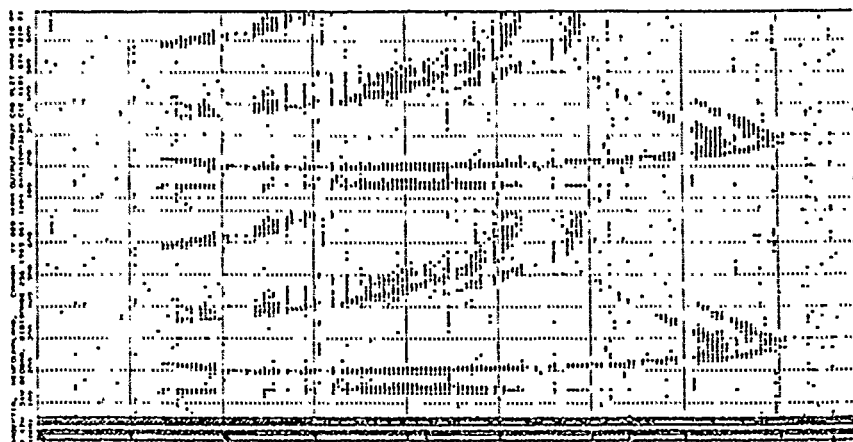
In conjunction with another experiment, oblique propagation between the University of Lowell Digisonde 256 at Millstone Hill, Massachusetts and the Air Weather Service Digisonde 256 at Argentina, Newfoundland was carried out. This path was used to establish the network characteristics of monitoring the reflection points between established ionosonde stations as proof of concept for routine oblique propagation experiments to define mid-path ionospheric characteristics.

Data exist from both stations on day 87293 (October 20, 1987) from 0018 to 0348 UT (Tables 2A and 2B) and from day 87296 (October 23, 1987) 1033 UT to day 87297 (October 24, 1987) 0433 UT (Tables 3 and 4).

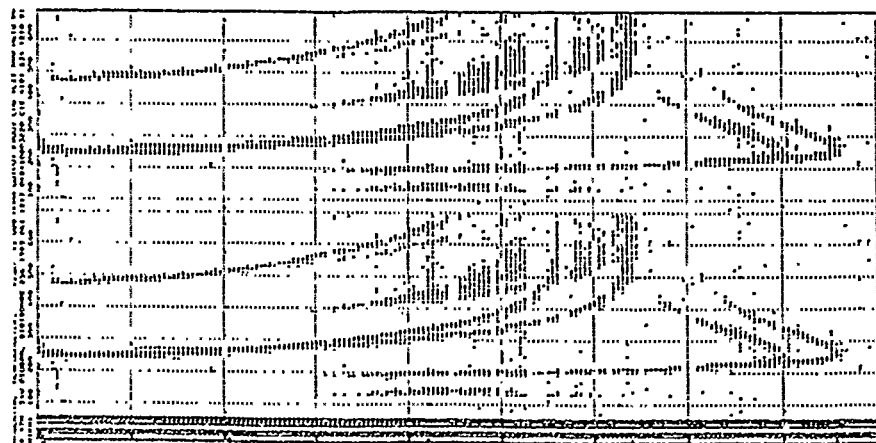
At least two time periods cover oblique ionograms recorded simultaneously on both stations which establishes the



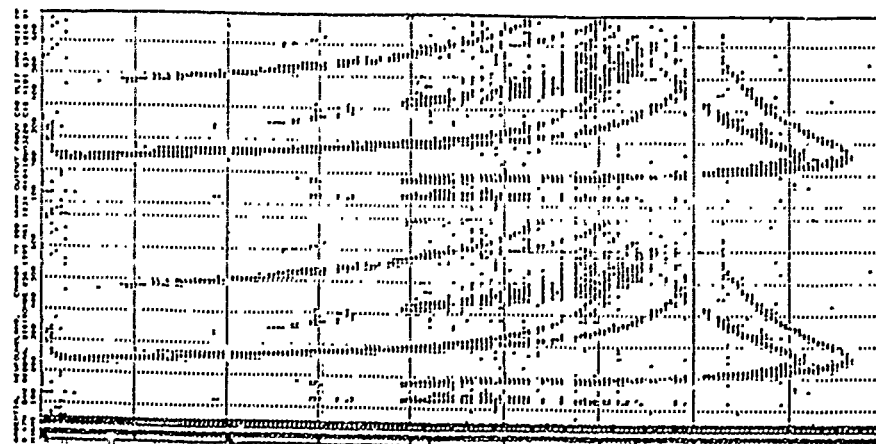
1147Z



1204Z



1217Z



1989 061 1234Z

Figure 8. Reception in Argentina of Oblique Ionograms from Goose Bay

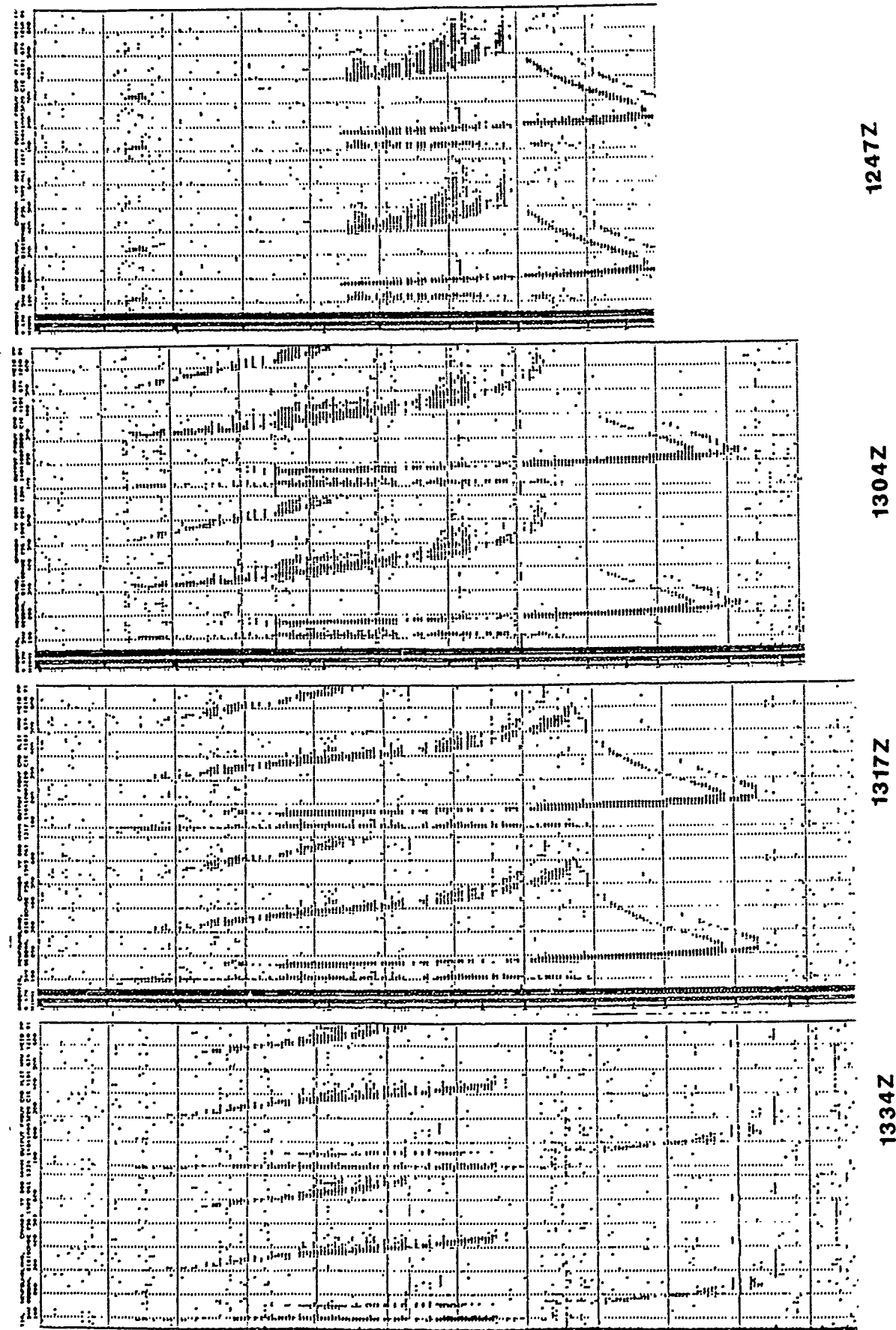


Figure 8. Reception in Argentina of Oblique Ionograms from Goose Bay (Continued)

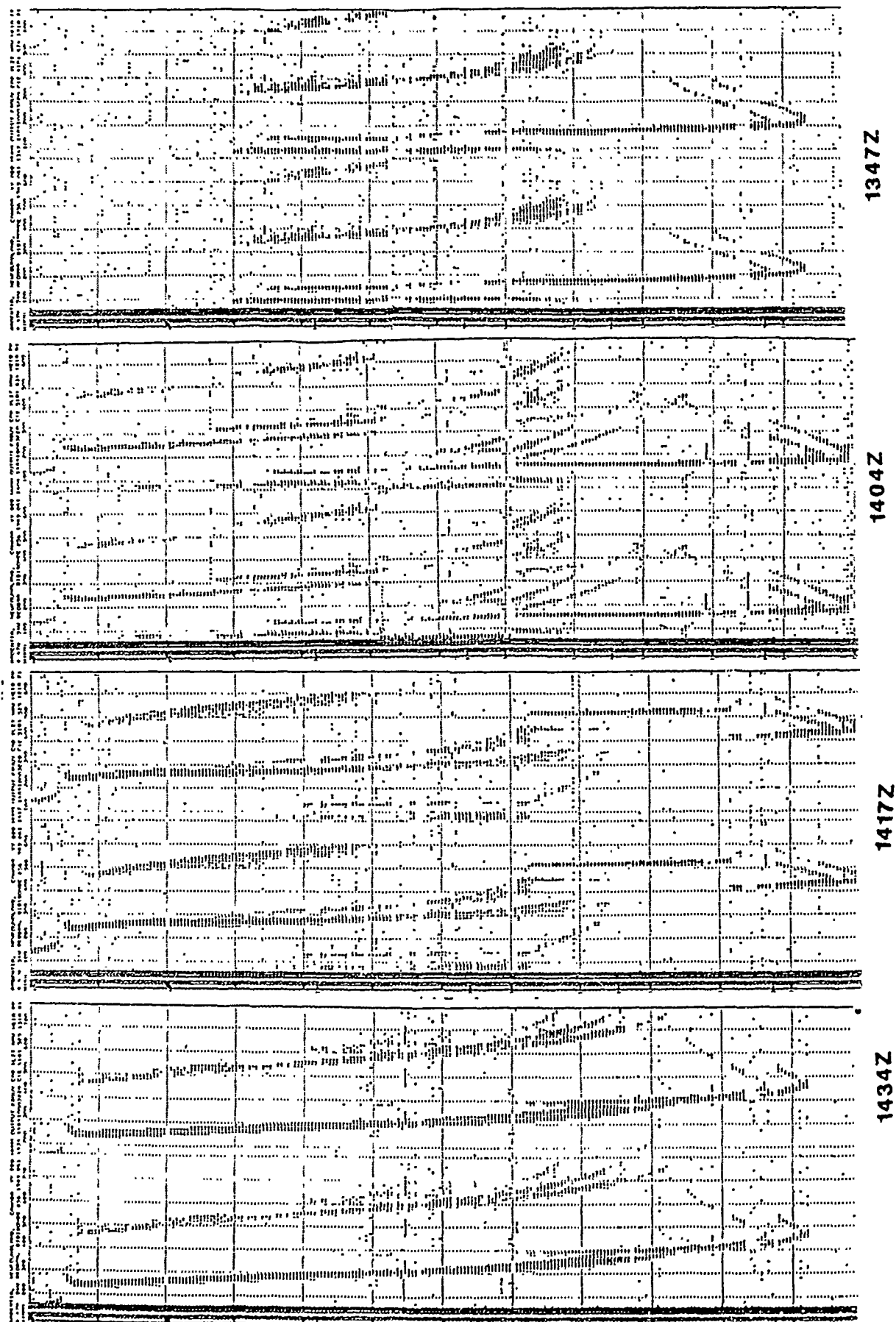
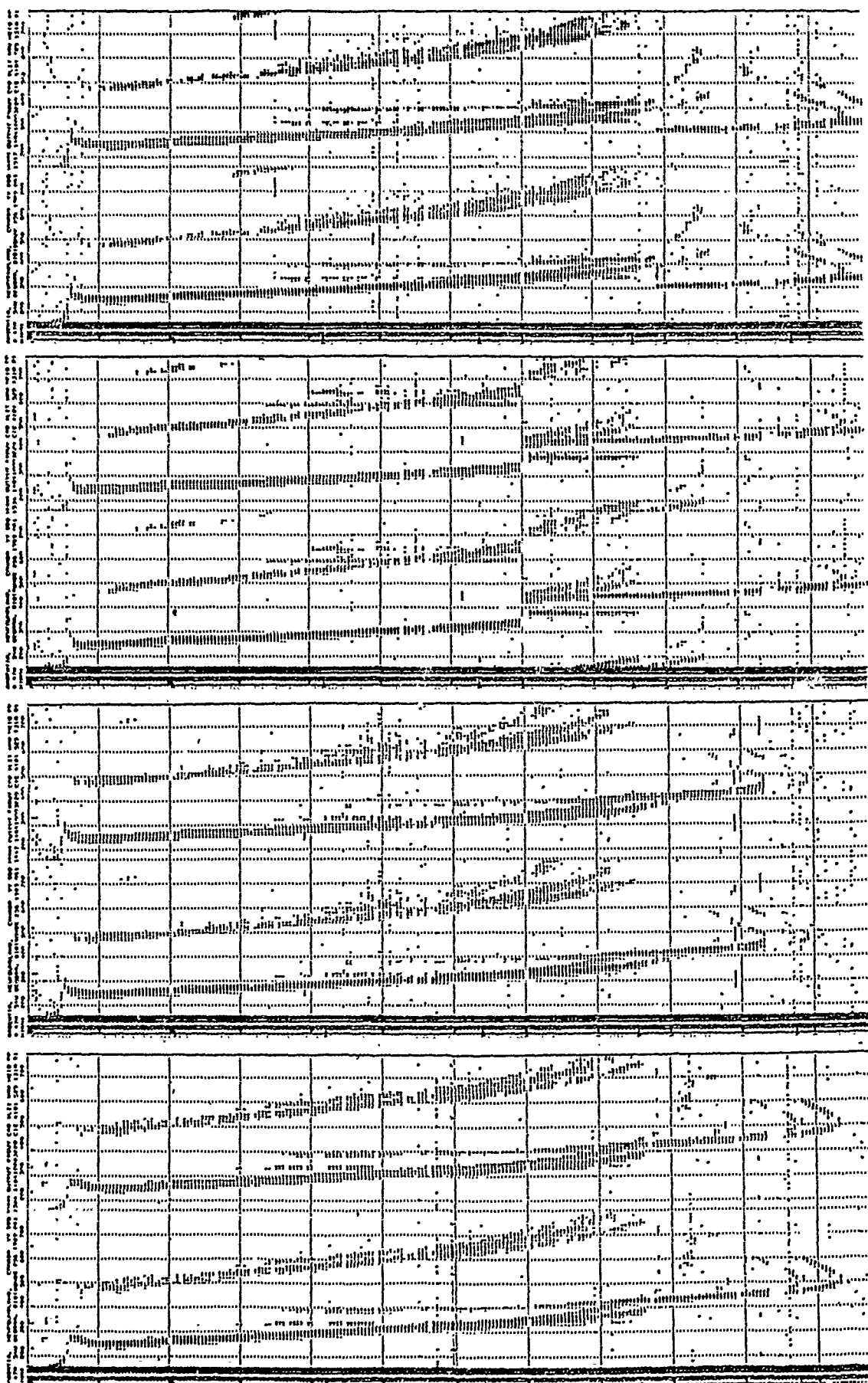


Figure 8. Reception in Argentina of Oblique Ionograms from Goose Bay (Continued)



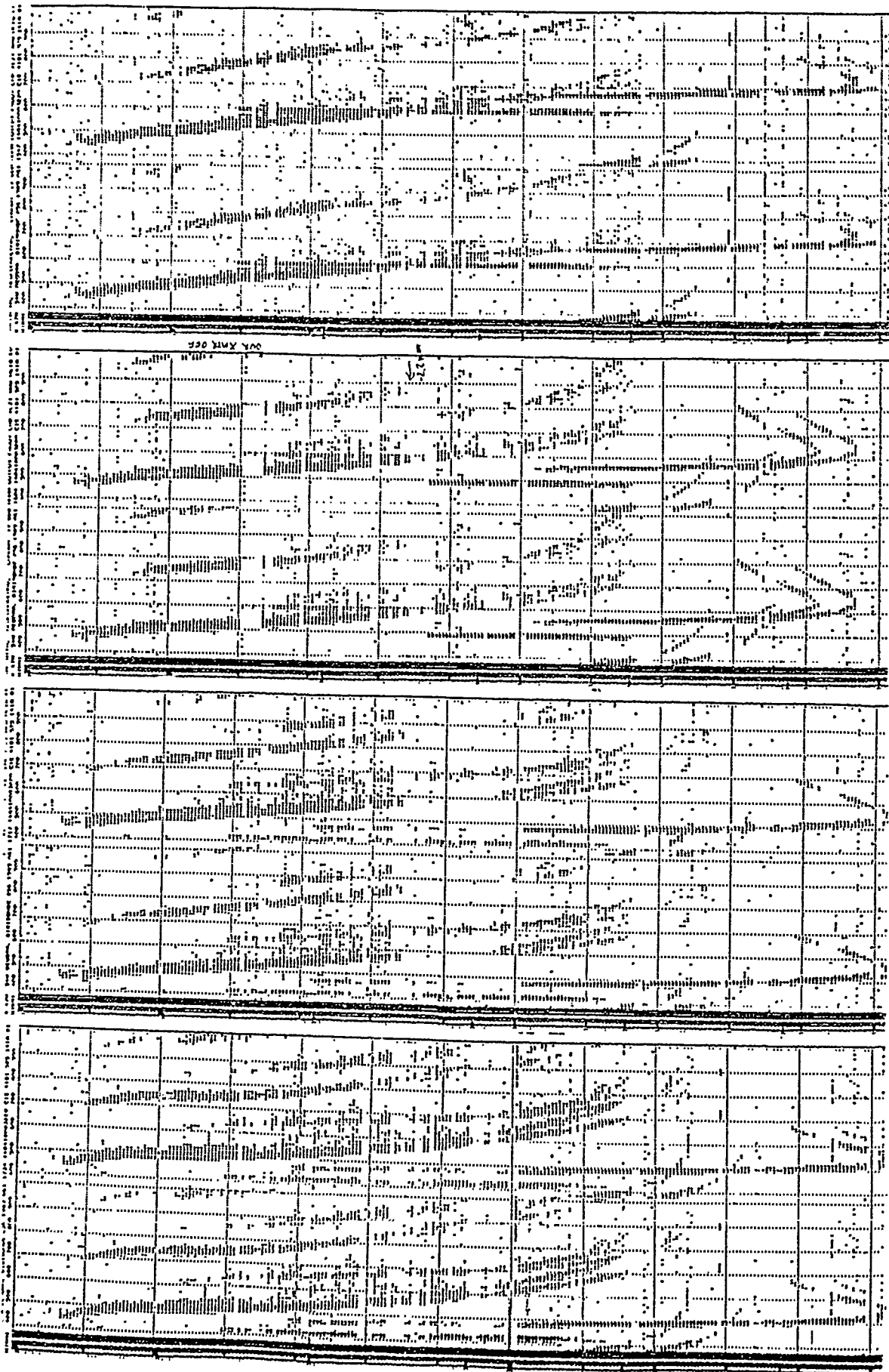
1504Z

1534Z

1547Z

1604Z

Figure 8. Reception in Antarctica of Oblique Ionograms from Goose Bay (Continued)



1647Z

1704Z

1717Z

1734Z

Figure 8. Reception in Argentina of Oblique Ionograms from Goose Bay (Continued)

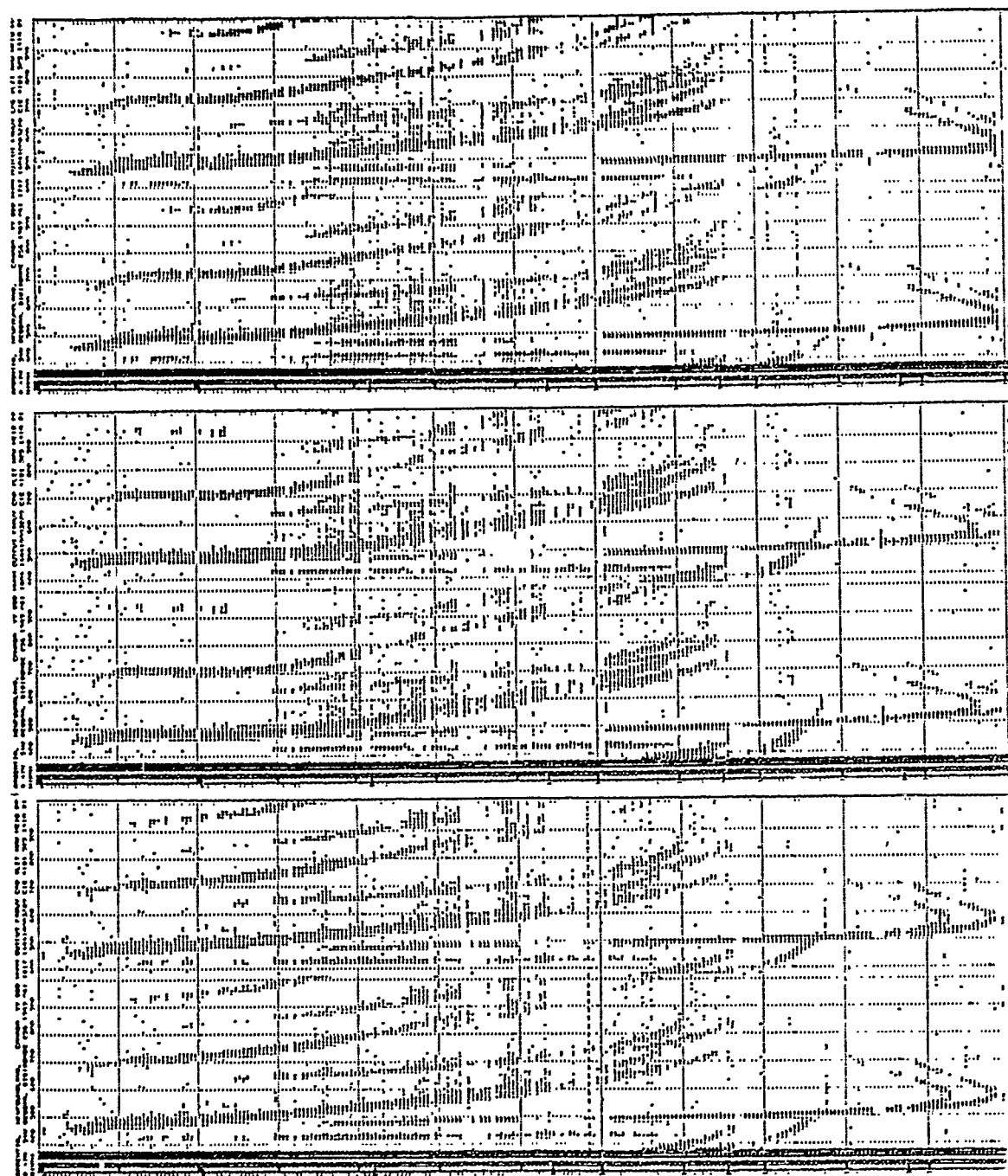


Figure 8. Reception in Argentina of Oblique Ionograms from Goose Bay (Continued)

Table 2A. Oblique Propagation (from Argentina) Received at Millstone

Day 293, October 20, 1987

TIME UT	foF2 (MHz)	1F MUF (MHz)	2F MUF (MHz)
0018	5.25	11.20	
0033	5.20	10.80	
0048	5.20	10.60	U9.30
0103	4.90	10.50	U8.30
0118	4.60	9.50	7.80
0133	4.50	9.20	
0148	4.10	9.25	
0203	3.90		

Note: "U" values are uncertain.

Table 2B. Oblique Propagation (from Millstone) Received at Argentina

TIME UT	foF2 (MHz)	1E MUF (MHz)	1F MUF (MHz)	2F MUF (MHz)	3F MUF (MHz)
0018	4.60		11.25		
0033	4.60	11.30	10.80		
0048	4.45	11.60	10.60	8.40	6.90
0103	4.30	10.50	10.50	8.40	
0118	4.00	11.60	9.30	7.80	
0133	4.00	11.50	9.15	7.80	
0148	3.90	11.60	9.25		
0203	3.60				
0318	3.30	10.70	7.10	5.70	4.80
0333	3.10	11.60	6.80	5.80	
0348		11.60	6.70		

Table 3A. Oblique Propagation (from Argentina) Received at Millstone

Day 296, October 23, 1987

TIME UT	foF2 (MHz)	1E MUF (MHz)	1F MUF (MHz)	2F MUF (MHz)	REMARKS
1029			6.90		
1033	4.10		7.80	5.05	Direct Backscatter
1044	4.60		8.50		
1059	4.80	7.30	10.40	6.25	
1103	U5.00		10.90	7.00	
1114	5.00				Change Tx Antenna Configura- tion
1118			>11.50		
1129	5.10				
1148		10.10	13.00		
1159	5.40				
1203		11.40	12.65	8.60	
1214	5.50				Change Tx Antenna Orientation
1218		11.10	13.80	8.70	
1229	5.50				
1233		11.70	14.25	9.05	

Table 3B. Oblique Propagation (from Millstone) Received at Argentina

Day 296, October 23, 1987

TIME UT	foF2 (MHz)	1E MUF (MHz)	1F MUF (MHz)	2F MUF (MHz)	3F MUF (MHz)	REMARKS
1018	2.35					Direct Backscatter First Oblique Echoes
1029	2.30		7.850			
1048	2.70		6.2 to (X)9.300			
1103	3.75		(X)10.850	7.000	4.80	
1118	4.00		>11.500	(O)7.200 (X)7.600		
1148	4.70	9.10	13.075	(O)7.870 (X)8.250	(X)6.95	
1203	5.00		12.650	(O)8.200 (X)8.650		
1218	5.40		13.800	(O)8.300		
1233	6.00		14.250	(X)9.000		
1248	6.30		15.000	(X)9.450		
1303	6.70 (F3)					Whip only (poor)
1318	6.80		14.750	U9.250	7.75	
1333	6.5/ 7.20					
1348	6.70		14.750	9.475		
1403	6.80		>16.000	10.000 + Nose		Large Rhombic
1418	6.90		>>16.000	10.950	9.20	
1433	7.10		>>16.000	11.600	U9.40	
1448	7.30		>16.000	11.475	9.20	Strong Direct Backscatter

Table 4A. Oblique Propagation (from Argentina) Received at Millstone

Day 296, October 23, 1987

TIME UT	foF2 (MHz)	1E MUF (MHz)	1F MUF (MHz)	2F MUF (MHz)	3F MUF (MHz)	REMARKS
2103	7.20	6.80	16.30	10.30	8.20	Loops
2110		13.45				
2118	7.10		15.40	9.20	8.20	Long High Ray E + F Mode Present
2133	6.90		13.10	8.60	6.90	
2148	6.50	9.00	12.40	(O)7.90	*U6.7	
2203	6.20		12.50	(O)7.80	*U6.5	
2218	5.90		12.45	(O)7.85		Strong E + F Mode E + F Mode Present Long High Ray, E + F Mode
2233	5.90	10.30	12.90	(X)8.30	(X)7.50	
2248	6.20	9.10	13.30	(X)8.40		
2303	5.90		12.50	(X)8.05	(O)6.40	
2318	5.00		11.10	(X)7.70		
2333	5.40		10.70		(O)5.40	
2348	5.30		10.25	6.80	*U5.5	

*Note: values are uncertain

Table 4B. Oblique Propagation (from Argentina) Received at Millstone

Day 297, October 24, 1987

TIME UT	foF2 (MHz)	1E MUF (MHz)	1F MUF (MHz)	2F MUF (MHz)	3F MUF (MHz)	REMARKS
0003	5.20		9.40			Spread F
0018	5.10		10.10	(.)	(.)	
0033	4.90		9.40	(.)	(X)4.90	
0048	4.70		8.70	(O)5.60	(X)4.90	
0103	4.70		(X)9.20	(O)5.40		
0118	4.30		(X)8.10	(O)5.20		Nose Extension 8.1 Nose to 7.6
0133	4.00		(X)8.10	5.20		
0148	3.90		(X)7.90	5.20		
0203	3.90		(X)7.60	5.05		
0218	4.00		(X)8.10	4.90		
0233	3.90		(X)7.70	4.90		
0248	3.90		7.30	4.80		
0303	3.80		7.10	4.70		
0318	3.80		(X)7.20	(O)4.50		
						Best Iono- gram. Good 2F Mode
0333	3.70		(X)7.10	(O)4.50		
0348	3.70		(X)6.85	(O)4.40		
0403	3.80		(X)6.85	(X)4.81		
0418	3.70		(X)6.95	(X)4.80		
0433	3.60	6.90	(X)6.90	(O)4.40		

Note: (.) indicates mode is present but MUF can't be scaled.

absolute group path between the stations. This occurred on day 87293 0018 UT to 0203 UT and on day 87296 from 1033 UT to 1233 UT (Table 5).

As expected, these periods show the same MOF on both records, but the vertical critical frequencies at the endpoint stations were often quite different. As Figure 9 shows, the transmission factor varies substantially between morning and evening hours. This is explained by the change in E-region ionization and the change in the profile of the F-region. But the variation of the transmission factor in each of these time periods is due to the change in local gradients of the maximum electron density. Thus it is inappropriate to linearly average foF2 between stations more than 1500 km apart.

3.2.3 Oblique Sounding Between Goose Bay and Millstone

Because of its excellent synchronization stability the best and most reliable oblique propagation data were obtained from the Goose Bay - Millstone link (see Figure 10). Although it was not considered necessary for the study of the ionospheric trough this link will improve the validity of the Argentia data. The necessary time transfer by more than one hour of the Argentia data must be verified as feasible. If the motion of the trough can be distinguished from other time-dependent changes, then the study of the three station net is sufficient. Also the lateral extension of the trough can be investigated.

3.2.4 Trough Studies

A substantial number of ionograms from the four stations: Goose Bay, Labrador; Argentia, Newfoundland; Millstone Hill, Massachusetts and Wallops Island, Virginia, have been presented as ionogram surveys for the study of the F region trough

Table 5A. Oblique Propagation Received Simultaneously at Millstone and Argentina

Day 293, October 20, 1987

TIME UT	foF2 (MHz)		1F MUF (MHz)			
	MILLSTONE	ARGENTIA	foF2 (MHz)	X-TRACE	O-TRACE	M-FACTOR
0018	5.25	4.60	4.90	11.25	10.75	2.19
0033	5.20	4.60	4.90	10.80	10.30	2.10
0048	5.20	4.45	4.80	10.60	10.10	2.21
0103	4.90	4.30	4.60	10.50	10.00	2.17
0118	4.60	4.00	4.30	9.30	8.80	2.05
0133	4.50	4.00	4.25	9.15	8.65	2.04
0148	4.10	3.90	4.00	9.25	8.75	2.19
				Evening	M-FAC	2.14

Table 5B. Oblique Propagation Received Simultaneously at Millstone and Argentina (Continued)

Day 296, October 23, 1987

TIME UT	foF2 (MHz)		1F MUF (MHz)			
	MILLSTONE	ARGENTIA	foF2 (MHz)	X-TRACE	O-TRACE	M-FACTOR
1033	2.30	4.10	3.20	7.85	7.35	2.30
1049	2.70	4.60	3.65	9.30	8.80	2.41
1057	3.75	4.80	4.30	10.90	10.40	2.42
1118	4.00	5.00	4.50	>11.50	11.00	2.44
1148	4.70	5.50	5.10	13.00	12.50	2.45
1203	5.00	5.50	5.25	12.65	12.15	2.31
1218	5.40	5.50	5.45	13.80	13.30	2.44
1233	6.00	5.50	5.57	14.25	13.75	2.39
			Morning	M-FAC	2.40	
			Average	M-FAC	2.27	

LOCAL TIME (ARGENTIA) = UT - 3 hr 30 min
 LOCAL TIME (MILLSTONE HILL) = UT - 4 hr 46 min

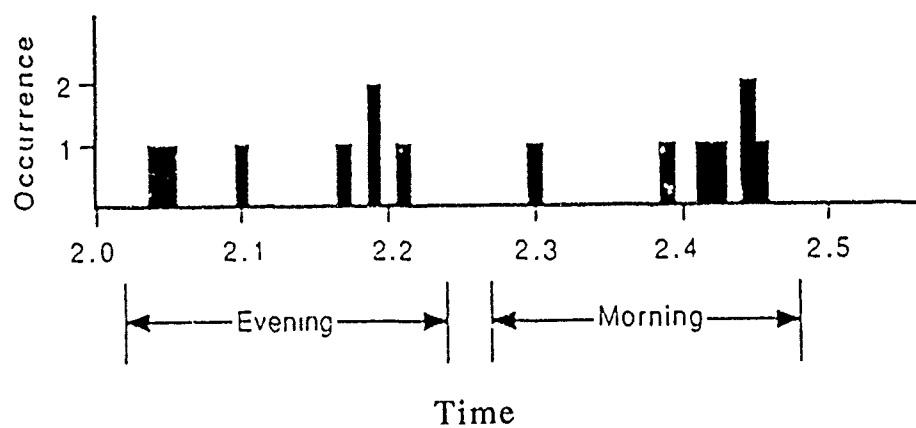


Figure 9. Variability of the Virtual Transmission Factor (M-Factor)
Assuming Linear Gradients in foF2. Argentina - Millstone
Day 87293

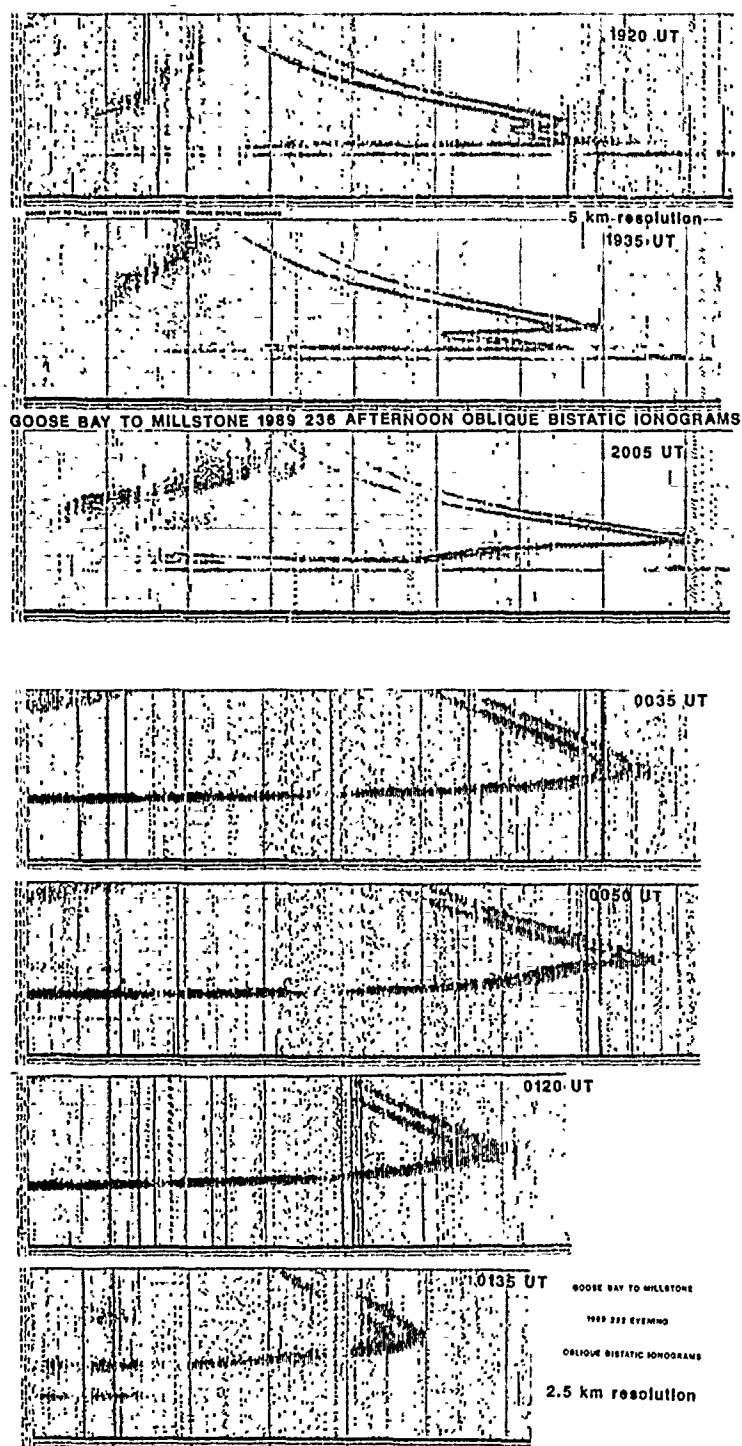


Figure 10. Goose Bay to Millstone Oblique Bistatic Ionograms

between the auroral and mid-latitude ionosphere. Table 6 gives a schedule of World Day data from 1988 and 1989 when ionogram surveys were available for at least three of the four stations. Many more days will be available from 1989 and in the future.

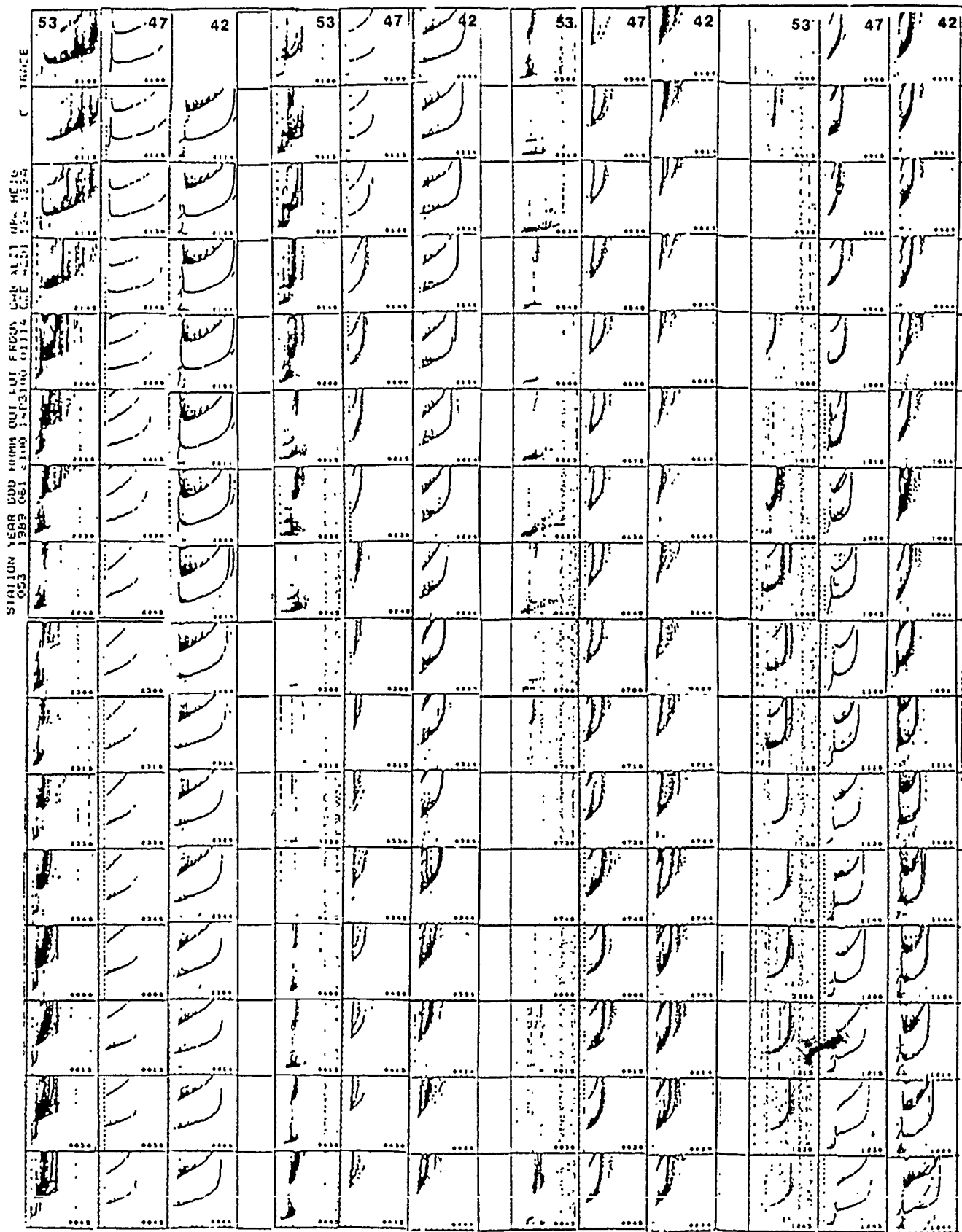
Analysis of digital data has the advantage of better discrimination of the vertical echo traces and of the ordinary component. Compared to the dense station net [Whalen, 1989], available during the International Geophysical Year 1958, the chain of available stations is very limited. To improve the situation an effort will be made for automatic bistatic sounding between the ionosondes to monitor the midpoint conditions. Note that Goose Bay data generally appear to be necessary to draw a cross-section of the maximum F-layer critical frequency, f_oF_2 , as a function of time of day.

One example of trough development is presented here. At the beginning of March 1989 (see Figures 11a and 11b) an intensive measurement campaign led to good data from the most significant stations. On Day 061 the ionospheric trough clearly reached Millstone Hill, MA and had its minimum between 06 and 07 UT, while before that time first Argentinia and later Millstone show additional echo traces of reflection from the trough walls. On Day 065 Argentinia shows echo traces from the walls of the trough since 0100 UT all the time until 1000 UT, while the Millstone ionosphere breaks down almost completely at 0700 UT.

In the future edited ARTIST data will be used for surveys of the trough onsets. The ADEP [Zhang, 1989] software package (ARTIST Data Editing and Printing) permits printing of the critical frequencies f_oF_2 , f_oE and f_oE_s , and the electron density contours as function of time. An example is shown in Figure 12 for 6 March 1989; the trough minimum occurs at 23 UT at Goose Bay, 04 UT at Argentinia and 06 UT at Millstone.

Table 6. Available Survey Ionograms

<u>1988</u>	Goose Bay	Argentina	Millstone	Wallops Is.
75	x	x	o Bad	x
76	x	x Absorption	x 08-10 Z Very low foF2	x
77	x	o	x	x
138	x 02-06 Z Aurora E	x 06 Z Low foF2	x 06 Z Low foF2	x
139	x Aurora E All night	x 06-07 Z Low foF2	x 08 Z Low foF2	x
140	x 07-15 Z foF2 and F1 F2	o	x 08 Z foF2 missing	x
166	x Aurora Es	x 0435 Z foF2 missing	x	x
167	x	x	x	x
194	x 830-930 Z Absorption Aurora 01-07 Z	o	x	x
195	x No morning data	o	x	x
196	x	x	x	xs
287	x	x Day missing	x	x
313	x Absorption	x 09-10 Z foF2 2.5 MHz	x 02-07 Z foF2 2.5 MHz	x
314	x	x	x	x
315	x	x	x	x
348	x	x	o	x
<u>1989</u>				
61	x	x	x	
65	x	x	x	



GOOSE BAY(53), ARGENTIA(47), MILLSTONE(42)

MOTION OF TROUGH OVER THREE STATION CHAIN 1989 061

Figure 11a. Motion of Trough Over Three Station Chain

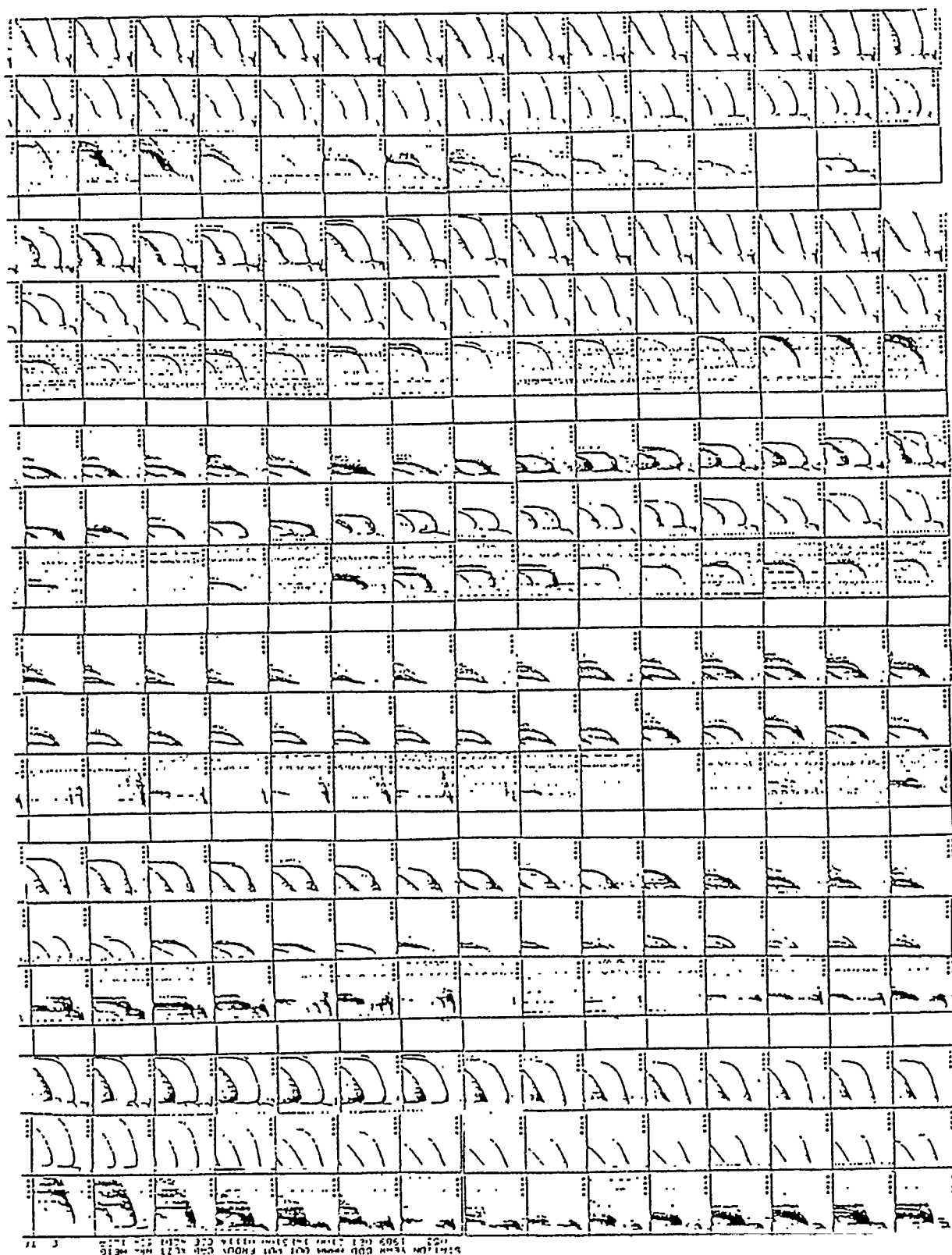
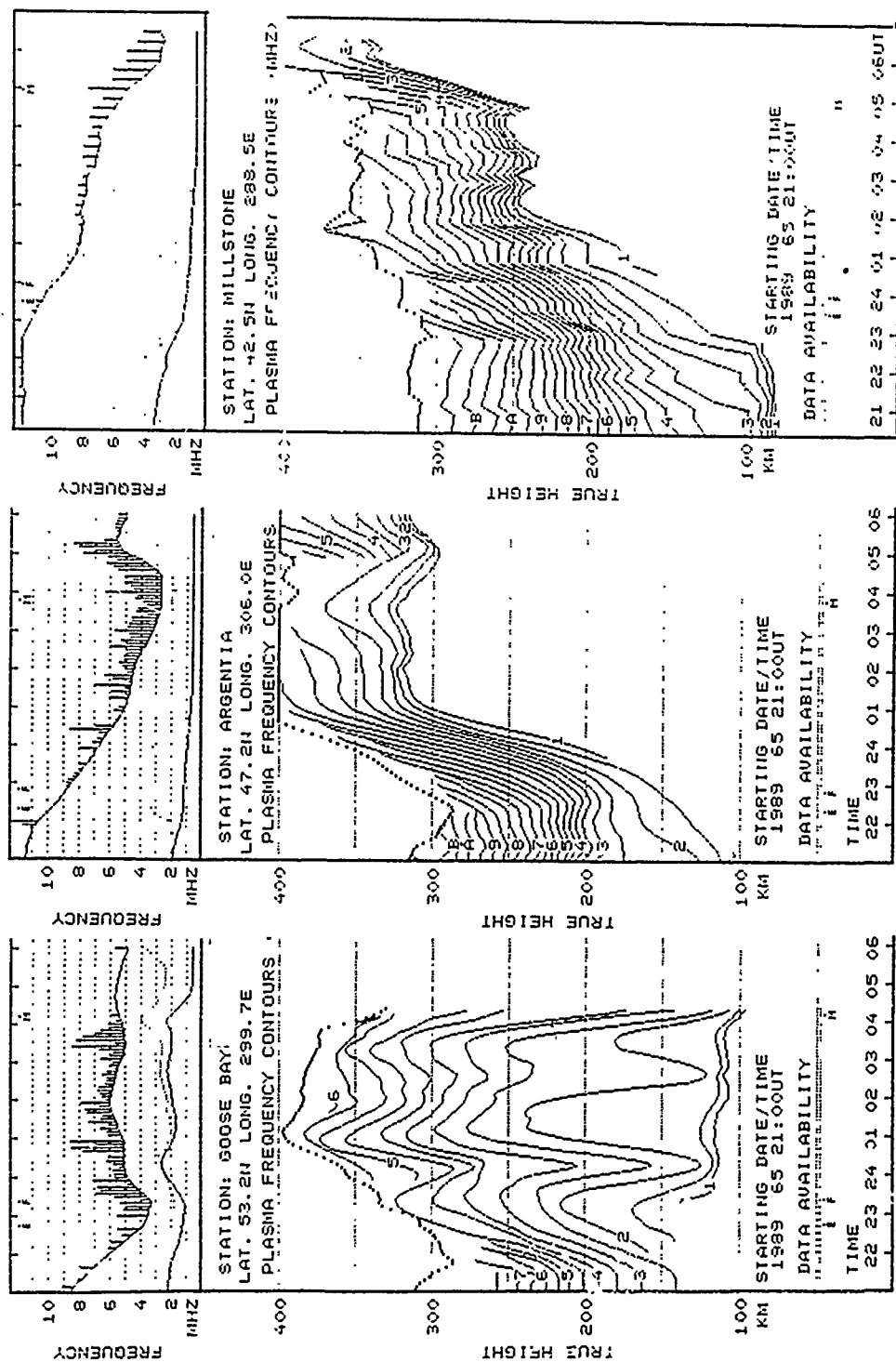


Figure 11b. Motion of Trough Over Three Station Chain



TROUGH ONSET

Along $\sim 300^\circ$ Meridian

Figure 12. Trough Onset 6 March 1989

3.3 Campaigns

Campaign studies have formed an integral part of this contract. The AWS Digisonde network is an important high latitude diagnostic available to both the geophysics and radar engineering communities. Several of the campaigns involving the Digisondes are summarized below (chronological order).

a) Viking/GL (October 28 - November 15, 1986)

This campaign focussed on the electrodynamics of polar cap sun-aligned F-region arcs, and velocity shears contiguous with arcs in the auroral oval. Diagnostics included the Viking and HILAT satellites, EISCAT and Sondrestrom radars, GL All Sky Imaging Photometers (ASIP's), and AWS Digisondes. The GL Airborne Ionospheric Observatory (AIO) was based at Thule early on in the campaign, and operated a Digisonde together with satellite scintillation receivers (250 MHz), ASIP and spectrometers. The AIO Digisonde operated in a 2.5 minute sequence during ground based and airborne observations. From 28 October to 3 November, the Digisondes at Qaanaaq and Argentia operated in a 5 min ionogram/drift sequence. On 3 November, the AIO transferred to Andoya, Norway, and participated in joint observations with EISCAT in Tromsø. Analysis of this data set contributed to a paper currently in preparation by Lars Bläü [1989 private communication].

b) Slant Es (July 26 - August 7, 1987)

A new direction-scanning ionosonde mode and the drift mode were implemented at Qaanaaq for this campaign, which was a collaborative effort between GL, ULCAR and DMI. In this mode, each frequency sounding within the ionogram is repeated 6 (or 12) times while the beam of the receiving antenna array scans through 6 (or 12) azimuth directions in 60° (or 30°) increments.

Analysis of slant Es data from this campaign and the one in 1986 resulted in a paper by Hoeg et al. [1987] that was presented at the Fall (1987) AGU meeting in San Francisco (see Appendix B).

Simultaneously with the slant Es, F layer patches were also studied. The patches often produced an interesting signature in the ionograms, consisting of a "nose" similar to that observed at oblique sounding (see Figure 8). The peculiar triangular shape in the spread F X-echoes on the ionograms (Figures 13 and 14) is caused by the oblique reflections from a patch, forming the nose that is typical for oblique ionograms. With plasma frequencies estimated to be only about 10% higher than the background, these patches return signals from distances maybe up to 200 km, resulting in a very flat nose. Often the nose of the O-trace is covered by X-echoes and is therefore not visible. But at 1456 UT (Figure 13) the O-nose is also visible.

(c) Structure and Dynamics of the Auroral Ionosphere (January 8 - 15, 1988)

The GL-AIO flew to the north of the EISCAT radar and performed 250 MHz phase and amplitude scintillation measurements, recorded all-sky auroral images at 6300 Å and 4278 Å and performed ionospheric sounding using a Digisonde. These measurements were coordinated with EISCAT observations, and DMSP-F8 overpasses in which precipitating electron and ion fluxes were measured, together with in-situ thermal plasma parameters at 850 km altitude.

Large scale ionospheric features such as F-layer blobs and the trough were observed. The location and intensity of small scale irregularities was mapped. All ionograms for the six AIO missions on January 8, 9, 15, 16, 17 and 18 have been scaled in terms of foF2, foE, foEs, and receiver gain (showing the level of

DIGISONDE 256 -- RAW DATA IONOGRAM ARMENU SETTINGS ARE P3=4 P4=4 P5=0

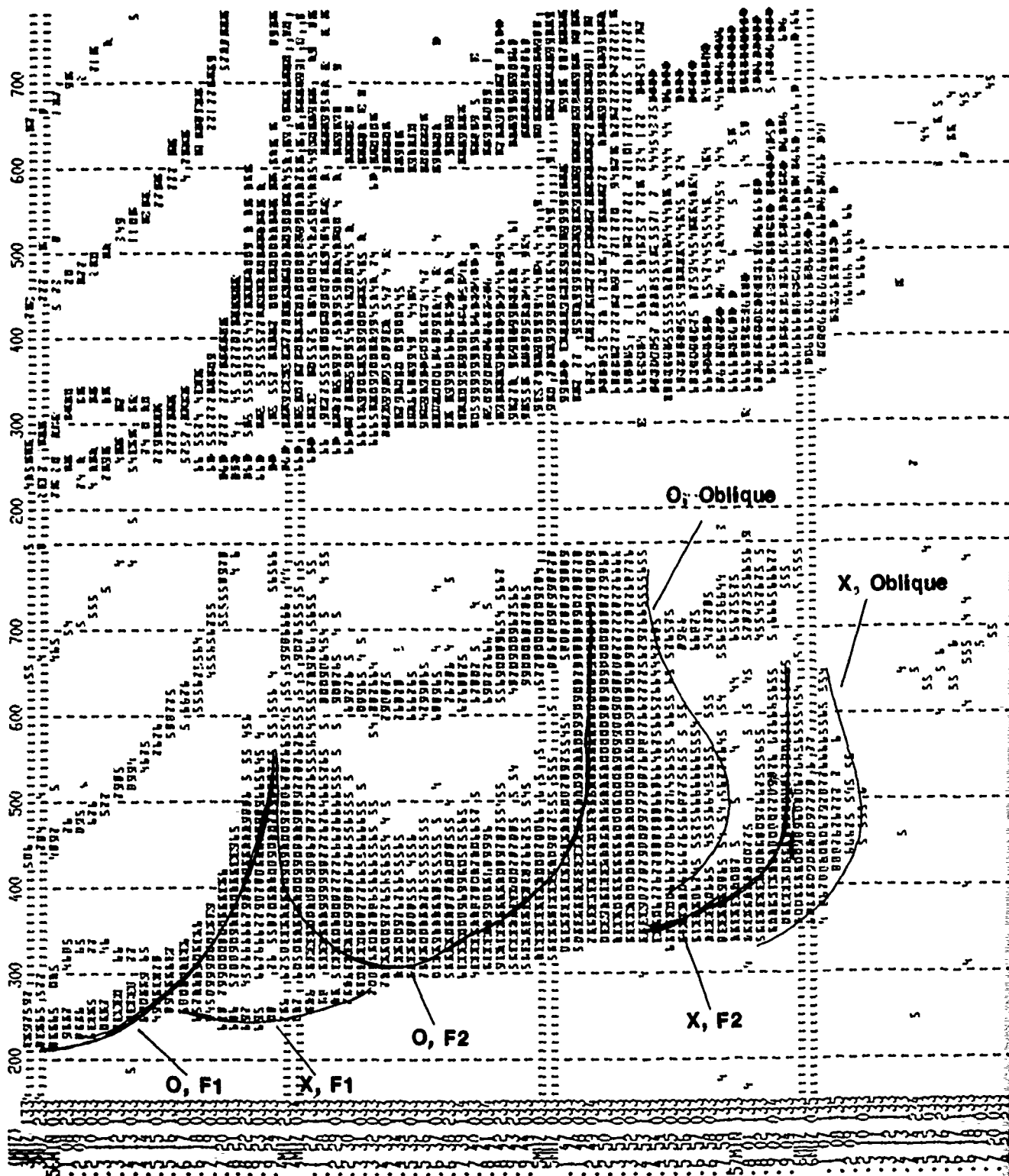


Figure 13. Qaanaaq, Greenland Digital Ionogram 14 August 1987, 1456 UT

DIGISONDE 256 -- ROW DATA IONOSPHERIC MENU SETTINGS ARE P2=4 P4=4 P5=0

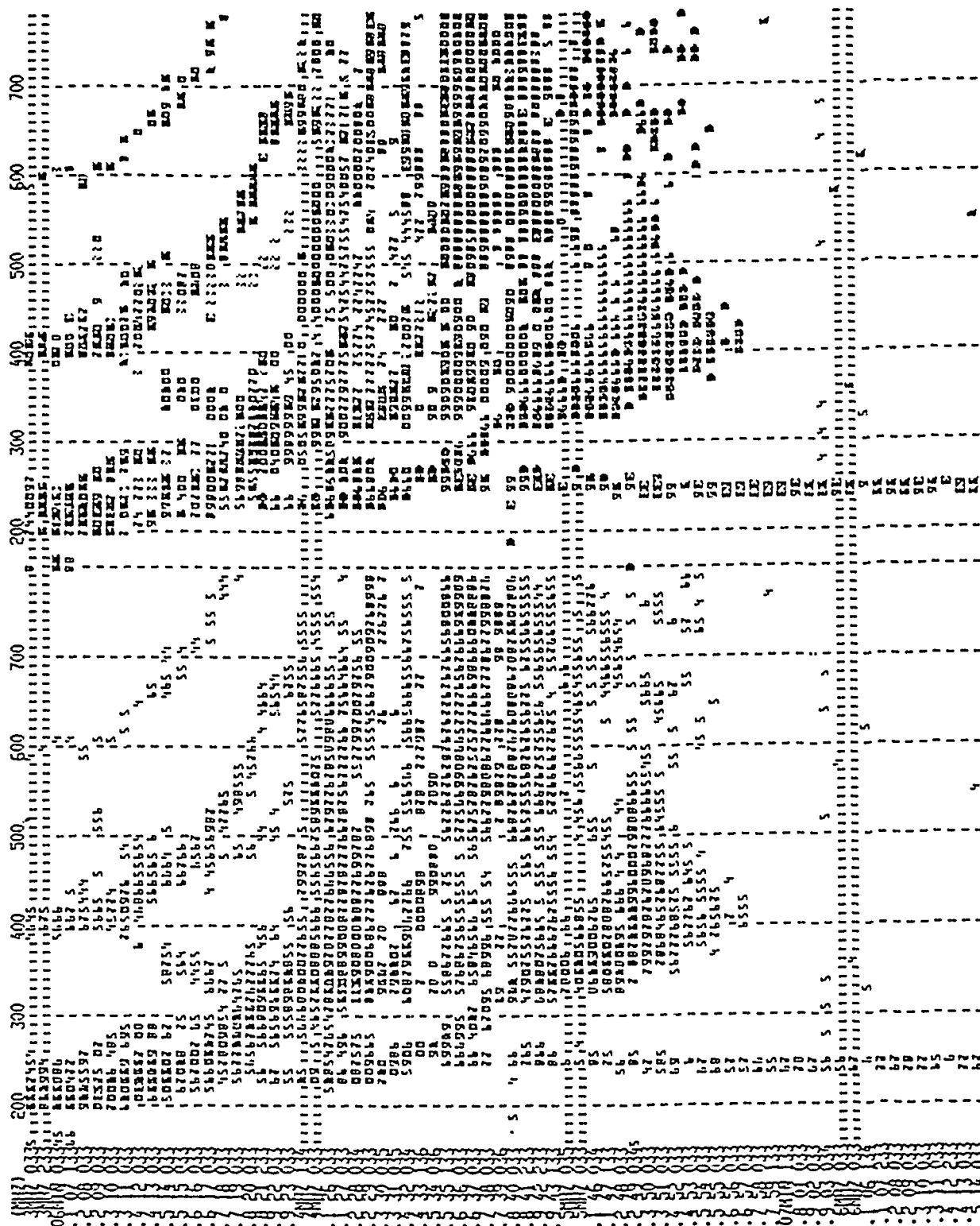


Figure 14. Qaanaaq, Greenland Digital Ionogram 14 August 1987, 1706 UT

absorption; high gain # = high absorption). Table 7 lists these parameters as a function of UT and aircraft location in terms of the corrected geomagnetic latitude (CGLAT). The ionization in the F region rarely went above $1 \times 10^5 \text{ cm}^{-3}$ (3 MHz plasma frequency). This is comparable to the ionization measured in the E region. The critical frequencies for the auroral E are generally just below 3 MHz, and sporadic E layers which are present most of the time vary between 3 and 9 MHz. In this environment it is difficult to derive vertical electron density profiles for the F region.

Figure 15 shows three AIO ionograms from the 18 January flight at 1809, 1816 and 1819 UT. The F layer is absent or blanketed in the last two ionograms, so a profile inversion was attempted only for the 1809 ionogram. The figure shows three different electron density profiles computed for 1809 UT using different assumptions about the electron distribution in the transition (valley) region between the E and F layers. The different valleys shown in the profile plots affect the calculation of the hmF2 values, causing them to vary from 236 km for the valley shown in the top panel to 227 km (middle) and to 209 km (bottom). In the latter case the transition region was assumed to be filled with ionization.

d) CEDAR-HLPS (February 6 - 24, 1988)

The CEDAR-High Latitude Plasma Structures (HLPS) initiative has as its objective the study of the source, evolution and ultimate fate of ionospheric irregularities at high latitudes. Digisondes obtained drift data and ionograms at Qaanaaq, Goose Bay, and Argentia. Time resolution was generally 15 minutes, but for two core periods (11-12 Feb. 21-02 UT; 18/19 Feb. 21-02 UT) it was five minutes. Ionograms were also recorded by the Digisonde 128 on board the GL-AIO parked at Thule. Table

Table 7. AIO Ionogram Observations
Andoya Round Trips 1988

1984 008 ANDOYA RRI					1984 009 ANDOYA RRI					1984 015 ANDOYA RRI					1984 016 ANDOYA RRI					1984 017 ANDOYA RRI					1984 018 ANDOYA RRI				
CELAT	UT	f _o F2	f _o E	Es	CELAT	UT	f _o F2	f _o E	Es	CELAT	UT	f _o F2	f _o E	Es	CELAT	UT	f _o F2	f _o E	Es	CELAT	UT	f _o F2	f _o E	Es	CELAT	UT	f _o F2	f _o E	Es
66.31	1746	3.2	2.5	8.0	66.50	1445	3.1	—	—	66.10	1701	—	3.1	9.2	66.90	1714	—	4.1	6	66.00	1649	—	—	—	66.00	1799	—	—	—
66.29	1745	3.1	2.4	8.0	66.50	1704	2.3	—	—	66.10	1706	—	3.1	9.4	66.90	1716	—	4.1	5	66.00	1654	—	—	—	66.00	1711	—	—	—
66.25	1751	2.8	2.7	8.0	66.70	1706	2.2	—	—	66.10	1709	—	—	8.7	66.70	1719	—	3.9	6	66.00	1704	—	—	—	66.00	1739	—	—	—
66.20	1754	2.9	2.3	8.0	66.90	1709	2.0	—	—	66.10	1711	—	—	9.3	66.70	1721	—	3.7	6	66.00	1706	—	—	—	66.00	1734	—	—	—
66.21	1756	2.8	2.6	8.0	67.10	1711	1.9	—	—	66.60	1714	—	—	9.6	66.70	1724	—	3.6	6	66.00	1709	—	—	—	66.00	1736	—	—	—
66.48	1759	—	3.4	8.0	67.60	1714	1.7	—	—	66.30	1716	—	—	9.6	66.70	1726	—	3.6	6	66.00	1711	—	—	—	66.00	1739	—	—	—
66.57	1801	—	—	7.0	67.90	1716	1.8	—	—	66.60	1719	2.7	2.8	9.4	66.70	1729	—	3.7	6	66.00	1714	2.6	2.4	9.4	66.00	1744	—	—	—
66.95	1804	—	—	6.0	68.00	1721	—	—	—	66.90	1721	—	2.5	9.3	66.70	1731	—	3.6	6	66.00	1719	—	—	—	66.00	1744	—	—	—
67.14	1806	—	—	7.0	68.30	1724	—	—	—	67.10	1724	2.3	2.7	9.3	66.80	1734	—	3.5	6	66.00	1721	—	—	—	66.00	1744	—	—	—
67.38	1809	—	3.4	5.9	68.70	1729	—	—	—	67.80	1731	—	2.7	9.3	66.80	1736	—	3.5	6	66.00	1724	—	—	—	66.00	1744	—	—	—
67.53	1811	2.8	—	6.8	69.00	1731	—	—	—	68.00	1734	—	—	9.3	66.90	1739	—	3.6	6	66.00	1726	—	—	—	66.00	1744	—	—	—
67.76	1814	2.4	—	5.0	69.30	1734	—	—	—	68.30	1736	—	—	9.3	66.90	1744	—	3.6	6	66.00	1729	—	—	—	66.00	1744	—	—	—
67.97	1816	2.5	—	5.7	69.50	1736	—	—	—	68.60	1739	—	—	9.3	66.90	1749	—	3.6	6	66.00	1731	—	—	—	66.00	1744	—	—	—
68.28	1819	2.8	2.4	5.9	69.10	1739	—	—	—	68.80	1741	—	—	9.3	66.90	1754	—	3.6	6	66.00	1734	—	—	—	66.00	1744	—	—	—
68.78	1824	2.6	—	5.2	68.90	1741	—	—	—	69.00	1744	—	—	9.3	66.90	1759	—	3.6	6	66.00	1736	—	—	—	66.00	1744	—	—	—
69.27	1829	2.5	—	3.5	68.70	1744	—	—	—	69.30	1746	—	—	9.3	66.90	1754	—	3.6	6	66.00	1739	—	—	—	66.00	1744	—	—	—
69.45	1831	2.6	—	3.7	68.10	1749	—	—	—	69.50	1749	—	—	9.3	66.90	1759	—	3.6	6	66.00	1741	—	—	—	66.00	1744	—	—	—
69.96	1836	2.7	—	4.5	67.80	1751	—	—	—	69.50	1751	—	—	9.3	66.90	1759	—	3.6	6	66.00	1744	—	—	—	66.00	1744	—	—	—
69.29	1839	2.8	—	4.9	67.50	1754	—	—	—	69.20	1754	—	—	9.3	66.90	1759	—	3.6	6	66.00	1744	—	—	—	66.00	1744	—	—	—
68.34	1841	2.8	—	4.1	67.10	1759	—	—	—	69.00	1756	—	—	9.3	66.90	1759	—	3.6	6	66.00	1744	—	—	—	66.00	1744	—	—	—
67.95	1844	—	—	5.7	66.80	1801	—	—	—	66.40	1759	—	—	9.3	66.90	1759	—	3.6	6	66.00	1744	—	—	—	66.00	1744	—	—	—
67.71	1846	—	—	5.8	66.50	1811	—	—	—	66.40	1801	—	—	9.3	66.90	1759	—	3.6	6	66.00	1744	—	—	—	66.00	1744	—	—	—
67.47	1849	—	—	5.7	66.70	1814	—	—	—	66.10	1804	—	—	9.3	66.90	1759	—	3.6	6	66.00	1744	—	—	—	66.00	1744	—	—	—
67.31	1851	—	—	5.3	67.00	1816	—	—	—	66.10	1804	—	—	9.3	66.90	1759	—	3.6	6	66.00	1744	—	—	—	66.00	1744	—	—	—
67.07	1854	—	—	5.3	67.30	1819	—	—	—	67.80	1806	—	—	9.3	66.90	1759	—	3.6	6	66.00	1744	—	—	—	66.00	1744	—	—	—
66.91	1856	—	—	5.8	67.50	1821	—	—	—	67.50	1809	—	—	9.3	66.90	1759	—	3.6	6	66.00	1744	—	—	—	66.00	1744	—	—	—
66.67	1859	—	—	5.8	67.80	1824	—	—	—	67.30	1811	—	—	9.3	66.90	1759	—	3.6	6	66.00	1744	—	—	—	66.00	1744	—	—	—
66.51	1901	—	—	5.7	68.00	1826	—	—	—	67.00	1814	—	—	9.3	66.90	1759	—	3.6	6	66.00	1744	—	—	—	66.00	1744	—	—	—
66.27	1904	—	—	5.8	66.30	1829	—	—	—	66.40	1816	—	—	9.3	66.90	1759	—	3.6	6	66.00	1744	—	—	—	66.00	1744	—	—	—
66.35	1906	—	—	5.9	66.60	1831	—	—	—	66.10	1819	—	—	9.3	66.90	1759	—	3.6	6	66.00	1744	—	—	—	66.00	1744	—	—	—
66.55	1909	—	—	5.9	66.90	1834	—	—	—	66.00	1821	—	—	9.3	66.90	1759	—	3.6	6	66.00	1744	—	—	—	66.00	1744	—	—	—
66.67	1911	—	—	4.4	69.10	1836	3.0	2.2	4	66.00	1824	—	—	9.3	66.90	1759	—	3.6	6	66.00	1744	—	—	—	66.00	1744	—	—	—
66.87	1914	—	—	4.4	65.30	1839	3.1	2.3	3.5	66.70	1826	—	—	9.3	66.90	1759	—	3.6	6	66.00	1744	—	—	—	66.00	1744	—	—	—
67.02	1916	—	—	4	69.50	1841	2.8	2.1	4	66.40	1829	—	—	9.3	66.90	1759	—	3.6	6	66.00	1744	—	—	—	66.00	1744	—	—	—
67.26	1919	—	—	5.8	69.70	1846	3.0	2.1	3.6	66.70	1829	—	—	9.3	66.90	1759	—	3.6	6	66.00	1744	—	—	—	66.00	1744	—	—	—
67.41	1921	—	—	5.7	69.70	1849	3.0	2.5	3.9	66.90	1831	—	—	9.3	66.90	1759	—	3.6	6	66.00	1744	—	—	—	66.00	1744	—	—	—
67.65	1924	—	—	5.8	69.50	1851	2.7	2.3	4.5	66.70	1834	—	—	9.3	66.90	1759	—	3.6	6	66.00	1744	—	—	—	66.00	1744	—	—	—
67.82	1926	—	—	5.9	69.20	1854	2.7	2.2	3.7	66.70	1836	—	—	9.3	66.90	1759	—	3.6	6	66.00	1744	—	—	—	66.00	1744	—	—	—
68.10	1929	—	—	5.8	68.90	1856	2.5	2.3	3.6	66.70	1839	—	—	9.3	66.90	1759	—	3.6	6	66.00	1744	—	—	—	66.00	1744	—	—	—
68.29	1931	—	—	5.1	68.60	1859	2.5	2.0	3.3	66.70	1841	—	—	9.3	66.90	1759	—	3.6	6	66.00	1744	—	—	—	66.00	1744	—	—	—
68.55	1934	3.1	2.8	5.8	66.40	1901	—	—	—	66.40	1846	—	—	9.3	66.90	1759	—	3.6	6	66.00	1744	—	—	—	66.00	1744	—	—	—
68.65	1936	—	—	5.8	66.10	1904	—	—	—	66.70	1849	—	—	9.3	66.90	1759	—	3.6	6	66.00	1744	—							

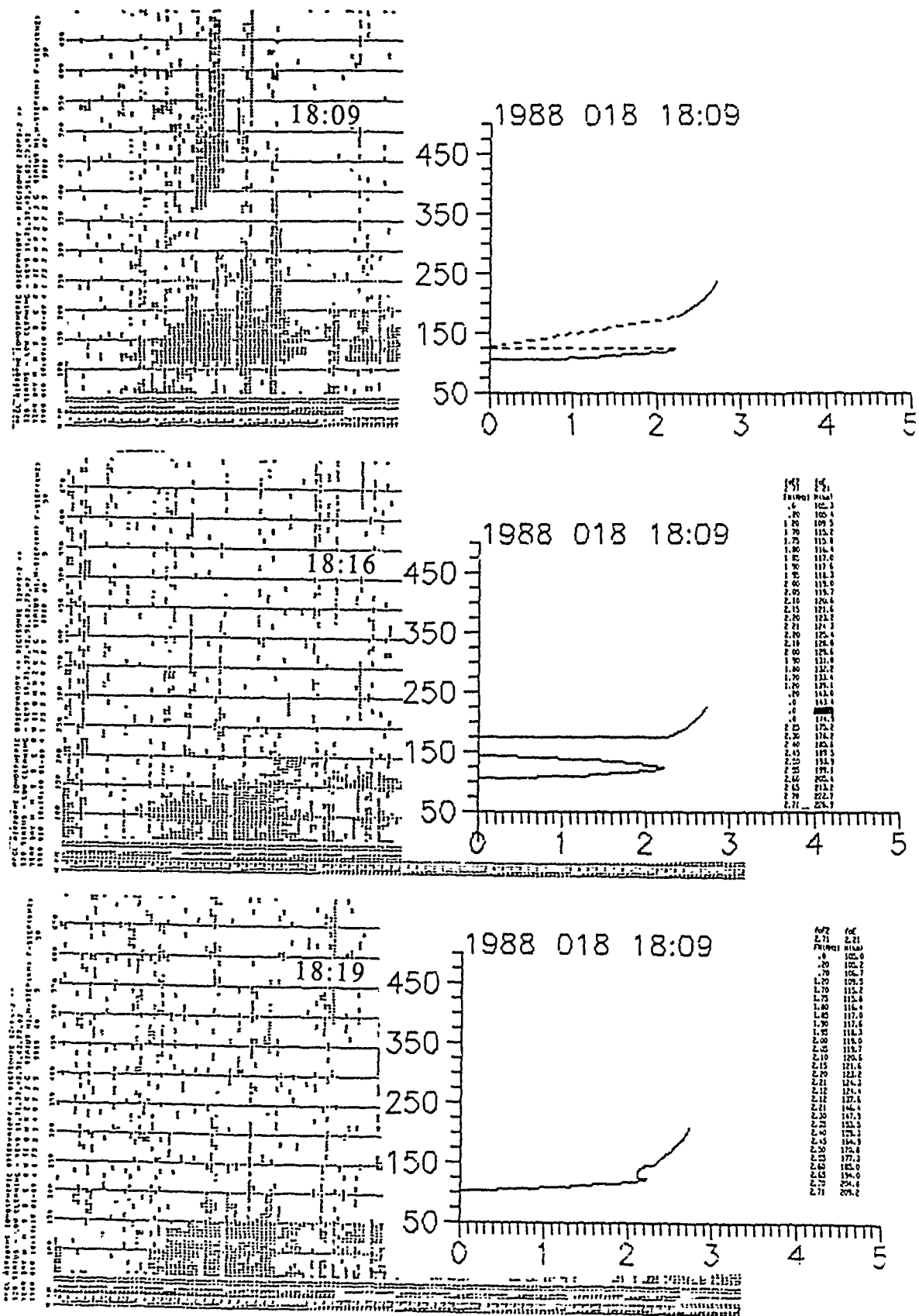


Figure 15. Andoya Ionogram and Electron Density Profiles

8 lists the available data for Goose Bay, Qaanaaq, Millstone Hill and Argentina.

Many other instruments supported this campaign, including ISRs, and ASIPs.

e) CEDAR-HLPS (December 5 - 13, 1988)

The format of this HLPS campaign was very similar to that described above.

Results from the analysis of the CEDAR-HLPS data have been presented at the NSF CEDAR meetings in Boulder 1988 and 1989, at the URSI meeting in Boulder in 1989 and Spring 1989 AGU meeting (see Section 5.0).

f) Slant-Es and Drift Measurements at Sondrestrom (July 7-11, 1989)

Drift mode operations were in effect at all three Air Force Digisondes: Qaanaaq, Goose Bay and Argentina. Unfortunately, the Sondrestrom ISR was also undergoing maintenance/repairs and only 1-2 hours of simultaneous observation was possible. Nature did not cooperate and the expected Slant-Es traces were not observed due to a lack of significant magnetic activity.

However, this trip was extremely valuable because it produced five days of drift data from the new AWS sounder at Sondrestrom: These data are discussed in Section 4.0 and yield some interesting geophysics in addition to confirming the correct operation of the new sounder. The experiment also revealed a problem with interference to communication systems which was resolved in November 1989.

(February 1988)

monogram

Equipment outlay

GOOSE HALL

1	2	3	4	5	6	7	8	9	10	11	12	13	14	15	16	17	18	19	20	21	22	23	24	25	26	27	28	29	30	31	32	33	34	35	36	37	38	39	40	41	42	43	44	45	46	47	48	49	50	51	52	53	54	55	56	57	58	59	60	61	62	63	64	65	66	67	68	69	70	71	72	73	74	75	76	77	78	79	80	81	82	83	84	85	86	87	88	89	90	91	92	93	94	95	96	97	98	99	100	101	102	103	104	105	106	107	108	109	110	111	112	113	114	115	116	117	118	119	120	121	122	123	124	125	126	127	128	129	130	131	132	133	134	135	136	137	138	139	140	141	142	143	144	145	146	147	148	149	150	151	152	153	154	155	156	157	158	159	160	161	162	163	164	165	166	167	168	169	170	171	172	173	174	175	176	177	178	179	180	181	182	183	184	185	186	187	188	189	190	191	192	193	194	195	196	197	198	199	200	201	202	203	204	205	206	207	208	209	210	211	212	213	214	215	216	217	218	219	220	221	222	223	224	225	226	227	228	229	230	231	232	233	234	235	236	237	238	239	240	241	242	243	244	245	246	247	248	249	250	251	252	253	254	255	256	257	258	259	260	261	262	263	264	265	266	267	268	269	270	271	272	273	274	275	276	277	278	279	280	281	282	283	284	285	286	287	288	289	290	291	292	293	294	295	296	297	298	299	300	301	302	303	304	305	306	307	308	309	310	311	312	313	314	315	316	317	318	319	320	321	322	323	324	325	326	327	328	329	330	331	332	333	334	335	336	337	338	339	340	341	342	343	344	345	346	347	348	349	350	351	352	353	354	355	356	357	358	359	360	361	362	363	364	365	366	367	368	369	370	371	372	373	374	375	376	377	378	379	380	381	382	383	384	385	386	387	388	389	390	391	392	393	394	395	396	397	398	399	400	401	402	403	404	405	406	407	408	409	410	411	412	413	414	415	416	417	418	419	420	421	422	423	424	425	426	427	428	429	430	431	432	433	434	435	436	437	438	439	440	441	442	443	444	445	446	447	448	449	450	451	452	453	454	455	456	457	458	459	460	461	462	463	464	465	466	467	468	469	470	471	472	473	474	475	476	477	478	479	480	481	482	483	484	485	486	487	488	489	490	491	492	493	494	495	496	497	498	499	500	501	502	503	504	505	506	507	508	509	510	511	512	513	514	515	516	517	518	519	520	521	522	523	524	5
---	---	---	---	---	---	---	---	---	----	----	----	----	----	----	----	----	----	----	----	----	----	----	----	----	----	----	----	----	----	----	----	----	----	----	----	----	----	----	----	----	----	----	----	----	----	----	----	----	----	----	----	----	----	----	----	----	----	----	----	----	----	----	----	----	----	----	----	----	----	----	----	----	----	----	----	----	----	----	----	----	----	----	----	----	----	----	----	----	----	----	----	----	----	----	----	----	----	----	-----	-----	-----	-----	-----	-----	-----	-----	-----	-----	-----	-----	-----	-----	-----	-----	-----	-----	-----	-----	-----	-----	-----	-----	-----	-----	-----	-----	-----	-----	-----	-----	-----	-----	-----	-----	-----	-----	-----	-----	-----	-----	-----	-----	-----	-----	-----	-----	-----	-----	-----	-----	-----	-----	-----	-----	-----	-----	-----	-----	-----	-----	-----	-----	-----	-----	-----	-----	-----	-----	-----	-----	-----	-----	-----	-----	-----	-----	-----	-----	-----	-----	-----	-----	-----	-----	-----	-----	-----	-----	-----	-----	-----	-----	-----	-----	-----	-----	-----	-----	-----	-----	-----	-----	-----	-----	-----	-----	-----	-----	-----	-----	-----	-----	-----	-----	-----	-----	-----	-----	-----	-----	-----	-----	-----	-----	-----	-----	-----	-----	-----	-----	-----	-----	-----	-----	-----	-----	-----	-----	-----	-----	-----	-----	-----	-----	-----	-----	-----	-----	-----	-----	-----	-----	-----	-----	-----	-----	-----	-----	-----	-----	-----	-----	-----	-----	-----	-----	-----	-----	-----	-----	-----	-----	-----	-----	-----	-----	-----	-----	-----	-----	-----	-----	-----	-----	-----	-----	-----	-----	-----	-----	-----	-----	-----	-----	-----	-----	-----	-----	-----	-----	-----	-----	-----	-----	-----	-----	-----	-----	-----	-----	-----	-----	-----	-----	-----	-----	-----	-----	-----	-----	-----	-----	-----	-----	-----	-----	-----	-----	-----	-----	-----	-----	-----	-----	-----	-----	-----	-----	-----	-----	-----	-----	-----	-----	-----	-----	-----	-----	-----	-----	-----	-----	-----	-----	-----	-----	-----	-----	-----	-----	-----	-----	-----	-----	-----	-----	-----	-----	-----	-----	-----	-----	-----	-----	-----	-----	-----	-----	-----	-----	-----	-----	-----	-----	-----	-----	-----	-----	-----	-----	-----	-----	-----	-----	-----	-----	-----	-----	-----	-----	-----	-----	-----	-----	-----	-----	-----	-----	-----	-----	-----	-----	-----	-----	-----	-----	-----	-----	-----	-----	-----	-----	-----	-----	-----	-----	-----	-----	-----	-----	-----	-----	-----	-----	-----	-----	-----	-----	-----	-----	-----	-----	-----	-----	-----	-----	-----	-----	-----	-----	-----	-----	-----	-----	-----	-----	-----	-----	-----	-----	-----	-----	-----	-----	-----	-----	-----	-----	-----	-----	-----	-----	-----	-----	-----	-----	-----	-----	-----	-----	-----	-----	-----	-----	-----	-----	-----	-----	-----	-----	-----	-----	-----	-----	-----	-----	-----	-----	-----	-----	-----	-----	-----	-----	-----	-----	-----	-----	-----	-----	-----	-----	-----	-----	-----	-----	-----	-----	-----	-----	-----	-----	-----	---

QALVO

	1	2	3	4	5	6	7	8	9	10	11	12	13	14	15	16	17	18	19	20	21	22	23	24	25	26	27	28	29	30	31	32	33	34	35	36	37	38	39	40	41	42	43	44	45	46	47	48	49	50	51	52	53	54	55	56	57	58	59	60	61	62	63	64	65	66	67	68	69	70	71	72	73	74	75	76	77	78	79	80	81	82	83	84	85	86	87	88	89	90	91	92	93	94	95	96	97	98	99	100	101	102	103	104	105	106	107	108	109	110	111	112	113	114	115	116	117	118	119	120	121	122	123	124	125	126	127	128	129	130	131	132	133	134	135	136	137	138	139	140	141	142	143	144	145	146	147	148	149	150	151	152	153	154	155	156	157	158	159	160	161	162	163	164	165	166	167	168	169	170	171	172	173	174	175	176	177	178	179	180	181	182	183	184	185	186	187	188	189	190	191	192	193	194	195	196	197	198	199	200	201	202	203	204	205	206	207	208	209	210	211	212	213	214	215	216	217	218	219	220	221	222	223	224	225	226	227	228	229	230	231	232	233	234	235	236	237	238	239	240	241	242	243	244	245	246	247	248	249	250	251	252	253	254	255	256	257	258	259	260	261	262	263	264	265	266	267	268	269	270	271	272	273	274	275	276	277	278	279	280	281	282	283	284	285	286	287	288	289	290	291	292	293	294	295	296	297	298	299	300	301	302	303	304	305	306	307	308	309	310	311	312	313	314	315	316	317	318	319	320	321	322	323	324	325	326	327	328	329	330	331	332	333	334	335	336	337	338	339	340	341	342	343	344	345	346	347	348	349	350	351	352	353	354	355	356	357	358	359	360	361	362	363	364	365	366	367	368	369	370	371	372	373	374	375	376	377	378	379	380	381	382	383	384	385	386	387	388	389	390	391	392	393	394	395	396	397	398	399	400	401	402	403	404	405	406	407	408	409	410	411	412	413	414	415	416	417	418	419	420	421	422	423	424	425	426	427	428	429	430	431	432	433	434	435	436	437	438	439	440	441	442	443	444	445	446	447	448	449	450	451	452	453	454	455	456	457	458	459	460	461	462	463	464	465	466	467	468	469	470	471	472	473	474	475	476	477	478	479	480	481	482	483	484	485	486	487	488	489	490	491	492	493	494	495	496	497	498	499	500	501	502	503	504	505	506	507	508	509	510	511	512	513	514	515	516	517	518	519	520	521	522	523	52
--	---	---	---	---	---	---	---	---	---	----	----	----	----	----	----	----	----	----	----	----	----	----	----	----	----	----	----	----	----	----	----	----	----	----	----	----	----	----	----	----	----	----	----	----	----	----	----	----	----	----	----	----	----	----	----	----	----	----	----	----	----	----	----	----	----	----	----	----	----	----	----	----	----	----	----	----	----	----	----	----	----	----	----	----	----	----	----	----	----	----	----	----	----	----	----	----	----	----	----	-----	-----	-----	-----	-----	-----	-----	-----	-----	-----	-----	-----	-----	-----	-----	-----	-----	-----	-----	-----	-----	-----	-----	-----	-----	-----	-----	-----	-----	-----	-----	-----	-----	-----	-----	-----	-----	-----	-----	-----	-----	-----	-----	-----	-----	-----	-----	-----	-----	-----	-----	-----	-----	-----	-----	-----	-----	-----	-----	-----	-----	-----	-----	-----	-----	-----	-----	-----	-----	-----	-----	-----	-----	-----	-----	-----	-----	-----	-----	-----	-----	-----	-----	-----	-----	-----	-----	-----	-----	-----	-----	-----	-----	-----	-----	-----	-----	-----	-----	-----	-----	-----	-----	-----	-----	-----	-----	-----	-----	-----	-----	-----	-----	-----	-----	-----	-----	-----	-----	-----	-----	-----	-----	-----	-----	-----	-----	-----	-----	-----	-----	-----	-----	-----	-----	-----	-----	-----	-----	-----	-----	-----	-----	-----	-----	-----	-----	-----	-----	-----	-----	-----	-----	-----	-----	-----	-----	-----	-----	-----	-----	-----	-----	-----	-----	-----	-----	-----	-----	-----	-----	-----	-----	-----	-----	-----	-----	-----	-----	-----	-----	-----	-----	-----	-----	-----	-----	-----	-----	-----	-----	-----	-----	-----	-----	-----	-----	-----	-----	-----	-----	-----	-----	-----	-----	-----	-----	-----	-----	-----	-----	-----	-----	-----	-----	-----	-----	-----	-----	-----	-----	-----	-----	-----	-----	-----	-----	-----	-----	-----	-----	-----	-----	-----	-----	-----	-----	-----	-----	-----	-----	-----	-----	-----	-----	-----	-----	-----	-----	-----	-----	-----	-----	-----	-----	-----	-----	-----	-----	-----	-----	-----	-----	-----	-----	-----	-----	-----	-----	-----	-----	-----	-----	-----	-----	-----	-----	-----	-----	-----	-----	-----	-----	-----	-----	-----	-----	-----	-----	-----	-----	-----	-----	-----	-----	-----	-----	-----	-----	-----	-----	-----	-----	-----	-----	-----	-----	-----	-----	-----	-----	-----	-----	-----	-----	-----	-----	-----	-----	-----	-----	-----	-----	-----	-----	-----	-----	-----	-----	-----	-----	-----	-----	-----	-----	-----	-----	-----	-----	-----	-----	-----	-----	-----	-----	-----	-----	-----	-----	-----	-----	-----	-----	-----	-----	-----	-----	-----	-----	-----	-----	-----	-----	-----	-----	-----	-----	-----	-----	-----	-----	-----	-----	-----	-----	-----	-----	-----	-----	-----	-----	-----	-----	-----	-----	-----	-----	-----	-----	-----	-----	-----	-----	-----	-----	-----	-----	-----	-----	-----	-----	-----	-----	-----	-----	-----	-----	-----	-----	-----	-----	-----	-----	-----	-----	-----	-----	-----	-----	-----	-----	-----	-----	-----	----

MILLSTONE

[illegible]

ARGENTINA

[illegible]

4.0 SONDRESTROM DRIFT OBSERVATIONS

The drift data obtained at Sondrestrom during the period 89188 - 89192 are illustrated in Figure 16. In the midnight sector, the drifts are generally close to antisunward, as expected for polar cap flows under B_z southward conditions. The antisunward direction is indicated by an oblique line in the frame marked A_z . Magnetic midnight is indicated by MM. Systematic offsets from straight antisunward, as seen e.g. 00-05 UT on 88-190, is likely due to the influence of B_y on the exact flow direction, as shown for the Qaanaaq data [Appendix B, Cannon et al., 1989]. Around 06 UT, the station passes through the convection reversal into a region of sunward (eastward) auroral flow. This remains strongly eastward until the noon sector when the direction switches through northward to strongly westward. In the late afternoon (18 UT) the convection reversal is crossed again, as Sondrestrom re-enters the polar cap. These changes are fairly abrupt in the data of Figure 16. In only one case, (Day 188, 18-24 UT) there is no clear transition from auroral to polar cap flow.

The drift speeds also varied dramatically during the five day period plotted in Figure 16. There is no dependence on time of day, although both the horizontal and vertical speeds measured in the polar cap tend to be larger than those in the auroral return flow. There is also no clear dependence on magnetic activity as defined by K_p (shown along the lower axis of the figure).

The most readily available corroborative data are the drift data from Qaanaaq (Figure 17). Qaanaaq is always inside the polar cap, and the nature of these measurements provides a strong indication of IMF conditions [see Appendix B, Cannon et al., 1989]. Again, the oblique lines plotted in the Frame marked Azimuth indicate the antisunward drift direction. The preliminary K_p indices

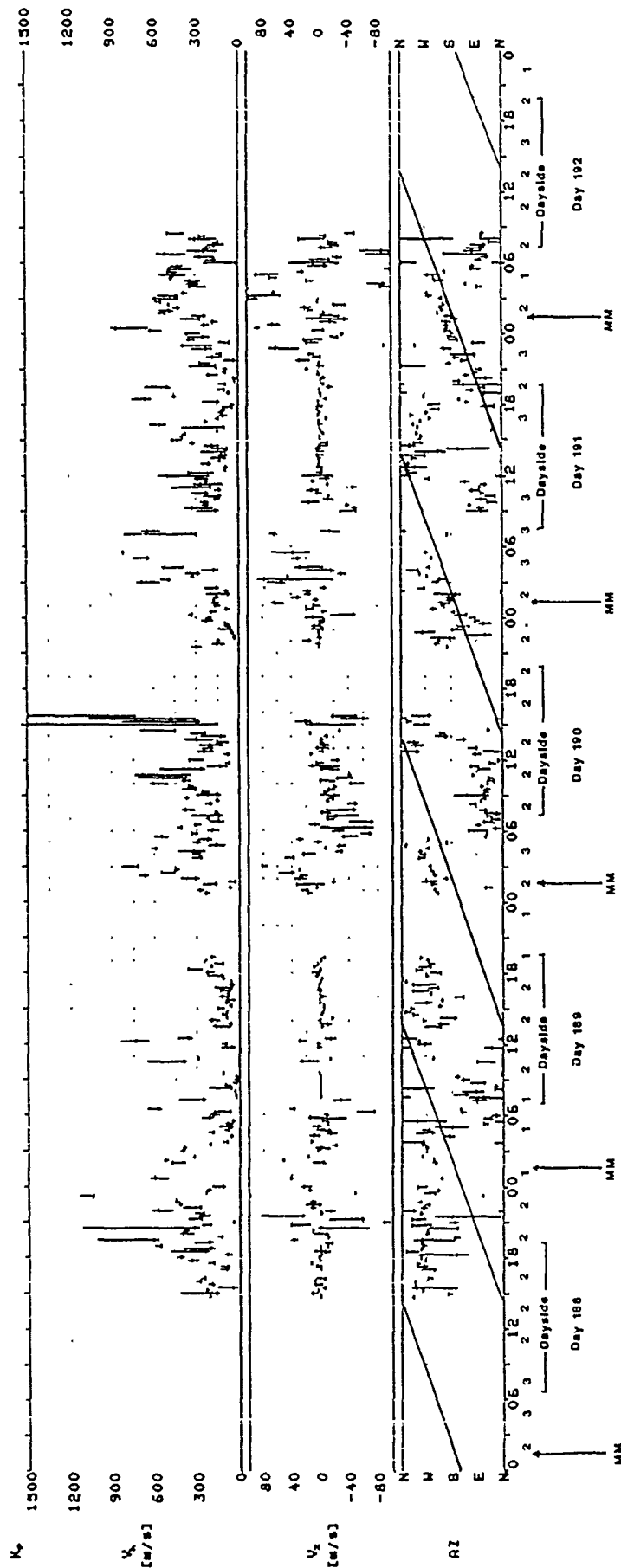


Figure 16. Sondrestrom Drift Data, 89188 to 898192

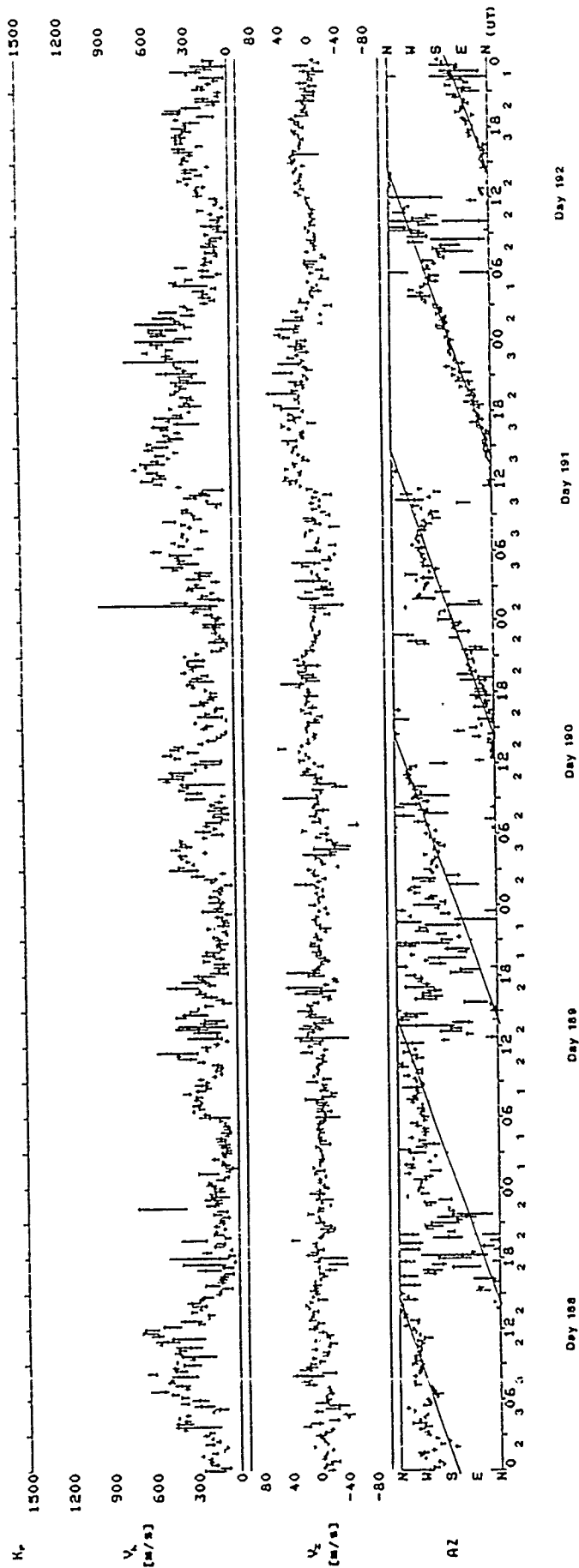


Figure 17. Qaanaaq Drift Data, 89188 to 898192

are shown along the lower axis of the figure, and vary from 1 to 3. The drift directions tend to be closer to antisunward for $K_p = 3$, while there is much more variation for lower K_p .

Since Sondrestrom and Qaanaaq are at approximately the same corrected magnetic local time (Figure 2), a polar plot in corrected magnetic coordinates provides an interesting opportunity to explore the large scale features of convection for that magnetic longitude. Figure 18 depicts the drift velocities observed at Sondrestrom and Qaanaaq as a function of CGLT for the 24 hour period between 06 UT Day 89191 and 0545 UT Day 89192. This was one of the most active intervals of the entire data set, according to the K_p index, and data from Sondrestrom and Qaanaaq were available almost continuously.

Several interesting features emerge from examination of Figure 18 (note that $UT \sim CGLT + 2$ hours). At the start of the interval, the Qaanaaq drifts diverge from the antisunward direction, becoming almost sunward by 09 CGLT, suggesting that the IMF B_z component is turning northward ($B_z > 0$). The Sondrestrom drifts are very variable during this interval, though sunward flows predominate from about 07 CGLT. At 0915 CGLT, the Qaanaaq flows change abruptly to antisunward, with high speeds around 600 ms^{-1} , typical of IMF B_z southward. The Sondrestrom flow also becomes antisunward before 10 CGLT, suggesting that plasma is entering the polar cap rapidly from the dayside.

At Qaanaaq, the drift direction remains antisunward for the entire day, until the last vector plotted at 0545, indicating that the IMF B_z component remained southward until 0545. The Sondrestrom drift variations are more complex. Using the result of Cannon et al. (1989) which is consistent with Heppner and Maynard (1987) for the influence of B_y on polar cap flows, it is possible to predict the sign of the IMF B_y component from the Qaanaaq flow direction. On average, B_y positive leads to deviations of 36° anti-

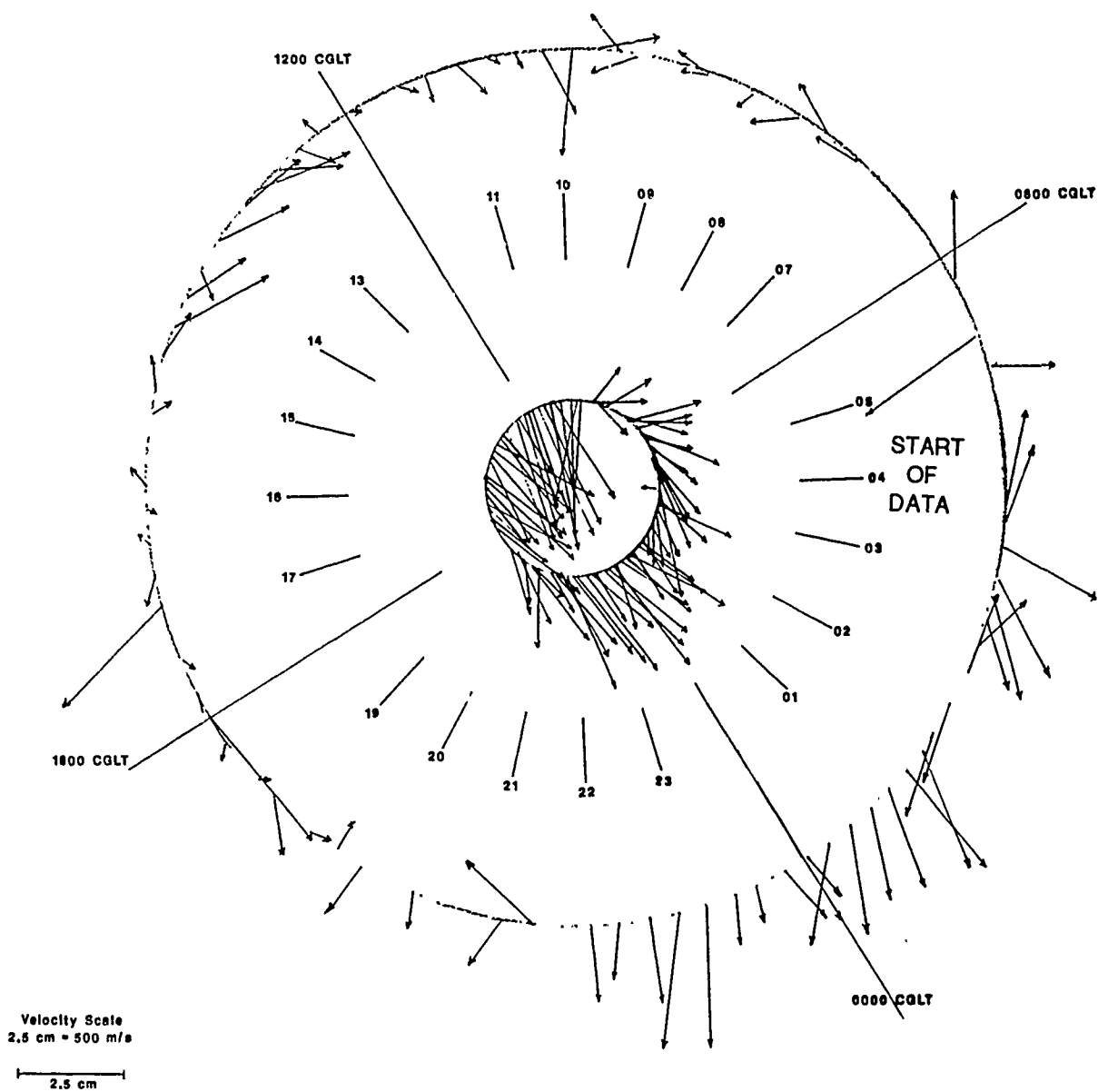


Figure 18. Drift at Sondrestrom and Qaanaaq

clockwise from the antisunward direction: B_y negative leads to deviations of -12° . Figure 19 depicts the predicted B_y direction based on the Qaanaaq data. For much of the time, the predictions based on Sondrestrom data are the same. For example at 03 UT the flow direction changes from approximately southward to strongly south westward, indicating an IMF B_y change from southward to northward. When IMF data become available in the near future, these predictions will be tested.

Unfortunately software is not yet available for plotting figures such as Figure 18 on a routine basis. Since these plots promise to be extremely useful, the appropriate software will be developed before other days are examined in detail.

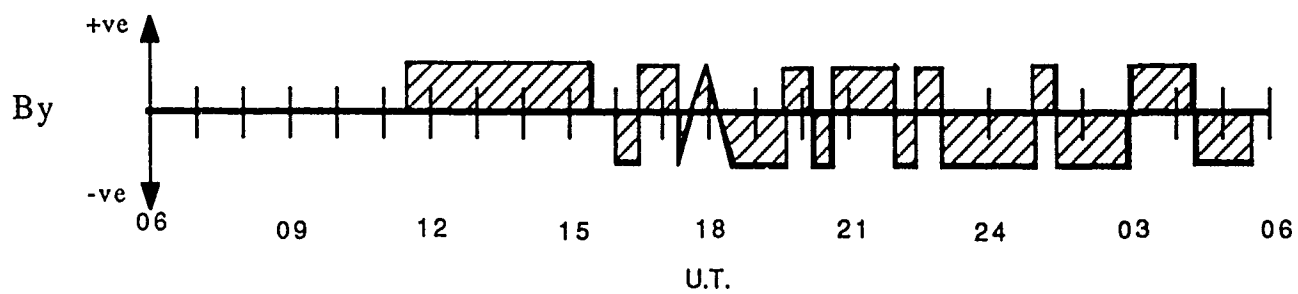


Figure 19. By Prediction Based on Qaanaaq Drift

5.0 SCIENTIFIC RESULTS

5.1 Published Papers

The research resulted in nine published papers as listed:

1. Basu, Sa., S. Basu, C. E. Valladares, E. J. Weber, J. Buchau, G. J. Bishop and B. W. Reinisch, "Coordinated Observations of High Latitude Ionospheric Turbulence," Physics of Space Plasmas (1988), SPI Conference Proceedings and Reprint Series, Vol. 8, pp. 137-151, 1988.
2. Bossy, L., R. R. Gamache and B. W. Reinisch, "Lay Functions for F2 Profiles," Adv. Space Res., Vol. 8, No. 4, pp. 4(201)-4(204), 1988.
3. Buchau, J., B. W. Reinisch, D. N. Anderson, E. J. Weber and C. G. Dozois, "Polar cap plasma convection measurements and their relevance to the modeling of the high-latitude ionosphere," Radio Sci., Vol. 23, No. 4, pp. 521-536, July-August 1988.
4. Cannon, P. S., B. W. Reinisch, J. Buchau and T. W. Bullett, "A Statistical Validation of the Digisonde Technique for Polar Cap F-Region Convection Measurements," submitted to JGR 1989.
5. McNamara, L. F., B. W. Reinisch and J. S. Tang, "Values of hmF2 Deduced from Automatically Scaled Ionograms," Adv. Space Res., Vol. 7, No. 6, pp. (6)53-(6)56, 1987.
6. Reinisch, B. W., J. Buchau and E. J. Weber, "Digital Ionosonde Observations of the Polar Cap F Region Convection," Physica Scripta, Vol. 36, pp. 372-377, 1987.
7. Reinisch, B. W., R. R. Gamache, X. Huang and L. F. McNamara, "Real Time Electron Density Profiles from Ionograms," Adv. Space Res., Vol. 8, No. 4, pp. (4)63-(4)72, 1988.

8. Reinisch, B. W., J. Buchau, K. Bibl and G. S. Sales, "Multistation/Multiparameter Observations with a Network of Digital Ionosondes," AGARD Conference Proceedings No. 441, pp. 37-1 - 37-9, 1988.
9. Reinisch, B. W., K. Bibl, G. S. Sales, J. Tang, Z.-M. Zhang, T. W. Bullett and D. F. Kitrosser, "The Digisonde 256 Ionospheric Sounder," SCOSTEP WITS Handbook #2, November 1989.

Appendix B of this report contains copies of papers 3 and 4; other papers were contained in Scientific Reports #1 and #2.

5.2 Scientific Reports

Two Scientific Reports have been published:

1. Reinisch, B. W., J. Buchau, E. J. Weber, L. F. McNamara and J. S. Tang, "Ionospheric Convection and Structure Using Ground-Based Digital Ionosondes," Scientific Report No. 1, AFGL-TR-88-0042, ULRF-440/CAR, February 1988. ADA194246
2. Reinisch, B. W., J. Buchau, R. R. Gamache, K. Bibl, G. S. Sales, X. Huang and L. F. McNamara, "Electron Density Profiles and Plasma Drift Measurements with Digital Ionosondes," Scientific Report No. 2, AFGL-TR-88-0233, ULRF-442/CAR, ADA205193, September 1988. ADA205193

5.3 Conference Presentations

Presentations were made at a number of conferences:

1. Buchau, J., D. N. Anderson, E. J. Weber, B. W. Reinisch and C. G. Dozois, "Polar Cap Plasma Convection and Real Time Modeling," Ionospheric Effects Symposium, Springfield, VA, May 1987.

2. Buchau, J., B. W. Reinisch, K. Bibl and D. F. Kitrosser, "New Research Opportunities with a Network of Digital Ionosondes," URSI General Assembly, Tel Aviv, Israel, 1987.
3. Cannon, P. S., J. Buchau, B. W. Reinisch, "Statistical Validation of Digisonde Drift Data from Qaanaaq," AGU, San Francisco, CA, December 1989.
4. Cannon, P. S., J. Buchau, B. W. Reinisch, G. Crowley and R. Lepping, "IMF Controlled Variations in the Convection Flow Direction Near the Corrected Geomagnetic Pole," US National URSI Meeting, Boulder, CO, January 1990.
5. Crowley, G. and B. W. Reinisch, "Qaanaaq Drift Observations in Support of the December 1988 CEDAR/HLPS Campaign," CEDAR Meeting, Boulder, CO, June 1989.
6. Crowley, G., J. Buchau and B. W. Reinisch, "First Results from the Digisonde at Sondrestrom," US National URSI Meeting, Boulder, CO, January 1990.
7. Hoeg, P., J. Buchau, B. W. Reinisch and J. K. Olesen, "Drift Measurements of E-Region Irregularities in the Polar Cap," AGU, San Francisco, CA, EOS December 1987.
8. Reinisch, B. W., J. Buchau and E. J. Weber, "Polar Cap F Region Plasma Convection," URSI General Assembly, Tel Aviv, Israel, 1987.
9. Reinisch, B. W. and J. Buchau, "Qaanaaq Drift Observations in Support of the January 88 CEDAR/HLPS Campaign," CEDAR Meeting, Boulder, CO, January 1988.
10. Reinisch, B. W., J. Buchau and P. S. Cannon, "Digital Ionosonde Measurements of High Latitude Ionospheric Convection," IAGA, Exeter, UK, July 1989.
11. Reinisch, B. W., J. Buchau and C. G. Dozois, "Correlating Polar Cap Plasma Drift with IMF," US National URSI Meeting, Boulder, CO, January 1989.

12. Reinisch, B. W., J. Buchau and C. G. Dozois, "Response of the Polar Cap Convection to Changes in the IMF," AGU Meeting, Baltimore, MD, May 1989.
13. Sales, G. S., B. W. Reinisch and C. G. Dozois, "A New Measure of Ionospheric Roughness," URSI General Assembly, Tel Aviv, Israel, 1987.

Papers #4, #7 and #11 are contained in Appendix B.

6.0 REFERENCES

Anderson, D. N., J. Buchau and R. A. Heelis, Origins of density enhancements in the winter polar cap ionosphere, Radio Sci., 23, No. 4, 1988.

Bibl, K. and B. W. Reinisch, The Universal Digital Ionosonde, Radio Sci., 13, p. 519, 1978.

Bibl, K. Resolves Multiple Reflectors with Multiplexed Closely Spaced Frequencies, in Commission F 1983 Symposium, Louvain, Belgium, pp. 1-4, June 1983.

Bibl, K., B. W. Reinisch and D. F. Kitrosser, Digisonde 256 - General description of the compact digital ionospheric sounder, University of Lowell Center for Atmospheric Research, 1981.

Bilitza, D., N. M. Sheik and R. Eyfrig, A global model for the height of the F2 peak using M3000 values from the CCIR numerical maps, Telecomm. J., 46, pp. 549-553, 1979.

Bossy, L., R. R. Gamache and B. W. Reinisch, Lay Functions for F2 Profiles, Adv. Space Res., Vol. 8, No. 4, pp. 4(201)-4(204), 1988.

Buchau, J., B. W. Reinisch, E. J. Weber and J. G. Moore, Structure and dynamics of the winter polar cap F region, Radio Sci., 18(6), p. 995, 1983.

Buchau, J., B. W. Reinisch, D. N. Anderson, E. J. Weber and C. Dozois, Polar cap plasma convection measurements and their relevance to the modeling of the high-latitude ionosphere, Radio Sci., 23, No. 4, pp. 521-536, 1988.

Bullett, T. W., Thesis, University of Lowell, 1990.

Cannon, P. S., B. W. Reinisch, J. Buchau and T. W. Bullett, "A Statistical Validation of the Digisonde Technique for Polar Cap F-Region Convection Measurements," submitted to JGR 1989.

Cauffman, D. P. and D. A. Gurnett, Satellite measurements of high-latitude convection field, *Space Sci. Rev.*, 13, p. 369, 1972.

Dozois, C. G., A high frequency radio technique for measuring plasma drifts in the ionosphere, Rep. AFGL-TR-83-0202, Air Force Geophys. Lab., Hanscom AFB, MA, ADA140509, 1983.

Dudeney, J. R., The accuracy of simple methods for determining the height of the maximum electron concentration of the F2 layer from scaled ionospheric characteristics, *J. Atmos. Terr. Phys.*, 45, pp. 629-640, 1983.

Dunge, J. W., Interplanetary magnetic field and the auroral zones, *Phys. Rev. Lett.*, 6, pp. 47-48, 1961.

Hakura, Y., Tables and maps of geomagnetic coordinates corrected by the higher order spherical harmonics terms, Rep. Ionos. Space Res. Jpn., 19, p. 121, 1965.

Heppner, J. P., Empirical models of high-latitude electric fields, *J. Geophys. Res.*, 82, 7, pp. 1115-1125, 1977.

Heppner, J. P. and N. C. Maynard, Empirical high-latitude electric field models, *J. Geophys. Res.*, 92, A5, pp. 4467-4489, 1987.

Hoeg, P., J. Buchau, B. W. Reinisch and J. K. Oleson, Drift Measurements of E-Region Irregularities in the Polar Cap, AGU, San Francisco, CA, EOS, December 1987.

Kelso, J. M., *Radio Ray Propagation in the Ionosphere*, McGraw-Hill, 1964.

Reinisch, B. W., New Techniques in Ground-Based Ionospheric Sounding and Studies, *Radio Sci.*, Vol. 21, No. 3, pp. 331-341, May-June 1986.

Reinisch, B. W., J. Buchau, K. Bibl and G. S. Sales, Multistation/Multiparameter Observations with a Network of Digital Ionosondes, AGARD Conference Proceedings No. 441, pp. 37-1 - 37-9, 1988b.

Reinisch, B. W., J. Buchau and E. J. Weber, Digital ionosonde observations of the polar cap F region convection, Phys. Scr., 36, p. 372, 1987.

Reinisch, B. W., R. R. Gamache, X. Huang and L. F. McNamara, Real Time Electron Density Profiles from Ionograms, Adv. Space Res., Vol. 8, No. 4, pp. (4)63-(4)72, 1988a.

Titheridge, J. E., Ionogram Analysis with the Generalized Program POLAN, World Data Center A for Solar Terrestrial Physics, Rep. UAG-93, 1985.

Weber, E. J., J. Buchau, J. G. Moore, J. R. Sharber, R. C. Livingston, J. D. Winningham and B. W. Reinisch, F layer ionization patches in the polar cap, J. Geophys. Res., 89(A3), p. 1683, 1984.

Whalen, J. A., Auroral oval plotter and nomograph for determining corrected geomagnetic local time, AFCRL-70-0422, ADA713170, 1970.

Whalen, J. A., The daytime F layer trough and its relation to ionospheric-magnetospheric convection, J. Geophys. Res., 94, A12, pp. 17,169-17,184, 1989.

Zhang, Z.-M., ARTIST Data Editing and Printing, ULCAR Report, 1989.

APPENDIX A

Invent of Drift Observations

from

Argentia, Goose Bay and Qaanaaq

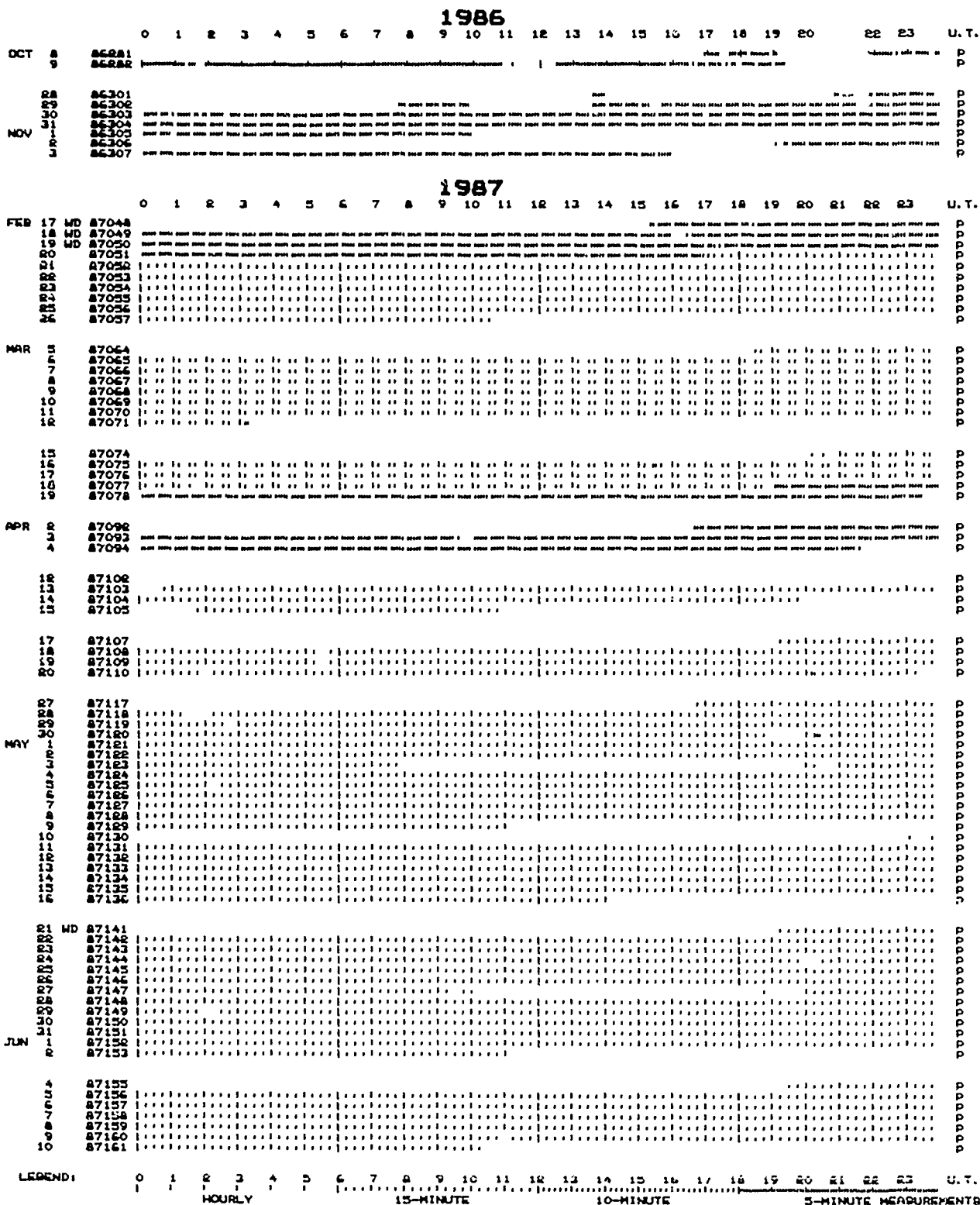


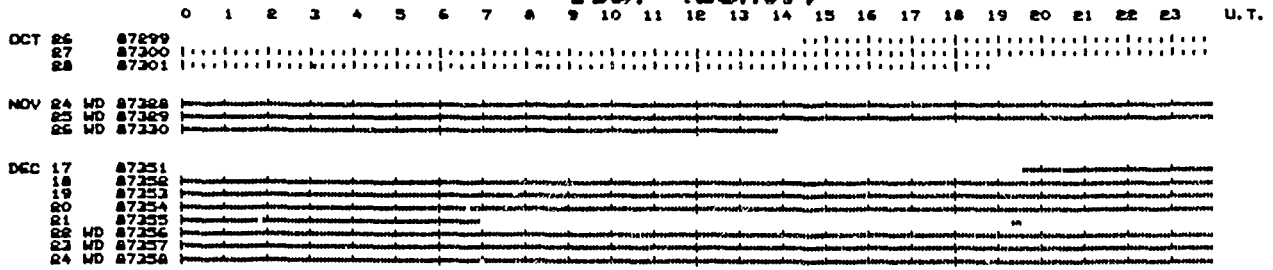
TABLE 1A: ARGENTIA DRIFT SURVEY

1987 (cont.)

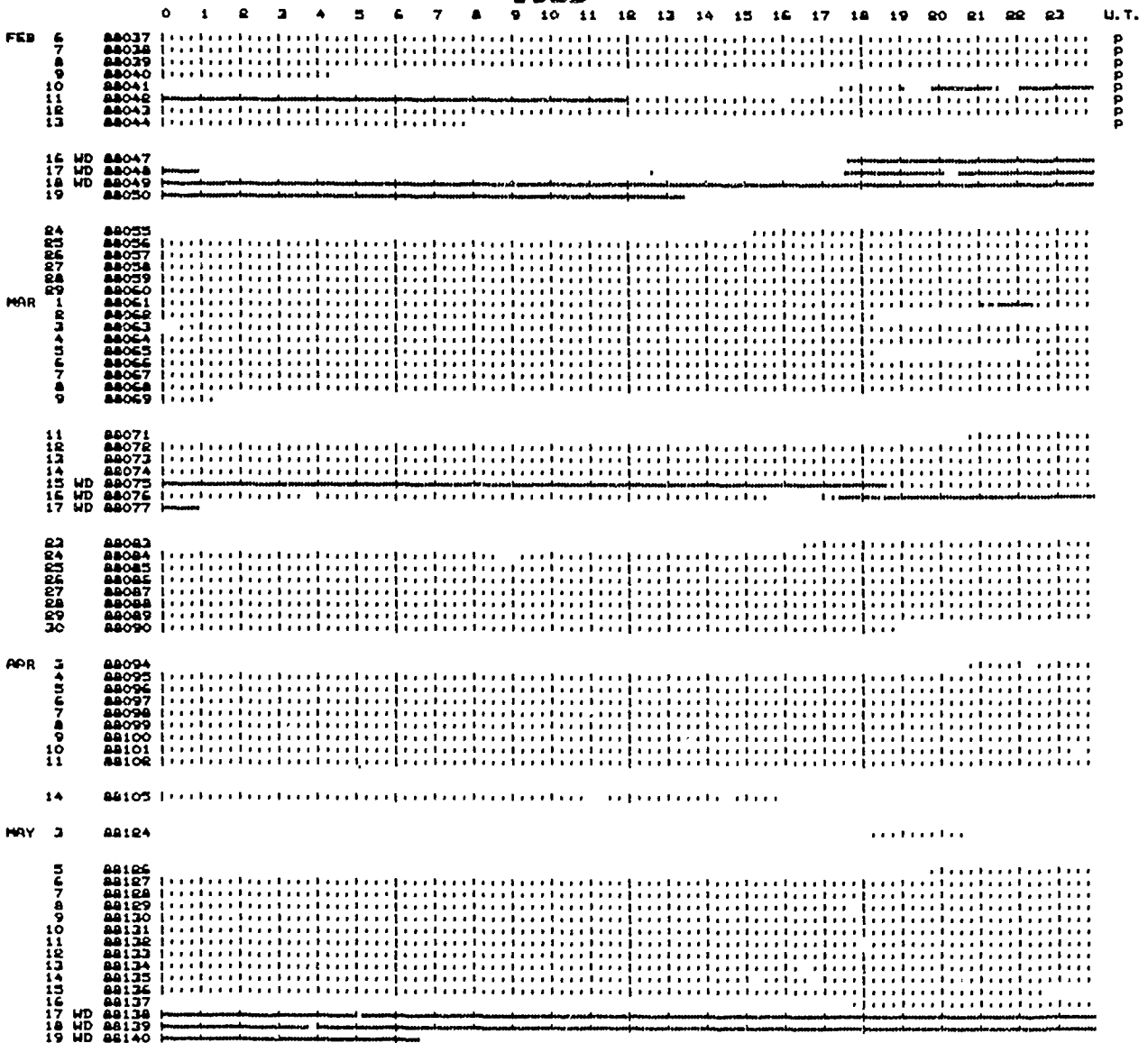
		0	1	2	3	4	5	6	7	8	9	10	11	12	13	14	15	16	17	18	19	20	21	22	23	U.T.	
JUN	12	87163																									P
	13	87164																									P
	14	87165																									P
	15	87166																									P
	16	87167																									P
	17	WD 87168																									P
	18	WD 87169																									P
	19	87170																									P
	20	87171																									P
	21	87172																									P
	22	87173																									P
	23	87174																									P
	24	87175																									P
	25	87176																									P
	26	87177																									P
	27	87178																									P
	28	87179																									P
	29	87180																									P
JUL	7	87188																									P
	8	87189																									P
	9	87190																									P
	10	87191																									P
	11	87192																									P
	12	87193																									P
	13	87194																									P
	14	87195																									P
	23	WD 87204																									P
	24	87205																									P
	25	87206																									P
	26	87207																									P
	27	87208																									P
	28	87209																									P
	29	87210																									P
	30	87211																									P
	31	87212																									P
AUG	1	87213																									P
	7	87219																									P
	8	87220																									P
	9	87221																									P
	10	87222																									P
	11	87223																									P
	12	87224																									P
	13	87225																									P
	14	87226																									P
	17	87229																									P
	18	WD 87230																									P
	19	WD 87231																									P
	20	WD 87232																									P
	21	87233																									P
	22	87234																									P
	23	87235																									P
	24	87236																									P
	25	87237																									P
	26	87238																									P
	27	87239																									P
	28	87240																									P
	29	87241																									P
	30	87242																									P
	31	87243																									P
SEP	1	87244																									P
	2	87245																									P
	3	87246																									P
	4	87247																									P
	5	87248																									P
	6	87249																									P
	7	87250																									P
	8	87251																									P
	9	87252																									P
	10	87253																									P
	13	87256																									P
	14	87257																									P
	15	87258																									P
	16	87259																									P
	17	87260																									P
	18	87261																									P
	19	87262																									P
	22	WD 87265																									P
	23	WD 87266																									P
	24	WD 87267																									P
	25	87268																									P
	26	87269																									P
	27	87270																									P
	28	87271																									P
	29	87272																									P
OCT	13	87284																									P
	14	87287																									P
	15	87288																									P
	16	87289																									P
	17	87290																									P
	18	87291																									P
	20	WD 87293																									P
	21	WD 87294																									P
	22	WD 87295																									P
	23	87296																									P

LEGEND: 0 1 2 3 4 5 6 7 8 9 10 11 12 13 14 15

1987 (cont.)



1988



LEGEND: 0 1 2 3 4 5 6 7 8 9 10 11 12 13 14 15 16 17 18 19 20 21 22 23 U.T.
 HOURLY 15-MINUTE 10-MINUTE 5-MINUTE MEASUREMENTS

TABLE 1C: ARGENTIA DRIFT SURVEY

1988 (cont.)

		0	1	2	3	4	5	6	7	8	9	10	11	12	13	14	15	16	17	18	19	20	21	22	23	U.T.	
MAY	22	00143																									
	23	00144																									
	24	00145																									
	25	00146																									
	26	00147																									
	27	00148																									
	28	00149																									
	29	00150																									
JUN	2	00154																									
	9	00151																									
	10	00152																									
	11	00153																									
	12	00154																									
	14 WD	00155																									
	15 WD	00157																									
	16 WD	00158																									
	17	00159																									
JUL	12 WD	00194																									
	14 WD	00196																									
	15	00197																									
	16	00198																									
	17	00199																									
	18	00200																									
	19	00201																									
	20	00202																									
	21	00203																									
	22	00204																									
	23	00205																									
	24	00206																									
	25	00207																									
	26	00208																									
	27	00209																									
	28	00210																									
	29	00211																									
AUG	1	00214																									
	2	00215																									
	3	00216																									
	4	00217																									
	5	00218																									
	6	00219																									
	7	00220																									
	25	00239																									
	27	00240																									
	29	00242																									
	30	00243																									
	31	00244																									
SEP	1	00245																									
	4	00248																									
	5	00249																									
	6	00250																									
	7	00251																									
	8	00252																									
	9	00253																									
	10	00254																									
	11	00255																									
	13 WD	00257																									
	14 WD	00258																									
	15 WD	00259																									
	16	00260																									
	17	00261																									
	18	00262																									
	19	00263																									
	20	00264																									
	21	00265																									
	22	00266																									
	23	00267																									
	24	00268																									
	25	00269																									
	26	00270																									
	27	00271																									
	28	00272																									
	29	00273																									
	30	00274																									
OCT	1	00275																									
	2	00276																									
	3	00277																									
	4	00278																									
	5	00279																									
	6	00280																									
	7	00281																									
	8	00282																									
	9	00283																									
	10	00284																									
	11 WD	00285																									
	12 WD	00286																									
	13 WD	00287																									
	14	00288																									
	15	00289																									
	16	00290																									
	17	00291																									
	18	00292																									
	19	00293																									
	20	00294																									
	21	00295																									
LEGEND:			0	1	2	3	4	5	6	7	8	9	10	11	12	13	14	15	16	17	18	19	20	21	22	23	U.T.
			HOURLY					15-MINUTE					10-MINUTE					5-MINUTE MEASUREMENT									

TABLE 1D: ARGENTIA DRIFT SURVEY

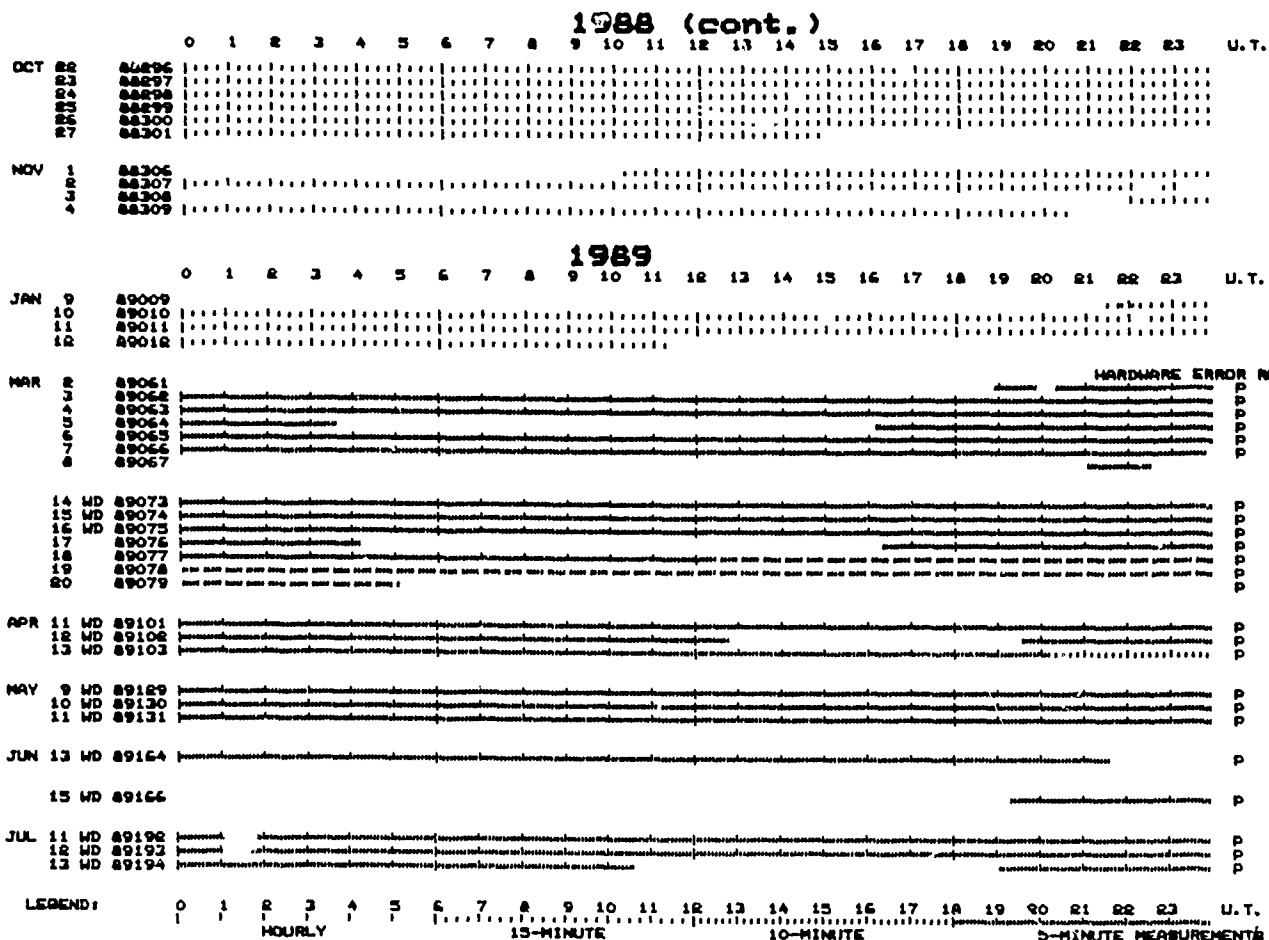


TABLE 1E: ARGENTIA DRIFT SURVEY

1988

		0	1	2	3	4	5	6	7	8	9	10	11	12	13	14	15	16	17	18	19	20	21	22	23	U.T.	
FEB	7	88038																									P
	8	88039																									P
	9	88040																									P
	10	88041																									P
	11	88042																									P
	12	88043																									P
	13	88044																									P
	14	88045																									P
	15	88046																									P
	16 WD	88047																									P
	17 WD	88048																									P
	18 WD	88049																									P
	19	88050																									P
	20	88051																									P
	21	88052																									P
MAR	14	88074																									P
	15 WD	88075																									P
	16 WD	88076																									P
	17 WD	88077																									P
	18	88078																									P
APR	19 WD	88110																									P
	24	88115																									P
	25	88116																									P
	26	88117																									P
	27	88118																									P
MAY	16	88137																									P
	17 WD	88138																									P
	18 WD	88139																									P
	19 WD	88140																									P
	20	88141																									P
JUN	14 WD	88166																									P
	15 WD	88167																									P
	16 WD	88168																									P
JUL	11	88193																									P
	12 WD	88194																									P
	13 WD	88195																									P
	14 WD	88196																									P
	15	88197																									P
AUG	26	88239																									P
	27	88240																									P
	28	88241																									P
	29	88242																									P
	30	88243																									P
SEP	13 WD	88257																									P
	14 WD	88258																									P
	15 WD	88259																									P
OCT	10	88284																									P
	11 WD	88285																									P
	12 WD	88286																									P
	13 WD	88287																									P
	14	88288																									P
NOV	8 WD	88313																									P
	9 WD	88314																									P
	10 WD	88315																									P
	11	88316																									P
DEC	2	88337																									P
	3	88338																									P
	5	88340																									P
	6	88341																									P
	7	88342																									P
	8	88343																									P
	9	88344																									P
	10	88345																									P
	11	88346																									P
	12	88347																									P
	13 WD	88348																									P
	14 WD	88349																									P
	15 WD	88350																									P
	16	88351																									P

1989

		0	1	2	3	4	5	6	7	8	9	10	11	12	13	14	15	16	17	18	19	20	21	22	23	U.T.	
JAN	16	89016																									
	17 WD	89017																									P
	18 WD	89018																									P
	19 WD	89019																									P

LEGEND:	0	1	2	3	4	5	6	7	8	9	10	11	12	13	14	15	16	17	18	19	20	21	22	23	U.T.	
	HOURLY					15-MINUTE					10-MINUTE					5-MINUTE MEASUREMENTS										

TABLE 2A: GOOSE BAY DRIFT SURVEY

0 1 2 3 4 5 6 7 8 9 10 11 12 13 14 15 16 17 18 19 20 21 22 23 U.T.

LEGEND: 0 1 2 3 4 5 6 7 8 9 10 11 12 13 14 15 16 17 18 19 20 21 22 23 U.T.
| | | | | | | | | | | | | | | | | | | | | | | | |
HOURLY 15-MINUTE 10-MINUTE 5-MINUTE MEASUREMENTS

85

1986

[illegible]

1987

		HOUR																								U.T.
		0	1	2	3	4	5	6	7	8	9	10	11	12	13	14	15	16	17	18	19	20	21	22	23	
JAN	20 WD	87060																								P
	21 WD	87061																								P
	22 WD	87062																								P
FEB	17 WD	87048																								P
	18 WD	87049																								P
	19 WD	87050																								P
	20	87051																								P
	21	87052																								P
	22	87053																								P
	23	87054																								P
	24	87055																								P
	25	87056																								P
	26	87057																								P
	27	87058																								P
	28	87059																								P
MAR	1	87060																								P
	2	87061																								P
	3	87062																								P
	4	87063																								P
	5	87064																								P
	6	87065																								P
	7	87066																								P
	8	87067																								P
	9	87068																								P
	10	87069																								P
	11	87070																								P
	12	87071																								P
	13	87072																								P
	14	87073																								P
	15	87074																								P
APR	16	87075																								P
	17	87076																								P
	18	87077																								P
	19	87078																								P
	20	87079																								P
	21	87080																								P
	22	87081																								P
	23	87082																								P
	24	87083																								P
	25	87084																								P
MAY	19 WD	87139																								P
	20 WD	87140																								P
	21 WD	87141																								P
JUN	16 WD	87167																								P
	17 WD	87168																								P
	18 WD	87169																								P
AUG	3	87214																								P
	4	87215																								P
	5	87216																								P
	6	87217																								P
	7	87218																								P
	8	87219																								P
	9	87220																								P
	10	87221																								P
	11	87222																								P
	12	87223																								P
	13	87224																								P
	14	87225																								P
SEP	15	87226																								P
	16	87227																								P
	17	87228																								P
	18	87229																								P

TABLE 3A: QANNAQ DRIFT SURVEY

1987 (cont.)

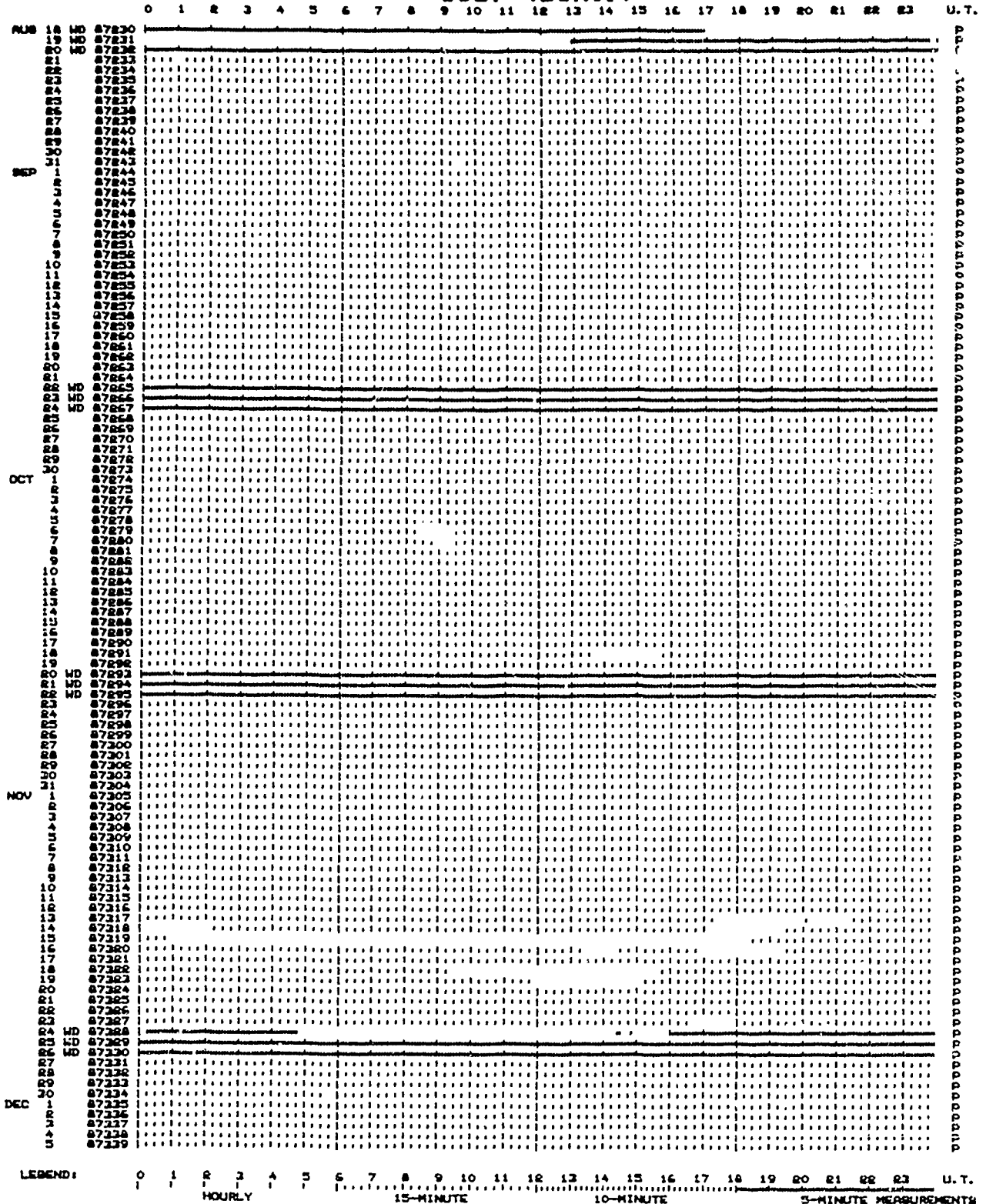


TABLE 3B: GAANAAG DRIFT SURVEY

1987 (cont.)

[illegible]

1228

[illegible]

LEGEND: 0 1 2 3 4 5 6 7 8 9 10 11 12 13 14 15 16 17 18 19 20 21 22 23 U.T.
| | | | | | | | | | | | | | | | | | | | | | | | | |
HOURLY 15-MINUTE 10-MINUTE 5-MINUTE MEASUREMENTS

TABLE 3C: QANNAQ DRIFT SURVEY

1988 (cont.)

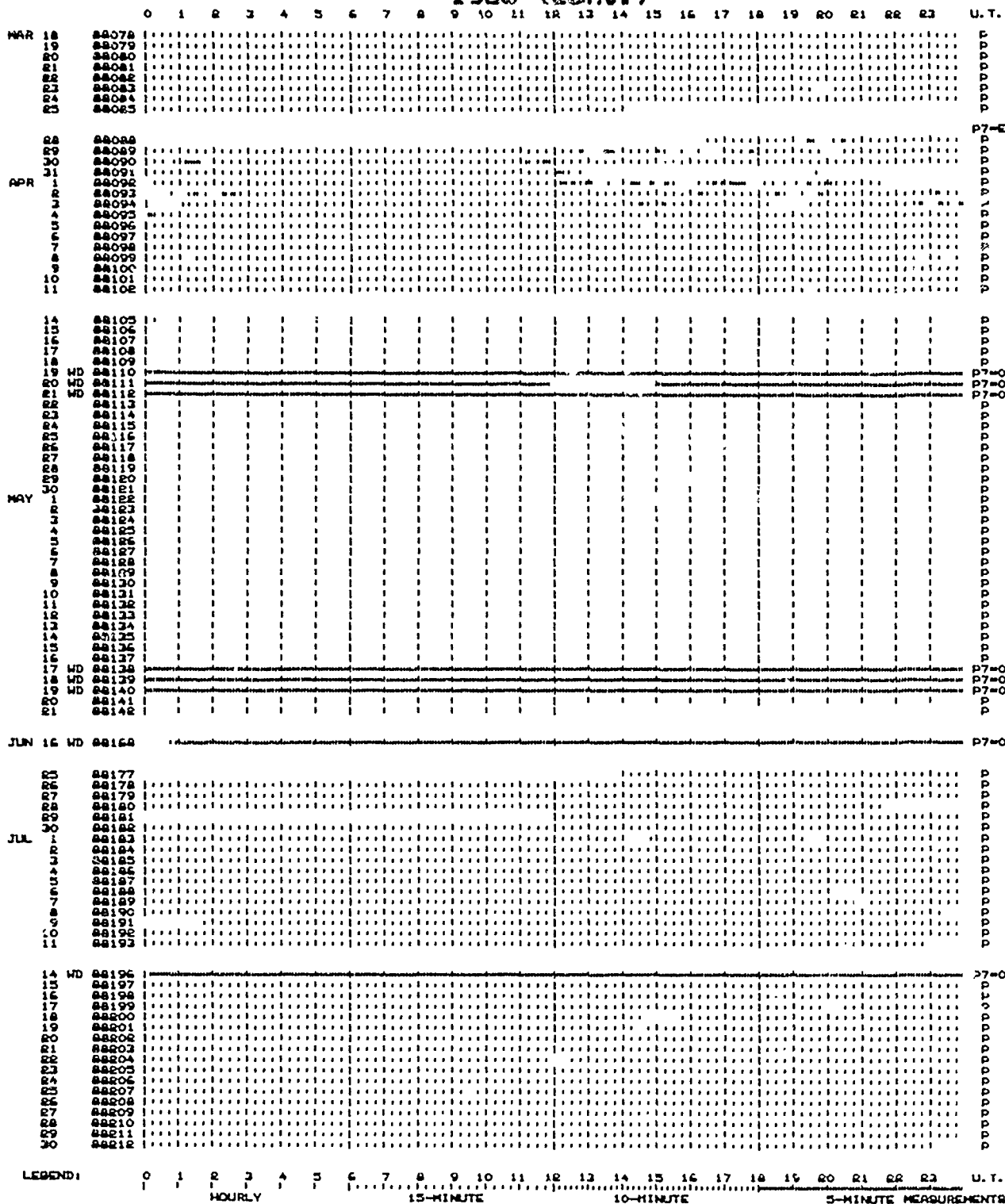


TABLE 3D: QAANAAQ DRIFT SURVEY

1988 (cont.)

[illegible]

TABLE 3E: QANAAQ DRIFT SURVEY

1988 (cont.)

[illegible]

1989

[illegible]

LEGEND :

0 1 2 3 4 5 6 7 8 9 10 11 12 13 14 15 16 17 18 19 20 21 22 23 U.T.
| | | | | | | | | | | | | | | | | | | | | |
HOURLY 15-MINUTE 10-MINUTE 5-MINUTE MEASUREMENTS

TABLE 3F: QANNAQ DRIFT SURVEY

1989 (cont.)

[illegible]

TABLE 3G: QANAAQ DRIFT SURVEY

1989 (cont.)

[illegible]

TABLE 3H: QANNAAG DRIFT SURVEY

APPENDIX B

Copies of Publications

For Presentation at the U.S. National URSI Meeting at Boulder, CO,
4-6 January 1989

Correlating Polar Cap Plasma Drift with IMF

Bodo W. Reinisch¹, Jurgen Buchau², and Claude G. Dozois¹

¹University of Lowell Center for Atmospheric Research,
450 Aiken Street, Lowell, Massachusetts 01854

²Air Force Geophysics Laboratory, Hanscom Air Force Base,
Bedford, Massachusetts 01731

Abstract

More than one year of polar cap drift data of the F region have been analyzed. The measurements were made at Qaanaaq, Greenland (87°N CGL) with a Digisonde 256 operated by the Danish Meteorological Institute. Drift velocities between 150 and 900 meters per second were observed. For several days in 1987 and for February 1988, interplanetary magnetic field (IMF) data were available and the direction of the F region drift was compared with the north-south component B_z of the IMF. For B_z negative, the drift is almost always antisunward; for B_z positive, it is irregular and often sunward. The response time of the ionosphere to sign changes in B_z is fast. Although fluctuations in B_z and the drift directions make it difficult to define a precise time, one can see a response often within less than 30 minutes.

Introduction

Since 1986 F region drift measurements were made in Qaanaaq, North Greenland (87° N CGL) with a Digisonde 256, operated by the Danish Meteorological Institute in cooperation with the Air Force Geophysics Laboratory and the University of Lowell. The general state of the ionosphere was observed with ionograms that were made every 5 or 15 minutes. Between the ionograms the Digisonde measured the F region drift using two different sounding frequencies, sampling the F layer at heights that are 50 to 150 km

apart. The sequence of ionogram/drift measurements is illustrated in Figure 1, which shows the on-line printout of an ionogram followed by eight consecutive drift measurements. The Digisonde drift technique has been previously described /1, 2/. This paper discusses some drift results for periods for which interplanetary magnetic field (IMF) data could be obtained from the National Space Science Data Center.

The Polar Cap Plasma Convection

The existence of polar plasma convection was first inferred from satellite-borne electric field measurements /3/ and plasma drift meter measurements /4/. Ground-based observations with the incoherent scatter radar (ISR) installations at Chatanika /5/ and Millstone Hill /6/ also determined the convection pattern. The Digisonde 256 can easily determine the plasma drift as function of time over long time periods. This allows to study in detail the effects of the IMF on the plasma convection for those times where IMF data are available.

Figure 2 shows Heelis's model /7/ of the convection pattern in a CGL/CGLT coordinate system. The Qaanaaq observatory moves around the magnetic north pole in 24 hours on the circle marked Q. The antisunward direction at Qaanaaq varies linearly with time, and since the plasma flow is expected to be antisunward for B_z south conditions, our data plots always show this direction.

Figure 3 shows the Qaanaaq drift data for 03 -05 March 1987, together with the z-component B_z of the IMF. The data are presented as function of universal time. The direction of the plasma drift is given in corrected geomagnetic coordinates, with south in the center of the panel, east is below and west above. The antisunward (asw) direction is indicated by the straight line. The magnitude of the drift vector, shown in the top panel, is given in m/s. For large data sets, this presentation is well suited for studies of the correlation between the orientation of the IMF and the direction of the plasma flow. It is not possible to determine the entire convection pattern with just one observing station. It would require at least 10 sounders strategically distributed to determine the shape of the convection pattern as function of time.

Case Studies

To illustrate the relation between B_z and the direction of plasma flow in the polar cap we briefly discuss the data shown in Figures 3 to 12, covering a number of days in March, May and June 1987, and in February 1988. The three days of drift data in Figure 3 show a typical behavior: the drift direction is largely antisunward (asw), with large deviations from asw when B_z turns positive. Determination of the response time of the ionospheric reaction to sign changes in B_z is only possible in some clearly defined cases. At 00 UT on March 4, it takes at least 30 min (there is a gap in the B_z data) for the plasma flow to become asw after B_z turns negative. On March 5 at 9:30 UT, the response time is about 2 hours.

On March 16 and 17 (Figure 4), B_z is predominantly positive and the plasma flow is very irregular. At 8:00 and 9:30 UT on March 16 (Figure 5), B_z goes through zero, and the drift direction changes within about 30 min. On March 18, B_z is predominantly positive and the drift direction is approximately sunward. At 20:30 UT, B_z turns negative and the drift directions becomes asw almost immediately. On March 22, B_z turns negative at 16:30 UT (Figure 6), and it takes about two hours before the drift turns asw.

The May data in Figure 7 show an exceptional situation. At 18:30 UT on May 20, B_z turns negative and remains negative for 9 hours, however, the drift does not turn asw. During the entire three days the drift velocity is unusually small, generally below 200 m/s. The June data (Figure 8) show a fairly regular asw drift; unfortunately, the B_z data have large gaps. An ionospheric response time of about one hour is seen at 19 UT on June 18, when B_z turns positive.

Figure 9 (February 9, 1988) shows another example at 21 UT where B_z is clearly negative, but the drift deviates significantly from asw. A similar behavior is seen for the first 90 min on February 25 (Figure 12). On February 10 (Figure 10) the drift turns sunward at 16:45 UT, about 30 min after B_z turns positive. A very clear B_z control can be seen for February 23: B_z oscillates through zero several times (Figure 11) and the drift changes accordingly from asw to sunward and back to asw with a response time of less than 15 min.

Conclusions

For the first time it has been possible to conduct extended ground-based measurements of the polar cap F region plasma flow and compare the response of the drift to the variations in B_z . It has been verified that the plasma flows asw when B_z is negative, and generally sunward when B_z is positive. There are exceptions, however, where the drift is not asw for some 4 hours, in one single case even 9 hours, even though B_z is negative. But these events are real exceptions. The response time of the plasma flow to sign changes of B_z varies from about 5 min to 2 hours. This explains why there are so widely differing statements in the literature about the response time. It was originally thought /8/ that the response time is 2 hours or more, while EISCAT observations suggested a 5 min or faster response /9/.

Acknowledgement

This research was supported by the Air Force Geophysics Laboratory under Contract F19628-86-K-0036. The authors thank Svend Erik Ascanius of DMI for the operation of the Digisonde 256.

References

1. Reinisch, B. W., J. Buchau and E. J. Weber, Digital ionosonde observations of the polar cap F region, Phys. Scr., 36, 372, 1987.
2. Buchau, J., B. W. Reinisch, D. N. Anderson, E. J. Weber and C. Dozois, Polar cap plasma convection measurements and their relevance to the modeling of the high-latitude ionosphere, Radio Sci., Vol. 23, No. 4, pp. 521-536, August 1988.
3. Cauffman, D. P. and D. A. Gurnett, Satellite measurements of high-latitude convection field, Space Sci. Rev., 13, 369, 1972.
4. Hanson, W. B. and R. A. Heelis, Techniques of measuring bulk gas motions from satellites, Space Sci. Instrum., 1, 493, 1975.
5. Foster, J. C., An empirical electric field model derived from Chatanika radar data, J. Geophys. Res., 88, 981, 1983.

6. Evans, J. V., J. M. Holt, W. L. Oliver and R. H. Wand, Millstone Hill incoherent scatter observations of auroral convection over $60^\circ \leq \lambda \leq 75^\circ$, 2, Initial results, J. Geophys. Res., 85, 41, 1980.
7. Heelis, R. A., J. K. Lowell and R. W. Spiro, A model of the high-latitude ionosphere convection pattern, J. Geophys. Res., 87(A8), 6339, 1982.
8. Wygant, J. R., R. Torbert and F. S. Mozer, J. Geophys. Res., 85, 5727, 1983.
9. Lockwood M., private communication.

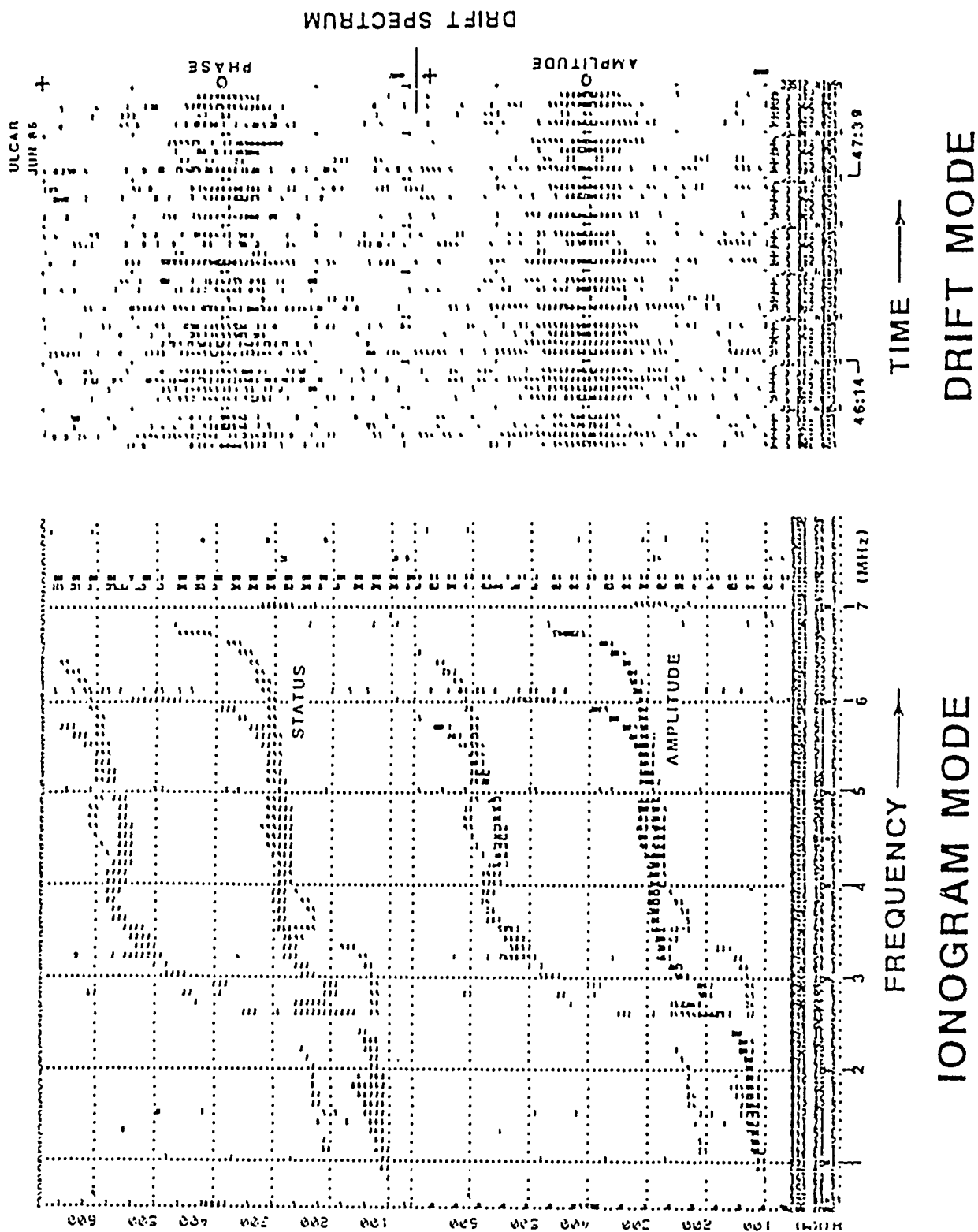


Fig. 1 IONOGRAM - DRIFT SEQUENCE

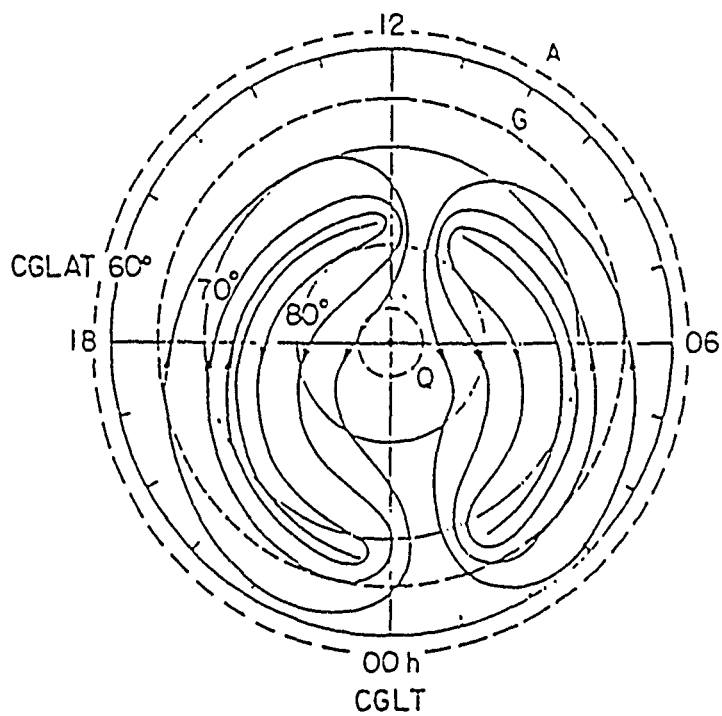
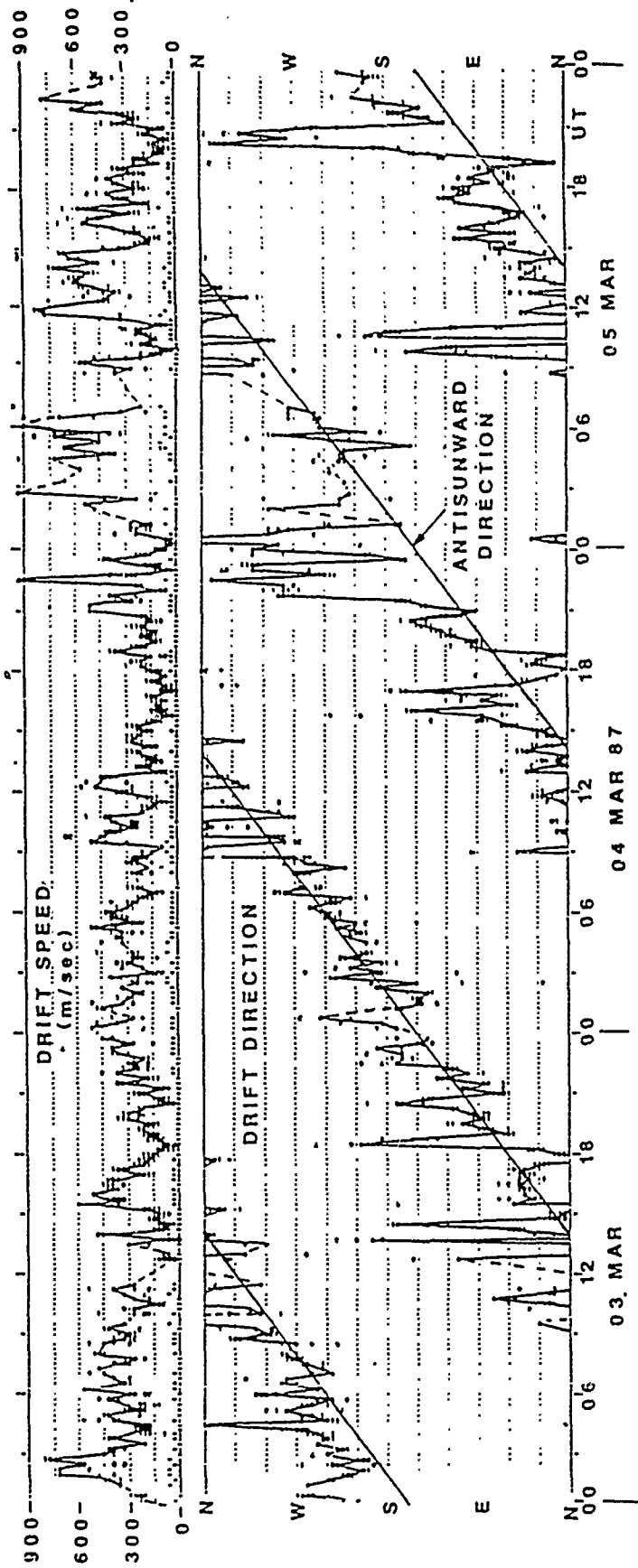


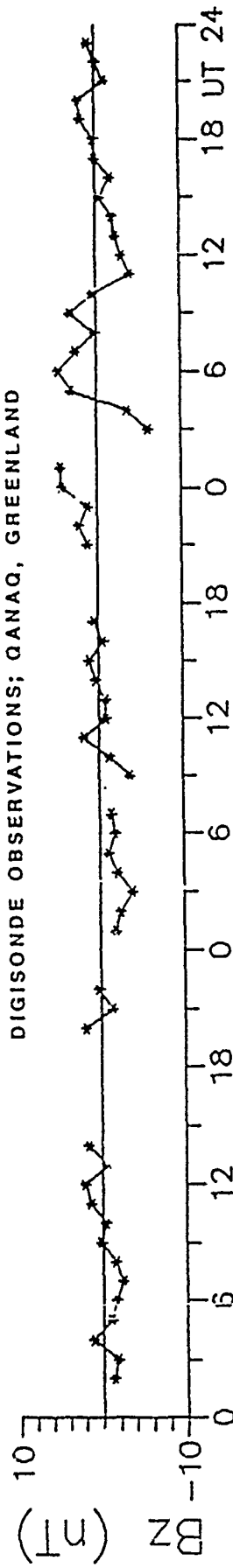
Fig. 2. Polar plasma convection pattern [Heelis et al., 1982] in CGL/CGLT coordinate system. The locations of the drift measuring stations Qaanaaq (Q), Goose Bay (G), and Argentina (A) are indicated by dashed circles.



104

F-REGION DRIFT

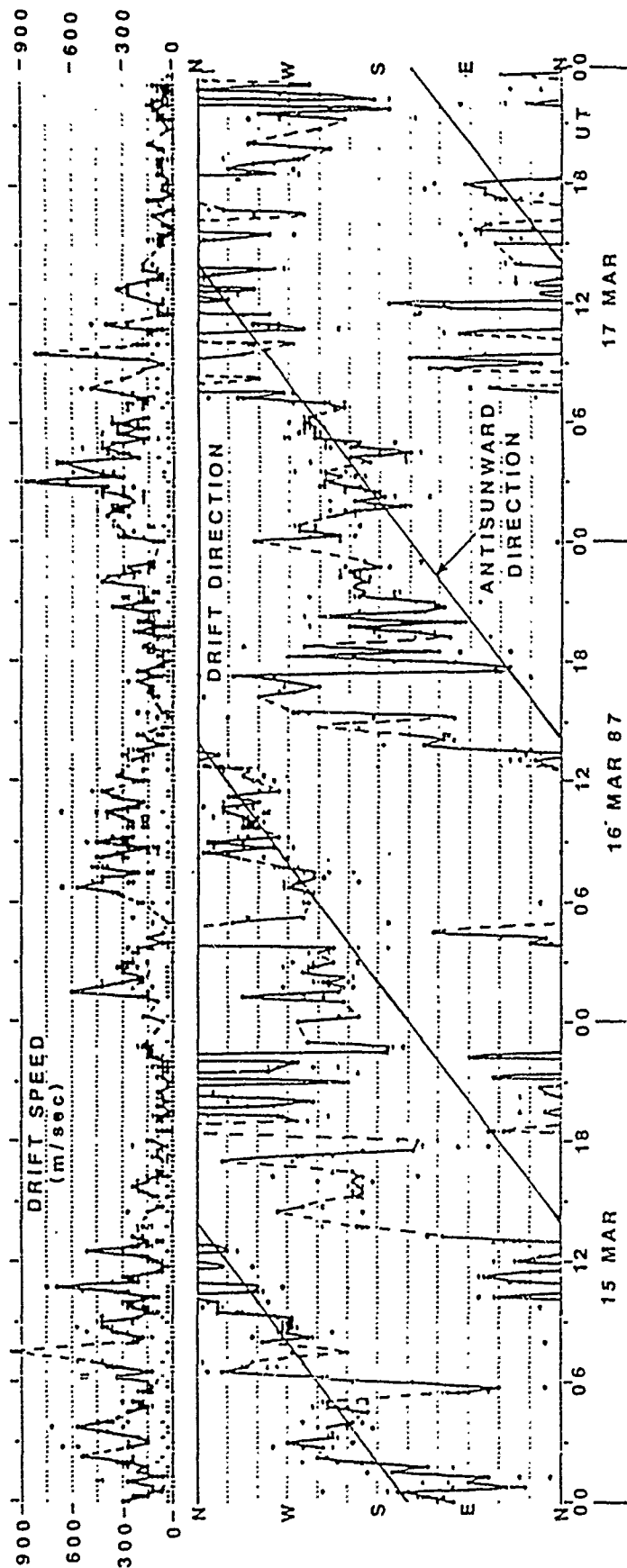
DIGISONDE OBSERVATIONS; QANAQ, GREENLAND



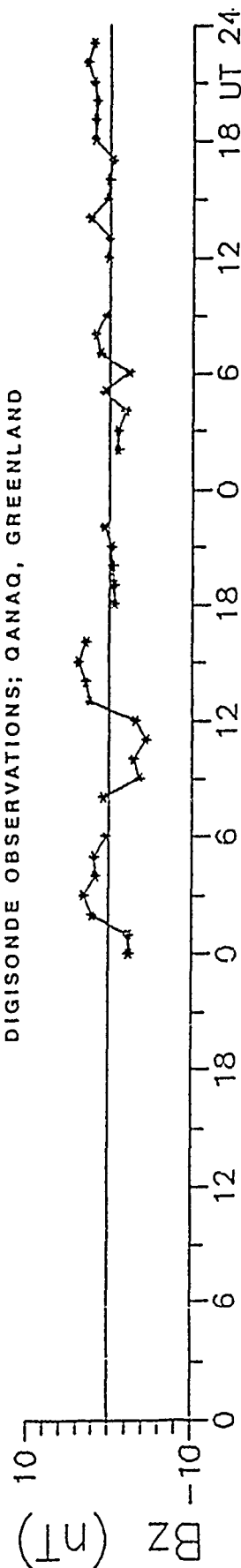
I.M.F. Bz 03-05 MARCH 1987

Bz data courtesy National Space Science Data Center

Fig. 3



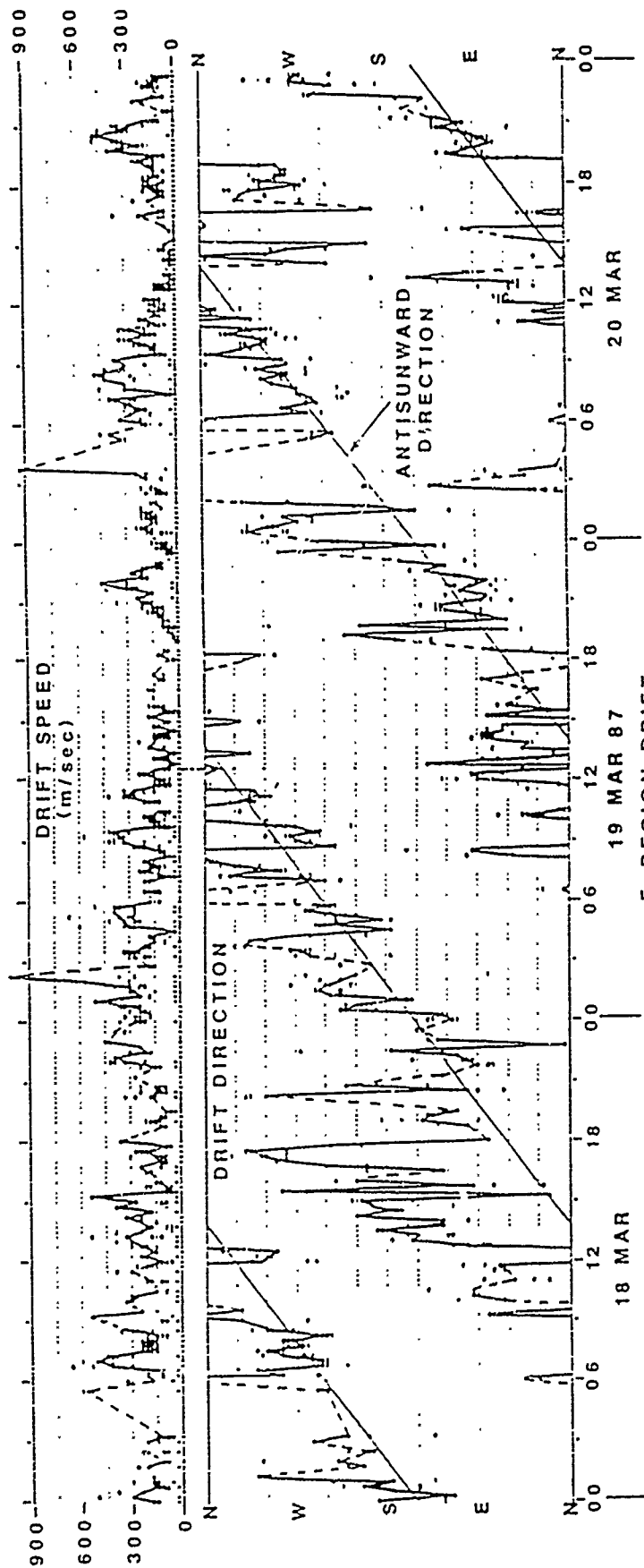
DIGISONDE OBSERVATIONS; QANAQ, GREENLAND



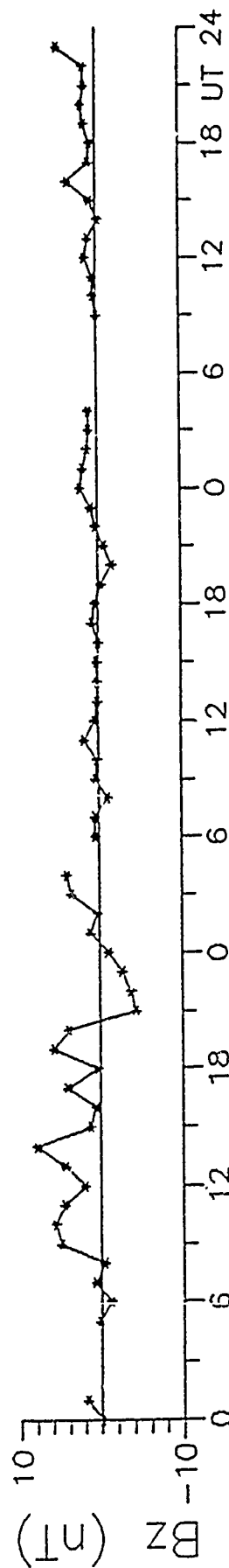
I.M.F. Bz 15-17 MARCH 1987

Bz data courtesy National Space Science Data Center

Fig. 4



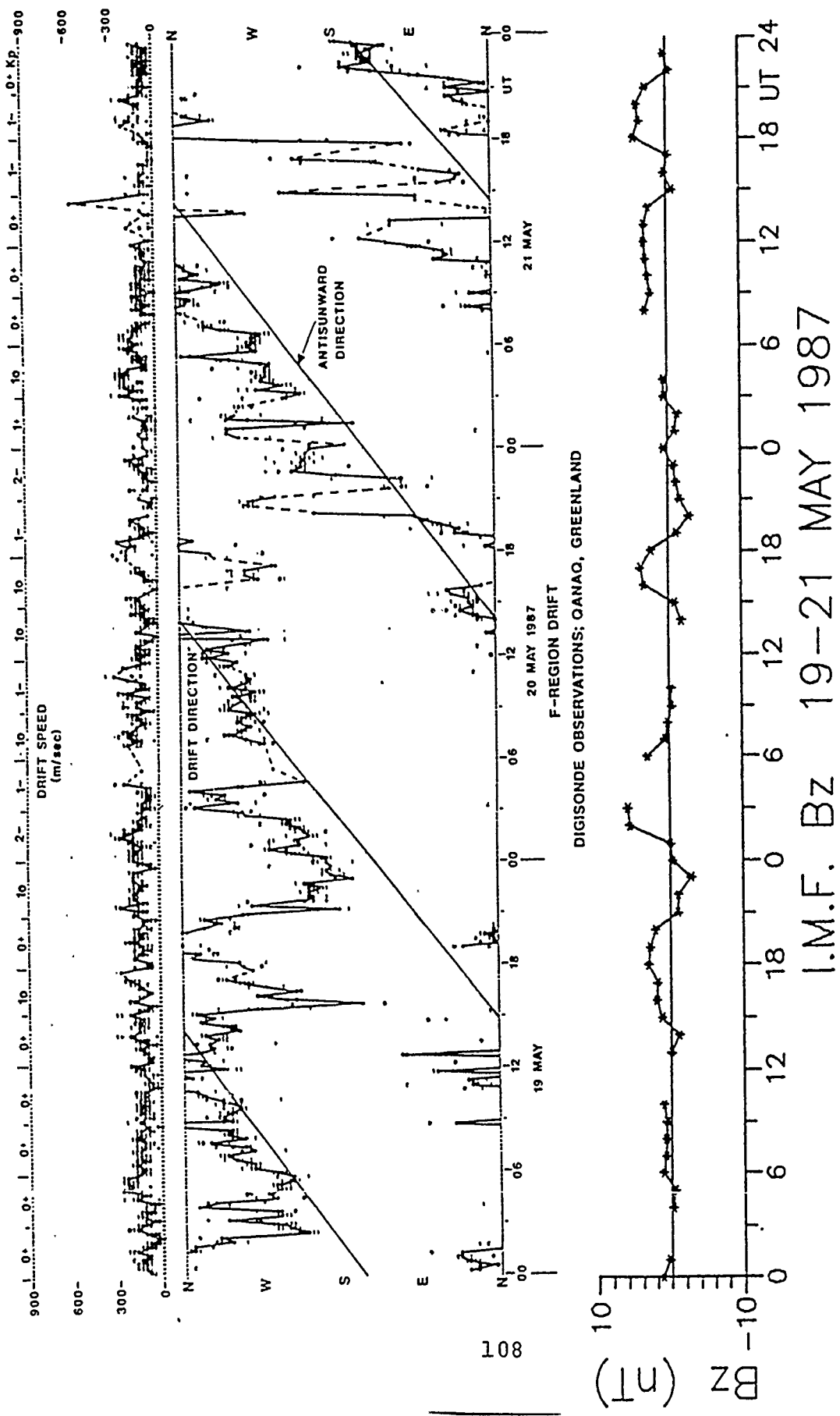
DIGISONDE OBSERVATIONS; QANAQ, GREENLAND



18-20 MARCH 1987

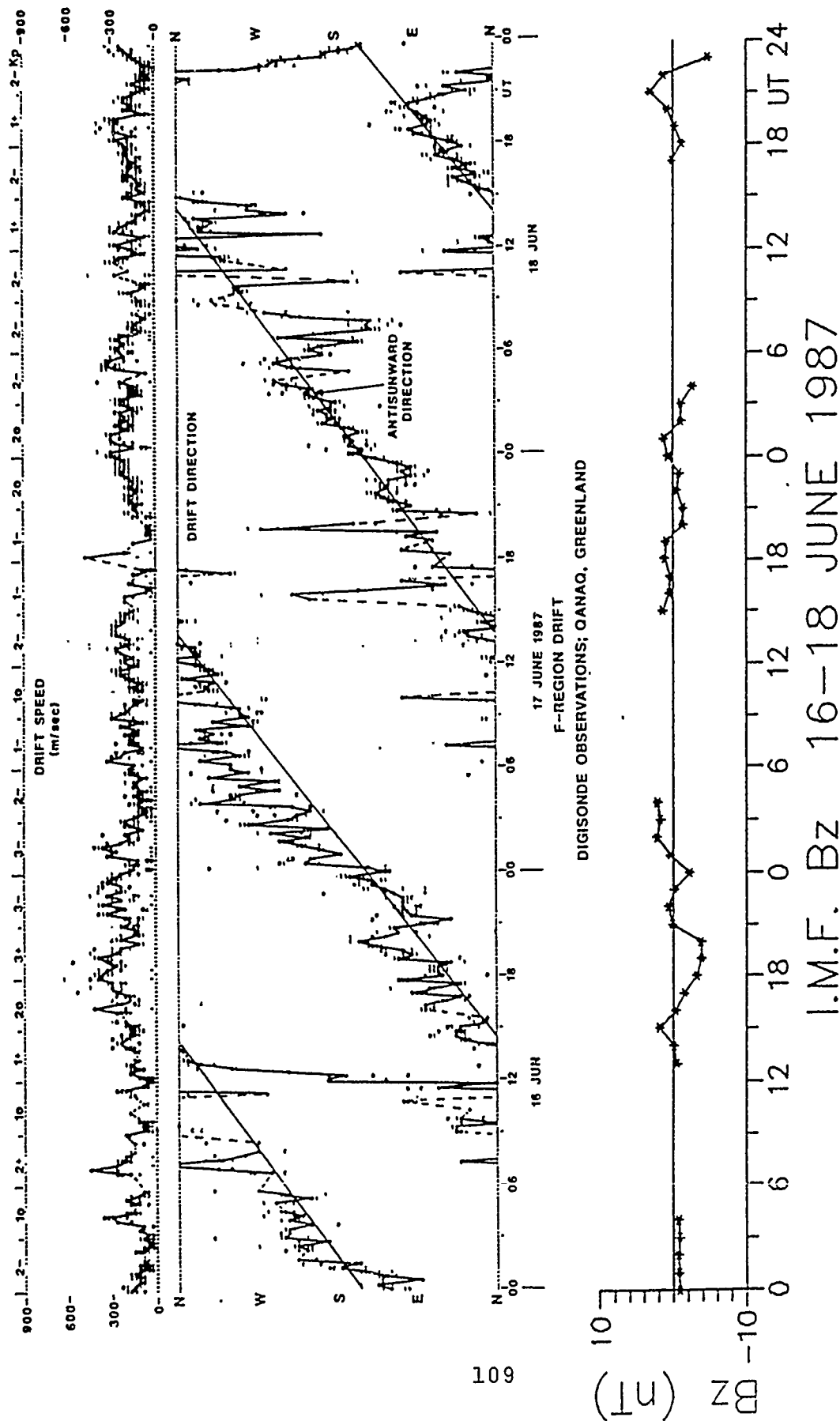
Bz data courtesy National Space Science Data Center

Fig. 5



Bz data courtesy National Space Science Data Center

Fig. 7



Bz data courtesy National Space Science Data Center

Fig. 8

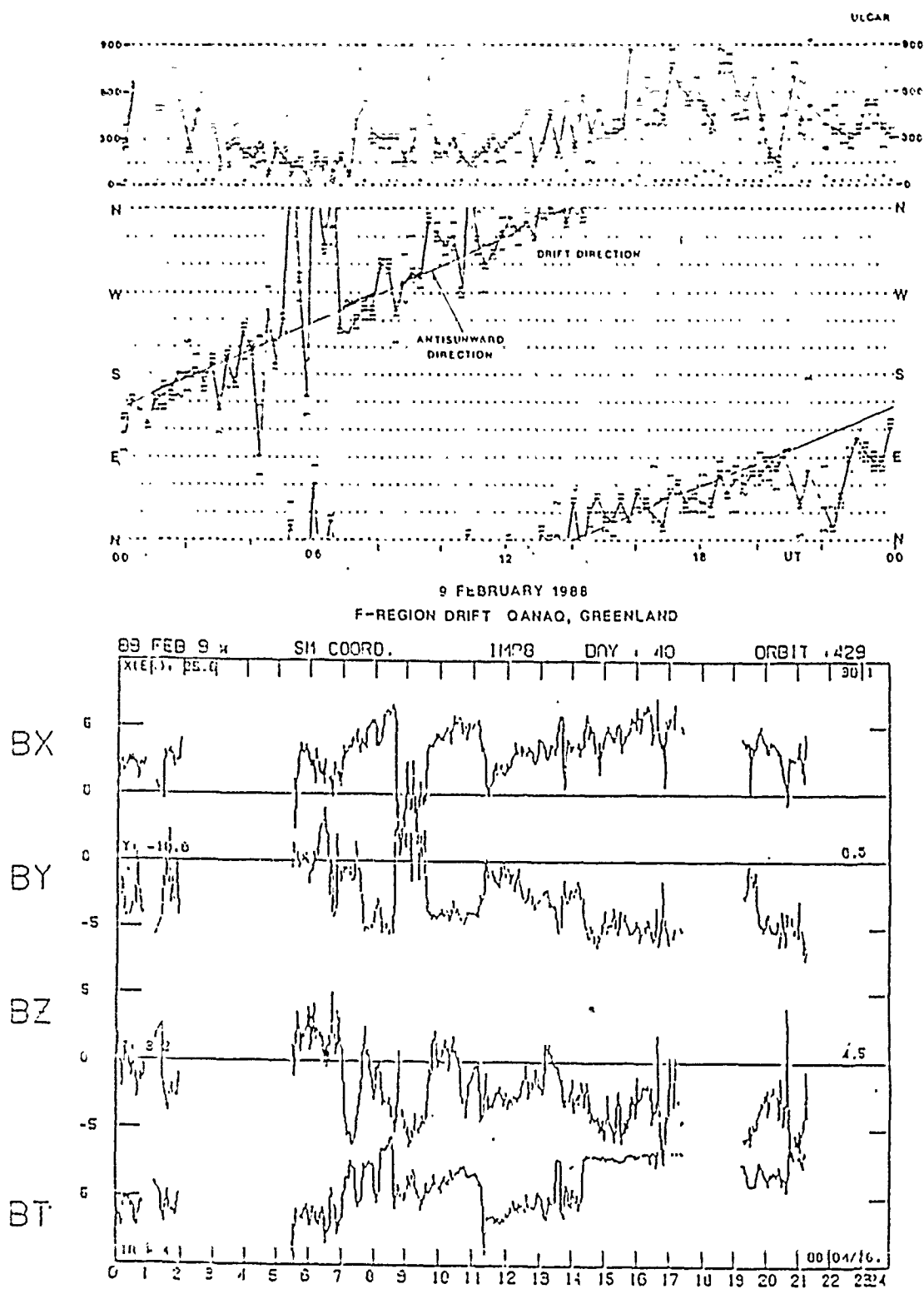
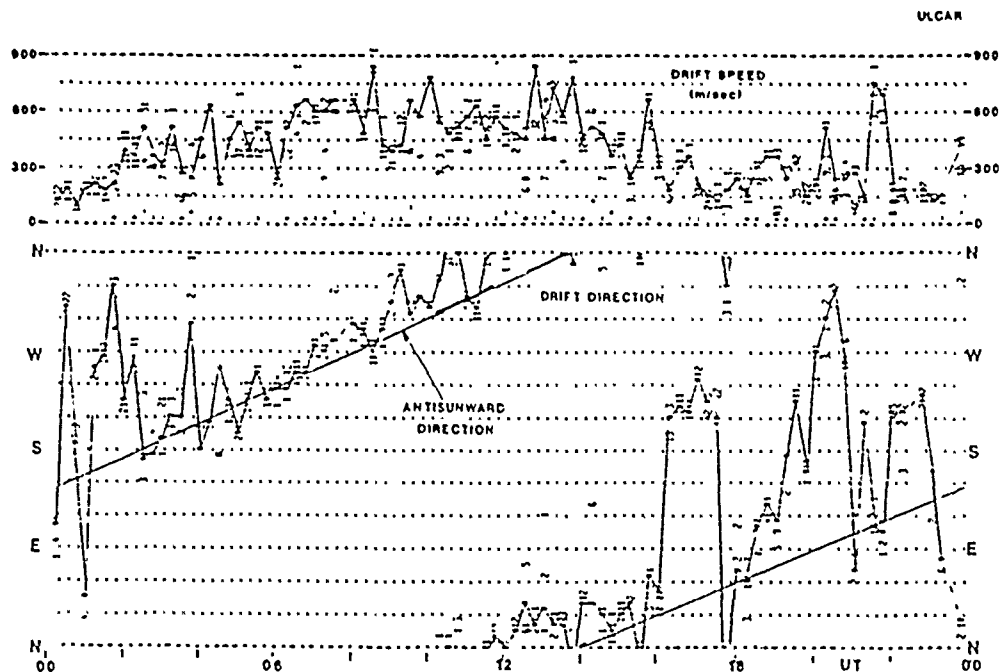


Fig. 9
110



10 FEBRUARY 1968

F- ION DRIFT OARAO, GREENLAND

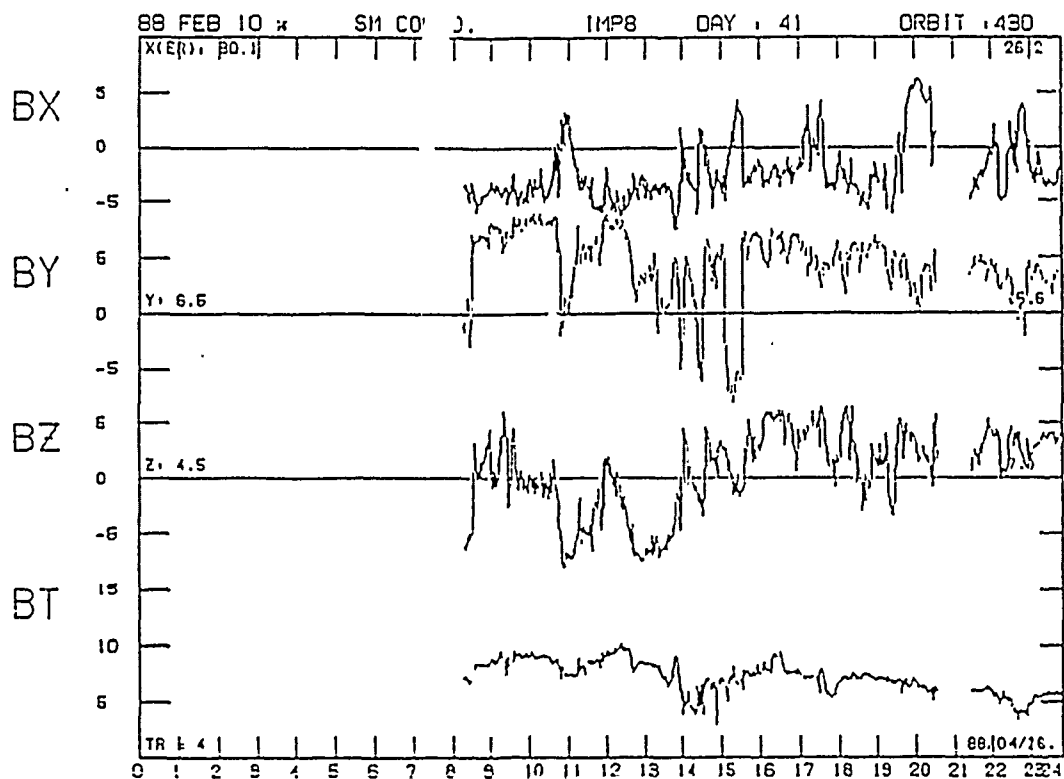


Fig. 10

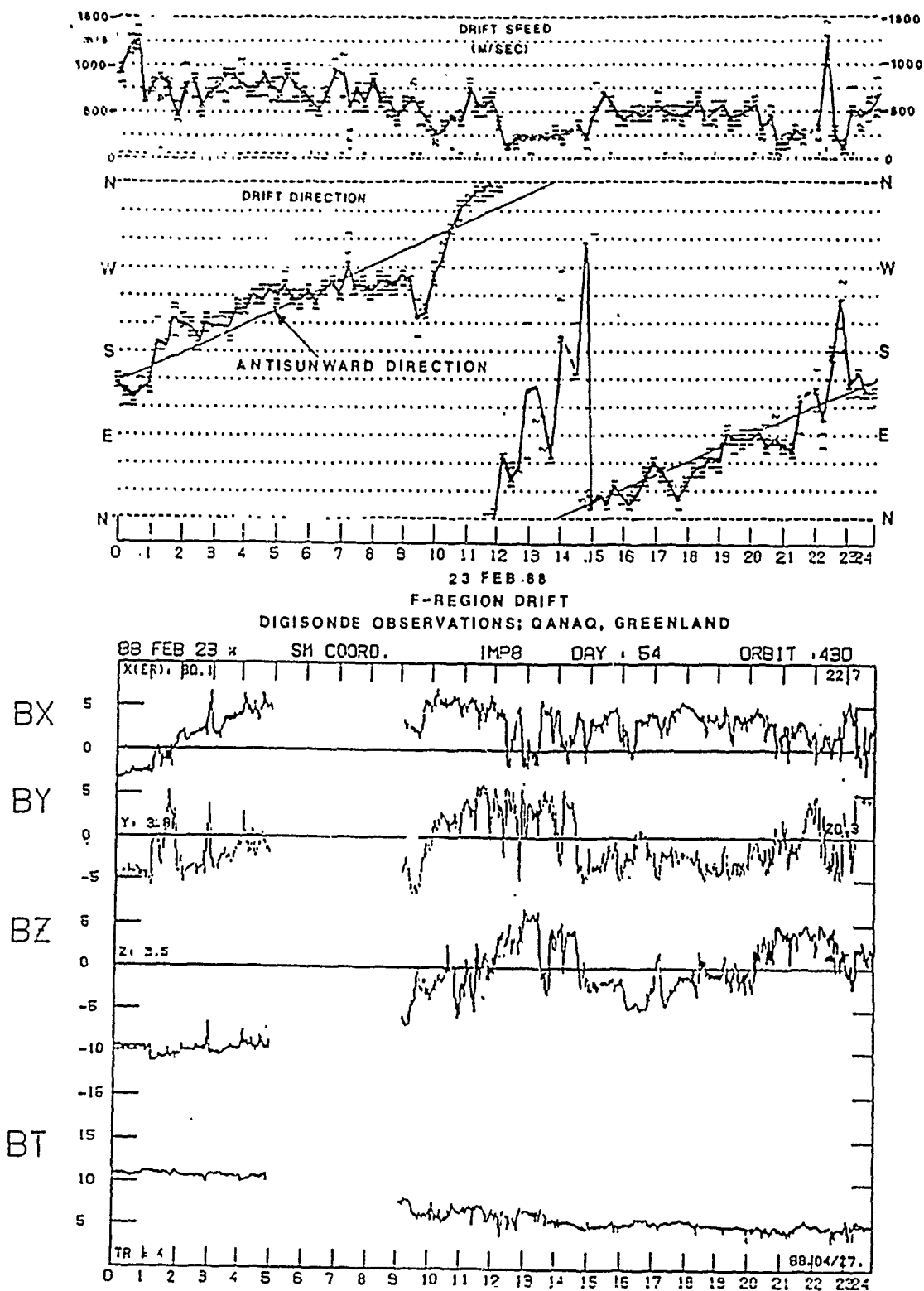


Fig. 11

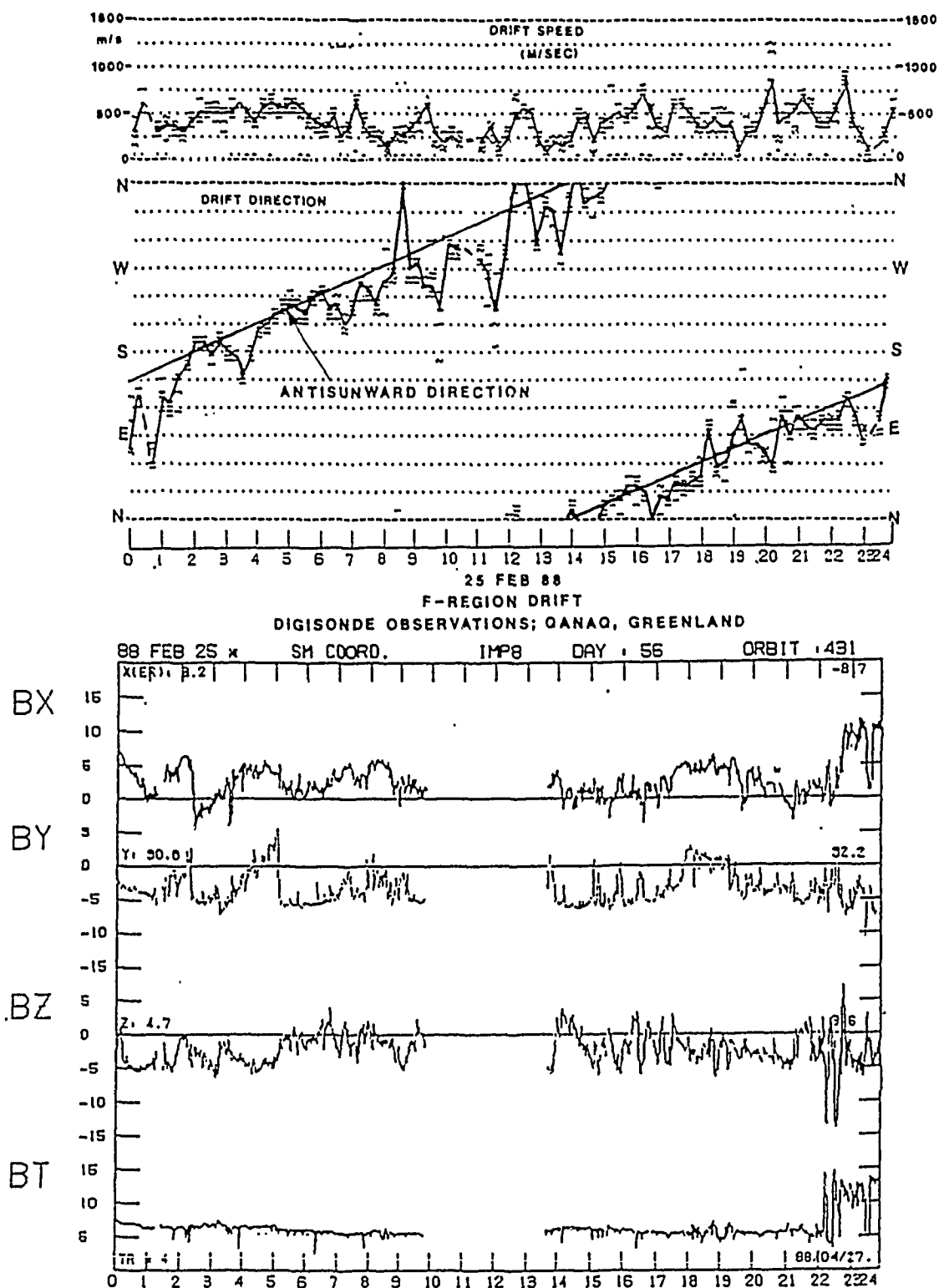


Fig. 12

For Submission to JGR.

A STATISTICAL VALIDATION OF THE DIGISONDE TECHNIQUE FOR POLAR CAP F REGION CONVECTION MEASUREMENTS.

Paul S. Cannon^{1,2}, Boris W. Reinisch,¹ Jurgen Buchau³ and Terence W. Bullett¹.

¹University of Lowell Center for Atmospheric Research, 450 Aiken Street, Lowell, Massachusetts 01854, USA

²Permanent Address - Applied Ionospheric Physics Laboratory, Flight Management Department, Royal Aerospace Establishment, Farnborough, Hampshire GU14 6TD, UK

³Geophysics Laboratory, Hanscom Air Force Base, Bedford, Massachusetts 01731, USA

ABSTRACT

Results of ionospheric drift measurements with a Digisonde 256 digital ionospheric sounder located at Qaanaaq, Greenland (87°N, corrected geomagnetic latitude), are presented. Digisonde drift data have been related to the interplanetary magnetic field (IMF) measured by the IMP8 satellite for thirty-two days during 1986, 1987 and 1988. Extremely good statistical agreement, between these measurements and convection directions derived from satellite instrumentation is demonstrated when the IMF z component is negative. For Bz negative and By negative the daily average convection direction is centred on -12° (anti-clockwise) from the anti-sunward direction. When Bz is negative but By is positive the convection direction is centred on +36°. These directions differ by respectively 3° and 9° from the models of Heppner and Maynard (1987). The variation about these values is $\sim \pm 20^\circ$. The excellent agreement between the Digisonde measurements and models derived from satellite measurements demonstrates the utility of the Digisonde for making ground based convection measurements in the polar cap F region when Bz is south. The convection directions under conditions of positive Bz have also been examined and we have measured three types of temporal variation in azimuth; namely an ordered and slowly (OS) varying change in direction, an ordered and quickly (OQ) varying change in direction, and disordered (D) variations in direction. The latter are believed to result from a breakdown of the analysis technique due to velocity shears in the vicinity of polar cap arcs and we estimate that they account for $\sim 25\%$ of the measurements when Bz > 0. When Bz is positive and By is negative our small subset of OS measurements supports the distorted two cell model of Heppner and Maynard (1987). The remainder of the measurements show no well defined daily average convection direction or diurnal variation. Likewise for Bz positive and By positive no well defined convection direction can be discerned, nor can any diurnal variation. The existence of OQ variations when Bz is > 0 suggests that meaningful average statistical convection patterns may be much harder to synthesize than similar patterns when Bz < 0.

1. INTRODUCTION

Magnetospheric electric fields play an important part in the control of the high latitude ionosphere. Ionospheric convection due to magneto-hydrodynamic coupling between the solar wind and the geomagnetic field was first suggested by Dungey (1961) who proposed a two cell pattern with antisunward flow across the polar cap when the interplanetary magnetic field (IMF) shows a southward directed component, (see also Axford and Hines, 1961). This simple two cell convection pattern has been further refined, extended and incorporated in models of the high latitude ionosphere (*eg* Sojka et al, 1986, Sojka and Schunk, 1987, Quegan et al., 1982). With this progress has come an improved understanding of the gross, and some of the detailed, aspects of the high latitude ionosphere.

Experimental information to act as the basis of the convection models and as a seed for the time dependent high latitude ionospheric models stems from a wide variety of sources (Sojka and Schunk, 1986). Satellite convection measurements have been made using double probe instrumentation aboard OGO6 (*eg* Heppner, 1972, 1977), instrumentation on board Atmosphere Explorer C (AE-C) (*eg* Heelis et al., 1976) and using data from Dynamics Explorer 2 (DE-2) (*eg* Heppner and Maynard, 1987). Other in-situ measurements of the electric field have been made by balloon probes (Mozer and Lucht, 1974) and rocket measurements (*eg* Maynard and Johnstone, 1974). Various ground based remote sensing techniques have also been employed including Incoherent Scatter Radars (ISR) located at Chatanika (Foster, 1981; 1983), Millstone Hill (Evans et al., 1980) and in Scandinavia using EISCAT (Folkestad et al, 1983). Coherent HF and VHF Radars have provided additional tools to investigate both E-region irregularities (Greenwald, 1978; Jones et al, 1985) and F-region irregularities (Greenwald et al. 1985; Ruohoniemi et al, 1987) and their associated electric fields.

Whilst these data have been used as input to theoretical models to deduce the temporal evolution of the ionosphere, they have been more usually employed, either separately or together, to derive average high latitude ionospheric convection patterns. When the IMF z (northward) component is negative many of these patterns exhibit the basically similar form of a two cell convection pattern. These include those derived by Heppner (1977) and later by Heppner and Maynard (1987) using pattern recognition of the cross polar cap potential distribution in order to minimise the spatial blurring which must necessarily be introduced by averaging. They also include the mathematically convenient models of Heelis et al. (1982) which describe the major features of the two cell convection pattern without undue complication. While the two cell models of these and other authors (see Schunk (1988) and references therein) concentrated on periods when the IMF z

component is southwards some models have examined the convection pattern for B_z north. Burke et al. (1979) suggested a four cell convection pattern and Lassen (1979) interpreted the polar cap auroral arcs, observed during magnetically quiet periods, as being the result of a shear associated with a third central polar cap cell. Potemra et al. (1984) also proposed three and four cell convection patterns with the number of cells and their size and location, dependent on the sign of B_y . Some of the expected ionospheric features of these multi-cell patterns have been modeled by Sojka and Schunk (1987). In contrast to the suggestion that three and four cell patterns represent the average convection pattern when B_z is northward Heppner and Maynard (1987) argued in favour of a distorted two cell model. The distortion proposed was that of a translational stretching of the evening cell focus towards and beyond noon, accompanied by a rotational twist of the streamlines around the foci. Progressively greater distortion was proposed as B_z increased.

Each of the different instruments, used in the derivation of the models, has advantages and disadvantages. Satellite-borne instrumentation provides good spatial coverage of the high latitude region at the expense of a long return time to any particular geographic region - typically the orbital period of a low altitude satellite is ~90 minutes. In addition, any deductions regarding the cross polar cap potential from satellite data must include some temporal blurring because the convection field is assumed to remain stable during the period (>10 min) that the satellite crosses the polar cap. Multistatic incoherent scatter radars provide excellent temporal resolution at the expense of some limitation on their spatial coverage. Monostatic ISR facilities are limited to making line of sight velocity measurements unless beam swinging techniques, coupled with assumptions of spatial uniformity and temporal stability of the bulk plasma velocity, are made. Other practical constraints also severely limit the operational availability of ISR facilities, making synoptic measurements difficult. The coherent HF and VHF radars provide good temporal resolution, their spatial coverage is significant, (particularly HF radars), and their near continuous operation makes them ideal for routine studies. The primary disadvantage of coherent radars is that the necessary radar wave vector to geomagnetic field orthogonality condition (Bates and Albee, 1970) cannot always be met in the desired region of the ionosphere. Further coverage restrictions are imposed by the logistics of locating the radar. These constraints are particularly severe for the high latitude VHF radars which are unable to benefit from ionospheric refraction to bring the ray path, at the interaction height, orthogonal to the local geomagnetic field. Nielsen and Schlegel (1985) have also shown that for metre scale irregularities in the E-region correction factors must be applied to accurately determine the drift magnitude and thus electric field. In the F-region this does not, however, appear to be a problem (Ruohoniemi et al, 1987).

An alternative and complementary form of instrumentation for ionospheric drift measurements is a digital, ground-based ionosonde employing an antenna array and

phase measurements to determine the arrival angles of the reflected signals. In this study a Digisonde 256, designed and built at the University of Lowell Center for Atmospheric Research (ULCAR) is employed. Like the coherent radars the Digisonde is ideal for synoptic measurements but unlike the coherent radars it does not rely on orthogonality between the ray direction and the geomagnetic field. Consequently, the logistical constraints of location are mitigated. The Digisonde can determine the drift by measuring the motion of isoionic contours. This is the most likely condition at mid-latitudes where the natural unevenness of these surfaces, accentuated by the transit of gravity waves, provides ample regions where off vertical perpendicularity is achieved. In the high latitude ionosphere, where the measurements described here were made, field aligned irregularities (FAIs) also exist throughout the ionosphere (*spread-F*). Here the orthogonality condition can often be met due to refraction, by the background ionisation, of the rather low frequency waves used in these measurements coupled with the large range and altitude extent of FAIs (Buchau and McNamara, 1986). The Digisonde also yields good time resolution with a nominal value of five minutes - under certain favourable conditions this may be improved upon. The disadvantage of the Digisonde is that it illuminates a relatively small area of the ionosphere above the antenna and current data reduction techniques require uniform ionospheric drift within the antenna beam.

Reinisch et al. (1987) showed good agreement between Digisonde measurements of F-region plasma drift and the major features of plasma convection patterns. Buchau et al. (1988), by examining various specific cases, showed that not only were the major convection features observed but also details such as convection reversals in response to quiet magnetic conditions. These two papers suggested that continuous monitoring of the large-scale features of the convection pattern, using a spatially diverse network of relatively inexpensive Digisondes, is possible.

The determination of drift velocities using the Digisonde is subject to certain assumptions which are not universally applicable. As a first step to investigating the ability of the technique for making ionospheric convection measurements in the high latitude region this paper discusses Digisonde drift measurements, from a site close to the corrected geomagnetic pole, as a function of the IMF. At this location, under $B_z < 0$ conditions, the plasma convection is known to be well ordered and quasi-laminar over large areas producing conditions for which the currently available Digisonde drift analysis technique has been developed. We demonstrate the efficacy of the technique for *polar cap* convection measurements by comparing our data with other measurements. Specifically, our statistical study will be compared to the extensive B_z negative statistical models of Heppner and Maynard (1987). A number of previous studies have demonstrated broadly anti-sunward flow during periods of negative B_z . The models of Heppner and Maynard (1987) show that when B_y is negative the convection streamlines, near the northern

geomagnetic pole, deviate in an anti-clockwise sense from the anti-sunward. Conversely, during periods when B_y is positive the average convection direction is rotated clockwise. We also discuss our measurements of ionospheric drift when B_z is positive. A statistical validation of the Digisonde drift measurement technique for plasma convection studies when B_z is northward is, however, difficult since there are no generally acceptable models of the plasma convection pattern.

Whilst the Digisonde is capable of measuring drift speeds, as well as directions, this paper will deal only with a comparison of the drift directions. The paper is divided into seven sections. In Section 2 a description of the Digisonde is given, together with a discussion of the assumptions built into the measurement technique, and in Section 3 the temporal evolution of the drift direction is examined by example. Section 4 describes the method of selecting Digisonde drift and IMF data with a view to examining the sensitivity of the measurement technique to variations in the IMF components B_y and B_z . Section 5 presents the results of these analyses and compares the results to the satellite convection models. Section 6 deals with the problem of how to interpret data during B_z positive periods which is more difficult to do than during periods when B_z is negative. In Section 7 we present the conclusions of the paper.

2. DESCRIPTION OF THE DRIFT MEASUREMENT TECHNIQUE AND HARDWARE AT QAANAAQ

The Digisonde (Bibl and Reinisch, 1978) drift technique uses *spectral analysis* of ionospheric echoes to locate the source of reflected signals (Pfister, 1974a, b); this is an important aspect of the technique which obviates the need for a large antenna array. Whilst the Digisonde drift technique can be employed to measure E-region drifts this paper is restricted to F-region measurements.

The hardware consists of a Digisonde 256 digital ionospheric sounder with one transmitter antenna and seven receiver antennas. The transmitter antenna has a beamwidth of $>90^\circ$ and illuminates a large area of the F-region above the ionosonde. The transmitter delivers 10 kW peak pulse power.

Seven receiver antennas are deployed on a 100 m equilateral triangle (Figure 1) although sometimes only the central four antennas are used. The array receives echo signals from a frequency dependent area which is $< 9 \times 10^4 \text{ km}^2$ in the F-region (equivalent to $(\sim 3^\circ)^2$ in latitude degrees). Specifically, at 10 MHz the 6 dB beamwidth of the array is $\sim 15^\circ$ with correspondingly larger values at the lower frequencies. Echoes are obtained from all points on a F-region isoionic surface where the plasma frequency is equal to the sounding frequency, and where the vector normal to the surface points towards the sounder (neglecting refraction

effects). In the polar cap F-region ionosphere kilometre scale irregularities and medium scale polar cap patches (eg Buchau et al., 1985; Weber et al., 1986) create a number of points off the vertical, where these conditions are met. The ionospheric drift is determined by measuring the Doppler frequencies of the individual echoes.

In the presence of multiple echoes a three dimensional drift velocity vector can be derived from this small array by using the radial Doppler velocity information associated with each echo. This may be achieved subject to two conditions. Firstly, the drift velocity must be uniform over the illuminated area. This is a particularly important restriction which we shall demonstrate is met in the polar cap under some IMF conditions. Secondly, the technique assumes that refraction effects can be ignored. The validity of this assumption has been demonstrated by Bullett (1990).

The Qaanaaq Digisonde records vertical ionograms every 5 or 15 minutes and the interval between each ionogram is utilised to make multiple measurements of the ionosphere bulk velocity. For these velocity measurements the single ionosonde receiver is multiplexed to either all seven or just four of the antennas at the pulse repetition frequency. The velocity measurements are made at two frequencies and two virtual ranges. The operating frequencies and range gates are automatically determined by a real time software system known as ARTIST (Automatic Real Time Ionogram Scaler with True height analysis). ARTIST is used to scale the ionogram immediately prior to the drift measurement and it selects two lower F-region frequencies ($\sim 0.5f_oF_2$) and two range gates which correspond to strong signals. Quadrature sampling of the signal received at each antenna is performed. These signals are Fourier transformed, in real time, to yield a complex Doppler spectrum for each antenna signal, $(A_i, \phi_i)_j$, with $i=1, \dots, 64$ (64 spectral lines) and $j=1, \dots, 4$ or 7 (for four or seven receiving antennas), which are recorded on magnetic tape for post processing.

Dozois (1983) has described how the echo data are being processed to generate the required drift information. In the post processing phase those Doppler lines which have significant signal energy are identified as "sources" of reflected signal. The spectral indices, i give the Doppler frequency, d_s of each source:

$$d_s = \frac{1}{\pi} \mathbf{v} \cdot \mathbf{k}_s \quad s = 1, 2, \dots (\text{source index})$$

where \mathbf{v} is the source drift velocity and \mathbf{k}_s the vector from the reflection point, s to the receiving antennas. From the spectral phases ϕ_{ij} across the antenna array, the source wave vector, \mathbf{k}_s is determined. The intersection of these \mathbf{k}_s vectors with the horizontal plane, at the virtual range gate, generates skymaps of the source locations. Figure 2 shows a skymap sequence covering one and a half hours.

The three-dimensional velocity vector \mathbf{v} is estimated from a collection of source locations, defined by \mathbf{k}_s and Doppler shifts d_s , by minimizing the least-square error :

$$\epsilon^2 = \sum_s \left[d_s - \frac{1}{\pi} \mathbf{v} \cdot \mathbf{k}_s \right]^2 \quad s = 1, 2, 3, \dots \text{ (source index).}$$

The technique breaks down when there are less than three sources and the errors become large when the sources are tightly clustered.

The unaliased upper limit of measurable drift velocities is constrained by the antenna sampling frequency. To maximize this limit more recent Qaanaaq Digisonde drift measurements use only four antennas and a 200 Hz pulse repetition frequency together with two frequencies and two ranges. Earlier measurements used a seven antenna configuration which decreased the sampling frequency. A ± 32 point spectrum is generated every 5.12 s with a spectral resolution of 0.1953 Hz. In the four antenna configuration the frequency range for unaliased signals is ± 6.25 Hz. This frequency range corresponds to a line of sight velocity of 312.5 ms^{-1} at 3.0 MHz, a typical measurement frequency. Most sources are, however, found nearer the zenith than the horizon and consequently the maximum horizontal velocity is significantly greater than 312 ms^{-1} . For a source located at 19° to the zenith the equivalent maximum horizontal velocity is 1000 ms^{-1} with a corresponding smaller cone appropriate to higher velocities. During each 5 minute period 40 measurements were made, 10 at each frequency and range. The combined sources (typically ten to several hundred) from each frequency were combined, assuming no variation in the bulk velocity over five minutes and no variation in height, to yield two ionospheric velocity vectors.

3. DRIFT DIRECTIONS

F-region ionospheric drift velocity vectors, recorded by a Digisonde 256 located at Qaanaaq, Greenland (77.5N, 290.8E geographic; 86.8N corrected geomagnetic latitude) have been determined for the days given in Table 1. The period studied covers data from a period of about two years and includes 1986, 1987 and 1988. Interplanetary magnetic field data from the IMP 8 satellite have been employed for comparison purposes. These days were chosen from a larger data set such that both the IMP8 satellite was correctly placed (see Section 4) and such that 5 minute resolution ionospheric drift vectors were available. The corrected geomagnetic

coordinate system (Hultqvist (1958a,1958b) has been used to reference directions using the coordinates computed by Gustafsson (1970).

As an example of the ionospheric drift measurements Figure 3 presents the drift directions, in the corrected geomagnetic coordinate system, for the days 040-042 (9-11 February) inclusive during 1988. Each point is the median drift direction vector calculated from measurements within frequency bins 0.5 MHz wide during a 5 minute period. For approximately 40% of the 5 minute intervals two median drift directions were obtained because the automatically selected operating frequencies fell in different frequency bins. The diagonal lines denote the anti-sunward direction along the corrected geomagnetic noon-midnight meridian. On all three days B_z (Figure 4) showed variability including periods of both significant negative and positive values (5-10 nT). Day 040 exhibited long periods when B_y was negative (Figure 5) while conversely, B_y was positive through much of days 041 and 042.

As expected from the results of numerous other experiments a comparison of the drift directions (Figure 3) and B_z (Figure 4) reveals that when B_z is predominantly negative there is a strong antisunward trend in the ionospheric drift direction, see day 040. When B_z is south the measured drift directions also vary in a systematic way from one measurement to the next. When B_z swings northward the drift direction variation is sometimes well ordered but sometimes badly ordered and there are also long periods when the drift direction departs significantly from the anti-sunward. At 2130 UT on day 041 the B_z component can be identified as directed northwards and except for a brief interlude between 00 and 01 UT on day 042 it remains so until ~ 0630 UT. Throughout the period 00 to 0630 UT on day 042 the drift directions are widely distributed over about 90° in azimuth and consistent ordering of the drift direction is not easily discernable. This should be contrasted with the period between 16 UT and 2330 UT on day 042 when B_z oscillates about zero remaining either positive or negative for up to 2 hours. When B_z is positive during this period the drift direction variation is well ordered (and quasi-periodic). Here also the drift direction deviates significantly from the anti-sunward.

The systematic or ordered variation in drift direction from one five minute estimate to the next is an important characteristic of nearly all of the data corresponding to B_z negative conditions together with much of the data corresponding to B_z positive conditions

During the period between 16 and 23 UT (Day 042) visual inspection of Figures 3, 4 and 5 reveals a well correlated and systematic variation of the drift direction in response to the changes in the IMF. There is also some indication that, during the one to two hour excursions in B_z , the drift direction fails to establish a quiescent

direction applicable to that Bz polarity. The delay of the ionospheric signature to the IMF change is short in this example.

4. COMPARISON OF DRIFT WITH IMF -TECHNIQUE

To determine the relationship between the IMF, measured in geocentric solar magnetospheric coordinates (GSM), and the drift direction it is necessary to know the direction of the IMF when the drift measurement was made. IMF data from the IMP 8 satellite have been used for this purpose. IMP 8 is in an ecliptic plane orbit which extends ~ 40 Re (earth radii) in the GSE (geocentric solar ecliptic) x-direction and ~ 30 Re in the GSE y direction. In these studies it is assumed that the magnetopause is located at $x=10$ Re and only IMP 8 data were considered when the satellite position was located at $x>10$ Re. Variations in the IMF, measured on IMP 8, then manifest themselves at the magnetopause and in the ionospheric F-region some time later. Like Heppner and Maynard (1987) we have defined a window preceding the drift measurement during which the IMF must remain stable if we are to know unequivocally the direction of the IMF at the time of the measurement. By stable we mean that each IMF component (in GSM coordinates) must remain either positive or negative during the whole of the window. This window may be divided into two parts. The first is the time delay for IMF disturbances to propagate between satellite and magnetopause. The second is the time delay of the ionospheric response due to a variation in the IMF at the magnetopause. The length of the first part was determined by considering both the corotation and the convective time delay approximation (Couzens and King, 1986) of IMF disturbances between the satellite and magnetopause at the sub-solar point. In order to estimate this delay we have assumed that the solar wind speed was 500 kms^{-1} , that the earth's speed was 30 kms^{-1} and the solar rotation speed was 428 kms^{-1} . The maximum corotation delay for satellite positions corresponding to $x > 10$ Re is then ~ 13 minutes, the maximum convective delay ~ 8 minutes and the maximum differential delay is ~ 10 minutes. Russell et al. (1980) have shown that neither approximation can generally be considered better than the other and, therefore, we have set the first component of the window to be 15 minutes in order to include the worst case propagation delay from satellite to magnetopause. With regard to the second part of the window Todd et al. (1988) and Etemadi et al. (1988) have demonstrated that the ionospheric response time is > 2 minutes but < 15 minutes. The total window requiring stable IMF components was, therefore, set at 30 minutes.

GSM coordinates rather than the GSE coordinates were selected because IMF statistical correlations with other geophysical parameters such as Kp and AE are better in the GSM coordinate system (eg Burch, 1974). This is, however, in conflict with Heppner and Maynard (1987) who used the GSE coordinate system. Another difference between our analysis procedure and that of Heppner and Maynard

(1987) is that their model is applicable to a range of Kp values between 3^+ and 4^- . We explored filtering our data according to these criteria but were unable to detect any statistically significant variations in average drift direction. All the results in this paper, therefore, reflect the full range of Kp values applicable to the data set.

5. COMPARISON OF DRIFT DIRECTIONS WITH IMF - RESULTS

The aforementioned criteria have been applied to the thirty-two days of data to determine how the drift direction varies when B_z is negative and B_y is negative and also how it varies when B_z is negative but B_y is positive. No account has been taken of the B_x condition except for the initial requirement of stability. A similar analysis has been carried out when B_z is positive. Drift direction data have been binned in 4° direction intervals. In order to ensure that the magnetosphere is responding strongly to the various IMF conditions an additional requirement of a 1 nT guard band has been imposed. That is any drift vector which corresponds to a 30 minute average IMF component such that $|B_y|$ or $|B_z| < 1$ nT is ignored. The number of points selected from each day are given in Figure 6. No attempt was made to select periods containing specific IMF conditions and there are relatively few drift data when B_z is positive and B_y is negative.

$B_z < 0, B_y < 0$

Four hundred and twelve drift vectors were selected meeting these various criteria and they are well distributed throughout the period 13 to 04 UT but with relatively few points at other times (Figure 7, top panel). Their deviation from the anti-sunward direction (Figure 7, bottom panel) shows the convection direction centred on -12° (clockwise rotation) from the anti-sunward. Simple inspection reveals a broad symmetrical spread of convection directions with the probability still at 50% of its maximum value at $\sim \pm 20^\circ$ of the modal drift direction.

Heppner and Maynard (1987) using satellite data presented two models for $B_z < 0$ and $B_y < 0$, corresponding to two polar cap potential distributions, with average convection directions at Qaanaaq of 0° for the A model and -15° for the DE model. Maynard (private communication, 1989) has indicated, however, that the A model is transitional between the DE and BC models for negative B_y and that its occurrence probability is less than the DE model. As a consequence, it may not be surprising that the Digisonde measurements do not reveal a secondary peak at 0° . The ground-based Digisonde average of -12° is in good agreement with the satellite average of -15° .

Associated with *each* individual five minute resolution drift direction estimate is a measurement inaccuracy (*ie* error). The magnitude of this error is controlled by a number of factors including the number and spatial distribution of reflection points on the skymap, the temporal stability of the drift direction within the antenna beam

and the spatial uniformity of the drift within the antenna beam. An examination of the error magnitudes consequently provides an indication of the validity of the Digisonde drift measurement technique, at least using the current data processing algorithm, for *F*-region polar cap drift measurements. The difference between the median and quartile drift direction estimates was used as a measure of this error. For each of the drift directions meeting the IMF selection criteria the difference between the median and both the upper and lower quartile drift direction estimate was evaluated. Figure 8a shows the mean of these two differences as a density plot. The large majority of the errors (75 %) are less than 5° . This, in association with the ordered variation of drift direction usually seen during these IMF conditions, is indicative of good data and processing reliability. Consequently, the distribution of drift directions about the mode (Figure 7) appears to be principally due to the physical variability of drift directions and does not appear to be an artifact of the equipment and data processing.

$B_z < 0, B_y > 0$

Four hundred and three drift vectors met these criteria and their time distribution is well spread over the entire day (Figure 9, top panel). The deviation from the anti-sunward direction peaks at 24° although a smooth curve is centred around 36° . Again there is a broad spread in convection directions. The Heppner and Maynard (1987) model places the average convection direction at Qaanaaq under these IMF conditions at 45° which is in good agreement with the Digisonde measurement of 36° .

The individual drift direction errors associated with this IMF configuration (Figure 8b) lead to identical conclusions to those drawn above for $B_z < 0$ and $B_y < 0$. The number of points with errors less than 5° is 72% which is very close to the value obtained for the $B_z < 0, B_y < 0$ condition.

$B_z > 0, B_y < 0$

A statistical examination of Digisonde data under positive B_z conditions cannot hope to validate the measurement technique, because there is no commonly held view on the average pattern. These data have, however, been examined in order to provide insight into the Digisonde measurement results for B_z north.

Figure 10 presents all the data when B_z was positive and B_y negative. Unfortunately, only 175 points were available; but surprisingly for this limited data set the average convection direction (bottom panel) is still relatively well defined and centred around -16° from the anti-sunward direction. Sixty eight of the points selected for inclusion in this figure were, however, derived from a relatively short period, between 0230 and 05 UT (approximately 2330 MLT to 02 MLT), on day 344, 1988 when the convection direction remained close to the anti-sunward. This

period is contained within a longer time frame from 0130 to 07 UT during which B_z was positive. (We are unfortunately unable to comment on the period immediately after 07 UT because IMP8 data were not available.) This B_z positive frame was preceded by a B_z negative frame lasting from 1930 UT on the previous day. The latter frame was characterised by strong antisunward convection and this continued into the B_z positive period until 05 UT. A characteristic of the anti-sunward drift is well ordered data with a change of only a few degrees between successive five minute estimates of the drift direction. After 05 UT the measured drift directions became highly variable and disordered. Likewise another 34 points which exhibit a slowly varying and ordered drift direction stem from the period between 20 UT and 2330 UT (approximately 17 MLT to 2030 MLT) on day 294, 1987. These two days of data severely bias the graph and without them no well defined average drift direction would be discernable.

The slowly varying ordered data also exhibit small errors associated with the individual drift measurements (Figure 8c) but the remaining selected points are associated with a wider distribution of errors ranging from the small to the large. For the entire category of data when $B_z > 0$ and $B_y < 0$ only 48% of the points exhibited errors less than 5° - a performance some 25% inferior to the B_z negative data set.

Heppner and Maynard (1987) argued in favour of a distorted two cell model when B_z was positive. This distortion places Qaanaaq, at 87° CG latitude, well into the morning cell and a complicated diurnal variation of convection direction results ranging from sunward through anti-sunward. The ordered data presented in Figure 10 are clustered in the period 20 - 2330 UT and 0230 - 5 UT which corresponds to convection directions, scaled from the weak B_z positive model of Heppner and Maynard (1987), of between 0° and -15° and -15° respectively. These data are, therefore, not in disagreement with this model; they are, however, in disagreement with the various three and four cell models which suggest anti-sunward flow during positive B_z periods. The significance of such a small data subset is, however, in question. How to interpret the remaining group of selected data points showing a wide scatter in azimuth, is discussed below in Section 6.

$B_z > 0, B_y > 0$

Four hundred drift vectors met this criterion. No clear statistically stable convection direction, which applies to the whole day, is evident in these data (Figure 11, bottom panel). During certain periods the convection direction is anti-sunward but at other times it is sunward. Figure 11 (top panel) fails to show any clear pattern which might be compared to either the distorted two cell pattern of Heppner and Maynard (1987) or a three or four cell model (eg Potemra et al, 1984).

In this IMF category only 42% of the drift directions estimates had an associated error of $<5^\circ$ (Figure 8d); a value similar to that obtained for the $B_z > 0$, $B_y < 0$ data set.

6. THE INTERPRETATION OF POLAR CAP DIGISONDE DRIFT VECTORS WHEN $B_z > 0$

When B_z is negative we have demonstrated that, at least on a statistical level, there is good agreement between the Digisonde drift directions and model convection directions. When B_z is positive we also propose to tentatively interpret well ordered variations in the drift direction as a measure of the convection direction. Whilst we are unable to support this assumption by comparison with measurements using other techniques we contend that there is no reason not to do this.

When $B_z > 0$ the ordered convection direction measurements, selected according to the IMF criteria, divide into two groups. Some vary slowly with time and examples of these occurred on Day 294, 1987 and Day 344, 1988 when $B_y < 0$. We designate those data which exhibit this behaviour *OS* (ordered and slowly varying). On other occasions the drift direction variation is also well ordered but the variation in direction with time is fast. An example of such a case was given in the post noon period of day 042 (Figure 3). Such points are spread over a wide range of azimuths and a large number of points, so selected from many days, has a tendency to appear disordered. These points which originate from periods when the azimuthal variation is ordered but quickly varying are designated *OQ*.

In addition to these periods of ordered variation in convection direction there are other periods when the convection direction appears to vary in a disordered manner from one 5 minute estimate to the next. After selection (according to IMF criteria) these individual drift directions, designated *D* (disordered), are indistinguishable from the *OQ* vectors except perhaps by the magnitude of their associated errors which are expected to be larger for *D* type measurements. An example of these *D* variations was given in Figure 3 between 00 and 06 UT, day 042. One reason for these disordered Digisonde drift vectors was proposed by Buchau et al. (1988). The Digisonde drift analysis algorithm assumes uniform drift across the sky and does not allow for flow variations within the antenna beam; if flow irregularities do exist the algorithm produces speeds and directions which are not meaningful. Carlson et al. (1984) have shown that velocity shears occur either side of sun aligned arcs and the latter are known to occur when B_z is positive (Gussenhoven, 1982). It, therefore, seems likely that visual or sub-visual sun aligned arcs were contained within the Digisonde antenna beam when *D* type measurements were made. A zeroth order measure of the probability of making *D*

measurements were made. A zeroth order measure of the probability of making D type measurements, rather than OS or OQ measurements can be made by examining the relative errors associated with the individual measurements when $B_z < 0$ as opposed to when $B_z > 0$. When $B_z < 0$ the errors were $< 5^\circ$ in azimuth for about 70% of the time where as when $B_z > 0$ this decreased to only $\sim 45\%$ of the time. This degradation in measurement accuracy indicates that when $B_z > 0$ the Digisonde measured significant velocity shears $\sim 25\%$ more of the time than when $B_z < 0$.

The summed effect of the OQ type variations and the D variations, rather than the D variations alone, are central to the reason why we are unable to determine any average convection direction when $B_z > 0$. With only ~ 20 to 30% of the selected measurements impaired by velocity shears a diurnal variation should be discernable given a good temporal distribution of data points over the day. No such variation is, however seen.

The existence of OQ variations also leads us to suggest that the synthesis of meaningful, average models, categorised simply by the sign of the IMF components may not be possible when B_z is positive. Inspection of the 32 days of data studied in this paper reveals that the azimuth of OQ variations may be tied, in a complicated manner, to the strength of the IMF components.

Another potential instrumentation and/or data analysis error which is considered to produce second order effects for polar cap observations, derives from the inability of the Digisonde to distinguish between electric field induced F region movements and movements induced by other forces. The major inaccuracy in this regard is believed to derive from gravity waves which will be most obvious when the induced gravity wave ionospheric velocities are large, or comparable to, the electric field induced drifts. When B_z is negative the polar cap electric field induced drift velocities are generally a few hundred metres per second or higher and the electric field induced movements are expected to dominate. When B_z is positive the electric field induced drift velocity falls to lower values and these other effects may disturb the data on occasion.

7. CONCLUSIONS

Thirty-two days of data have been analysed and Figure 12 gives a synopsis of the results.

When B_z is negative and when B_y is positive and negative these data indicate a clear shift in the convection drift direction respectively positive and negative of the anti-sunward direction. Heppner and Maynard (1987) propose two models for the

negative B_y case - one with the stream lines flowing anti-sunward (*ie* 0°) and the other offset by -15° . Our measurements indicate a single median direction of -12° . For the positive B_y case Heppner and Maynard give an offset of $\sim 45^\circ$ positive whereas our measurements indicate a modal convection direction of 36° . We conclude that when B_z is negative the ground based Digisonde has been shown to produce average, daily polar cap drift directions which are close to those reported by Heppner and Maynard (1987) from satellite measurements. The usefulness of the Digisonde for making polar cap convection measurements, when $B_z < 0$, has, therefore, been demonstrated when data are averaged over several hours to several days. Generally there is also consistency of drift azimuth from individual measurement to individual measurement which is suggestive that the Digisonde can be used for case studies (Buchau et al., 1988), however, this aspect has not been addressed in this paper.

When B_z is positive and B_y negative the data divides into three groups - convection directions which are ordered and vary slowly with time (OS), convection directions which are ordered and which vary quickly with time (OQ) and convection directions which are disordered (D) with time. The latter are believed to be due to the breakdown of the measurement procedure as a result of velocity shears. Using the analysis selection procedures described in this paper OQ and D are indistinguishable from each other but there is hope that this might be overcome by examining the errors associated with the individual 5 minute resolution measurements. For the small sub-group OS there is a favoured convection direction centred on between 0° and -20° from the anti-sunward during the periods 2330 to 02 MLT and 17 to 2030 MLT. This flow direction is in good agreement with the distorted two cell (satellite) data model of Heppner and Maynard (1987).

For B_z positive and B_y positive the original drift data divides into two groups OQ and D and no diurnal variation of drift direction can be identified.

The existence of OQ variations, which represent significant variations in drift directions over intervals of 5 to 10 minutes, illustrates one of the problems of using satellites which take 10 minutes or more to traverse the polar cap and which require temporal stability over that period. The low probability of OQ variations when $B_z < 0$ (which may also be inferred from the relatively narrow drift direction spread of $\pm 20^\circ$ from the daily modal direction) indicates that less severe problems are to be expected by temporal averaging of convection data during these IMF conditions.

The magnitude and direction of plasma drift has not been quantified on a short time scale with respect to other techniques. In the polar cap this involves comparison of the convection data from Qaanaaq with satellite or ground based optical measurements. In the auroral region it awaits the analysis of data from another Digisonde at Sondre Stromfjord and comparison with data from the co-located ISR.

At mid latitudes it involves comparative measurements at Millstone Hill between a Digisonde and the ISR. Due to the assumption that the ionospheric bulk velocity remains constant over the antenna field of view and the varying velocity shears that are expected in each of these regions a series of measurement comparisons and improvements in the analysis technique will be required to validate the measurement technique. The Digisonde drift measurements are also susceptible to movements induced by other ionospheric dynamic effects, such as travelling ionospheric disturbances generated by neutral gravity waves, which may induce a degree of variability on the calculated convection velocities. The percentage error will be a function of the induced plasma convection velocity and may be expected to be small, under the expected high plasma velocities at auroral and polar cap latitudes, but relatively more important at middle latitudes.

ACKNOWLEDGEMENTS

We are indebted to the Directors of the Danish Meteorological Institute and its Division for Geophysics for their interest and support. This research was conducted with the approval of the Commission for Scientific Research in Greenland under Project 28-88. We thank the commission members for their interest and support. The provision of IMP8 data by Dr R Lepping and Dr J King at NSSDCA, Goddard Space Flight Center is gratefully acknowledged. Some of the Digisonde drift data was collected as part of the collaborative CEDAR HELPS programme. BWR and TWB acknowledge the support of their work by the Geophysics Laboratory, Air Force Systems Command under contract FY 19628-86-K-0036. PSC would like to thank Director, Royal Aerospace Establishment, UK for leave of absence to work at the University of Lowell.

REFERENCES

- Axford, W. I. and C. O. Hines, A unifying theory of high latitude geophysical phenomena and geomagnetic storms, *Can. J. Phy.*, 69, 1181, 1961.
- Bates, H. F. and P. R. Albee, Aspect sensitivity of F-layer HF backscatter echoes, *J Geophys. Res.*, 75, 165, 1970.
- Bibl, K. and B. W. Reinisch, The universal digital ionosonde, *Radio Sci.*, 13, 519, 1978.
- Buchau, J. and L.F. McNamara, Simulation of ionograms obtained during the October 1979 Platteville heater experiment, *Radio Sci.*, 21, 3, 286, May-June, 1986.
- Buchau, J., E. J. Weber, D. N. Anderson, H. C. Carlson, Jr., J. G. Moore, B. W. Reinisch and R. C. Livingston, Ionospheric structures in the polar cap: Their origin and relation to 250 MHz scintillation, *Radio Sci.*, 20, 325, 1985.
- Buchau, J., B. W. Reinisch, D. N. Anderson, E. J. Weber and C. G. Dozois, Polar cap plasma convection measurements and their relevance to the modeling of the high-latitude ionosphere, *Radio Sci.* 23, 4, 521-536, August 1988.
- Bullett, T., Doctoral Thesis, University of Lowell, Lowell, MA 01854, USA, 1990.
- Burch, J. L., Observations of interactions between interplanetary and geomagnetic fields, *Rev. Geo. Space. Phys.*, 12,3, 363-378, 1974.
- Burke, W. J., M. C. Kelley, R. C. Sagalyn, M. Smiddy and S. T. Lai, Polar cap electric field structures with a northward interplanetary magnetic field, *Geophys. Res. Lett.*, 6, 21, 1979.
- Carlson, H. C., Jr., V. B. Wickwar, E. J. Weber, J. Buchau, J. G. Moore and W. Whiting, Plasma characteristics of polar cap F layer arcs, *J Geophys. Res. Lett.*, 11, 895, 1984.
- Couzens, D. A. and J. H. King, Interplanetary medium data book, Supplement 3 1977-1985, NSSDC/WDC-A-R2586-04, National Space Science Data Center, NASA, Goddard Space Flight Center, Greenbelt, MD 20771, 1986.

Dozois, C. G., A high frequency radio technique for measuring plasma drifts in the ionosphere, Rep. AFGL-TR-83-0202, Air Force Geophys. Lab., Hanscom AFB, Mass., 1983. ADA140509

Dungey, J. W., Interplanetary magnetic field and the auroral zones, Phys Rev. Lett., 6, 47-48, 1961.

Evans, J. V., J.M. Holt, W.L. Oliver, and R H Wand, Millstone Hill incoherent scatter observations of auroral convection over $60^{\circ} \leq \Lambda \leq 75^{\circ}$, 2, Initial results, J. Geophys. Res., 85, 41, 1980

Foster J. C., J. R. Doupnik, G. S. Stiles, Ionospheric convection and currents in the midnight sector on November 8, 1979, J. Geophys. Res. 86, 2143, 1981.

Foster, J. C., An empirical electric field model derived from Chatanika radar data, J. Geophys. Res. 88, 981, 1983.

Folkestad K., T Hagfors and S Westerlund, EISCAT. An updated description of technical characteristics and operational capabilities, Radio Sci., 18, 867, 1983.

Greenwald R. A., W. Weiss, E. Nielsen, and N. R. Thomson, STARE: A new radar auroral backscatter experiment in northern Scandinavia, Radio Sci., 13, 1021, 1978.

Greenwald, R. A., K. B. Baker, R. A. Hutchins, and C. Hanuise, An HF phased-array radar for studying small-scale structure in the high latitude ionosphere, Radio Sci., 20, 63, 1985

Gussenhoven, M. S., Extremely high latitude auroras, J. Geophys. Res., 87, 2401-2412, 1982.

Gustafsson, G., A revised corrected geomagnetic coordinate system. Ark Geofy, 5, 595, 1970.

Hultqvist, B., The spherical harmonic development of the geomagnetic field, epoch 1945, transformed into rectangular geomagnetic coordinate systems, Ark Geofy, 3, 53-61, 1958a.

Hultqvist, B., The geomagnetic field lines in higher approximation. Ark Geofy. 3, 63-77. 1958b.

Heelis, R. A., W. B. Hanson. J. L. Burch, Ion convection reversals in the day-side cleft, J. Geophys. Res., 81, 3803, 1976.

Heelis, R. A., J. K. Lovell and R. W. Spiro, A model of the high latitude ionospheric convection pattern, J. Geophys. Res. 87, A8, 6339-6345, 1982.

Heppner, J. P., Polar cap electric field distributions related to the interplanetary magnetic field direction, J. Geophys. Res., 77, 4877, 1972.

Heppner, J. P., Empirical models of high-latitude electric fields, J. Geophys. Res. 82, 7, 1115-1125, 1977.

Heppner, J. P. and N. C. Maynard, Empirical high-latitude electric field models, J. Geophys. Res. 92, A5, 4467-4489, May 1987.

Jones, T. B., J. A. Waldock, E. C. Thomas, C. P. Stewart and T. R. Robinson, SABRE radar observations in the auroral ionosphere, AGARD Conf. Proc. 382, *Propagation Effects on Military Systems in the High Latitude Region*, Fairbanks Alaska, June 1985.

Lassen, K., The quiet-time pattern of auroral arcs as a consequence of magnetospheric convection, Geophys. Res. Lett., 6, 777, 1979.

Maynard N. C. and A.D. Johnstone, High Latitude dayside electric field and particle measurements, J. Geophys. Res., 79, 3111, 1974.

Mozer, F.S., and P. Lucht, The average auroral zone electric field, J. Geophys. Res., 79, 1001-1006, 1974.

Nielsen, E and K Schlegel, Coherent radar Doppler measurements and their relationship to the ionospheric electron drift velocity, J Geophys. Res., 90, 3498, 1985.

Pfister, W., Drift measurement with spectral analysis during period of chemical releases into the ionosphere, Space Res., XIV, 401., 1974a.

Pfister, W., Pulse sounding with closely spaced receivers as a tool for measuring atmospheric motions and fine structure in the ionosphere, V, Period of chemical releases (as example of spectral analysis), Rep. AFCRL-TR-74-0105, Environ. Res. Pap., 468, Air Force Cambridge Res. Lab., Bedford, Mass., 1974b. AD781040

Potemra, T. A., L.J. Zanetti, T. A., P. F. Bythrow, A.T.Y. Lui and T. Iijima, By-dependent convection patterns during northward interplanetary magnetic field. J. Geophys. Res., 89, 9753-9760, 1984.

Quegan, S., G., J. Bailey, R. J. Moffett, R. A. Heelis, T. J. Fuller-Rowell, D. Rees, and R. W. Spiro, A theoretical study of the distribution of Ionisation in the high latitude ionosphere and the plasmasphere: First results on the mid-latitude trough and the light-ion trough, *J Atmos. Ter. Phys.*, 44, 619, 1982.

Reinisch, B. W., New techniques in ground-based ionospheric sounding, *Radio Sci.*, 21, 331, 1986.

Reinisch, B. W., J. Buchau and E. J. Weber, Digital ionosonde observations of the polar cap F region convection, *Phys. Scr.*, 36, 372, 1987.

Ruohoniemi, J. M., R A Greenwald, K B. Baker, and J P Villain, Drift motions of small-scale irregularities in the high-latitude F region: An experimental comparison with plasma drift motions, *J. Geophys. Res.*, 92, A5, 4553-4564, 1987.

Russell, C. T., G. L. Siscoe and E. J. Smith, Comparison of ISEE-1 and -3 interplanetary magnetic field observations, *Geophys. Res. Letters*, 7, 5, 381-384, 1980.

Schunk, R. W., Magnetosphere-ionosphere-thermosphere coupling processes, *Sym. on Solar-terrestrial energy program (STEP): Major Scientific Problems*, Helsinki, Finland, July, 1988.

Sojka, J. J. and R. W. Schunk, Problems with deducing ionospheric convection patterns, *J. Geophys Res.*, 91, 259, 1986.

Sojka, J. J., C. E. Rasmussen, and R. W. Schunk, An Interplanetary magnetic field dependent model of the ionospheric convection electric field, *J. Geophys Res.*, 91, 11,281-11,290, 1986, 1986.

Sojka, J. J. and R. W. Schunk, Theoretical study of the high-latitude ionosphere's response to multicell convection patterns *J. Geophys Res.*, 92, A8, 8733-8744, 1987.

Weber, E. J., J. A. Klobuchar, J. Buchau, H. C. Carlson, Jr., R. C. Livingston, O. de la Beaujardiere, M. McCready, J. G. Moore, G. J. Bishop, Polar cap F layer patches: Structure and dynamics, *J. Geophys. Res.* 91.11,12121,1986

Table 1
Selected Data Periods

Year	Day Number	Date
1986	302-305	29 Oct-1 Nov
1987	139-141	19-21 May
	167-168	16-17 June
	265-267	22-24 September
	293-294	20-21 October
	328-330	24-26 November
	356	22 December
1988	039-042	8-11 February
	052-055	21-24 February
	340-345	5-10 December

Captions

- Figure 1 Receiver antenna geometry.
- Figure 2 A skymap survey for part of day 052. Each panel shows the positions of oblique ionospheric sources scaled in degrees with zenith angles varying from 0° to $\pm 80^\circ$. Under each panel is shown the universal time, the number of drift soundings contributing to the panel and the number of sources mapped onto the panel.
- Figure 3 Drift directions for days 040 to 042, 1988. *OS* indicates ordered and slowly varying drift direction variations; *OQ* ordered and quickly varying and *D* disordered variations, see Section 6.
- Figure 4 IMF B_z component (nT) at IMP8 on days 040 to 042, 1988
- Figure 5 IMF B_y component (nT) at IMP8 on days 040 to 042, 1988

- Figure 6 No of drift vectors selected per day per IMF category.
- Figure 7 Selected drift data when $B_z < 0$ and $B_y < 0$:top panel, temporal distribution of selected data, bottom panel, deviation of convection direction from the anti-sunward.
- Figure 8 Diurnal variation of the quartile error of each (five minute resolution) drift direction estimate: a) $B_z < 0, B_y < 0$; b) $B_z < 0, B_y > 0$; c) $B_z > 0, B_y < 0$; d) $B_z > 0, B_y > 0$.
- Figure 9 Selected drift data when $B_z < 0$ and $B_y > 0$: Top panel, temporal distribution of selected data; bottom panel deviation of convection direction from the anti-sunward.
- Figure 10 Selected drift data when $B_z > 0$ and $B_y < 0$: Top panel, temporal distribution of selected data; bottom panel deviation of convection direction from the anti-sunward.
- Figure 11 Selected drift data when $B_z > 0$ and $B_y > 0$: Top panel, temporal distribution of selected data; bottom panel deviation of convection direction from the anti-sunward.
- Figure 12 Synopsis of measured convection directions: polar plot, shading indicates no clear convection direction.

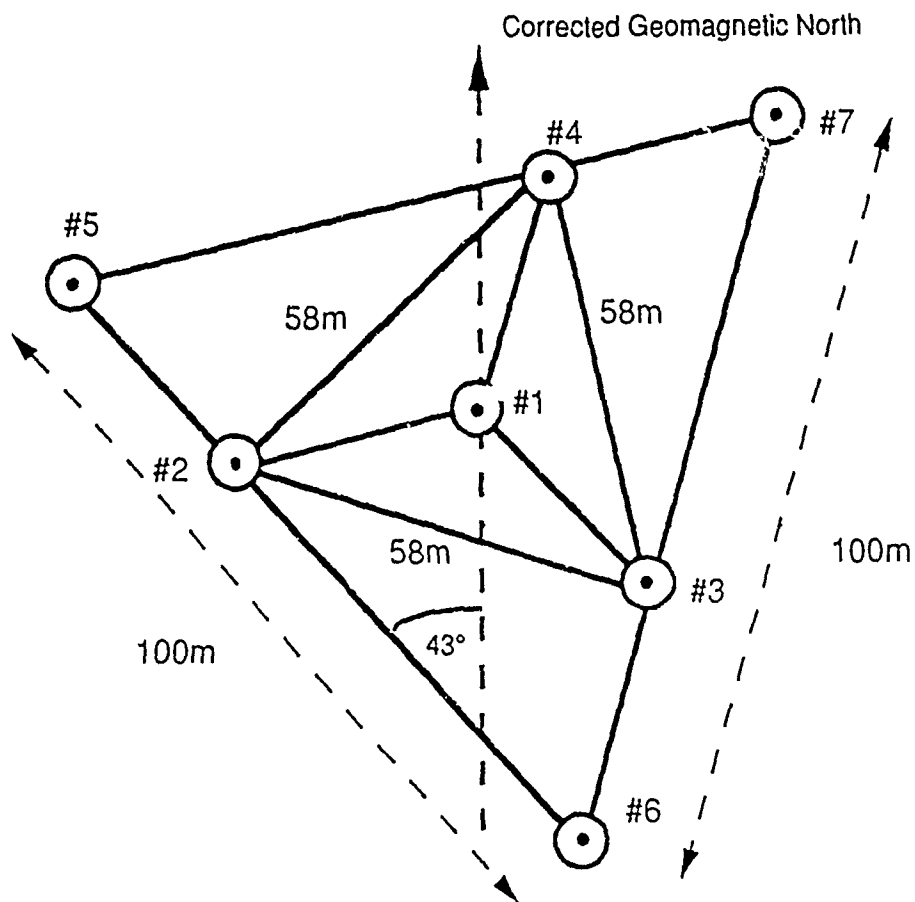


Figure 1. Receiver Antenna Geometry

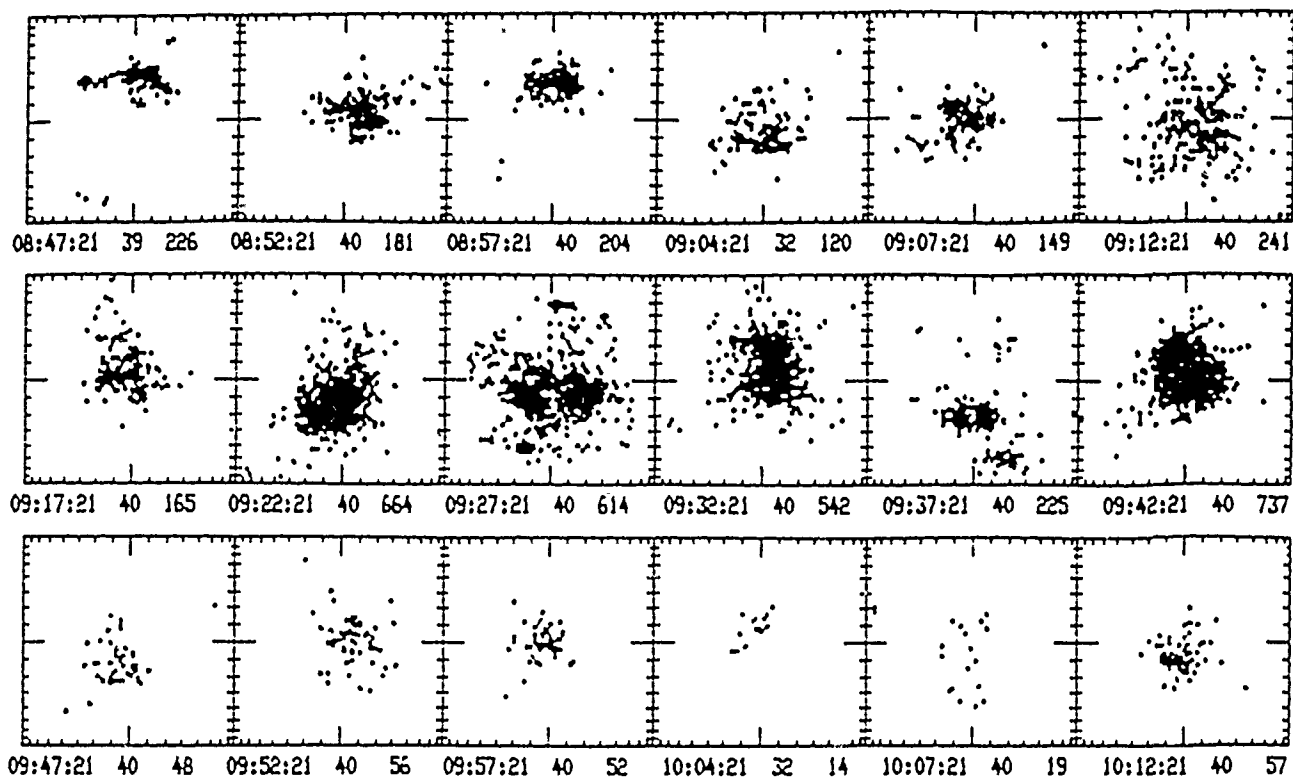


Figure 2

Figure 3

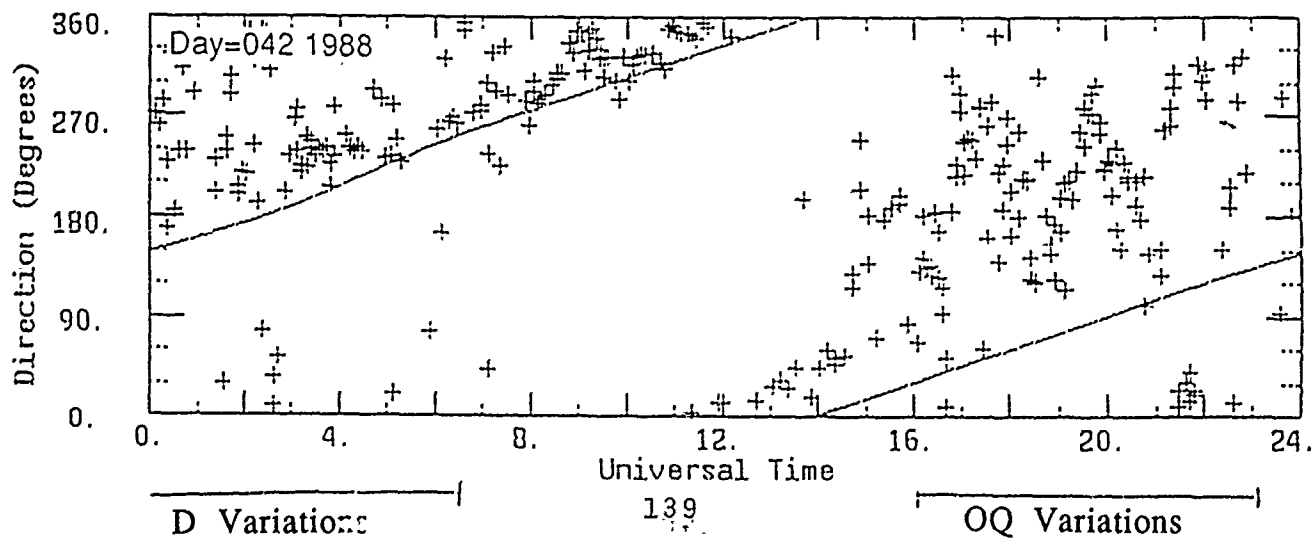
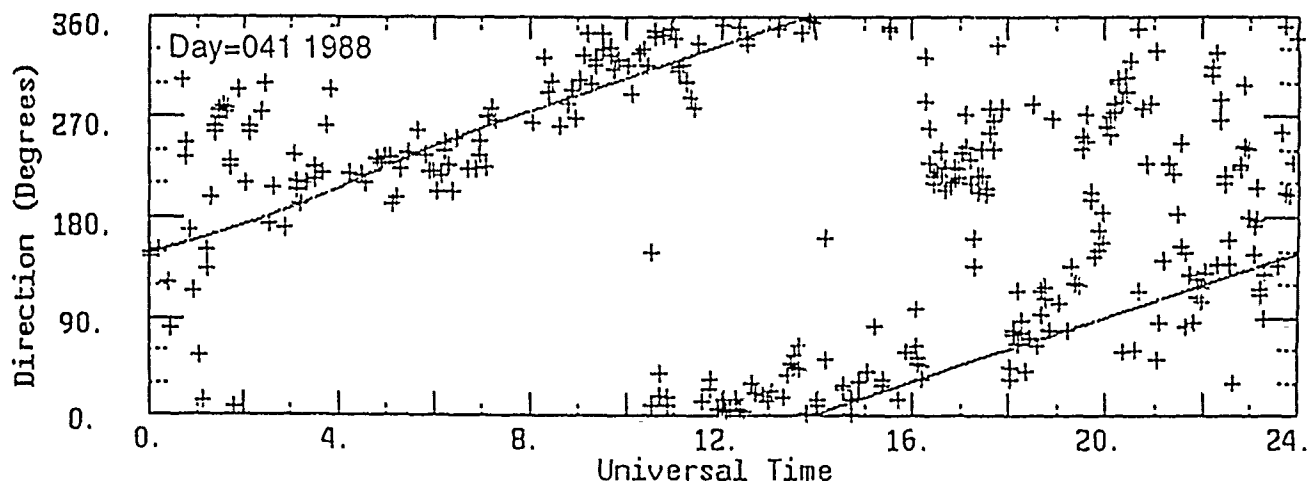
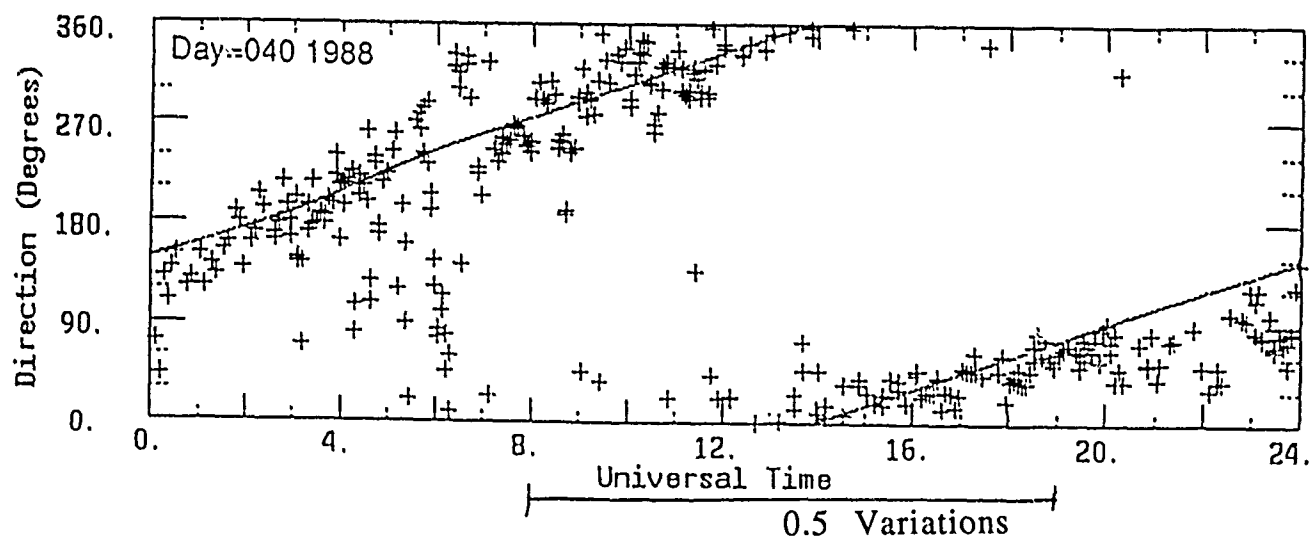


Figure 4

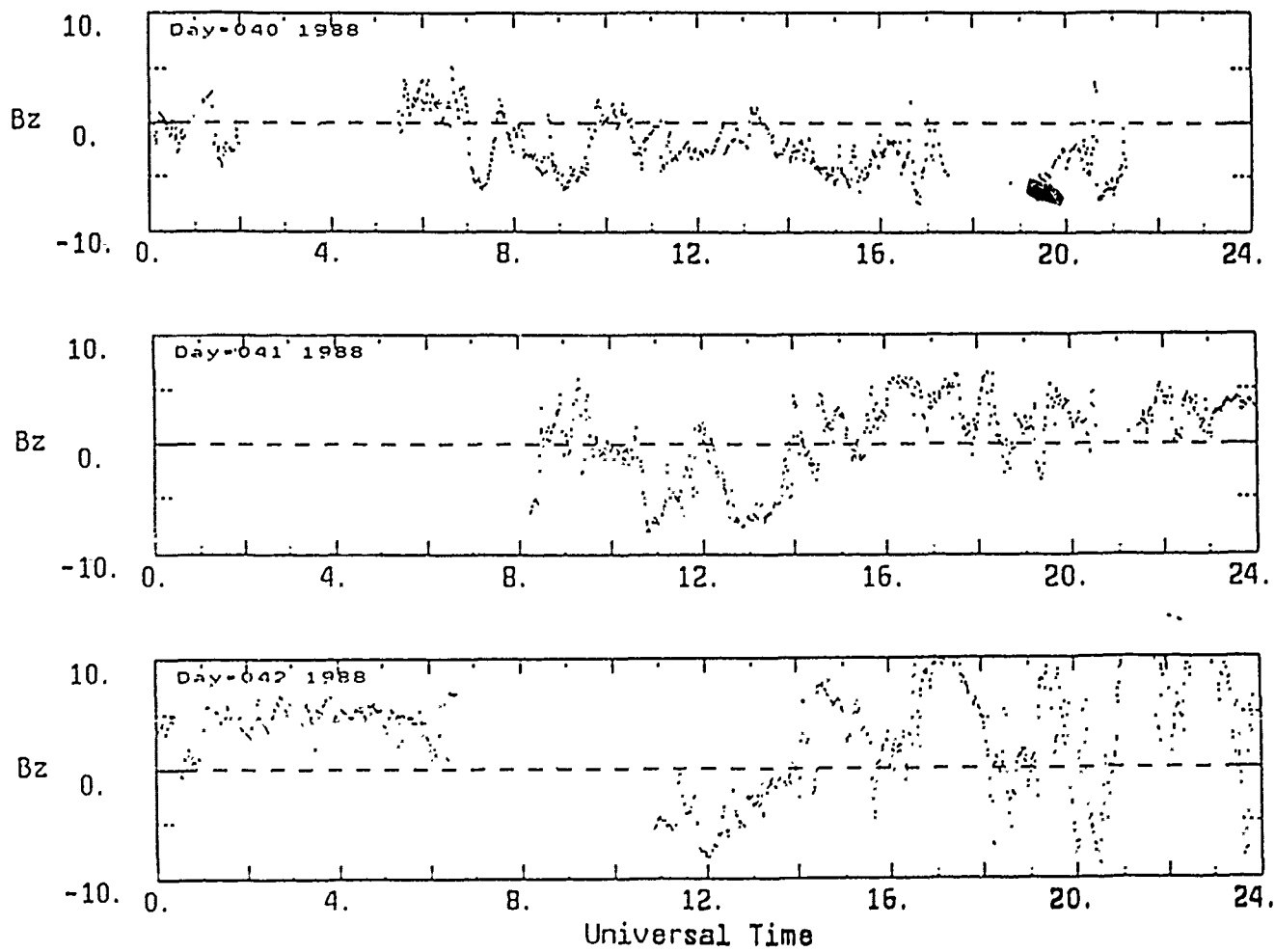
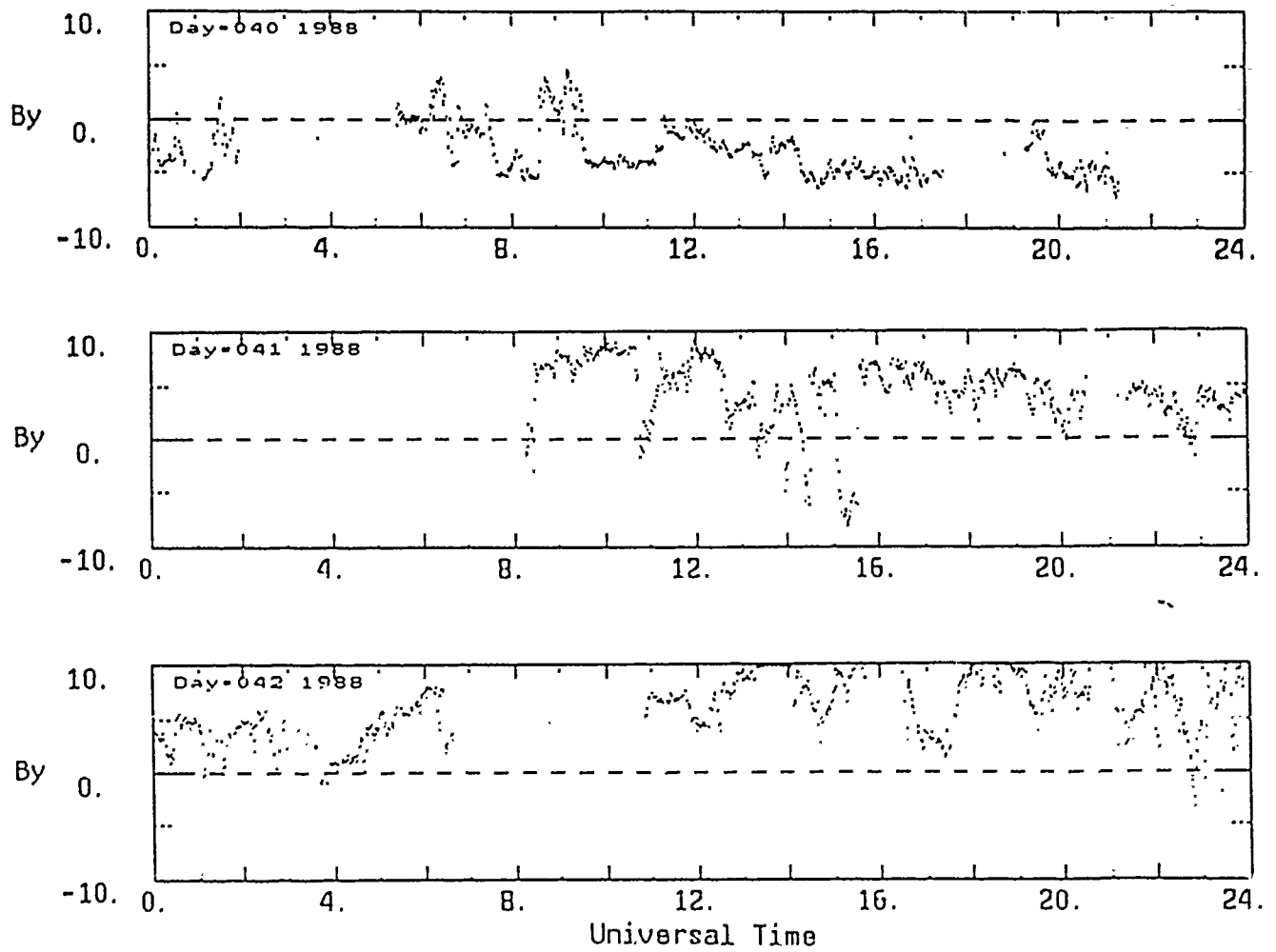
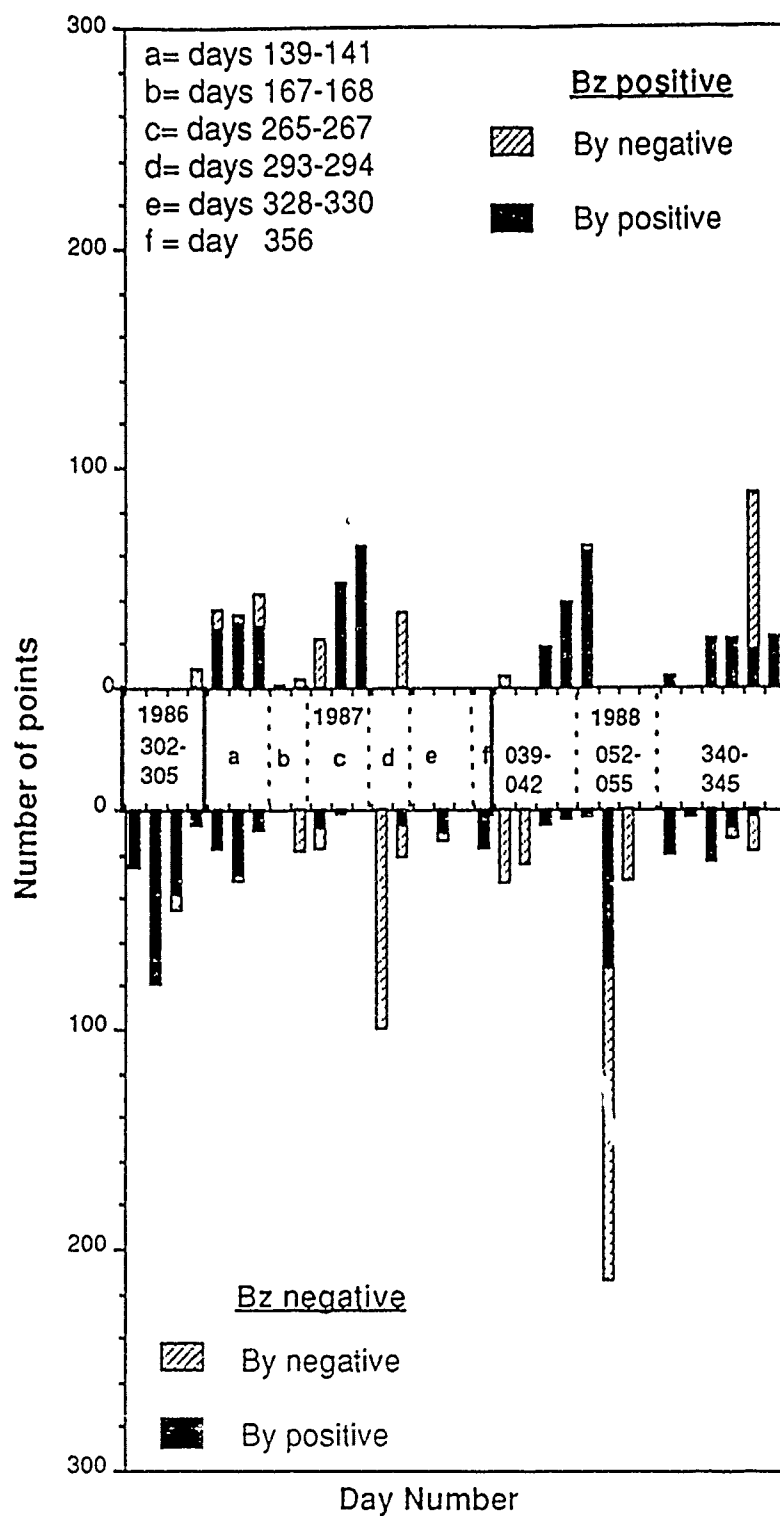


Figure 5





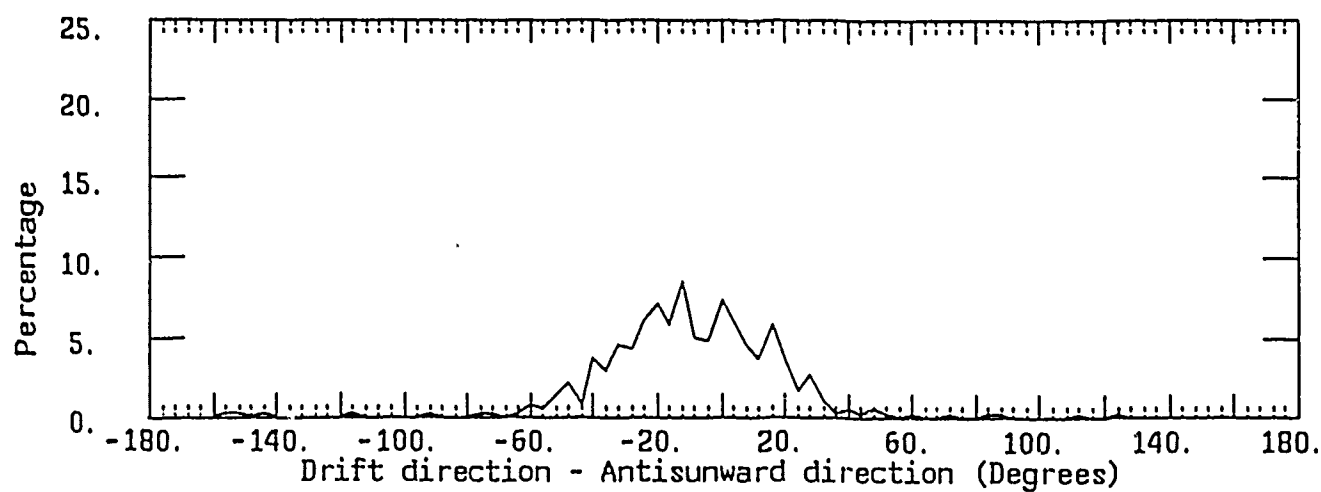
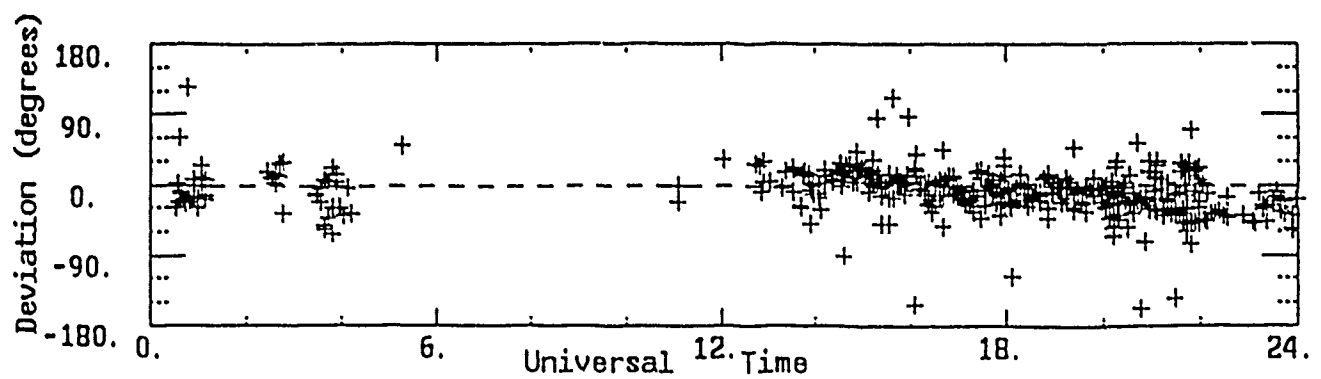


Figure 7

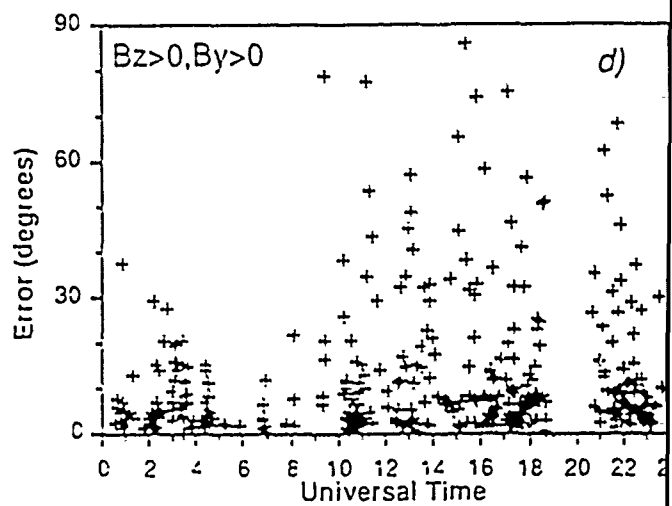
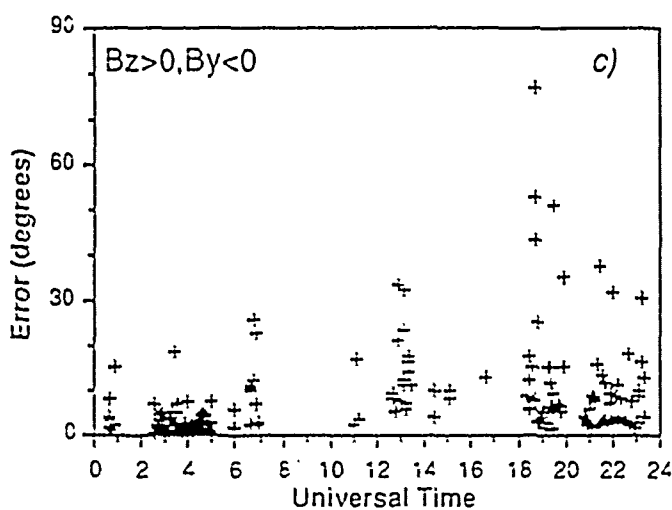
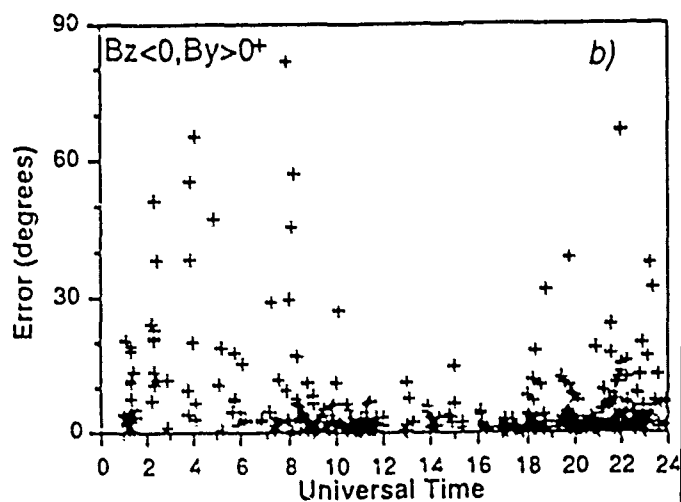
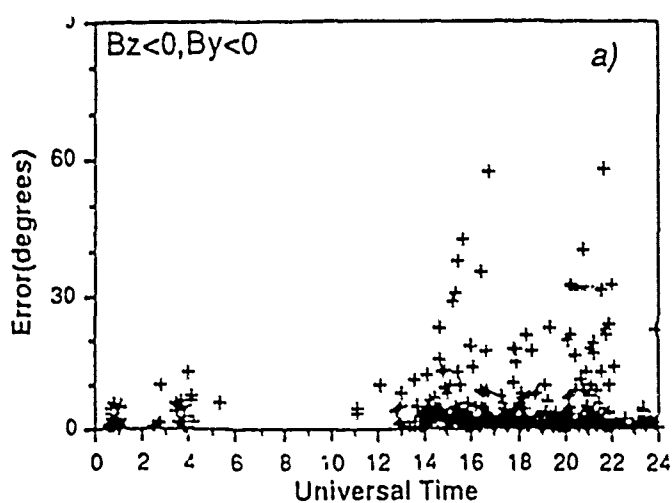


Figure 8

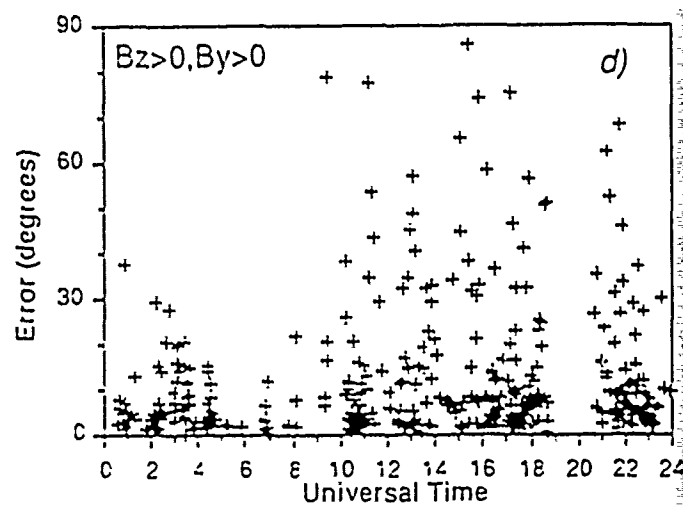
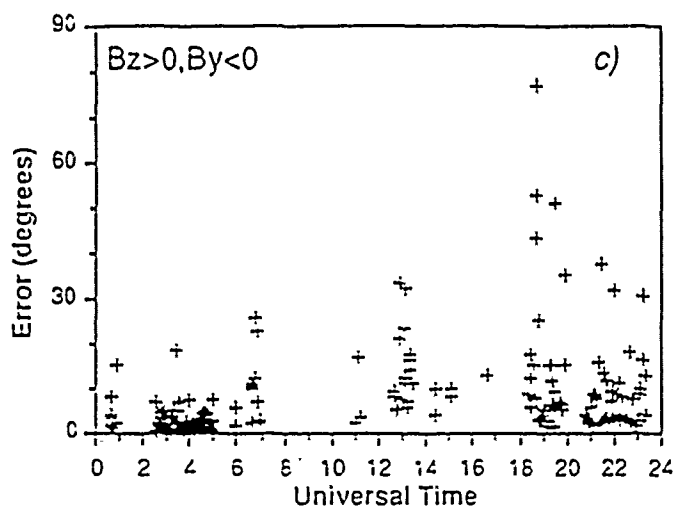
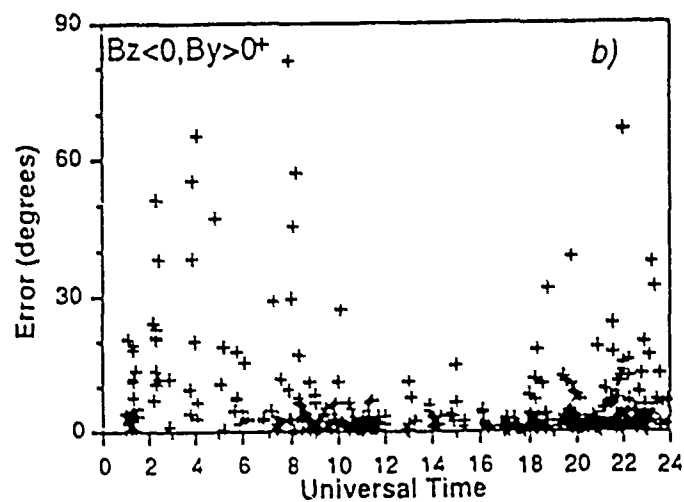
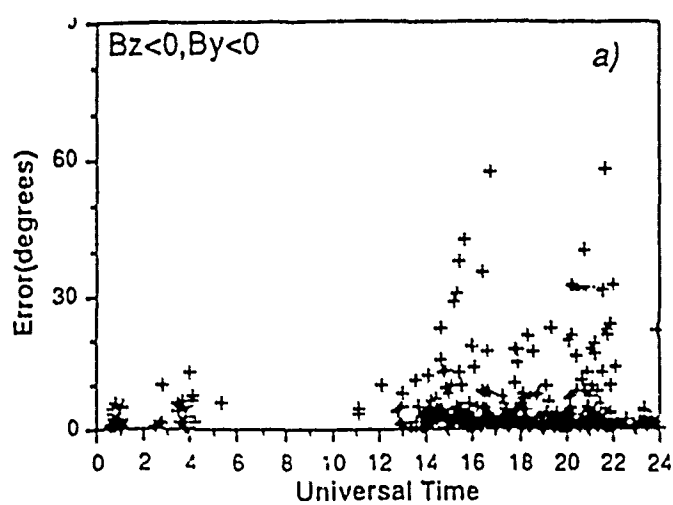


Figure 8

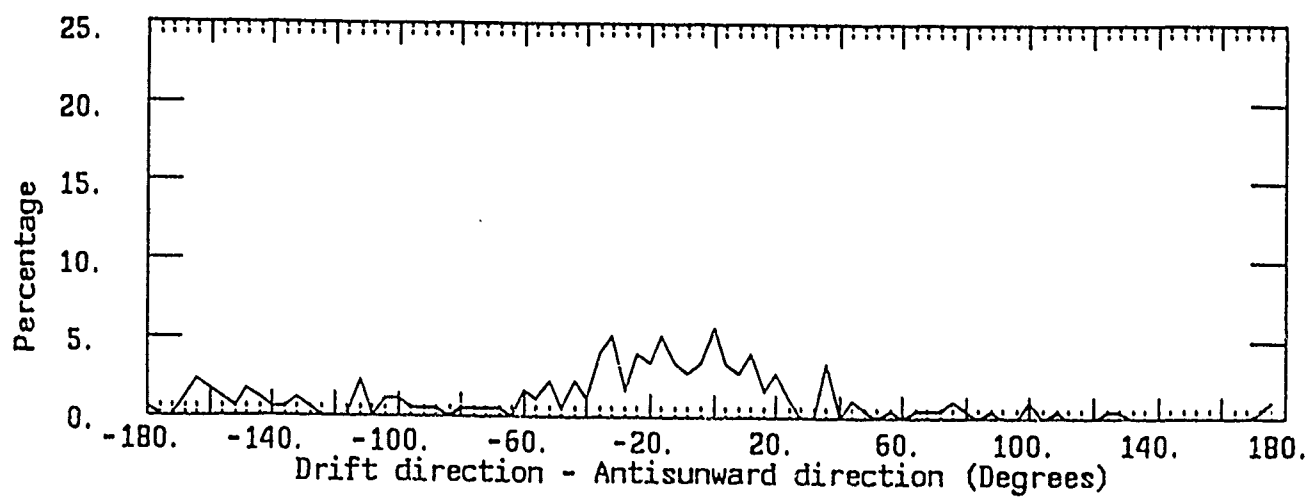
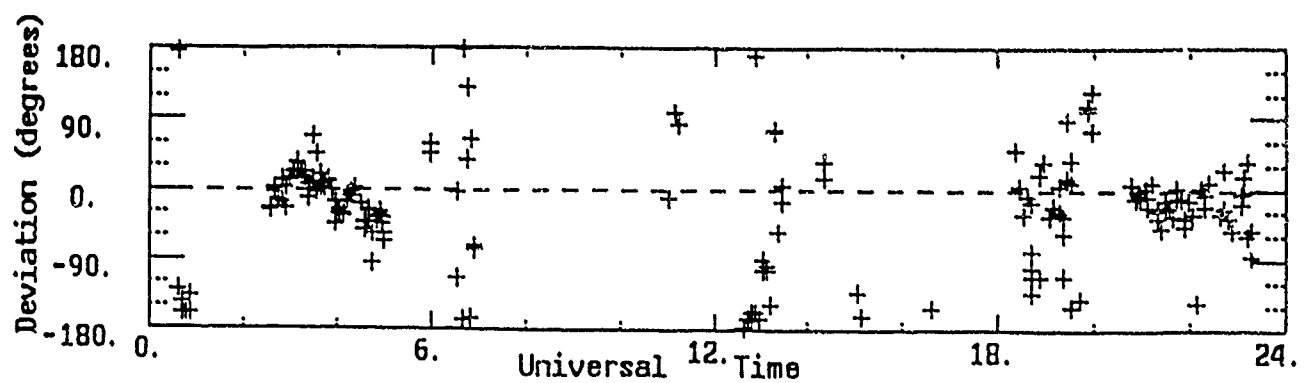


Figure 10

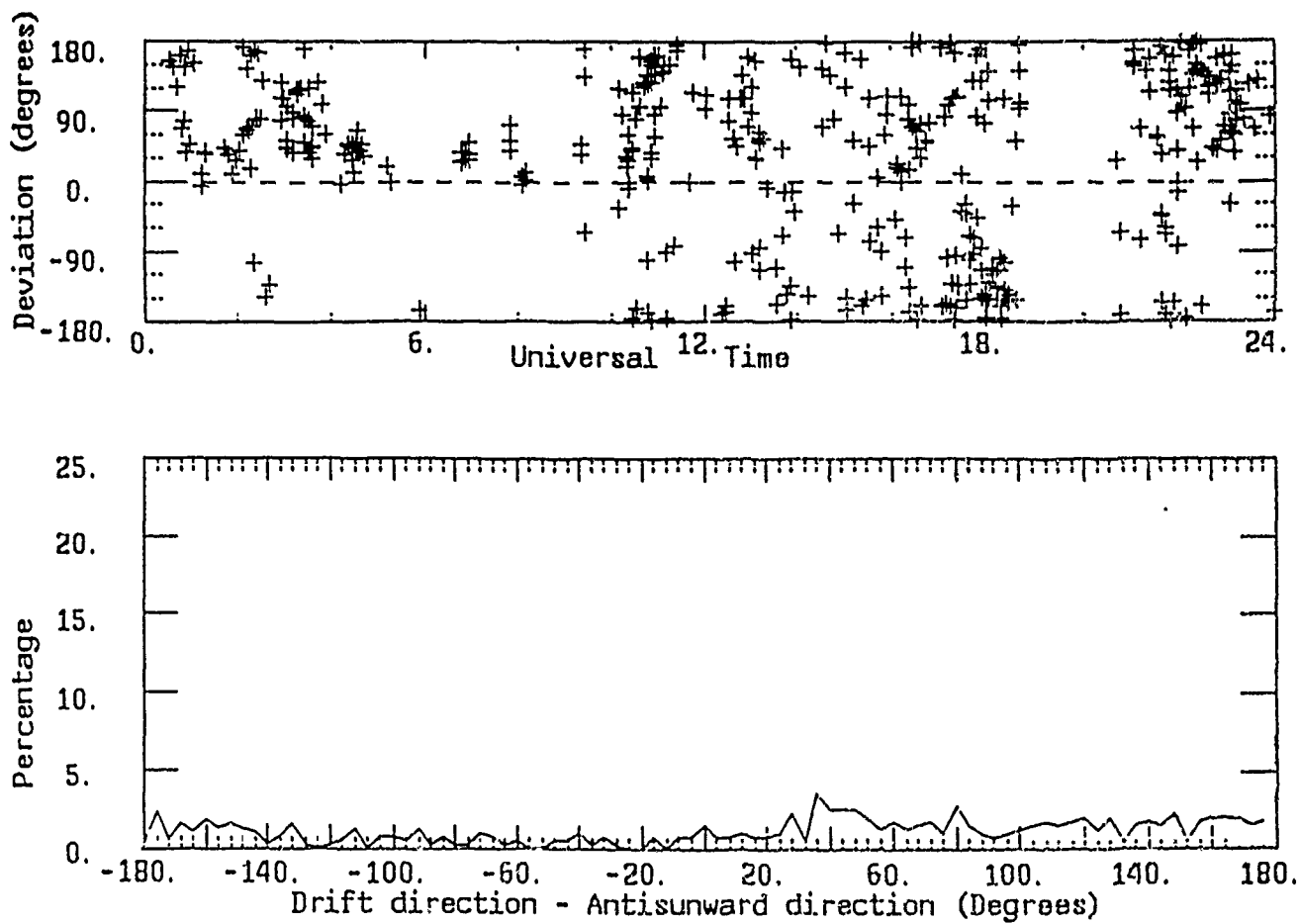


Figure 11

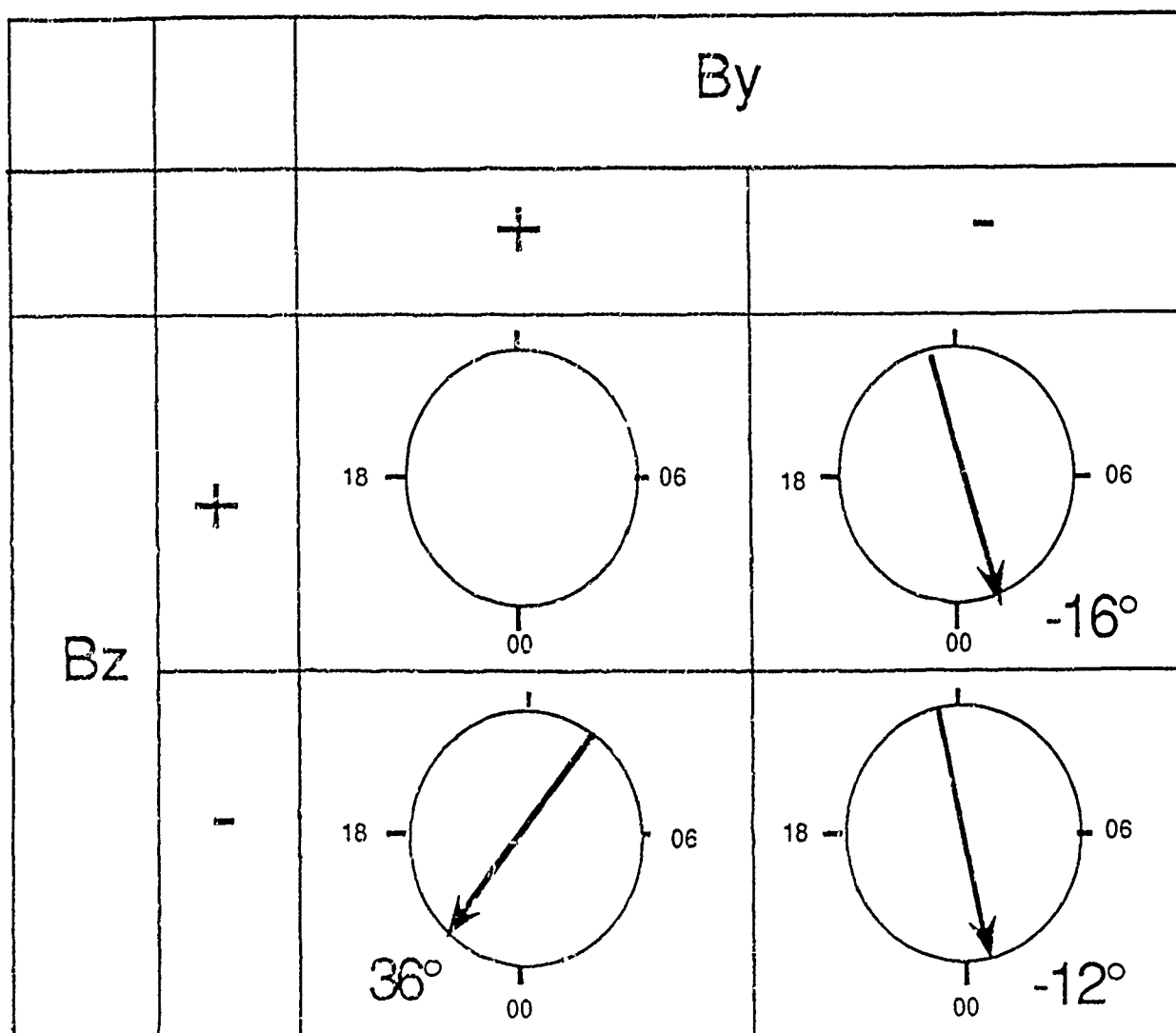


Figure 12. Synopsis of measured convection directions: polar view, shading indicates no clear convection direction

Polar cap plasma convection measurements and their relevance to the modeling of the high-latitude ionosphere

Jurgen Buchau,¹ Bodo W. Reinisch,² David N. Anderson,¹ Edward J. Weber,¹ and Claude Dozois²

(Received September 29, 1987; revised April 18, 1988; accepted May 18, 1988.)

Plasma convection measurements, using Digisonde ionospheric sounders, have been conducted in the central polar cap at Thule, Greenland (86° CGL) and more recently at Qaanaaq, Greenland (87° CGL), in the auroral oval at the Air Force Geophysics Laboratory Goose Bay Ionospheric Observatory (65° CGL), and at suboval latitudes at Argentia NAS (57° CGL). The plasma convection or ionospheric drift measurements conducted at Thule and Qaanaaq during campaigns from the 1983-1984 winter to the present provide evidence that antisunward convection dominates in the polar cap with velocities typically between 300 and 900 m s⁻¹. Velocity reversals or shears were observed in association with polar cap *F* layer auroras during quiet magnetic conditions. Observations of the plasma drift at Goose Bay show, as expected, a drift reversal from westward to eastward around midnight CGLT, indicating the rotation of Goose Bay from the evening into the morning convection cell. Observations at Argentia, typically a suboval/trough station, provide evidence under magnetically disturbed conditions for the midnight reversal of the antisunward flow pattern. However, the data at Argentia are generally less consistent under magnetically quiet conditions. This likely indicates the proximity of Argentia to the boundary between rotating and convecting plasma. Recent theoretical calculations of electron density profiles within the high-latitude/polar cap ionosphere demonstrate that the diurnal f_oF_2 variation observed at Thule is controlled by the plasma convection pattern and the associated drift velocities. The model calculations for $B_z < 0$ and $B_z \approx 0$ show factors of 2 to 3 differences in N_{max} over Thule, supporting the stated importance of convection pattern and velocity measurements for the modeling of the high-latitude ionosphere.

1. INTRODUCTION

The high-latitude ionosphere exhibits several large-scale characteristics, for example, winter polar cap UT dependence [Sato and Rourke, 1964; Buchau *et al.*, 1985]; longitudinal variation in the *F* region densities in the nightside auroral zone [de la Beaujardiere *et al.*, 1985]; and the main *F* layer trough. These large-scale characteristics, at least to a large extent, are a result of the plasma convection across the polar cap [Knudsen, 1974; Knudsen *et al.*, 1977; Watkins, 1978; Sojka *et al.*, 1981] and the displacement of the geomagnetic pole from the geographic pole [Sojka *et al.*, 1979].

The existence of polar plasma convection was inferred from electric field measurements from satellites [Cauffman and Gurnett, 1972], or by directly mea-

suring the convection with satellite-borne plasma drift meters [Hanson and Heelis, 1975]. Ground-based high-latitude plasma convection measurements have been conducted during the decade-long measuring campaign of the Chatanika incoherent scatter radar (ISR) [Foster, 1983] and by the northward looking Millstone Hill ISR [Evans *et al.*, 1980]. The large body of plasma convection data shows that in its simplest form the convection occurs in a two-cell pattern. Models of this two-cell convection pattern developed by Volland [1975] and improved by Heelis *et al.* [1982] have been used extensively to model the ionosphere under the influence of the convection (above references). Figure 1 [from Heelis *et al.*, 1982] shows the two-cell configuration, with anti-sunward plasma flow across the polar cap and sunward return flow along the morning and evening flanks of the auroral oval.

Past observations and modeling work have shown that knowledge of the convection pattern is a prerequisite for understanding the polar ionosphere. The two-cell pattern occurs most clearly when the interplanetary magnetic field (IMF) has a southward component ($B_z < 0$), while the exact flow geometry is controlled by B_y [Heelis, 1984]. For $B_z > 0$, dusk to

¹Air Force Geophysics Laboratory, Hanscom Air Force Base, Massachusetts.

²Center for Atmospheric Research, University of Lowell, Lowell, Massachusetts.

Copyright 1988 by the American Geophysical Union.

Paper number 8S0375.
0048-6604/88/008S-0375\$08.00

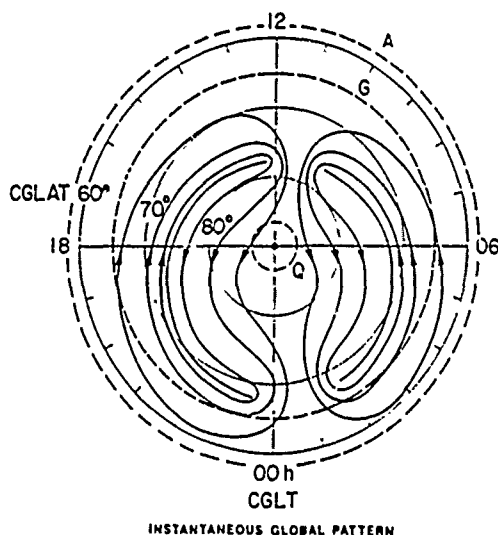


Fig. 1. Polar plasma convection pattern [Heelis *et al.*, 1982] in CGL/CGLT coordinate system. The locations of the drift measuring stations Qaanaq (Q), Goose Bay (G), and Argentia (A) are indicated by dashed circles.

dawn polar cap electric fields have been measured, which cause sunward plasma flow across the central polar cap [Burke *et al.*, 1979], leading to the model of a four-cell convection pattern. Satellite magnetometer measurements [Zanetti *et al.*, 1984] suggest a three- or four-cell pattern depending on the sign of B_y . Lassen [1979] interpreted the polar cap auroral arcs, observed during magnetically quiet periods, as being the result of a shear associated with a third central polar cap cell, with the shear occurring either at the edge of the morning (when $B_y < 0$) or the evening cell (when $B_y > 0$). Recent analysis of Dynamics Explorer (DE) 2 data [Heppner and Maynard, 1987] indicates that it is possible to explain the data for the full range of B_z and B_y with a basic two-cell pattern. For the $B_z > 0$ condition this approach results in substantial distortion of the two cells to explain sunward flow in the central polar cap. However, the resulting pattern agrees with observations in other regions of the high-latitude ionosphere.

In this paper we describe a ground-based coherent HF radar (digital ionosonde) technique, which allows continuous measurement of the plasma convection at selected sites. Early observations [Reinisch *et al.*, 1987] show good agreement between the measurements and the major features of the plasma convection patterns. The analysis presented here indicates that not only are the major features observed, but also details such as shears and drift reversals in response to quiet magnetic conditions are detected.

The digital ionosonde measurements suggest that continuous monitoring of at least the large-scale features of the convection pattern with a ground-based technique is possible and useful.

2. SPACED ANTENNA DOPPLER DRIFT TECHNIQUE

The Digisonde [Bibl and Reinisch, 1978] drift technique uses spectral analysis of ionospheric echoes [Pfister, 1974a, b]. This technique has been refined for automatic data processing [Dozois, 1983] and is an integral part of all modern Digisondes [Reinisch, 1986].

The drift measurements are conducted using phase coherent pulse transmission on two HF frequencies which are selected to sample desired heights in the F region. These transmitted HF waves typically illuminate a large overhead F region area of several hundred kilometers diameter. An array of four or seven antennas (depending on the site) deployed in a 100-m baseline triangle receives the signals reflected from the ionosphere (the technique is equally applicable to E region studies). The individual antennas of the receiving array are multiplexed at the pulse repetition rate (typically 200 Hz). For each of the two frequencies the time series of the echo received and sampled at each of the antennas is Fourier transformed in real time, resulting in four (or seven) complex spectra at the end of each measurement period, one for each antenna.

During a normal measurement campaign, ionograms are taken in 5-min intervals to monitor proper frequency and sample gate selection in a dynamic environment. The time between ionograms is used to collect a series of (nominally eight) drift measurements of typically 20-s each. Figure 2 shows an example of such a sequence of ionogram/drift measurements. On the left is the representation of the digital ionogram (bottom, amplitude; top, status, i.e., coded information on Doppler/direction/polarization); and to the right, a subset of the collected Doppler spectra, displayed to permit inspection of data quality during data acquisition. Data time runs from left to right as indicated. Spectral frequencies are displayed vertically, with 0, plus, and minus Doppler as indicated. The bottom right half of Figure 2 (labeled "amplitude") gives the amplitude spectrum; the top half (labeled "phase") shows the phase of each corresponding Doppler line; jointly these two data sets provide a set of complex spectra. For a 20-s sampling period the Doppler resolution is 0.05 Hz, and the Doppler range is ± 1.6 Hz with 64 Doppler lines. These values

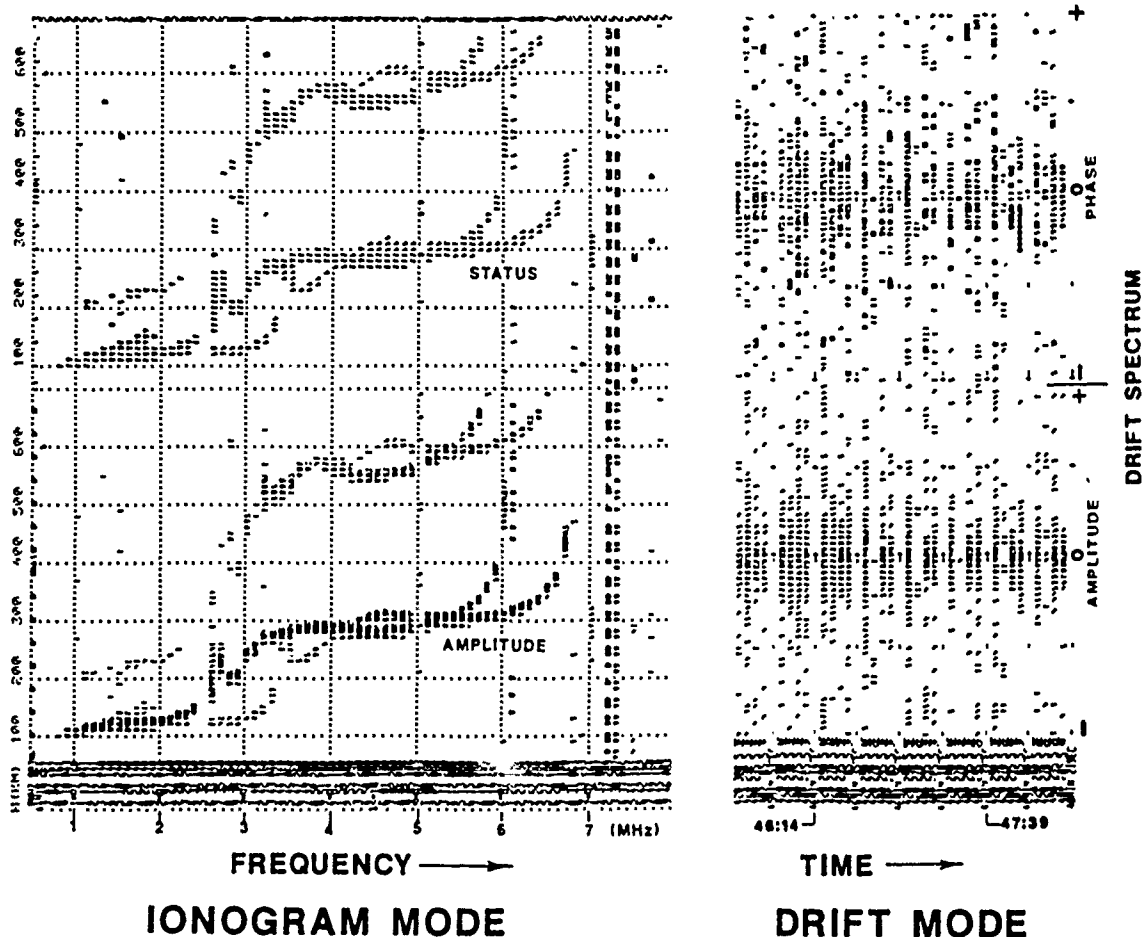


Fig. 2. A typical example of a sequence of ionogram and drift measurements collected during a drift campaign at Argentina, Newfoundland. Such a data set is collected every 5 min.

can be changed over a certain range to adjust to changing ionospheric conditions by selecting different sampling rates (pulse repetition frequencies) and sampling windows.

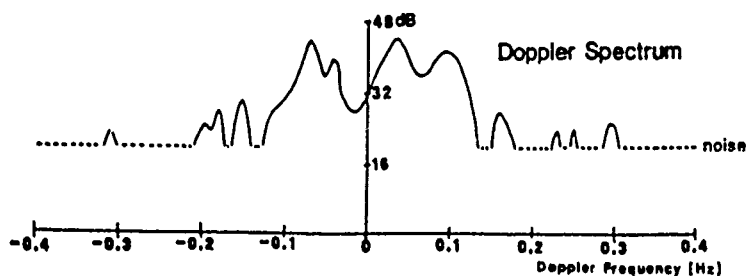
Spatial cross correlation [Bibl *et al.*, 1975] of the complex spectra (see Figure 3) determines the angle of arrival for each spectral component containing significant energy. As a result of this analysis one can construct a "sky map" showing the location of each reflection point, or source [Dozois, 1983], specified by a given Doppler frequency. The Doppler frequency provides the radial velocity component of the moving plasma for this source. The returns from all sources superimpose as a combined signal at each antenna. The Doppler frequency is given by

$$d_s = (1/\pi) \cdot v \cdot k_s \quad s = 1, 2, \dots$$

where s is the source index, v is the drift velocity, and k the wave vector from source s . The sky map covers

the area of the antenna array's main lobe, a frequency dependent area, nominally smaller than 400 km along each side for F region reflections ($<45^\circ$ half beam width). In the sky map of Figure 3 the majority of the sources are in the NW quadrant; the letters indicate positive and the numbers negative Doppler shifts. By assuming that the observed Doppler shifts are the result of a uniform motion of the reflecting plasma, one can determine the three-dimensional velocity vector v which in the least squares error sense best represents the Doppler frequencies d_s measured at the source locations specified by k_s . The drift direction for the sky map in Figure 3 is approximately to the east-northeast.

The size (or diameter) of the convection pattern and the actual convection velocities are important quantities in modeling the polar ionosphere. Three Digisonde stations, Qaanaaq, Greenland (87° CGL), Goose Bay, Labrador (65° CGL), and Argentina,



Cross correlation P of complex Doppler spectrum F from 4 antennas:

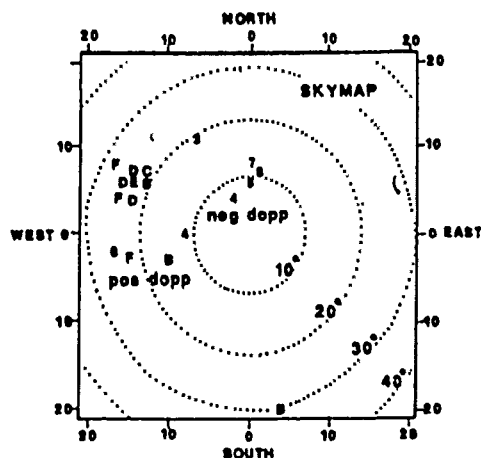
$$P_{kl} = \sum_j \sum_{j'} F_{jl} F_{j'l}^* \exp -i k \cdot [a_j - a_{j'}]$$

l - spectral line

j - antenna

a - antenna position

yields angle of arrival of each reflected spectral line.



Least Squares Fit for Drift Velocity V :

$$\xi^2 = \frac{\sum_s w_s (V \cdot R_s - \frac{1}{2} \frac{\Delta f_s}{f} c)^2}{\sum_s w_s}$$

R_s - unit position vector of reflector s

Δf_s - Doppler frequency of reflector s

f - sounding frequency

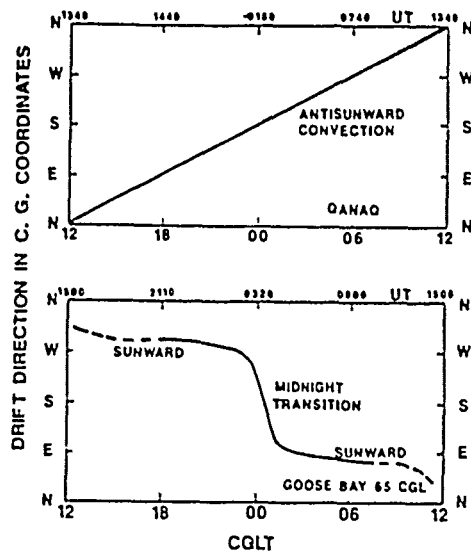
w_s - weighing factor

c - speed of light in vacuo

Fig. 3. The identification of the location of reflecting areas (sources) for those Doppler components of the ionospheric returns which contain energy above a threshold level is made by spatial cross correlation. The result is a sky map (bottom) of source locations. Letters indicate sources with positive, numbers those with negative Doppler. The three-dimensional drift vector is obtained by least squares fit, assuming uniform drift over the sky map area.

NAS, Newfoundland (57° CGL) provide a first step at continuously measuring features of the convection. Their respective locations over a full day are indicated in Figure 1 by dashed circles marked Q (Qaanaaq), G (Goose Bay), and A (Argentia). The figure shows that for the conditions represented by this pattern, Qaanaaq is fully embedded in the antisunward flow in the central polar cap, while Goose Bay is under the influence of westward (sunward) flow before midnight and of eastward (sunward) flow after

midnight. Under quiet conditions, Argentia is equatorward of the high-latitude convection and observes mid-latitude corotating plasma. Under more active magnetic conditions (in response to $B_z < 0$) the convection pattern expands in diameter, bringing Argentia under its influence for part of the night and extending the duration during which Goose Bay observes sunward return flow. Figure 4 presents diurnal variation of the drift direction in a corrected geomagnetic (CG) direction, CG local time diagram which



TIME HISTORIES AT POLAR AND AURORAL STATIONS

Fig. 4. Expected diurnal change of the drift direction (assuming the convection shown in Figure 1) for Qaanaaq and Goose Bay in a CG direction and CG local time coordinate system.

would be observed at Qaanaaq (top) and Goose Bay (bottom), assuming the convection pattern of Figure 1. At Qaanaaq the drift direction rotates linearly through 360° , while at Goose Bay the westward drift

before midnight changes to eastward at or near midnight CGLT.

3. DRIFT MEASUREMENTS

3.1. Thule—Magnetically active period

Several winter measurement campaigns were conducted by the Airborne Ionospheric Observatory while on the ground at Thule AB, Greenland (86° CGL) to study the structure and dynamics of the polar cap ionosphere. During these campaigns the antisunward convection of large nonauroral plasma patches was observed with an all-sky imaging photometer (ASIP) [Weber *et al.*, 1984], and the UT dependence of the maximum electron densities in these patches was established [Buchau *et al.*, 1985]. For the campaigns in December 1983, January–February 1984 and March 1985 a four-antenna array was deployed near the aircraft to provide measurements of the plasma drift independent of the optical observations. The patches observed by the ASIP under active conditions in the 1200 to 0000 UT time window permit an independent measurement of the convection velocities. Between 0000 and 1200 UT the patches are generally not detectable by the ASIP owing to the low plasma densities [Buchau *et al.*, 1985]. Drift results (Figure 5) for measurements

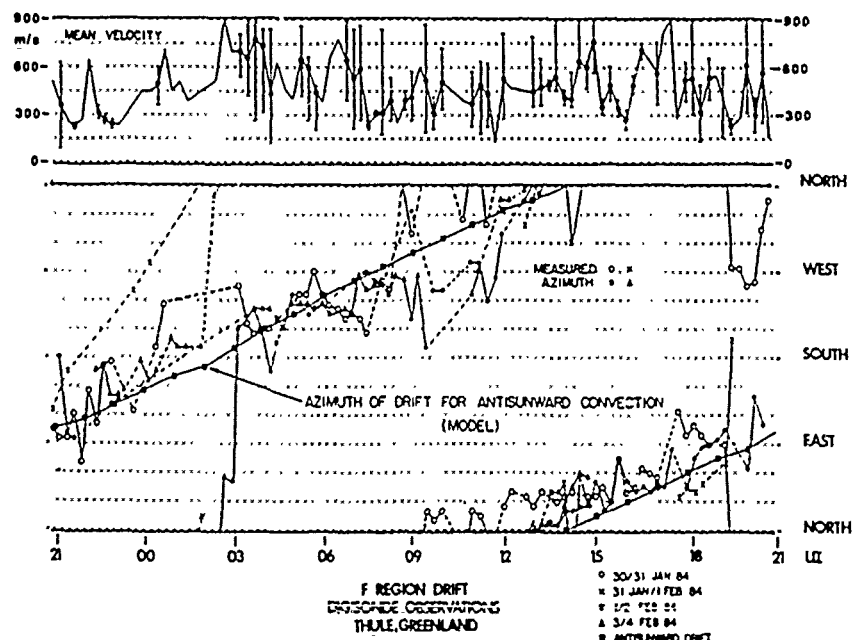


Fig. 5. F region drift direction (bottom) and velocity (top, showing mean velocity and range of observations) taken during four moderately disturbed days in January and February 1984 at Thule AB, Greenland. The anti-sunward direction is indicated for reference.

taken at Thule during four disturbed to moderately disturbed days between January 30 and February 4, 1984 (ΣKp for January 30 and 31 and February 1–4 was 34, 29–, 23+, 22–, 23, and 41+, respectively) show a predominantly antisunward drift (the antisunward direction, rotating through 360° in 24 hours, is indicated). This agrees with the analysis of simultaneous optical observations for February 3–4, 1984 [Weber *et al.*, 1986] and earlier results derived from optical data of antisunward plasma transport under disturbed conditions [Weber *et al.*, 1984]. The observed velocities shown in the top panel of Figure 5 (mean velocity and range) fluctuate between 150 and 900 m s⁻¹, well within the range of previous satellite measurements and in general agreement with the optical observations. With the confidence in the technique gained from these measurements, permanent digital sounding capabilities were established at the Qaanaaq Geophysical Observatory of the Danish Meteorological Institute, in northern Greenland (87° CGL), and at a suboval station (Argentia, Newfoundland, 58° CGL). Together with the Air Force Geophysics Laboratory (AFGL) Goose Bay Ionospheric Observatory (65° CGL) these stations form a meridian chain along approximately 20°E CG longitude.

3.2. Thule—Magnetically quiet period

Earlier campaigns had established that sun-aligned polar cap arcs, especially subvisual *F* layer arcs, occur in the polar cap under magnetically quiet conditions [Weber and Buchau, 1981; Buchau *et al.*, 1983]. Reiff *et al.* [1978] showed that current continuity at plasma flow shears requires upward (or downward) Birkeland currents, therefore producing subvisual and visual signatures, i.e., auroras in the region of upward currents. Lassen [1979] concluded that polar cap arcs are optical signatures of shears and flow irregularities in the magnetospheric convection. The analysis of Sondrestrom ISR data in the context of ASIP arc observations has confirmed that arcs delineate plasma shears [Carlson *et al.*, 1984].

The Thule drift data taken on December 9–10, 1983 cover a 9-hour period at the end of a 27-hour-long quiet period (December 9 $\Sigma Kp = 5+$). During the quiet period from 1900 to 2300 UT on December 9, 1983, subvisual and visual arcs typical for quiet periods were observed in the ASIP data to occupy major parts of the sky and to drift from dawn to dusk. The concurrent drift measurements are shown in Figure 6 (bottom). The drift direction oscillates

dramatically throughout the three magnetically quiet 3-hour periods at the beginning of the data sample (Kp is indicated below the abscissa), suggesting the transit of several shear boundaries through the station zenith. As magnetic activity increases, the convection direction becomes more orderly, with a general direction 30°–45° clockwise from antisunward. The drift velocities are low (150–300 m s⁻¹) during the quiet period and increase somewhat (150–600 m s⁻¹) during the disturbed period.

Also of significance here is the first comparison of drift data with IMF data, shown in the top part of Figure 6. The large fluctuations in drift direction, indicating the presence of shears, as well as the arc observations occur during times when $B_z > 0$, $B_y \approx 0$, and $B_x > 0$. As B_x decreases and B_y increases with still (strongly) positive B_z , the plasma drift becomes more orderly, but skewed by 60°–90° clockwise from antisunward. For the steady $B_z < 0$ conditions from 1100 to 2100 UT, the flow is steady antisunward (skewed 30° clockwise). As B_z becomes positive again after 2100 UT, shears start to dominate again. No clear effects of B_y and B_x on the drift direction (under $B_z < 0$ conditions) can be derived from this short measurement.

For the drift analysis the convection is assumed to be uniform across the sky map. This clearly is not the case during the 9-hour period of arc observation, and the resulting drift directions and the calculated velocities are not meaningful but merely give an indication of the existence of shears. A preliminary attempt to separate sky maps into regions within and on either side of arcs, using ASIP images as a guide, shows evidence of shears. A detailed discussion of this analysis is beyond the scope of this paper.

3.3. Qaanaaq—First extended drift measurements

Drift measurements until early 1986 had been made by manually selecting frequencies and setting sampling gates, thereby requiring continuous manning of the Digisonde. Since 1986 this procedure has been automated for all Digisonde 256 stations. The automation is based on the ARTIST trace identification software for the Digisonde ionograms [Reinisch and Huang, 1982; Reinisch *et al.*, 1982] that resides in an IBM AT microcomputer which is part of the Digisonde 256.

The data (Figure 7) cover a continuous period of almost 6 days of drift measurements, from October 29 to November 3, 1986. A cursory inspection suggests at least for the first four days steady anti-

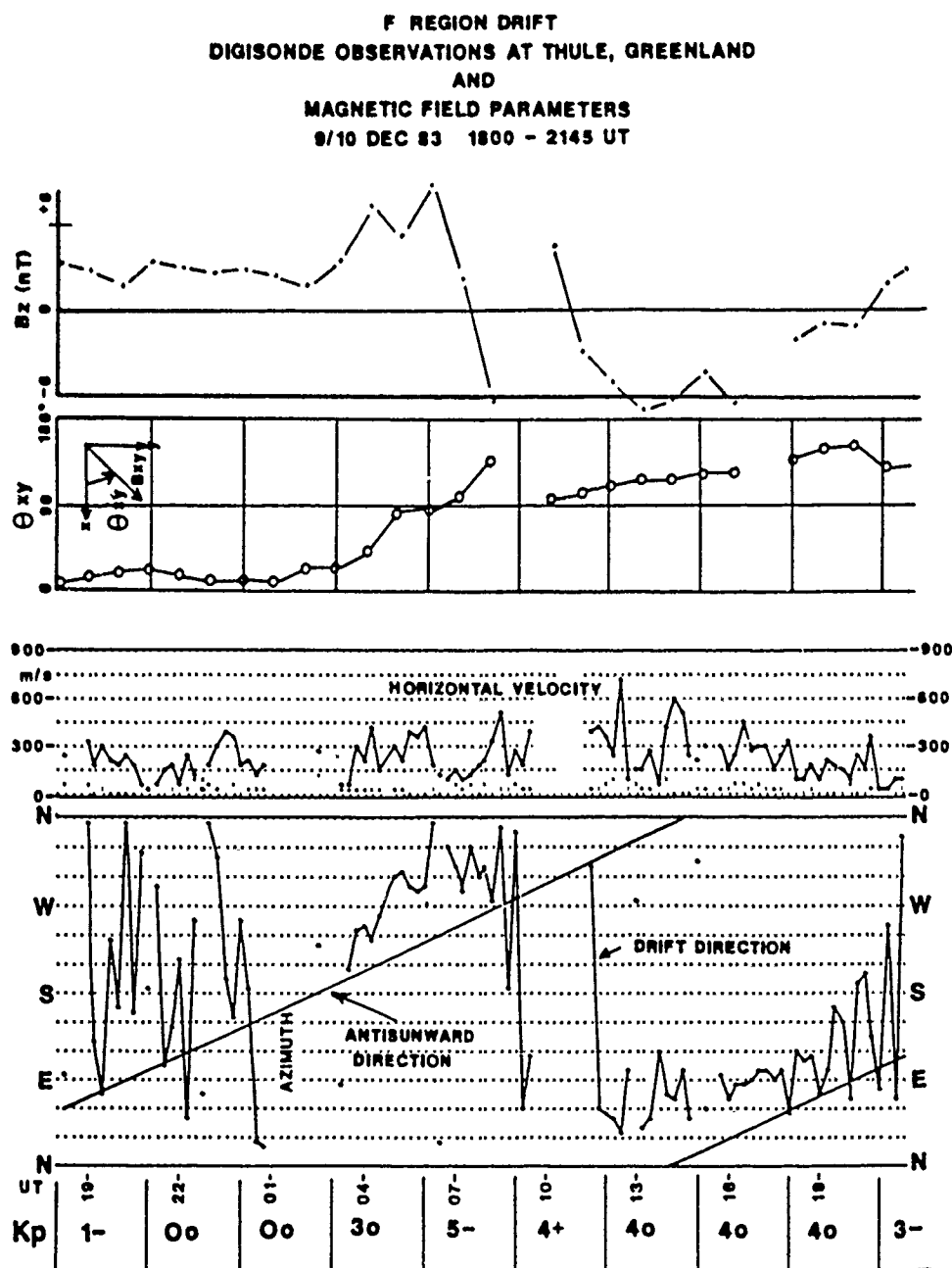


Fig. 6. First comparison of *F* region drift measurements, taken on December 9–10, 1983 at Thule, and interplanetary magnetic field (IMF) data (for discussion see text). Also shown are the *Kp* values for the measurement period.

sunward drift direction. However, clear deviations are seen for the period 1500–1800 UT on October 29, and 1200–1600 UT on November 1. Significant oscillations in direction, similar to those discussed in section 3.2, indicate the presence of shears/arcs starting 1700 UT on November 1 and continuing more or

less unabated throughout the remainder of the measurement period.

Comparison of magnetic activity (*Kp*) and drift measurements in Figure 7 indicates antisunward convection at velocities greater than 300 m s^{-1} during more disturbed periods ($Kp > 3$) on October 29 and

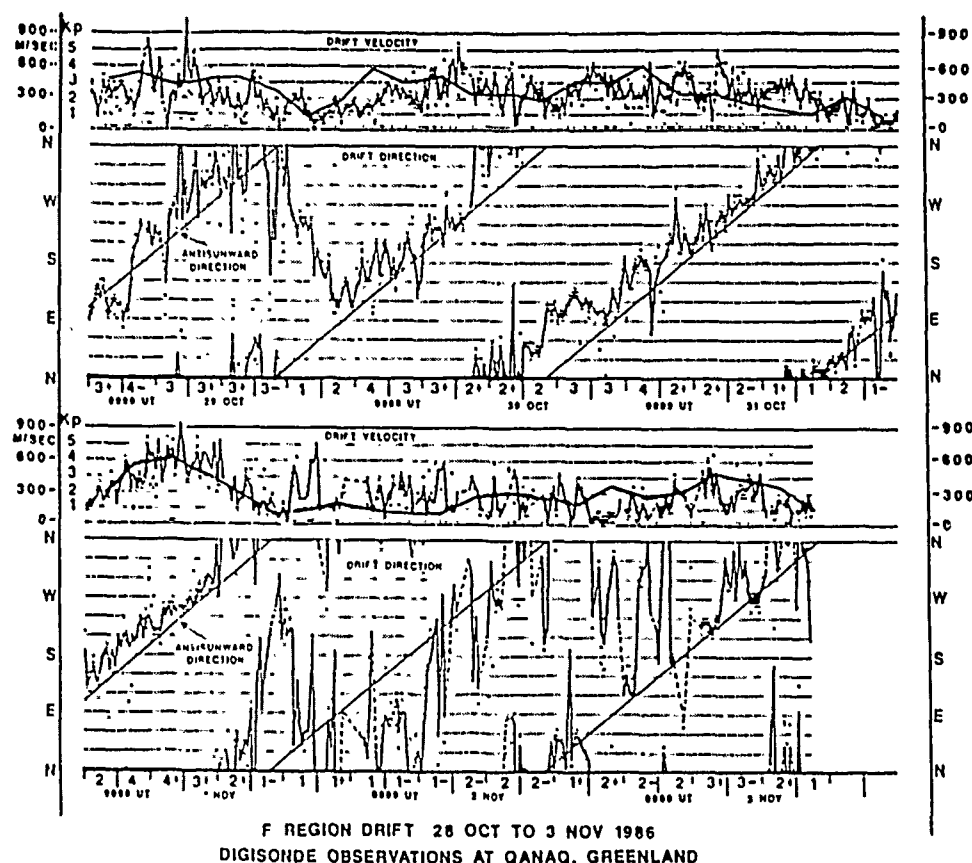


Fig 7. Continuous *F* region drift measurements taken at Qaanaq, Greenland, from October 28, 1986 (2100 UT) to November 3, 1986 (1500 UT). *Kp* values are shown between corresponding 3-hour tick marks. Superimposed on the presentation of the drift velocity for comparison is an analog representation of the *Kp* time variation.

early October 30, 1986. This active period was interrupted by a 3-hour quiet period ($Kp = 1$, 1500 to 1800 UT on October 29) during which the drift turned sunward, in agreement with the previously mentioned satellite observation for $B_z > 0$. Sunward drift during quiet times following disturbed conditions was again observed on November 1, 1986. Magnetically active conditions ($Kp = 4, 4+, 3+, 2+$) during the first half of the day were interrupted by quiet ($Kp = 1-$) conditions from 1200 to 1500 UT, during which period well-organized antisunward drift with velocities greater than 600 m s^{-1} was measured. From here to the end of the measurements the magnetic activity remained generally quiet, and clear evidence of shears was observed throughout. A short period of moderate activity ($Kp = 3+, 3-$) within this quiet period tended to show somewhat more antisunward organization of the drift. While the previously discussed measurements from Figure 7 agree with generally accepted behavior of convection

during various levels of magnetic activity, this is not the case for October 31, 1986, when despite extended quiet magnetic conditions the drift is consistently antisunward, with velocities decaying from ~ 450 to 75 m s^{-1} by the end of the quiet period.

The (horizontal) drift velocities are shown above the respective drift direction panels. Superimposed is the variation of *Kp* as a function of time in analog presentation (continuous line). There is evidence that higher *Kp* values correlate with higher velocities and lower *Kp* values with lower velocities (for example, 2100 UT on October 31 to 1500 UT on November 1). The correlation breaks down during the extended period of shear observation (second half of November 1, and all of November 2–3, 1986).

3.4. Qaanaq—Drift measurements under sunlit conditions

A limited set of drift measurements taken at Qaanaq under fully sunlit conditions corroborates the

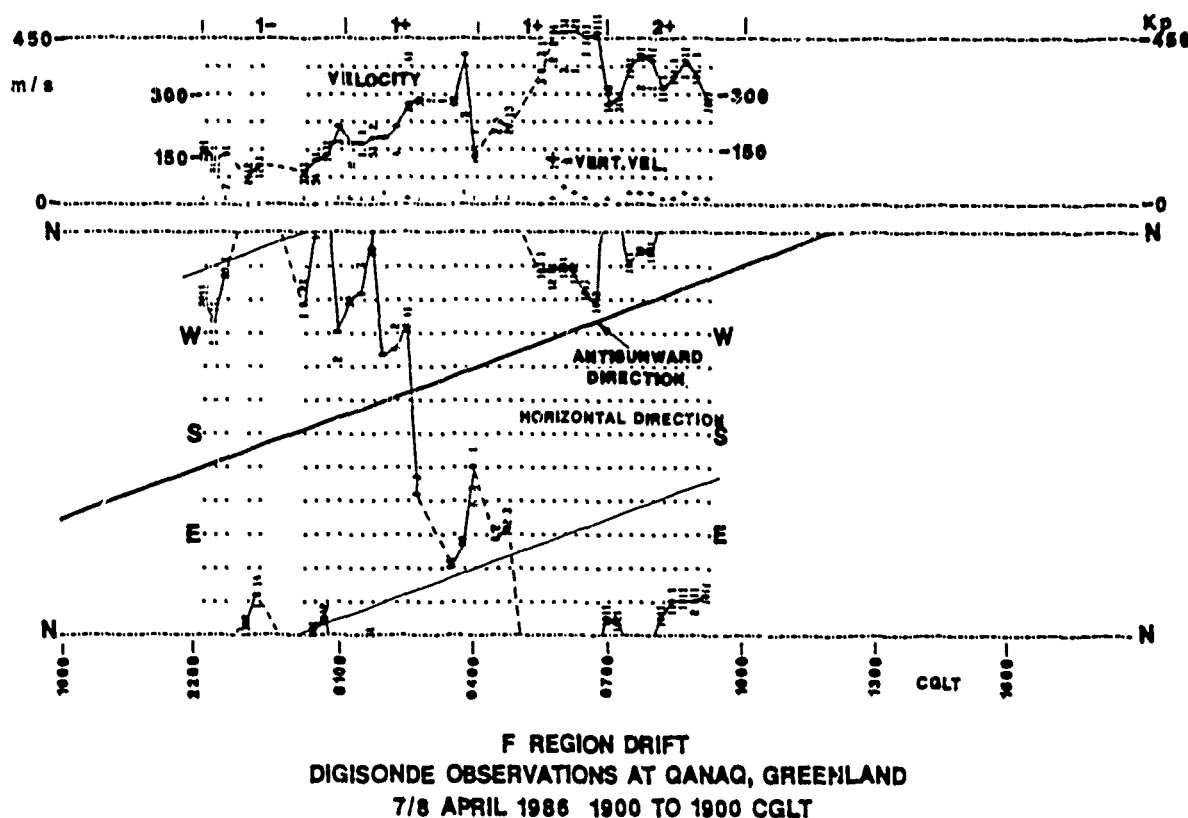


Fig. 8. F region drift observations from Qanaaq, Greenland, taken on April 7-8, 1986 taken under magnetically quiet conditions.

observations in darkness. Drift measurements conducted at Qanaaq on July 29-31, 1986 (data not presented here) show consistent antisunward convection with velocities from 150 to 450 m s^{-1} for the prevailing moderately active conditions ($\Sigma Kp = 26-, 20, 20+,$ respectively, or $Kp > 2$). For measurements taken under magnetically quiet conditions, in full sunlight on April 8, 1986 (Figure 8), with $Kp = 1-, 1+, 1+, 2+, 2+$ for the period of measurements (0000 to 1200 UT on April 8, 1986 or 2200 to 0900 CGLT) the convection is initially sunward, as expected for quiet or (inferred) $B_z > 0$ conditions. As magnetic activity increases through $Kp = 1+$ to $2+$, the drift direction turns antisunward, skewed clockwise by 30° - 60° .

It is clear from the set of Qanaaq observations discussed so far that Kp is at best a coarse ordering parameter for the drift observations, especially since $B_z > 0$ does not necessarily correspond to quiet magnetic conditions as Figure 6 indicates. There a jump from $B_z = +3$ nT to $+6$ nT corresponds to a change in Kp from 0_0 to 3_0 , contrary to an expectation of continued quiet conditions.

3.5. Goose Bay observations

As Figures 1 and 4 indicate, Goose Bay, for the selected average convection pattern, is under the influence of the sunward return plasma flow for ± 6 hours around CG midnight, with westerly flow expected prior to and easterly flow past midnight. At other times, Goose Bay is under the influence of corotating plasma, measuring the lower drift velocities of the mid-latitude ionosphere [Kent and Wright, 1968].

A typical example of Goose Bay drift measurements are the data from January 14-15, 1983 (Figure 9) taken under moderately disturbed conditions ($\Sigma Kp = 16+$ and $28+$ for January 14 and 15, respectively). The convection in the premidnight sector is consistent and toward the west (sunward). After CG midnight the convection switches toward the east, moving smoothly through the expected southerly direction. A valid measurement indicating a quick switch back to westerly drift at 0200 AST interrupts the smooth transition toward easterly flow. It should be noted that the velocities are consider-

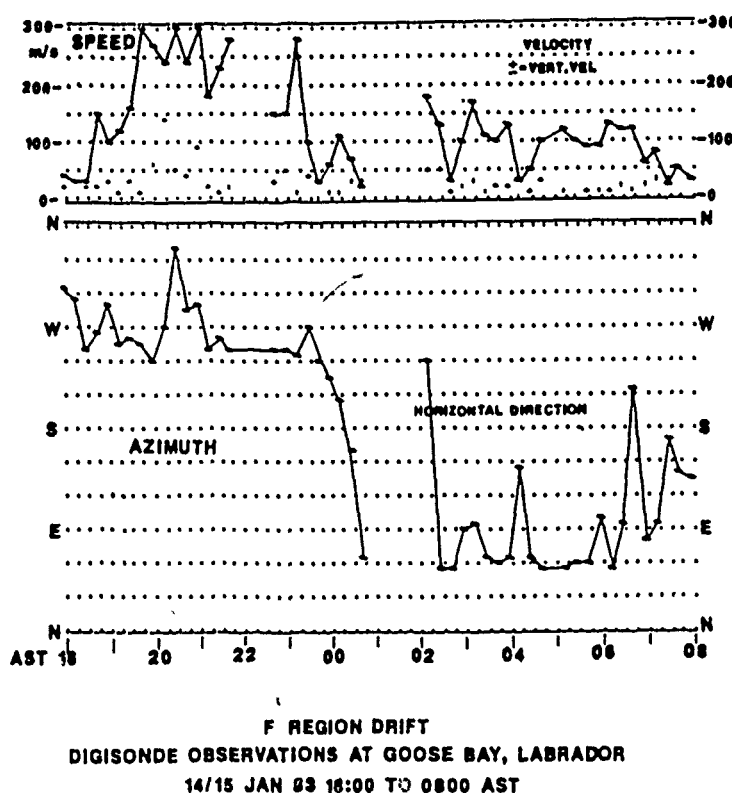


Fig. 9. *F* region drift observations at Goose Bay on January 14–15, 1983 show the expected switch of the sunward convection return flow from westward to eastward near midnight.

ably lower than those observed in the polar cap, with premidnight velocities measured at 250 m s^{-1} and postmidnight velocities at 100 m s^{-1} .

A substantial data set (38 full or partial days) collected between 1981 and 1985 during the development of the drift technique is not of the same quality and consistency as the polar cap data set. This is due to (1) manual data collection, (2) interference with the *F* layer measurements by blanketing *E_s* during magnetically disturbed periods, and (3) lack of solid echoes during low- f_oF_2 (trough) conditions, coinciding with quiet magnetic activity and small oval and convection pattern diameter. But throughout the measurement set, consistent premidnight westward/postmidnight eastward drift direction is observed. Short 15 min to 1 hour drift reversals are, however, not uncommon, especially in the postmidnight sector. The drift velocities shown in Figure 9 are typical of the higher velocities observed in the full data set; however, the high velocities may be observed after midnight as well as before. Low velocities ($< 50 \text{ m s}^{-1}$) are more routinely observed and are more typi-

cal for times away from midnight. A thorough analysis in the context of available IMF data is planned, focusing specifically on the time of the midnight switch from west to east, the relation of short-lived drift reversals to IMF conditions, and the daily duration of distinct convection conditions. This latter measurement may provide information on the diameter of the convection pattern.

3.6. *Argentia* observations

Our southernmost measurements have been taken at Argentia NAS, Newfoundland (57° CGL). Under quiet and moderate magnetic conditions, Argentia is likely to remain under the influence of the corotating ionosphere, at or south of the plasmopause (Figure 1). For low magnetic activity ($\Sigma Kp < 25$), observed drift directions to date do not exhibit any recognizable patterns. Measured velocities are in the $50\text{--}150 \text{ m s}^{-1}$ range. Figure 10, however, provides evidence that for the magnetically active period of February 9–12, 1986 the diameter of the convection

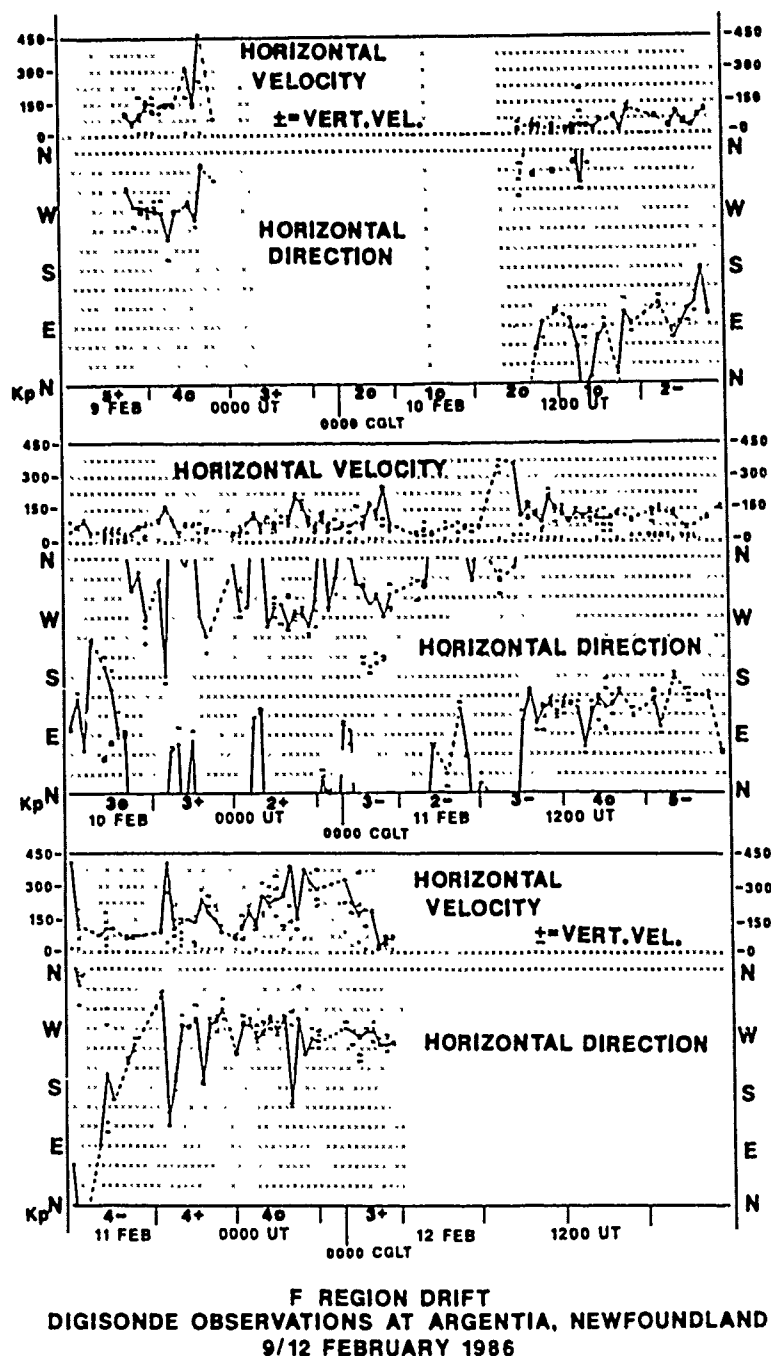


Fig. 10. *F* region drift observations at Argentia, Newfoundland on February 9–12, 1986 during moderately disturbed conditions.

pattern expands to bring Argentia into the area of sunward return flow. For this station, magnetic midnight occurs at 0400 UT. For each of the 3-hour periods marked on the time axes of the three panels, the *Kp* values are indicated.

Inspection of Figure 10 shows evidence for westward (sunward) drift at $75\text{--}150\text{ m s}^{-1}$ for $Kp \geq 4$ prior to local magnetic midnight, with occasional velocity increases to 450 m s^{-1} . During less active conditions ($2 < Kp < 4-$) the data for February 10–11

show switching between sunward (westward) and antisunward (eastward) flow prior to magnetic midnight. This suggests a sequence of convection pattern contractions and expansions, alternately shifting the convection pattern or the corotating plasma over the station. The postmidnight (CGLT) data on February 10 and 11 indicate generally east to southeast (sunward) drift with velocities between 50 and 100 m s^{-1} for quiet conditions (February 10) and between 100 and 300 m s^{-1} for more active conditions (February 11). Short deviations from the east drift toward northerly were observed in both morning periods.

4. DISCUSSION OF DRIFT MEASUREMENTS

A newly developed digital ionosonde ground-based technique to measure plasma drift at high latitudes has produced data which agree with previous observations from satellites and from incoherent scatter radars:

1. In the central polar cap we find antisunward convection for $B_z < 0$ or for $Kp > 3$.
2. During quiet conditions, especially when following an active period, sunward convection is observed in the polar cap.
3. For extended quiet periods and $B_z > 0$, shear conditions are observed typical of the Sun-aligned polar cap arcs.
4. At oval/suboval latitudes we observe sunward flow (westward before midnight and eastward after midnight) under magnetically disturbed conditions.
5. Argentia (57° CGL) and to some extent also Goose Bay (65° CGL) show random switches from westward to eastward and back under moderate ($Kp \leq 2$) conditions. This suggests that the station(s) move alternately under the influence of convecting or corotating plasmas.

Important parameters of the plasma convection, namely the antisunward convection velocity and the approximate diameter of the convection pattern, can be measured for part of the day.

5. DRIFT MEASUREMENTS AND MODELING OF THE HIGH-LATITUDE IONOSPHERE

The importance of polar convection measurements lies in the relation of the convection pattern and the convection velocities (magnitude and direction) to the condition of the interplanetary magnetic field (IMF). The latter controls the polar cap potential Φ_{pc} through the solar wind to magnetosphere energy coupling function ϵ [Akasofu, 1981, 1984; Reiff et al.,

1981]. Ionospheric modeling has shown that polar cap and auroral oval ionization and the development of the F layer trough to the south of the oval are controlled (location and intensity) by the magnitude of the polar cap potential and are, therefore, related to the polar cap convection velocities. We expect that future studies will lead to the development of either ϵ (IMF) or Φ_{pc} (IMI) dependent high-latitude ionospheric models which can, in the absence of measurements for either parameter, be driven by polar cap plasma convection measurements.

As an example, we have investigated the effects of B_z on the electron densities in the central polar cap. Using solar production for the time dependent modeling of the ionization buildup (and decay) within a flux tube (for details see Anderson et al. [this issue]) as it travels along a trajectory described by a B_z dependent convection model [Heelis, 1984], the time history of the maximum electron density (N_{max}) in flux tubes which cross Thule at selected times has been computed. The effects due to particle precipitation have been neglected. The contribution to N_{max} by the cusp precipitation is small ($\sim 2.4 \times 10^4 \text{ cm}^{-3}$), as the flux tubes that typically travel at 500–1000 m s^{-1} spend little time traversing the cusp [Knudsen et al., 1977].

Figure 11 shows the trajectories of the flux tubes which traverse Thule at 1400 CGLT (squares) and 2000 CGLT (triangles) in a CGL/CGLT coordinate system: for $B_z < 0$ and $B_z \approx 0$ condition, respectively. Other trajectories are also shown but are not discussed further. The locations of the flux tubes are indicated in $\Delta t = 30$ min increments; the starting point of each trajectory is 6 hours before the time of crossing over Thule. The figure illustrates the large difference in convection pattern diameter and in the convection velocities (v is proportional to the distance between half-hour marks) for the two selected B_z conditions. Of special importance is the exposure of the relevant flux tubes to solar UV. The relation of the flux tube trajectories to the terminator for December is shown in Figure 12. For $B_z < 0$ the flux tubes arriving at Thule at 1400 and 2000 CGLT spend at least 4.5 hours in sunlight, much of that time at solar zenith angles of $< 80^\circ$. Because of the high convection velocities, it takes the flux tubes only between 15 and 30 min to reach Thule, after crossing the terminator into darkness, a time short in comparison to the recombination time of the F layer ionization. In contrast, for $B_z \approx 0$ the respective flux tubes experience sunlight for only 1.5–3.5 hours and

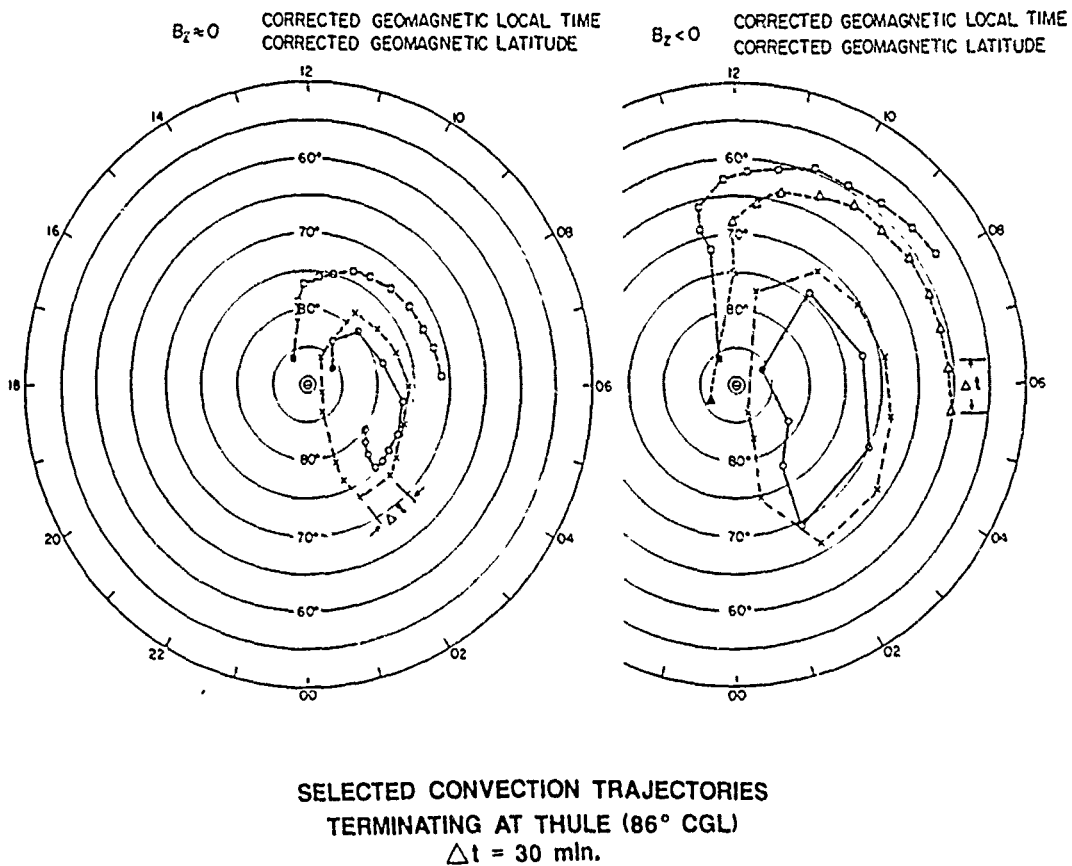


Fig. 11. Convection trajectories for flux tubes crossing Thule at 0200 CGLT (crosses), 0800 CGLT (circles), 1400 CGLT (squares) and 2000 CGLT (triangles) for $B_z < 0$ and $B_z \approx 0$ conditions, in CGL/CGLT coordinates ($\Delta t = 30$ min). The 2000 CGLT trajectory has not been shown in the left diagram, for clarity, since it follows closely the 1400 CGLT trajectory.

only with solar zenith angles of $> 25^\circ$. As a consequence of the low convection velocities it takes the flux tubes between 45 min. and 1.5 hours to move from the terminator to Thule. Figure 13 shows the results of the modeling of the ionization time histories, as the flux tubes travel along the respective trajectories. The results differ by a factor of 3 (2) in N_{\max} for ionization observed at Thule at 1400 (2000) CGLT, for the two considered conditions, $B_z = 0$ and $B_z < 0$, respectively.

6. CONCLUSION

A chain of Digisondes, with automatic plasma drift measurement capabilities, is able to continuously measure features of the polar cap convection patterns, which previously had been derived from many "snapshot" measurements by polar satellites, and

from a limited (in location and time) set of incoherent scatter radar measurements.

Digisonde drift measurements in the central polar cap identified antisunward convection under disturbed conditions, and sunward convection when magnetic conditions switched from active to quiet. Under extended quiet conditions the existence of shears has been documented, which is expected to accompany the simultaneously occurring polar cap auroral E and/or F layer arcs. The observed velocities in the polar cap tended to increase with magnetic activity, corresponding to the positive correlation between magnetic activity and the polar cap potential drop [Heppner and Maynard, 1987]; however, a clear overall correlation between activity and velocity could not be established. This may possibly be due to incorrect drift velocities obtained during arc or quiet

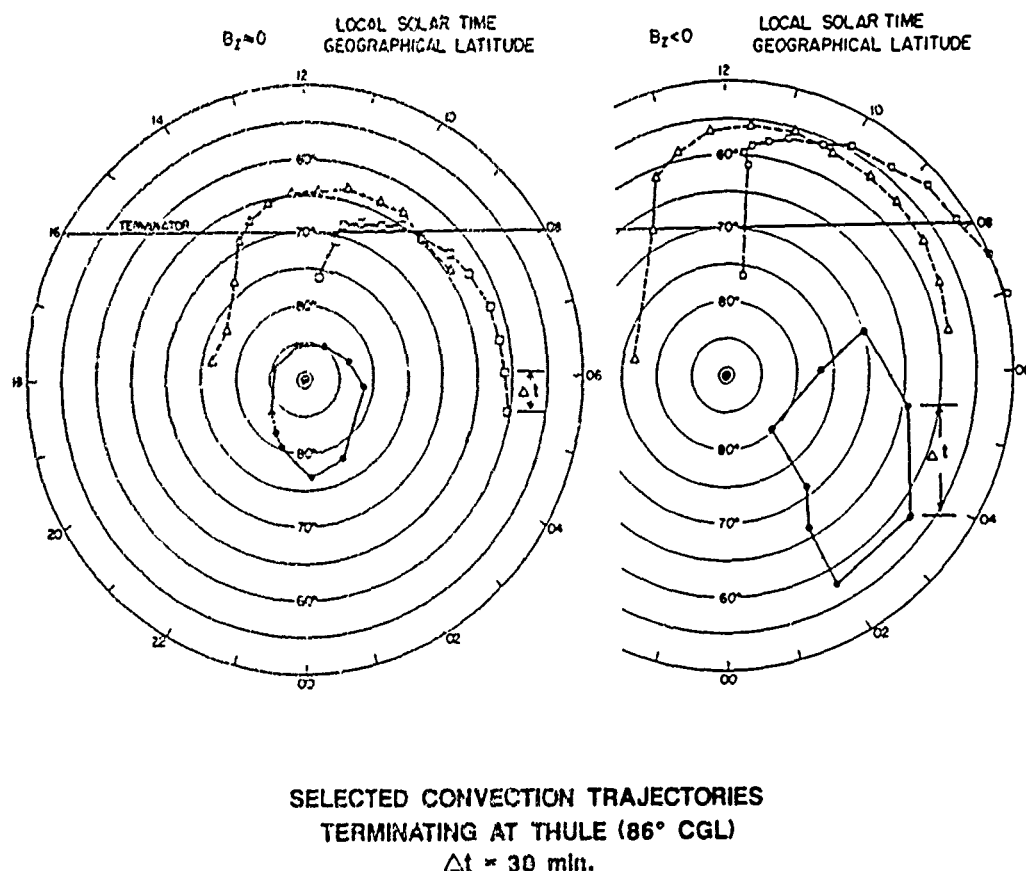


Fig. 12. The same convection trajectories as in Figure 11, here in geographic latitude, local solar time coordinates. Also shown is the terminator ($\chi = 90^\circ$).

conditions, when the assumption of uniform drift over the sky map area does not hold.

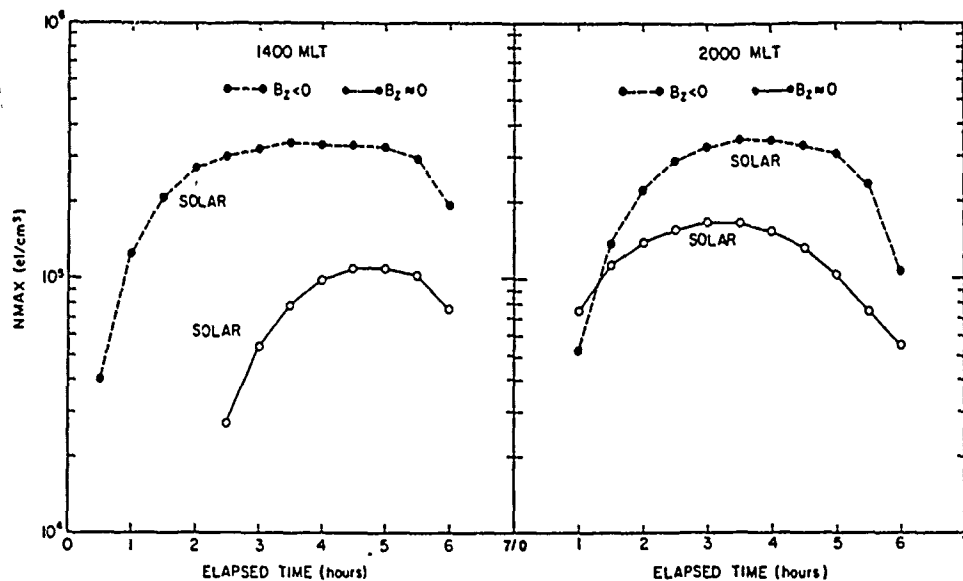
At the auroral and subauroral stations Goose Bay and Argentia the sunward return flow is observable for several hours near magnetic local midnight, including the expected drift reversal from westward to eastward, as long as the activity is high enough to bring the convection pattern over the station(s). During more quiet or changing magnetic conditions the switching of a station from inside the convecting region into the corotating region has been observed at the southernmost station (57° CGL). Thus such drift measurements may allow determination of the dimensions of the region under the influence of convection for at least part of the day.

Our previously discussed measurements and other studies of polar cap convection under $B_z > 0$ condition [Burke et al., 1979; Frank et al., 1986; Heppner and Maynard, 1987] suggest that the highly structured, often turbulent convection, represented in multiple-cell or contorted flow patterns, cannot be

determined with any degree of accuracy by a limited (even large) set of ionosonde drift measurements. However, the data discussed here, backed up by data from a full year of Regular World Day measurements (Qaanaaq, 1986), provide evidence that the drift measurements can readily identify this turbulent condition.

In general, the slow convection under $B_z > 0$ condition is not as important to the maintenance or enhancement of the polar cap (and auroral oval) F layer plasma densities as the higher convection velocities for $B_z \leq 0$ (increasing magnetic activity). The previous ionospheric model study supports this assumption, where 3 times higher plasma densities over Thule resulted from the stronger convection for the $B_z < 0$, in comparison to those for the $B_z \sim 0$. It is expected that the continuous drift measurements will define the basic parameters of the convection pattern at least for periods when the more regular two-cell configuration prevails, i.e., for $B_z \leq 0$.

But even for $B_z < 0$ it will not be possible to speci-



Calculated NMAX Values Along Convection
Trajectories Crossing Thule at 14 and 20 MLT

Fig. 13. Calculated N_{max} values along convection trajectories crossing Thule at 1400 and 2000 CGLT.

fy the details of the convection pattern for the whole polar region with the limited number of polar stations currently envisioned (five to 10). We do expect, however, on the basis of the data presented in this paper, that a detailed analysis of the existing and growing drift data base will lead to a technique of selecting (for at least part of the day) the convection model and the polar cap potential drop which best represent the observations. The improving convection models, the addition of Digisonde drift measurements at locations significant to the determination of the convection pattern, and the combined use of ion drift data from satellites (Defense Meteorological Satellite Program) and time continuous Digisonde drift measurements hold the promise for a convection pattern specification capability. A first step in this direction is the planned deployment of a Digisonde at Sondrestrom to measure the skewing of the trans-cusp plasma flow under the influence of B_z [Heelis, 1984] with the goal of providing in the skewing another parameter for the selection of the best fitting model.

Acknowledgment. We thank the Danish Commission for Scientific Research in Greenland for permission to conduct ground and aircraft experiments at Thule AB. We thank the scientists and engineers from the Danish Meteorological Institute, in Copenhagen and at the Qaanaaq Geophysical Observatory, for their enthusiastic support in establishing the Digisonde facility at Qaa-

naaq. The establishment of a Digisonde facility at Qaanaaq was sponsored by the AFGL Laboratory Director's Fund. We thank personnel from the Canadian Marconi Corporation, operating the Goose Bay Ionospheric Observatory, for the skillful collection of the Goose Bay drift data. Special thanks go to Jack B. Waaramaa, Robert W. Howell, Sgt. Douglas L. Carter, and Sgt. Wendall Randolph for their strong efforts during the many arctic field campaigns. We also acknowledge the technical support by David F. Kitrosser and Siu W. Li from the University of Lowell during these experiments. A. L. Snyder, University of Lowell, provided the comparison of drift and IMF data shown in Figure 6.

REFERENCES

- Akasofu, S. I., Prediction of development of geomagnetic storms using the solar wind-magnetosphere energy coupling function ϵ , *Planet. Space Sci.*, 29(11), 1151, 1981.
- Akasofu, S. I., Development of a geomagnetic storm prediction scheme, paper presented at 1984 Ionospheric Effects Symposium, Naval Res. Lab., Alexandria, Va., May 1-3, 1984.
- Anderson, D. N., J. Buchau, and R. A. Heelis, Origins of density enhancements in the winter polar cap ionosphere, *Radio Sci.*, this issue.
- Bibl, K., and B. W. Reinisch, The universal digital ionosonde, *Radio Sci.*, 13, 519, 1978.
- Bibl, K., W. Pfister, B. W. Reinisch, and G. S. Sales, Velocities of small and medium scale ionospheric irregularities deduced from Doppler and arrival angle measurements, *Space Res.*, XV, 405, 1975.
- Buchau, J., B. W. Reinisch, E. J. Weber, and J. G. Moore, Structure and dynamics of the winter polar cap F region, *Radio Sci.*, 18(6), 995, 1983.
- Buchau, J., E. J. Weber, D. N. Anderson, H. C. Carlson, Jr., J. G. Moore, B. W. Reinisch, and R. C. Livingston, Ionospheric struc-

- tures in the polar cap: Their origin and relation to 250-MHz scintillation, *Radio Sci.*, 20, 325, 1985.
- Burke, W. J., M. C. Kelley, R. C. Sagalyn, M. Smiddy, and S. T. Lai, Polar cap electric field structures with a northward interplanetary magnetic field, *Geophys. Res. Lett.*, 6, 21, 1979.
- Carlson, H. C., Jr., V. B. Wickwar, E. J. Weber, J. Buchau, J. G. Moore, and W. Whiting, Plasma characteristics of polar cap *F* layer arcs, *Geophys. Res. Lett.*, 11, 895, 1984.
- Cauffman, D. P., and D. A. Gurnett, Satellite measurements of high-latitude convection field, *Space Sci. Rev.*, 13, 369, 1972.
- de la Beaujardiere, O., G. Caudal, J. Holt, J. Craven, V. B. Wickwar, L. Brace, D. Evans, and J. D. Winningham, Universal time dependence of nighttime *F* region densities at high latitudes, *J. Geophys. Res.*, 90, 4319, 1985.
- Dozois, C. G., A High frequency radio technique for measuring plasma drifts in the ionosphere, *Rep. AFGL-TR-83-0202*, Air Force Geophys. Lab., Hanscom AFB, Mass., 1983.
- Evans, J. V., J. M. Holt, W. L. Oliver, and R. H. Wand, Millstone Hill incoherent scatter observations of auroral convection over $60^\circ \leq \lambda \leq 75^\circ$, 2, Initial results, *J. Geophys. Res.*, 85, 41, 1980.
- Foster, J. C., An empirical electric field model derived from Chatanika radar data, *J. Geophys. Res.*, 88, 981, 1983.
- Frank, L. A., et al., The theta aurora, *J. Geophys. Res.*, 91, 3177, 1986.
- Hanson, W. B., and R. A. Heelis, Techniques of measuring bulk gas motions from satellites, *Space Sci. Instrum.*, 1, 493, 1975.
- Heelis, R. A., The effects of interplanetary magnetic field orientation on dayside high-latitude ionospheric convection, *J. Geophys. Res.*, 89, 2873, 1984.
- Heelis, R. A., J. K. Lowell, and R. W. Spiro, A model of the high-latitude ionosphere convection pattern, *J. Geophys. Res.*, 87(A8), 6339, 1982.
- Heppner, J. F., and N. C. Maynard, Empirical high-latitude electric field models, *J. Geophys. Res.*, 92, 4467, 1987.
- Kent, G. S., and R. W. H. Wright, Movements of ionospheric irregularities and atmospheric winds, *J. Atmos. Terr. Phys.*, 30, 657, 1968.
- Knudsen, W. C., Magnetospheric convection in the high-latitude *F*₂ ionosphere, *J. Geophys. Res.*, 79, 1046, 1974.
- Knudsen, W. C., P. M. Banks, J. D. Winningham, and D. M. Klumpp, Numerical model of the convecting *F*₂ ionosphere at high latitudes, *J. Geophys. Res.*, 82, 4784, 1977.
- Lassen, K., The quiet-time pattern of auroral arcs as a consequence of magnetospheric convection, *Geophys. Res. Lett.*, 6, 777, 1979.
- Pfister, W., Drift measurement with spectral analysis during period of chemical releases into the ionosphere, *Space Res.*, XIV, 401, 1974a.
- Pfister, W., Pulse sounding with closely spaced receivers as a tool for measuring atmospheric motions and fine structure in the ionosphere, V. Period of chemical releases (as example of spectral analysis), *Rep. AFCRL-TR-74-0105*, Environ. Res. Pap., 468, Air Force Cambridge Res. Lab., Bedford, Mass., 1974b.
- Reiff, P. H., J. L. Burch, and R. A. Heelis, Dayside auroral arcs and convection, *Geophys. Res. Lett.*, 5, 391, 1978.
- Reiff, P. H., R. W. Spiro, and T. W. Hill, Dependence of polar cap potential drop on interplanetary parameters, *J. Geophys. Res.*, 86, 7639, 1981.
- Reinisch, B. W., New techniques in ground-based ionospheric sounding, *Radio Sci.*, 21, 331, 1986.
- Reinisch, B. W., and X. Huang, Automatic calculation of electron density profiles from digital ionograms, 1, Automatic O and X trace identification for topside ionograms, *Radio Sci.*, 17(2), 421, 1982.
- Reinisch, B. W., J. S. Tang, and R. R. Gamache, Automatic scaling of Digisonde ionograms test and evaluation report, *Rep. AFGL-TR-82-0324*, Air Force Geophys. Lab., Hanscom AFB, Mass., 1982.
- Reinisch, B. W., J. Buchau, and E. J. Weber, Digital ionosonde observations of the polar cap *F* region convection, *Phys. Scr.*, 36, 372, 1987.
- Sato, T., and G. F. Rourke, *F* region enhancements in the Antarctic, *J. Geophys. Res.*, 69, 4591-4607, 1964.
- Sojka, J. J., W. J. Raitt, and R. W. Schunk, Effect of the displaced geomagnetic and geographic poles on high-latitude plasma convection and ionospheric depletions, *J. Geophys. Res.*, 84, 5943, 1979.
- Sojka, J. J., W. J. Raitt, and R. W. Schunk, A theoretical study of the high-latitude winter *F* region at solar minimum for low magnetic activity, *J. Geophys. Res.*, 86, 609, 1981.
- Volland, H., Models of the global electric fields within the magnetosphere, *Ann. Geophys.*, 31, 154, 1975.
- Watkins, B. J., A numerical computer investigation of the polar *F* region ionosphere, *Planet. Space Sci.*, 26, 559, 1978.
- Weber, E. J., and J. Buchau, Polar cap *F* layer auroras, *Geophys. Res. Lett.*, 8, 125, 1981.
- Weber, E. J., J. Buchau, J. G. Moore, J. R. Sharber, R. C. Livingston, J. D. Winningham, and B. W. Reinisch, *F* layer ionization patches in the polar cap, *J. Geophys. Res.*, 89(A3), 1683, 1984.
- Weber, E. J., J. A. Klobuchar, J. Buchau, H. C. Carlson, Jr., R. C. Livingston, O. de la Beaujardiere, M. McCready, J. G. Moore, and G. J. Bishop, Polar cap patches: Structure and dynamics, *J. Geophys. Res.*, 91, 12,121, 1986.
- Zanetti, L. J., T. A. Potemra, T. Iijima, W. Baumjohann, and P. F. Bythrow, Ionospheric and Birkeland current distribution for northward interplanetary magnetic field. Inferred polar convection, *J. Geophys. Res.*, 89, 7453, 1984.
- D. N. Anderson, J. Buchau, and E. J. Weber, Air Force Geophysics Laboratory, Hanscom AFB, MA 01731.
- C. Dozois and B. W. Reinisch, University of Lowell, Center for Atmospheric Research, Lowell, MA 01854.